

UNIVERSITY OF THE WESTERN CAPE

**Formation Evaluation And Assessment Of Flow Units
Of Some Selected Wells In The Bredasdorp**

Basin, Offshore South Africa

By

Ubong Moses Okon

(Student Number: 3762295)

B.Sc. Hons (Geology/Applied Geology), B.Th, C.Th



**A thesis submitted in fulfilment of the requirements for the Degree of
Master of Science (MSc) in Applied Geology (Petroleum Option)
Faculty of Natural Sciences, Department of Earth Sciences, University of
the Western Cape, Bellville, South Africa.**

Supervisor: *Prof. Mimonitu Opuwari*

September 2022

DECLARATION

I the undersigned hereby declare that this thesis entitled “*Formation Evaluation and Assessment of Flow Units of Selected Wells in Bredasdorp Basin, Offshore South Africa*” is my original work. The work has never been submitted before for any degree or examination in any other university. All the sources I have used or quoted have been indicated and acknowledged using complete references.

Ubong Moses Okon

30th September 2022



Copyright © 2022 University of Western Cape

All rights reserve

DEDICATION

This research is dedicated to three important women in my life.

In Loving Memories of

My Dearly Beloved Mum, Late Deaconess/Mrs. Eno Moses Okon

My Dearly Beloved One, Late Mrs. Udeme-Obong Afaha Bassey

And

My Dearly Beloved Senior Sister, Late Mrs. Glory (Hossana) Okon



ACKNOWLEDGEMENTS

I thank the **Almighty God** for the grace, courage, strength and help He alone has provided for me throughout this study with the supporting family, friends and all who played a significant role in this accomplishment. To you I say, thank you very much indeed for your contributions. Acknowledgment is due to the **Petroleum Agency of South Africa (PASA)**, especially **Mr. Leon Koopman** (Supervisor) for providing the data and training on core data and to the **Information and Communication Services (ICS)** of the **University of the Western Cape (UWC)**, especially **Mrs. Renska Cupido** (ICS Technical Support) and the **STU-Team** for creating a conducive environment during this research, for all their support throughout this study and for believing in my abilities.

I would like to thank the staff members and my fellow professional colleagues and friends in the **Earth Science Department University of the Western Cape**, especially **Prof. Tapas K. Chatterjee** for his guidance and mentoring on the choice of the research area (Petrophysics), **Mr. Richard Harrison** for his guidance during the use of equipment during this research, **Mrs. Janine Botha** for her guidance during the crushing and milling of the core sample and **Nehemiah Dominick, Maxwell Dacosta and Fritz Ako** (Ph.D. candidates), **Zaki Ongeziwe** (MSc.candidate) and **Hlakametsa Vincent** (BSc. Hons Candidate) for all their motivations.

I would like to express my profound gratitude and appreciation to my thesis Supervisor **Prof. Mimonitu Opuwari**, for his guidance, invaluable discussion and encouragement throughout this research. I feel grateful to my thesis co-supervisor **Dr. Saeed Mohammed** for his continuous advice and cooperation.

I am very grateful to **Mr. Anthony Fielies** who helped me in contacting PASA for the matching of the core plugs for the mineralogy analyses in this study after waiting for a very long time.

I would like to extend my thanks to **Mr. Musharraf Fooroskar** (My work Supervisor) for his assistance and **Mr. Shawn Squire** (My Boss) for his understanding, **Mr. Blessing afolayan** for his technical support and **Mr. Sibusiso Skhosana** for the graphics and design in this thesis.

Many thanks to my extended family in Nigeria, especially my dad, **Bishop Moses Udoh and** brother (last born) **Mr. Ndiana-Abasi Moses** including my Father-Inlaw and Mother-Inlaw **Dr.& Mrs. Ogunyiriofor Okoroh** for always checking on me and for all those who encouraged me, I say thanks a million for all your encouragement, concern and love.

I would like to sincerely thank **Prof Thokozani** for reading and editing this thesis amidst his busy schedule and despite the short notice, limited time, few days to the due date for the submission of this work and particularly the ongoing load-shedding and his feedback “Dear Moses, this is a well written and presented thesis. All the best”. I am so humbled.

Lastly and most importantly, my sincere appreciation goes to my immediate family; my dear wife **Mrs. Malin Okoroh (MD)** and my dear son **Prince Micah Okon (PMUM)** for their enormous patience, sacrifices, encouragement, love, understanding and continuous support during these three years of hard work. To God be all the glory forever and ever for the great things He has done and will continue to do. Amen!!

OUTCOME OF RESEARCH

The Impact of Detrital Minerals on Reservoir Flow Zones in the northeastern Bredasdorp Basin, South Africa, Using Core Data. Minerals 2022, August 12, 1009.

<https://doi.org/10.3390/min12081009>



Keywords: Formation Evaluation, Hydraulic Flow Units, Flow zone, Permeability, Porosity.



ABSTRACT

Petroleum geologists have long recognized the need to apply secondary and tertiary hydrocarbon recovery techniques for an accurate understanding of the internal architecture of a reservoir. The approach to effective incorporation of geological heterogeneity in numerical models for stimulating reservoir behaviour, detailed petrophysical zonation and mineralogy composition analyses are required. These include the delineation of sandstone reservoirs and characterization of the sedimentological and petrophysical properties into a system for reservoir description in the Gas Field, the grouping of rock units into flow zones from core porosity and permeability and understanding of the effects of minerals on reservoir flow zones for the assessment and construction of the flow units.

This approach provides a means of uniquely subdividing reservoirs into volumes that approximate the architecture of a reservoir at a scale consistent with reservoir simulations. This approach also has advantage over more traditional methods of reservoir zonation whereby model layers are determined based on vertical distributions of porosity and permeability from core analyses and wireline logs. Primarily, the porosity and permeability distributions are considered and the variation of reservoir properties gives rise to different flow units within a lithological formation. It is also imperative to know how much hydrocarbon and water exist in situ and how the fluids will move through the reservoir.

This study focuses on the formation evaluation of the F-AH Gas Field. Uses petrophysical methods to improve the delineation of the sandstone reservoir and classify a grouping of rock units into flow zones. It also uses core permeability and porosity to identify flow units by integrating core parameters and wireline logs in the northeastern Bredasdorp Basin, offshore South Africa. The study evaluates the three selected Wells (F-AH1, F-AH2 and F-AH4) located northeastern, Bredasdorp Basin, off the coast of South Africa and was drilled in a Gas Field

known as F-AH. The datasets utilized for this study include geological well completion reports, conventional core analysis reports, well completion reports, special core analysis reports, digital wireline logs (LAS format), core photographs and petrographic assessment reports. In the present work, a suite of geophysical wireline logs consists of Gamma Ray (GR), spontaneous potential (SP) neutron (NPHI), density (RHOB), resistivity (ILD/MSFL), sonic (DT) and caliper (CL). The reservoir zone of interest ranged between 2363.9m-2560.8m depending on the position of the wells and the core intervals varied with depth and were strongly correlated with log data. The study aims to carry out a petrophysical and petrographic evaluation and integration of the sandstone reservoir zonation for the identification of flow zones in the F-AH Gas Field, north-eastern Bredasdorp Basin. The clay volume was calculated using the linear Gamma Ray method. Across the reservoir interval, well F-AH1 had an average clay volume of 16.8 %, well F-AH2 had an average volume of 24.1 % and well F-AH4 had 18.3 % all of which are relatively clean sand formations with little clay and silt impact. Log-derived porosity was calculated using density, neutron and sonic log data with an emphasis on estimating porosity within the non-reservoir sections of each well. These wells have a good average log-derived porosity of 12.3 %, 13.1 % and 15.7%. The core permeability distribution across the studied wells ranged from 0.001 mD to 2767 mD. Water and gas were recorded within the core intervals of the well. Well F-AH1 to F-AH4 had average gas saturation of 61%, 57% and 27% respectively. Average core water saturations of 39%, 43% and 73% were measured per well. The average log-derived water saturations for the three wells were 45 %, 14 % and 42 %.

Cut-off parameters were established to distinguish between pay and non-pay intervals. Pay potential intervals must have a porosity of at least 4 %, clay volume less than 40 %, and water saturation less than 65 %. Nine of seventeen reservoirs met the cut-off criteria for net pay potential. Gross thicknesses of the reservoir intervals ranged from 3.30 –80.62 m and net

thicknesses ranged from 0-79.84 m respectively. Reservoir 1 of well F-AH2 had the highest gross and net thicknesses of 80.75 m and 79.84 m at a net/gross ratio of 0.989.

Flow capacities and storage were determined using the Stratigraphic Modified Lorenz Plot (SMLP) method. The facies classification from core data was used in identifying the reservoir zones in the studied wells and the main objective of detailing the drill core samples is to identify characteristic facies based on grain size in each well. The scanning electron microscopy results of the morphological studies helped to describe the pores and grain textures by mapping clay distributions and dominant pore and clay types as the quantitative XRD results did not show the distribution and type of minerals in the pore spaces. Results show five flow zones grouped as high, moderate, low, very low and tight reservoir rocks. The High Flow Zone is the best reservoir quality rock, with porosity and permeability values ranging from 12 to 20% and 100 to 1000 mD. The high and moderate zones contribute more than 60% to the flow capacity of each well. The moderate and low flow zone extends laterally to all boreholes. The tight flow zone is impervious rock and has the lowest rock quality with porosity and permeability values of less than 8% and 1 mD, respectively. This zone contributes less than 1% to the flow capacity. Overall, this work has contributed to evaluating the predominantly gas-bearing sandstone reservoir quality distribution based on petrophysical and petrographic properties and integration of the sandstone reservoir zonation for the identification of flow zones in the F-AH Gas Field.

TABLE OF CONTENTS

UNIVERSITY OF THE WESTERN CAPE	i
Formation Evaluation And Assessment Of Flow Units.....	i
<i>DECLARATION</i>	<i>i</i>
<i>DEDICATION</i>	<i>ii</i>
<i>ACKNOWLEDGEMENTS</i>.....	<i>iii</i>
<i>OUTCOME OF RESEARCH</i>.....	<i>v</i>
<i>Keywords: Formation Evaluation, Hydraulic Flow Units, Flow zone, Permeability, Porosity</i>.....	<i>vi</i>
<i>ABSTRACT</i>.....	<i>vii</i>
<i>TABLE OF CONTENTS</i>.....	<i>x</i>
<i>LIST OF FIGURES</i>.....	<i>xv</i>
<i>LIST OF TABLES</i>.....	<i>xx</i>
<i>CHAPTER ONE</i>	<i>1</i>
<i>1. INTRODUCTION</i>.....	<i>1</i>
1.1 BACKGROUND OF STUDY	1
1.2 LOCATION OF STUDY AREA	2
1.3 AIM AND OBJECTIVES	5
1.4 THESIS OUTLINE.....	7
1.4.1 Chapter 1.....	7
1.4.2 Chapter 2.....	7
1.4.3 Chapters 3	7

1.4.4 Chapter 4.....	7
1.4.5 Chapter 5.....	7
1.4.6 Chapter 6.....	7
1.4.7 Chapter 7.....	8
CHAPTER TWO.....	9
2. GEOLOGICAL BACKGROUND OF THE BREDASDORP BASIN	9
2.1 REGIONAL GEOLOGY	9
2.2 TECTONOSTRATIGRAPHY	11
2.3 STRUCTURAL FRAMEWORK	14
2.4 DEPOSITIONAL SETTING	15
2.5 PETROLEUM SYSTEMS OF THE BREDASDORP BASIN	15
2.5.1 Petroleum Source Rock.....	16
2.5.2 Reservoir Rock.....	17
2.5.3 Seals and Traps.....	18
CHAPTER THREE	19
3. MATERIALS AND RESEARCH METHODOLOGY.....	19
3.1 INTRODUCTION.....	19
3.2 WIRELINE DEPTHS AND CORE INTERVALS FOR WELLS	20
3.3 LOG EDITING	21
3.3.1 Depth Shifting/Matching.....	22
3.4 RESEARCH METHODOLOGY	23
3.5 WIRELINE LOGS.....	24
3.5.1 Gamma Ray (GR) Log.....	24

3.5.2 Spontaneous Potential (SP) Log	24
3.5.3 Neutron (NPHI) Log	25
3.5.4 Density (RHOB) Log	25
3.5.5 Resistivity (LLD/ILD/MSFL) Log.....	26
3.5.6 Sonic (DT) Log.....	27
3.5.7 Caliper Log (CL).....	27
CHAPTER FOUR.....	28
4. CONVENTIONAL CORE ANALYSIS AND INTERPRETATION OF WIRELINE	
LOGS	28
4.1 INTRODUCTION.....	28
4.2 CONVENTIONAL CORE ANALYSIS.....	28
4.2.1 Intervals Cored	29
4.2.1.1 Well F-AH1	29
4.3 CORE-LOG DEPTH MATCH.....	40
4.4 LITHOFACIES DESCRIPTION.....	40
4.4.1 Well F-AH1 Litho-facies Description.....	43
4.4.2 Well F-AH2 Litho-facies Description.....	46
4.4.3 Well F-AH4 Litho-facies Description.....	49
4.5 RESULTS AND INTERPRETATION	52
4.5.1 Well Correlation	52
4.5.2 Grain Density.....	55
4.5.3 Sediment Logs.....	57
4.6 INTERPRETATION OF WIRELINE LOGS.....	57
4.6.1 Well F-AH1 wireline logs interpretation.....	60
4.6.2 Well F-AH2 wireline logs interpretation.....	64

4.6.3 Well F-AH4 wireline logs interpretation.....	68
CHAPTER FIVE	73
5. PETROPHYSICAL MODEL	73
5.1 ESTIMATION OF THE SHALE VOLUME.....	73
5.1.1 Gamma Ray Shale Volume	73
5.2 DETERMINATION OF THE POROSITY	81
5.2.1 Porosity from Density Log	81
5.2.2 Porosity from Neutron Log.....	82
5.2.3 Porosity from Sonic (acoustic) Log	83
5.2.4 Effective Porosity	84
5.2.5 Comparison of Log and Core Porosity	85
5.3 PERMEABILITY	91
5.3.1 Permeability from Core Analysis (Porosity-Permeability Crossplot).....	91
5.3.2 Comparison of Estimated Log Permeability with Core Permeability	97
5.4 WATER SATURATION MODEL.....	104
5.4.1 Parameters.....	104
5.4.2 Water Saturation (Sw) Models.....	107
5.4.3 Comparison of Conventional Core and Log-Derived Water Saturation	110
CHAPTER SIX	115
6. CUT-OFF AND NET PAY DETERMINATION AND ESTIMATION OF STORAGE AND FLOW CAPACITIES.....	115
6.1 INTRODUCTION.....	115
6.1.1 Determination of Petrophysical Properties in Non-cored wells	116
6.2 CUT-OFF DETERMINATION.....	117
6.2.1 Volume of Clay Cut-off Determination.....	118

6.2.2 Porosity Cut-off Determination.....	120
6.2.3 Water Saturation Cut-off Determination	122
6.3 NET PAY DETERMINATION	124
6.3.1 Determination of Reservoir Flow Units from Core Data	136
6.4 FLOW ZONE MODELLING.....	137
6.4.1 Windlandr35	137
6.4.2 Flow Zone Indicator.....	140
6.5 ESTIMATION OF STORAGE AND FLOW CAPACITIES	142
6.5.1 Stratigraphy-Modified Lorenz Plot (SMLP).....	142
6.5.2 Effect of Mineral on Flow Units.....	144
CHAPTER SEVEN.....	146
7. CONCLUSION AND RECOMMENDATIONS	146
7.1 RECOMMENDATIONS	147
REFERENCES	148
APPENDICES	157



LIST OF FIGURES

Figure 1- 1: Map showing the location of the selected wells in the Bredasdorp Basin (PASA, 2004/2005).....	4
Figure 2- 1: Major tectonic elements of the Outeniqua Basin (PASA, 2012).	10
Figure 2- 2: Sequence chronostratigraphic framework of the Bredasdorp Basin (PASA, 2012)	13
Figure 2- 3: The main elements of a petroleum system (Magoon and Dow, 1994).	16
Figure 3- 1: Flow chart of the research methodology.....	23
Figure 4- 1: Well F-AH1 showing core facies in track 6.....	45
Figure 4- 2: Well F-AH2 showing core facies in track 6.....	48
Figure 4- 3: Well F-AH4 showing core facies in track 6.....	51
Figure 4- 4: Well correlation between well F-AH1, F-AH2 and F-AH4 using Gamma Ray log.	53
Figure 4- 5: Well correlation between well F-AH1, F-AH2 and F-AH4 using Gamma Ray, neutron porosity, sonic and resistivity log	54
Figure 4- 6: Example of a potential Sandstone Reservoir in well F-AH2	59
Figure 4- 7: Reservoir interval in well F-AH1 (Zone 1, 2411.5 – 2428.1 m depth).....	61
Figure 4- 8: Reservoir interval in well F-AH1 (Zone 2, 2429.5 – 2454.2 m depth).....	62
Figure 4- 9: Reservoir interval in well F-AH1 (Zone 3, 2495.8 – 2503.0 m depth).....	63
Figure 4- 10: Reservoir interval in well F-AH1 (Zone 4, 2560.8 – 2569.5 m depth).....	63
Figure 4- 11: Reservoir interval in well F-AH2 (Zone 1, 2363.9 – 2444.7 m depth).....	65
Figure 4- 12: Reservoir interval in well F-AH2 (Zone 2, 2457.1 – 2462.3 m depth).....	66

Figure 4- 13: Reservoir interval in well F-AH2 (Zone 3, 2487.2 – 2490.5 m depth).....	67
Figure 4- 14: Reservoir interval in well F-AH2 (Zone 4, 2553.8 – 2557.9 m depth).....	67
Figure 4- 15: Reservoir interval in well F-AH4 (Zone 2, 2369.1 – 2376.7 m depth).....	68
Figure 4- 16: Reservoir interval in well F-AH4 (Zone 2, 2377.7 – 2429.4 m depth).....	69
Figure 4- 17: Reservoir interval in well F-AH4 (Zone 3, 2450.1 – 2458.4 m depth).....	70
Figure 4- 18: Reservoir interval in well F-AH4 (Zone 4, 2476.7 – 2483.8 m depth).....	71
Figure 4- 19: Reservoir interval in well F-AH4 (Zone 5, 2516.4 – 2524.8 m depth).....	71
Figure 4- 20: Reservoir interval in well F-AH4 (Zone 6,7 and 8, 2526.8 – 2561.1 m depth).72	
Figure 5- 1: Log-derived volume of clay models of well F-AH1	75
Figure 5- 2: Log-derived volume of clay models of well F-AH2.....	76
Figure 5- 3: Log-derived volume of clay models of well F-AH4.....	77
Figure 5- 4: Well F-AH1 Gamma Ray Histogram plot	78
Figure 5- 5: Well F-AH2 Gamma Ray Histogram plot	79
Figure 5- 6: Well F-AH4 Gamma Ray Histogram plot	80
Figure 5- 7: Well F-AH1 comparison of log and core porosity.....	86
Figure 5- 8: Well F-AH2 comparison of log and core porosity.....	88
Figure 5- 9: Well F-AH4 comparison of log and core porosity.....	90
Figure 5- 10: Porosity-permeability cross-plot relationships for well F-AH1.....	93
Figure 5- 11: Porosity-Porosity-permeability cross-plot relationships for well F-AH2	94
Figure 5- 12: Porosity-permeability cross-plot relationships for well F-AH4.....	95
Figure 5- 13: Porosity-permeability cross-plot relationships for all wells	96
Figure 5- 14: Predicted permeability together with core permeability for Well F-AH1	98
Figure 5- 15: Predicted permeability together with core permeability for Well F-AH2	100
Figure 5- 16: Predicted permeability together with core permeability for Well F-AH4	102

Figure 5- 17: Example of resistivity of water from SP method.....	106
Figure 5- 18: Comparison of core and log water saturation models for well F-AH1	111
Figure 5- 19: Comparison of core and log water saturation models for well F-AH2.....	112
Figure 5- 20: Comparison of core and log water saturation models for well F-AH4.....	113
Figure 5- 21: Comparison of log water saturation over hydrocarbon zone for well F-AH4 .	114
Figure 6- 1: Multi-well Volume of Clay-Porosity plot for cut-off determination	119
Figure 6- 2: Multi-well porosity-permeability plot for cut-off determination.....	121
Figure 6- 3: Multi-well Water saturation plot for cut-off determination.....	123
Figure 6- 4: Well F-AH1 showing calculated reservoir parameters and pay flags in reservoir 1	125
Figure 6- 5: Well F-AH1 showing calculated reservoir parameters and pay flags in reservoir 2	126
Figure 6- 6: Well F-AH1 showing calculated reservoir parameters and pay flags in reservoir 3	126
Figure 6- 7: Well F-AH1 showing calculated reservoir parameters and pay flags in reservoir 4	127
Figure 6- 8: Well F-AH2 showing calculated reservoir parameters and pay flags of reservoir 1	128
Figure 6- 9: Well F-AH2 showing calculated reservoir parameters and pay flags of reservoir 2	129
Figure 6- 10: Well F-AH2 showing calculated reservoir parameters & pay flags of reservoir 3	129
Figure 6- 11: Well F-AH2 showing calculated reservoir parameters & pay flags of reservoir 4	130

Figure 6- 12: Well F-AH4 showing calculated reservoir parameters & pay flags of reservoir 1	131
Figure 6- 13: Well F-AH4 showing calculated reservoir parameters & pay flags of reservoir 2	132
Figure 6- 14: Well F-AH4 showing calculated reservoir parameters & pay flags of reservoir 3	133
Figure 6- 15: Well F-AH4 showing calculated reservoir parameters & pay flags of reservoir 4	134
Figure 6- 16: Well F-AH4 showing calculated reservoir parameters & pay flags of reservoir 5	134
Figure 6- 17: Well F-AH4 showing calculated reservoir parameters & pay flags of reservoir 6	135
Figure 6- 18: Well F-AH4 showing calculated reservoir parameters & pay flags of reservoir 7	135
Figure 6- 19: Well F-AH4 showing calculated reservoir parameters & pay flags of reservoir 8	135
Figure 6- 20: Well F-AH4 showing calculated reservoir parameters & pay flags of reservoir 8	136
Figure 6- 21: Calculated Windland r35 pore throat radius showing five different petrophysical rock types (PRT1-5) plotted on the standard Windland graph on permeability against porosity	139
Figure 6- 22: Calculated FZI used to identify different HFUs from RQI versus NPI.....	141
Figure 6- 23: Permeability versus porosity plot showing different hydraulic flow units, HFU 1-5.	141

Figure 6- 24: Plot of cumulative flow and storage capacities for wells showing five different
flow units, FU1-5..... 143



LIST OF TABLES

Table 1- 1: Well coordinates and various depths involved during drilling.....	5
Table 3- 1: Summary of the data used for the study	20
Table 3- 2: Suit of wireline depths and core intervals in each well	21
Table 4- 1: Well F-AH1 core analysis results and lithology description.....	30
Table 4- 2: Well F-AH2 core analysis results and lithology description.....	33
Table 4- 3: Well F-AH4 core analysis results and lithology description.....	37
Table 4- 4: Litho-facies description and classification of reservoir facies	41
Table 4- 5: Summary of identified lithofacies for well F-AH1	44
Table 4- 6: Summary of identified lithofacies for well F-AH2	47
Table 4- 7: Summary of identified lithofacies for well F-AH4	50
Table 4- 8: Matrix density of common lithology (Source: Schlumberger, 2013)	55
Table 4- 9: Summarised grain density statistics of Well F-AH4 core sections	57
Table 5- 1: Parameters for clay volume estimation	74
Table 5- 2: Parameters used for the calculation of effective porosity	84
Table 5- 3: Porosity-permeability functions per wells.....	97
Table 5- 4: Porosity –permeability functions per well.....	108
Table 6- 1: Summary of calculated net pay parameters for Well F-AH1	125

Table 6- 2: Summary of calculated net pay parameters for Well F-AH2	127
Table 6- 3: Summary of calculated net pay parameters for Well F-AH4	130
Table 6- 4: Results of calculated petrophysical rock types and flow zone indicators used to classify rocks into different flow zones	138
Table 6- 5: Storage and flow capacities estimated for wells	143
Table 6- 6: Qualitative XRD results showing the mineral content of different minerals	145



CHAPTER ONE

1. INTRODUCTION

1.1 BACKGROUND OF STUDY

Formation evaluation is key to a successful hydrocarbon development program. The recovery efficiency of any reservoir is influenced by its heterogeneities due to its complicated nature, in particular the distribution of permeability and porosity. To develop a reservoir model that represents the reservoir properties, there is a need to define the vertical distribution of flow behaviour and the understanding of flow units to allow the identification of preferred flow zones.

The concept of “flow units” is very essential to providing exploration geologists and reservoir engineers with the formation’s geological and physical parameters necessary for the construction of the flow zones model of the reservoir. [Ebanks, 1987](#), defined flow units according to geological properties to include texture, mineralogy, sedimentary structures, bed contacts, and the nature of permeability barriers in combination with quantitative petrophysical properties such as porosity, permeability, capillarity, and fluid saturation. According to [Opuwari et al., 2020a](#), a flow unit is an interval that is vertically and laterally continuous within the zone of the reservoir and has similar permeability and porosity characteristics that differ from those in other sections of the reservoir.

A conceptual petrophysical flow zonation scheme for the F-AH Gas Field in the northeastern Bredasdorp basin offshore South Africa was carried out using petrophysical analysis, quantitative X-ray diffraction (XRD), Scanning Electron Microscopy (SEM) and core data. One-hundred and sixty-eight (168) core porosity and permeability data were used to establish reservoir zones from the flow zone indicator (FZI) method and Winland’s methods. Storage and flow capacities were determined from the stratigraphy-modified Lorenz plot (SMLP)

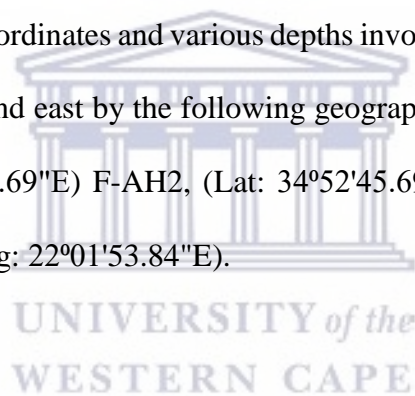
method. To understand the effects of the mineralogy on the flow zones from mineralogical composition analyses, petrography analysis was established using four (4) samples for quantitative X-ray diffraction (XRD) and Scanning Electron Microscopy (SEM) to identify and quantify the clay minerals of the sandstones. In addition, the SEM micrographs was useful to estimate the type and distribution of porosity and cement.

The study aims to carry out a formation evaluation of the sandstone reservoir zonation for the identification of flow zones. Correlation with the identified zones in the other parts of the basin in the F-AH Gas Field in the northeastern Bredasdorp basin off the coast of South Africa with the use of core data. Generate a grouping of rock units from core permeability and porosity using two graphic methods; Petrophysical Rock Type (PRT) from the Winland r35 and Flow Zone Indicator (FZI) and Stratigraphic Modified Lorenz Plot (SMLP) from mineralogy composition analyses. The objective was to make use of the available well logs (Gamma Ray, spontaneous potential, neutron, density, sonic, resistivity, caliper and conventional), sedimentological (XRD, SEM and petrological description) and core data to establish reservoir zones from the flow zone indicator (FZI) and Winland's methods and to determine storage and flow capacities from the stratigraphy modified Lorenz plot (SMLP) method. Three (3) wells viz: F-AH1, F-AH2 and F-AH4 were used for the petrophysical evaluation and analysis of the reservoir. The Petroleum Agency South Africa (PASA) provided the data used for this study and SOEKOR (Southern Oil Exploration Corporation) drilled the three wells (F-AH1, F-AH2 and F-AH4).

1.2 LOCATION OF STUDY AREA

The study area for this research is located in the northeastern Bredasdorp Basin off the coast of South Africa, approximately 79 km SSW of Mossel Bay in the F-A field. It is situated 100km offshore of Mossel Bay and it is a gas-bearing shallow marine, syn-rift reservoir discovered in

1970 and started producing gas in 1992. The reservoir is generally good with an average permeability of 100 mD and porosity of 12%. The basin is part of the five sub-basins in the Outeniqua Basin off the southern coast of South Africa and stretches for approximately 18,000 km. The Outeniqua Basin includes offshore rift and post-rift basins north of the Alguhas Falkland Fracture Zone (AFFZ) and includes four syn-rift subbasins, namely the Bredasdorp and Pletmos Drift Basins, located in the southern region of the Outeniqua Basin and the Algoa and Gamtoos that occur in the eastern region of the northern Outeniqua Basin (Brown et al., 1995). The Outeniqua Basin is bounded by Alguhas Columbine Arch on the west and St Francis Arch on the east (Brown et al., 1995). **Figures 1-1** are the well maps generated with Petrel software and Petrosa, showing the distribution of wells in this study area of the Bredasdorp Basin. **Table 1-1** shows well coordinates and various depths involved during drilling. The study area is delimited to the south and east by the following geographic coordinates: F-AH1, (Lat: 34°58'28.35"S, Long: 22°01'40.69"E) F-AH2, (Lat: 34°52'45.69"S, Long: 22°00'03.61"E) F-AH4, (Lat: 34°52'58.98"S, Long: 22°01'53.84"E).



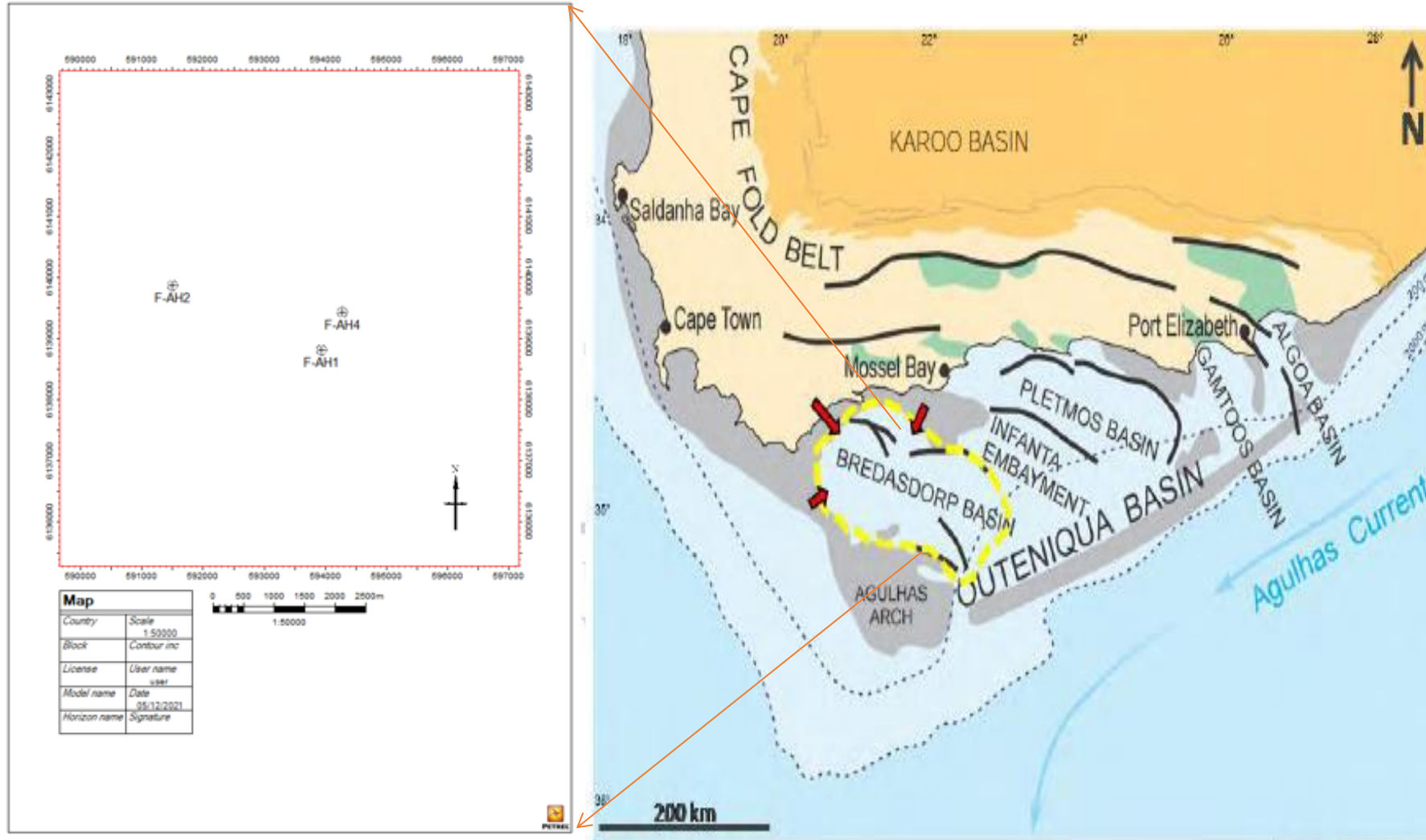
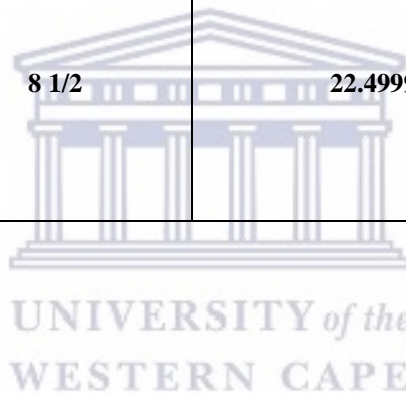


Figure 1- 1: Map showing the location of the selected wells in the Bredasdorp Basin (PASA, 2004/2005).

Table 1- 1: Well coordinates and various depths involved during drilling

<i>Well Name</i>	<i>Coordinates</i>	<i>Hole size (in)</i>	<i>Kelly Bushing to Sea level (m)</i>	<i>Total Depth Drilled (m)</i>	<i>Block</i>
<i>F-AH1</i>	Latitude: 34°58'28.35"S	8 1/2	26	2688	<i>Block 9</i>
	Longitude: 22°01'40.69"E				
<i>F-AH2</i>	Latitude: 34°52'45.69"S	8 1/2	26	2678	<i>Block 9</i>
	Longitude: 22°00'03.61"E				
<i>F-AH4</i>	Latitude: 34°52'58.98"S	8 1/2	22.49999	2670	<i>Block 9</i>
	Longitude: 22°01'53.84"E				



1.3 AIM AND OBJECTIVES

The study aims to carry out a formation evaluation of the F-AH Gas Field for the identification of flow zones and correlation with the identified zones in the other parts of the basin in the northeastern Bredasdorp Basin off the coast of South Africa with the use of core data and to generate a grouping of rock units from core permeability and porosity using two graphic methods; Petrophysical Rock Type (PRT) from the Winland r35 and Flow Zone Indicator (FZI) and Stratigraphic Modified Lorenz Plot (SMLP) from mineralogy composition analyses consisting of wells ((F-AH1, F-AH2 and F-AH4).

To achieve the stated study aim, five specific objectives are formulated as follows:

1. Delineate and identify the sandstone reservoir
2. Identify and classify lithofacies
3. Estimate petrophysical properties (shale volume, porosity, permeability, and water saturation) from wireline logs
4. Determination of cut-off and Net Pay
5. Estimate the storage and flow capacities in the flow zones



1.4 THESIS OUTLINE

This work consists of a written report of the study, divided into seven chapters

1.4.1 Chapter 1

Chapter one provides an elaborate introduction of the current study in terms of the background of the study, location of the study, study aim and objectives of the research and the outline of the study.

1.4.2 Chapter 2

Chapter two discusses the geological background of the Bredasdorp Basin which includes the regional geology, tectonostratigraphy, structural framework, depositional environment and Bredasdorp Basin petroleum system off the coast of South Africa.

1.4.3 Chapters 3

Chapter three outlines the various materials, research methodology and techniques, used to obtain results and in writing this thesis.

1.4.4 Chapter 4

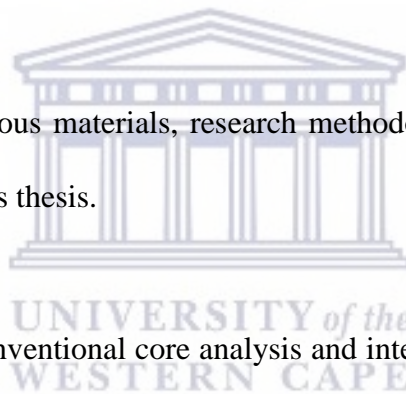
Chapter four focuses on the conventional core analysis and interpretation of the wireline logs within the cored and non-cored intervals of the studied wells.

1.4.5 Chapter 5

Chapter five describes the petrophysical model used to obtain the results of the following parameters: shale volume, porosity, permeability and water saturation determinations.

1.4.6 Chapter 6

Chapter six first discusses the cut-off and net pay determination used to attain the desired results and finally discusses the estimation of storage and flow capacities and the effect of minerals on the flow units in the northeastern Bredasdorp Basin, offshore of South Africa.



1.4.7 Chapter 7

Chapter seven provides the summary and conclusion of the study and recommendations for future work.



CHAPTER TWO

2. GEOLOGICAL BACKGROUND OF THE BREDASDORP BASIN

This chapter discusses the geological background of the Bredasdorp basin Offshore South Africa. The Bredasdorp Basin, Southwest of Mosselbay extends along the Southern Coast of South Africa at approximately 18,000 km² and the water depth is less than 200m, underneath the Indian Ocean. It is believed that this basin is essentially filled with post-divergence rocks of the Cenozoic and Cretaceous including Lower Cretaceous syn-rift and Upper Jurassic continental and marine strata (McMillan et al., 1997).

2.1 REGIONAL GEOLOGY

South Africa's offshore basin is divided into three (3) zones; the western zone, the southern zone and the eastern zone. The western zone region known as the Orange Basin includes a passive marginal basin associated with the opening of the South Atlantic during the Cretaceous, while the eastern zone region, often referred to as the Durban and Zululand Basins during the Jurassic passive margin setting was formed because of the disintegration of Africa, Madagascar and Antarctica. In the study area, during the Late Jurassic-Early Cretaceous dissolution and separation of Gondwana, the Southern Zone region was defined by the Outeniqua Basin, which is a large composite intracratonic rift basin representing strong strike-slip movement and several authors have reported that the Bredasdorp Basin in Gondwana arose due to South Atlantic movement along the Agulhas-Falkland fracture zone (**Figure 2-1**).

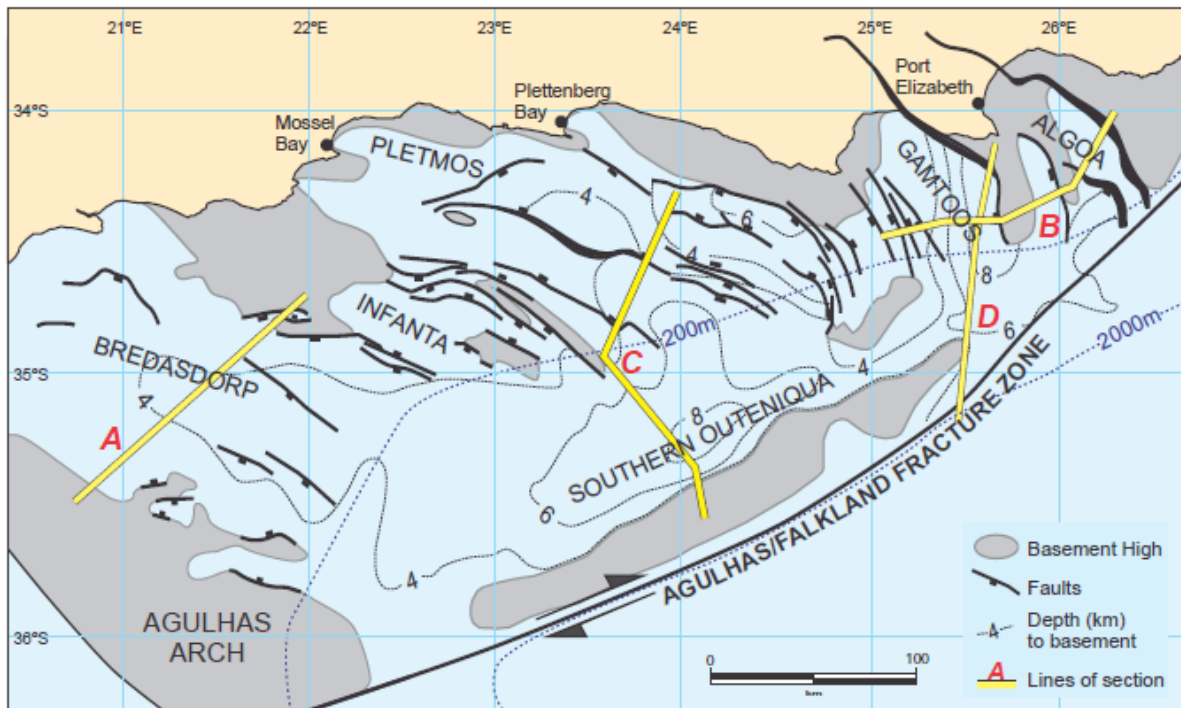


Figure 2- 1: Major tectonic elements of the Outeniqua Basin (PASA, 2012).

The Outeniqua Basin comprises several en-echelon sub-basins (i.e., Bredasdorp, Algoa, Gamtoos and Pletmos Basin), although they share a comparable history, the responses to specific events affecting these sub-basins are different in each case often distinctly different and the oldest sediments have been recovered by drilling in the Gamtoos and Algoa Basins and have been dated to the Kimmeridgian (later Jurassic) in age (McMillan et al., 1997).

The study area is approximately 200 m long and 80 km wide (Broad et al., 2006) and bounded by two arches, namely the Infanta Arch and the Columbine-Agulhas Arch (Brown et al., 1995). These arcs in the study area are elongated basement rocks composed of Cape Supergroup metasediments, granite and Precambrian metamorphic rocks.

2.2 TECTONOSTRATIGRAPHY

The tectonic elements that occurred in the Bredasdorp Basin are mainly in the form of normal faults; however, compression structures are also known to have evolved. These normal faults are typically listric in geometry and detach at common planes of decollement at greater depths (Schalkwyk, 2005).

The offshore region of South Africa can be divided into three major tectonostratigraphic zones:

- ❖ The Orange Basin, the largest offshore basin on the West Coast, lies on a broad passive margin associated with the opening of the South Atlantic during the Early Cretaceous (Petroleum Agency S A, Brochure, 2004/5).
- ❖ During the Jurassic, the breakup of Antarctica, Madagascar and Africa resulted in an eastern offshore passive margin of limited deposition and is known as the Durban and Zululand Basins (Petroleum Agency S A, Brochure, 2004/5).
- ❖ The Outeniqua Basin is a large composite intracratonic rift basin in the south offshore region showing strike-slip faulting during the Late Jurassic to Early Cretaceous split and Gondwana breakup. The Outeniqua Basin consists of five rift subbasins, east to west; Algoa, Gamtoos, Pletmos, Infanta and Bredasdorp basins, and each of these basins consists of a rift semi-graben overlain by drift sediments of varying thickness.

The Bredasdorp Basin hosts an Oxfordian-Recent stratigraphic column as shown in **Figure 2-2** (PASA, 2012). It contains no equivalent onshore and is situated between anticlinal basement highs at Cape Infant and Cape Agulhas. In the western section of the Bredasdorp Basin, two episodes of sedimentation are associated with the stratigraphy of the basin, the Syn-Rift and the Drift. Synrift and drift episodes have clearly defined the active rift tectonics and sedimentation associated with the early continental fracture period and post-rift phase of thermal subsidence (Dingle et al., 1983; Broad et al., 2006). However, geological and geophysical evidence shows that the syn-rift and drift events are less pronounced in the western

Bredasdorp Basin than, for example, in the Orange Basin ([Petroleum Agency S A, Brochure, 2008](#)).

The Bredasdorp Basin in the study area underwent two syn-rift phases recorded from the first two sequences separated by a Type 1 sequence boundary as follows: The first syn-rift phase during the Late to Mid Jurassic-early Cretaceous (157.1 Ma to 121 Ma) and the second during the Hauterivian (121.5 Ma to 117.5 Ma). It should be noted that a transition phase (117.5 Ma to 103 Ma) was documented that controlled the deposition of a low-level, progressive wedge near the edge of the shelf and the bottom and slanting fans of the basin to the deepest part of the basin. However, in this transition phase, the organic-rich shale rock with high potential as a hydrocarbon-producing parent rock was deposited. The 14At1 unconformity (produced by the onset of thermally induced sagging) indicates the onset of the drift phase in the Bredasdorp Basin.

Due to the diverse elements that contribute to the formation, the potential for deposit development in low-lying sequence swaths is favourable and these low-lying sequence swaths have been identified as relatively good-quality hydrocarbon deposits. [Broad, 2004](#), suggests that high erosion anomalies (Type 1) exhibiting incised valleys and canyons present surfaces where:

- ❖ Hilly and slab-like submarine/basin bottom fans
- ❖ Submarine channel fill and associated hills and fans
- ❖ Progressive Delta/Coastal Depressions Wedges

Fans, wedges and channel fills are sourced and sealed at the top from transgressive shales deposited during sea-level rise. Low-level system tracts are considered to consist of turbidity fans, channels and/or layers at the bottom of the basin since the Bredasdorp Basin is composed of terrigenous clastic material ([Broad, 2004](#)). Poorly defined transgressive tracts are due to shelf flooding occurring with relative sea-level rise. With the newly found shoreline, well-

defined clinoforms and extensively formed delta/coastal systems, spreading basin-ward, developed due to sea-level rise. Turbidite fans and channel fills are located in the sloping coastal sands that contain hydrocarbon deposits in the Low Stand System tract (Broad, 2004).

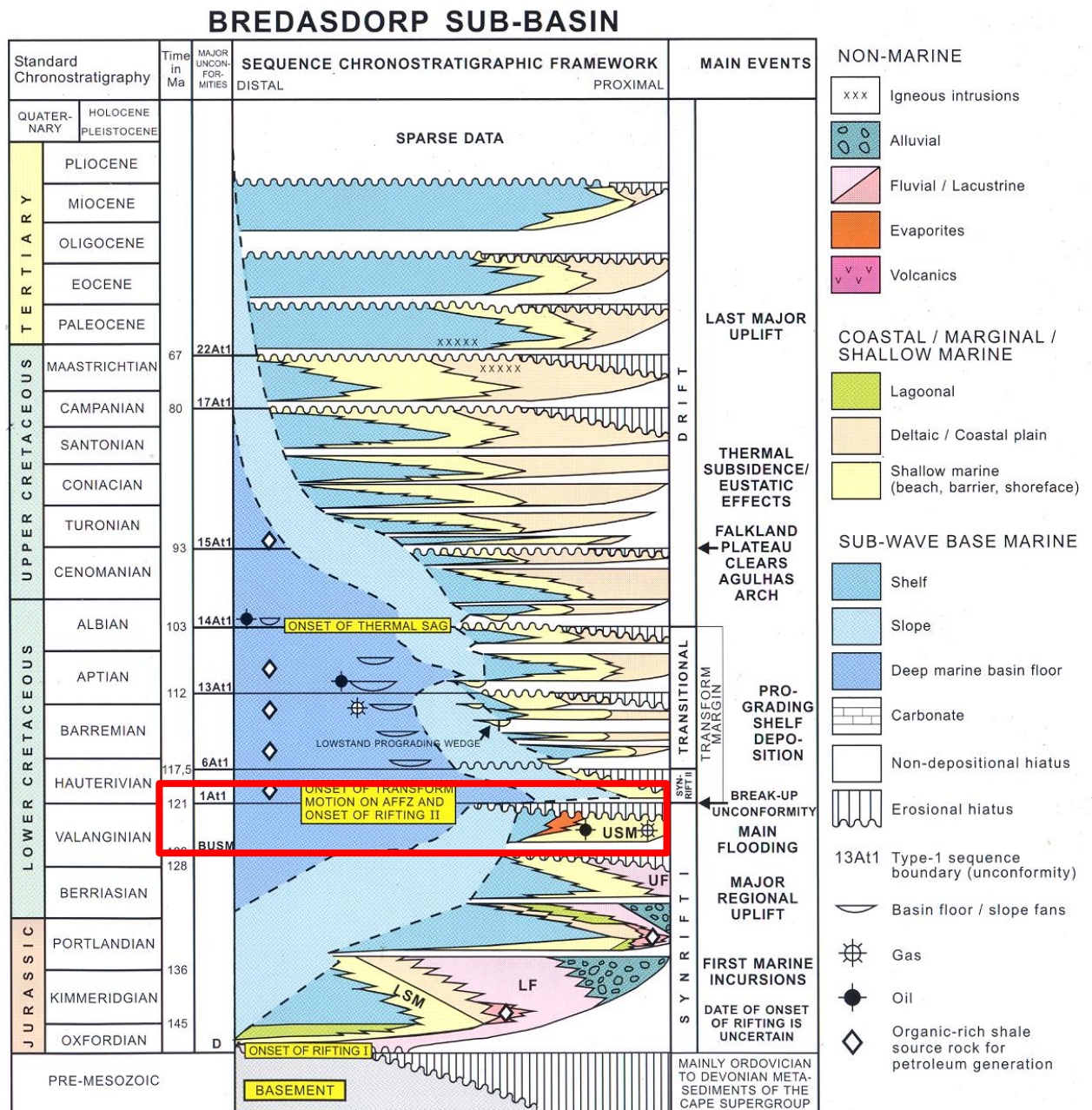


Figure 2- 2: Sequence chronostratigraphic framework of the Bredasdorp Basin (PASA, 2012)

2.3 STRUCTURAL FRAMEWORK

The Bredasdorp basin has been defined as a broad, asymmetric cross-section basement depression that can best be described as a graben structure. The western portion of the basin floor generally dips in a northwesterly direction, with the deepest extents of the basin near the northern rim (Dingle et al., 1983). He further explained that the western part of the basin does not extend on land, but breaks up into small, narrow, northwest-southeast ridges and ditches that spread to the coast connecting Cape Agulhas and Cape Infanta. The result of a major dissolution and separation of the West Gondwana supercontinent into the African and South American plates initiated and led to the existence of the South African continental margins, which further orchestrated the process that initiated the formation of the Outeniqua Basin (McMillan et al., 1990).

Broad et al., 2006 reported that major processes include extensional forces, rifting, continental separation and drifting of the constructed South African continental margin, in addition to the breaking up and drifting that occurred in the early Mesozoic and early Cretaceous respectively. It extends across the southern and eastern margins of South Africa and was formed due to the dextral (right-lateral) strike-slip movement of the African and South American tectonic plates as they slid past each other, followed by a drift of the Falkland Plateau across the African plate (Ben-Avraham et al., 1997; Broad et al., 2006). However, a number of these different dynamic processes, such as the onset of strike-slip movement of the (AFFZ) in the Early Cretaceous at the onset of drifting, led to the truncation of the pre-existing structural trends of the rift basin (i.e. Outeniqua-Bredasdorp, Pletmos and Gamtoos and Algoa basins) and the latter developed structures have been termed failed rifts because they may have opened up and evolved into mid-oceanic spreading centers that led to the formation of the South African offshore rift sub-basins. The Outeniqua Basin consists mainly of Middle Aptian to Maastrichtian deposits spreading over pre-existing rift basins and showing a transverse structural gain.

2.4 DEPOSITIONAL SETTING

The Bredasdorp Basin developed from fan deltas and stream overwhelmed to wave-dominated deltas and also coastal systems (PASA brochure 2004/2005). Slope and basin settings that evolved from the fine-grained thickness and suspended deposits into the leveed incline and basin floor turbidite fans have also been identified with the fine-grained turbidite settings. The progression is in response to second-order tectonic episodes that have produced the diversity in sediment supply rates and rates of subsidence or settlement and the expansion of untamed sea forms (PASA brochure 2004/2005). Four relatively separate sub-basins of the fault forming the Bredasdorp Basin throughout Supercycle 1-5 (126-117.5 Ma) were fed sediments by high-angle flow settings. River-dominated delta frameworks prograde southward over the northern rim of the central sub-basin (PASA Brochure 2004/2005).

The depositional sequence in the study area consists predominantly of Type 1 sequences (Brown et al., 1995) and the assessed reservoir sediments are from a shallow marine depositional environment. The sediments of the Bredasdorp Basin originate predominantly from the processes of erosion and stripping of the shallow, deep and transitional marine environments of the Cape Supergroup and Karoo Supergroups. Hence, the primary source of hydrocarbons in the basin is the deep marine shales deposited in the mid-Aptian. The Synrift shelf and drift section of deep-marine turbidite sandstone form the two main reservoirs of the basin, while the marine-origin drift shales act as the primary seals (Opuwari et al., 2022). The major anomalies bounding the assayed third-order sequences in the Bredasdorp Basin have been entered into the well logs based on data provided by PetroSA.

2.5 PETROLEUM SYSTEMS OF THE BREDASDORP BASIN

Magoon and Beaumont, 1999, defined a petroleum system as the systemic interaction of a geological configuration that could lead to the commercial accumulation of hydrocarbons. All

the different elements and processes of petroleum geology are encompassed by this unifying concept. The petroleum source rock, reservoir rock, and seals and traps represent the necessary elements for the accumulation of hydrocarbons and consist of all components of the petroleum system present in the study area.

A petroleum system was also defined by Magoon and Dow, 1994, as a geological system that includes the hydrocarbon source rocks and all associated hydrocarbon and that includes all geological elements and processes essential for the existence of a hydrocarbon accumulation (Figure 2-7). This section discusses the essential elements of the Bredasdorp Basin petroleum systems, which include petroleum source rock, reservoir rock, and seals and traps.

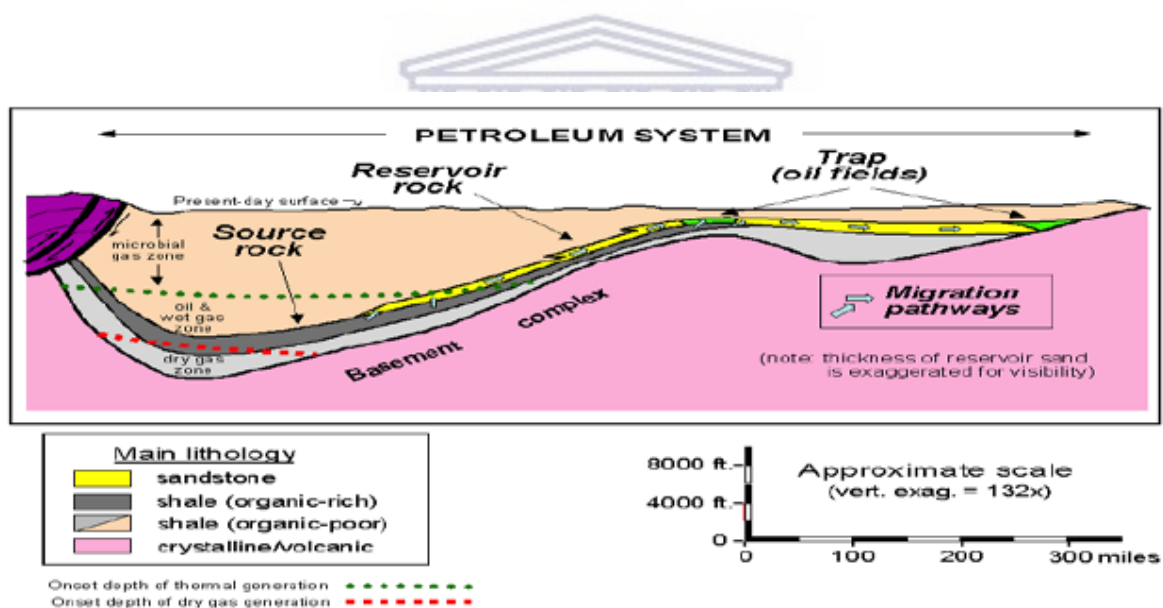


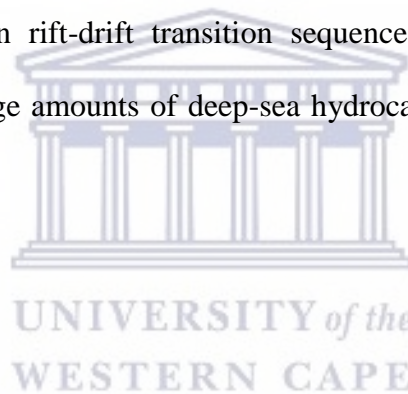
Figure 2- 3: The main elements of a petroleum system (Magoon and Dow, 1994).

2.5.1 Petroleum Source Rock

Petroleum source rock is any source rock that can produce and eject sufficient hydrocarbons to form a pool of hydrocarbon (Hunt, 1996). These source rocks are rich in hydrocarbon-susceptible organic matter and are typically shale or limestone. Source rocks are classified based on the kerogen type they contain and can be classified as hydrocarbon susceptible.

Exploration activity in the Bredasdorp Basin to date indicates that deep-sea hydrocarbon will be developed in the Rift-Drift transition sequence (lower Valanginian to mid-Aptian, 1A-13A sequences) where the 13A well (mid-Aptian) is likely to be the main source for the gas condensate fields ([Petroleum Agency SA, Brochure, 2003](#)).

The best-producing source rocks are mudrock deposits developed in the syn-rift and transitional rift-drift phases during the early Valanginian to mid-Aptian i.e. the (1A to 13A sequences) within the Bredasdorp Basin and most of the source rocks tend to be matured over large parts of the area and these hydrocarbons tend to be contained in deposits below 1A1, while the thick (more than 100 m) mudrocks of 13A contain mainly source rocks for hydrocarbon and minor sources for gas condensate fields ([PASA, 2012](#)). The Lower Valanginian to Middle Aptian rift-drift transition sequence (1A-13A sequences) of the Bredasdorp Basin contains large amounts of deep-sea hydrocarbon-susceptible source rocks ([Van Der Spuy, 2000](#)).

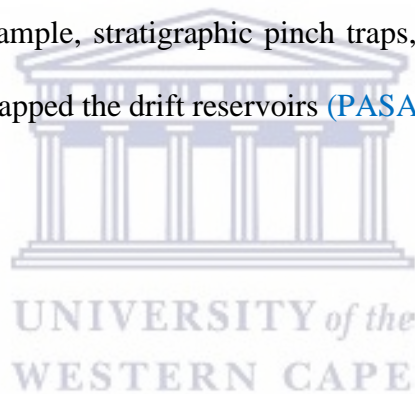


2.5.2 Reservoir Rock

Reservoir rock is a rock in which hydrocarbon accumulates under sufficient trapping conditions with appropriate porosity (space between rock grains where hydrocarbon accumulates) and permeability (the ease with which hydrocarbon can move effectively, such as mudstone or anhydrite) accumulate. [Rider, 2002](#), defined a reservoir rock as a porous and permeable rock containing interconnected pores or openings that occupy the spaces between the mineral grains of the rock. It is the type of rock that has sufficient porosity and permeability to store hydrocarbons and allow production, and most reservoir rocks worldwide are either sandstone or carbonate rocks. Shelf sandstones of the Syn-Rift section and deep-marine turbidite sandstone of the drift sections are the two types of reservoir rocks that are found in the Bredasdorp Basin ([PASA, 2012](#)).

2.5.3 Seals and Traps

Seals are rocks that hydrocarbon cannot move through effectively (such as mudstone or anhydrite). It is any rock with relatively low permeability, preventing liquids from migrating beyond the reservoir, and rock that prevents leakage from the trap. A trap is a structural and stratigraphic configuration that concentrates hydrocarbon in aggregation, and it is a 3-D configuration that “pools” the hydrocarbon. The seals of the Bredasdorp Basin originate from the marine shale of the drift phases and these marine shales function as the main seals within the basin. However, syn-rift seals are present but only occur as non-connecting tilted faults or as mud deposits in marine or lagoon environments (Williams, 2014). Both truncational and structural traps are available within the shallow sea up to the fluvial syn-rift reservoir, while different types of traps, for example, stratigraphic pinch traps, reversal-related closures and compactional traps anticlines trapped the drift reservoirs (PASA Brochure, 2004/2005).



CHAPTER THREE

3. MATERIALS AND RESEARCH METHODOLOGY

This chapter outlines various techniques, materials and research methodologies used for the research project.

3.1 INTRODUCTION

Data and well logs were provided by the Petroleum Agency of South Africa (PASA). Porosity and permeability measurements from nine (9) core samples of the three (3) exploration wells (3 samples from F-AH1, 2 samples from F-AH2 and 4 samples from F-AH4) in the northeastern Bredasdorp Basin, Offshore of South Africa were also provided by PASA. Data processing commenced with the creation of the database and the implementation of quality control on the data. The dataset was loaded into the Interactive Petrophysics (IP 4.7) © 2021 and the well logs were used to identify the reservoir intervals and lithology. The well log-core measurements shift was performed, followed by the crushing and milling of the 9 core samples for Wells F-AH1, F-AH2, and F-AH4. Well logs correlation and delineation of reservoir sand units along with reservoir studies using reports, X-Ray Diffraction (XRD) and Scanning Electron Microscopy (SEM) were performed to characterise the reservoir quality and improve the delineation of the sandstone reservoir. Interactive Petrophysics (IP 4.7) © 2021, Schlumberger Petrel software © 2015 and Sedlog software program was used to generate results.

In this study, a suit of composite Well logs from Wells F-AH1, F-AH2, and F-AH4 respectively, obtained from Schlumberger Service Company and provided by the Petroleum Agency South Africa (PASA) were used for this study and the datasets containing digital wireline logs (LAS Format), conventional core analysis report, special core analysis reports, Petrographic appraisal report, geological well completion reports, well completion reports and

core photographs. The geophysical wireline logs consist of Gamma-ray (GR), Spontaneous Potential (SP) Neutron (NPHI), Density (RHOB), Resistivity (ILD/MSFL), Sonic (DT) and Caliper (CL). These logs were used to analyze and evaluate the petrophysical properties such as porosity and permeability etc. The Interactive Petrophysics (IP 4.7) ® 2021 workstation was used to display the log curves, interpretation, modeling and analyses of the available digitalized wireline logs (LAS Format) data, the Schlumberger Petrel software ® 2015 was used specifically for well location map and well correlation and the Sedlog software program was used to create graphic sediment logs.

The datasets used for this study are summarized in **Table 3-1** including Gamma Ray well log, core analysis (porosity and permeability), and sedimentology data (reports, SEM and XRD analyses), which are available for the studied wells (F-AH1, F-AH2, and F-AH4) of the northeastern Bredasdorp Basin Offshore of South Africa.

Table 3- 1: Summary of the data used for the study

<i>Well Name</i>	<i>Conventional Logs</i>	<i>Conventional Core Report</i>	<i>Special Core Analysis</i>	<i>Petrography</i>	<i>Core Photographs</i>	<i>Completion Report</i>
<i>F-AH1</i>	✓		✓		✓	✓
<i>F-AH2</i>	✓	✓	✓		✓	✓
<i>F-AH4</i>	✓		✓	✓	✓	✓

3.2 WIRELINE DEPTHS AND CORE INTERVALS FOR WELLS

The basic wireline suites from a series of wireline logging suites were run downhole for each well and recorded in log-ASCII format (LAS) which recorded measurements of depth, Gamma Rays, spontaneous potential, resistivity, calipers, neutrons, density and sonic logs. The logs

were loaded into the Interactive Petrophysics (IP 4.7) © 2021 Workstation and data such as core permeability and porosity values were extracted from printed reports. **Table 3-2** shows the suit of wireline depths and core intervals in each well.

Table 3- 2: Suit of wireline depths and core intervals in each well

<i>Well</i>		<i>F-AH1</i>	<i>F-AH2</i>	<i>F-AH4</i>
<i>Drilling</i>	Depth Planned (m)		2766	2750
	Depth reached (m)	2688	2915	2670
	Water depth (m)	106	105	107
<i>Wireline</i>	Start depth (m)	1600	1585	1400
	End depth (m)	2687	2677	2650
	Logging Service	Gearhart Geodata	Gearhart Geodata	Halliburton
<i>Core Interval</i>		C1 to C4 (2415.1- 2443.3m)	C1 to C6 (2368.2- 2436.8m)	C1 to C5 (2369.2- 2428.2m)

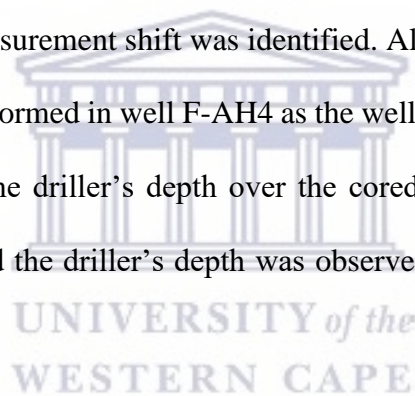
3.3 LOG EDITING

Log editing is a form of log interpretation, usually aimed at correcting or eliminating the problem affecting the logging environment, such as the type of drilling mud and the salinity of the mud to get the actual log's response and to give in-situ properties recorded and measured by the logs. Well-log data is the result of the physical measurement of subsurface properties obtained within the confined spaces of a well (Jarvis, 2006). However, well log data requires some time to clean up the error associated logs through editing, normalization, correction and interpretation to obtain consistent and accurate logs from well to well before they can be used

for the formation evaluation study. In this study, log editing such as environment corrections and normalization was performed on the selected well log data.

3.3.1 Depth Shifting/Matching

During quantitative interpretation, one of the problems encountered by logs that need to be edited before use is depth shifting/matching. When performing a depth shifting/matching, the available log curves are usually placed side-by-side for comparison purposes with the Gamma Ray log as the reference log curve that forms the basis of a depth shifting/matching relative to the other relevant curves. In this study, the Interactive Petrophysics (IP 4.7) © 2021 software (made available by Earth Science, University of the Western Cape) was used to create a database and well log-core measurement shift was identified. All the datasets were loaded and a well-core depth shift was performed in well F-AH4 as the well logs indicate that the logger's depth is 2.45 m deeper than the driller's depth over the cored interval. Moreover, a match between the logger's depth and the driller's depth was observed in wells F-AH1 and F-AH2 respectively.



3.4 RESEARCH METHODOLOGY

The flow chart (**Figure 3-1**) shows the summary of the research methodology used for this research which begins with the data collection and ends with thesis writing and submission.

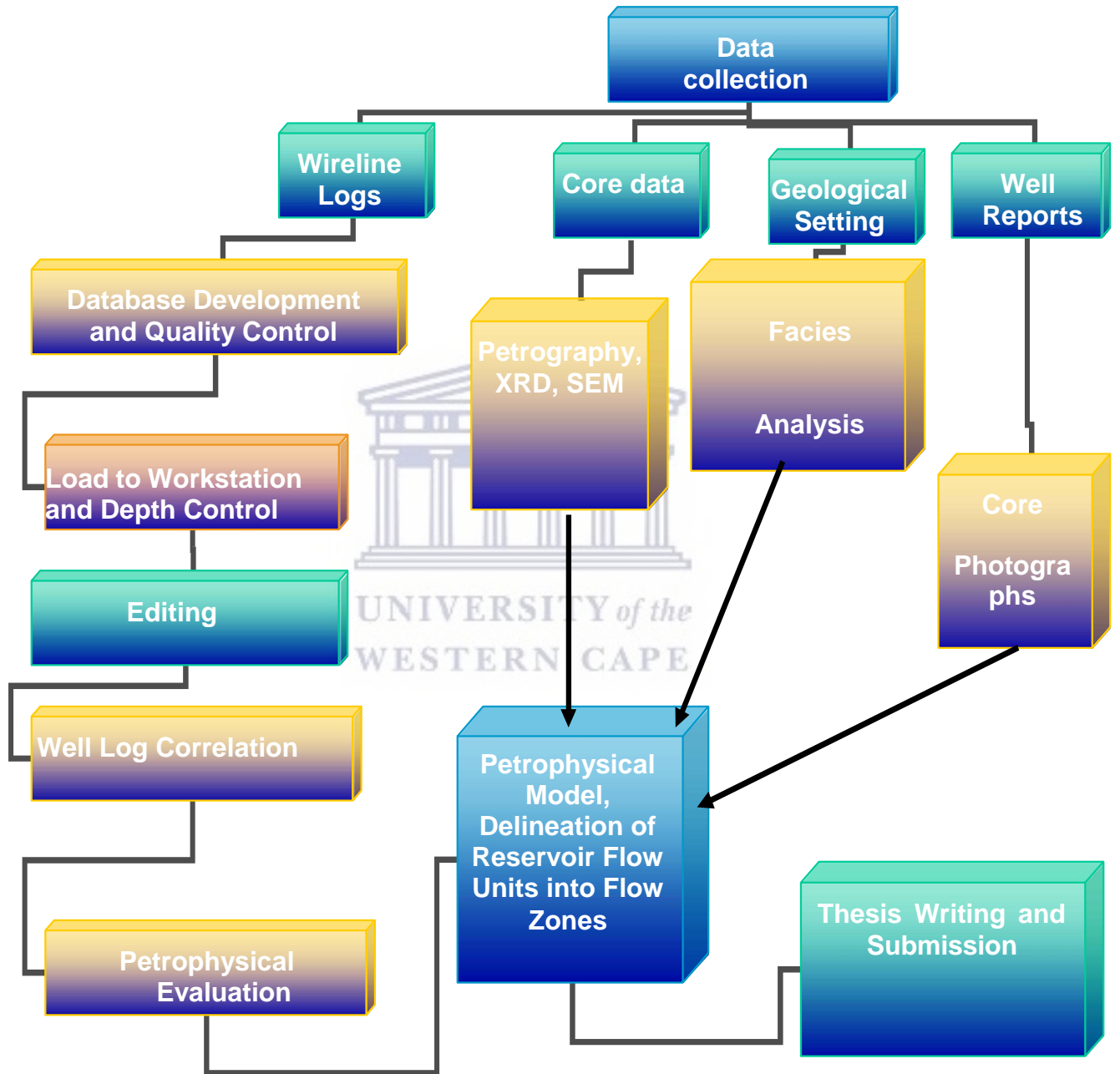


Figure 3- 1: Flow chart of the research methodology

The petrophysical parameters such as effective porosity (ϕ), water saturation (S_w), formation resistivity (R_w), hydrocarbon saturation (S_o) and true resistivity (R_t) are all evaluated using well log data

3.5 WIRELINE LOGS

3.5.1 Gamma Ray (GR) Log

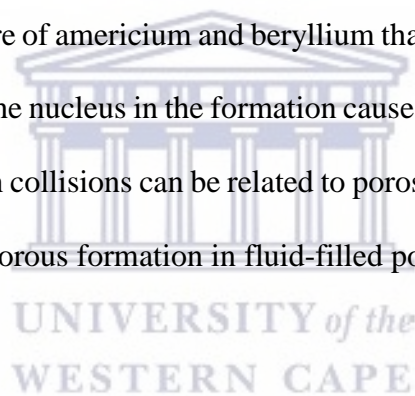
The Gamma Ray log is a measure of the production of natural radioactivity. The three radioactive series found on the earth's crust produced by the emission of Gamma Ray includes Uranium-series, Thorium series and potassium (K_{40}) series and these emissions that pass through rock are slowed down and absorbed at a rate that depends on the formation (Rider, 2002). Since shale is more radioactive than sands or shale, Gamma Ray log can be used to calculate the volume of clay in the porous reservoirs and can also be used for correlating zones and identifying lithologies. Moreover, in shale formations, the response of Gamma Ray logs increases due to the high concentration of radioactive materials in the shale formations and a shale-free formation may also have a high Gamma Ray response if the formation contains potassium feldspar, glauconite, uranium-rich water, and mica because these minerals have high radioactive concentrations. The units for Gamma Ray are API.

3.5.2 Spontaneous Potential (SP) Log

The Spontaneous Potential log is a measurement of very small electrical voltages resulting from electrical currents in the borehole caused by the differences between the salinities of the formation water and the drilling mud filtrate. The voltage changes are measured by a downhole electrode relative to the ground surface. They are naturally occurring potentials within the earth. The reading of the SP curve depends on the salinity in the liquid. If the salinity of the formation water is higher than the salinity of the mud filtrate, the deflection occurs to the left, in the opposite case, the deflection occurs to the right.

3.5.3 Neutron (NPHI) Log

Neutron logs are porosity logs that measure the concentration of hydrogen ions in a formation and the response of the neutron log is controlled by various things like the difference in detector types, the distance between source and detector, and finally by lithology, sandstone, limestone or dolomite (Rider, 2002). The two types of neutron log tools include the sidewall neutron log which is a neutron device that has both the source and detector in a pad that is pushed against the borehole wall and the compensated neutron log, which has one neutron source and two detectors. These two types of neutron log tools can be recorded in sandstone, dolomite and limestone units but the compensated neutron log is the most preferred because it is less affected by borehole irregularities. The chemical source in the neutron log produces neutrons and this chemical source can be a mixture of americium and beryllium that continuously emits neutrons. The collision of neutrons with the nucleus in the formation causes some neutrons to lose energy and the amount of energy lost in collisions can be related to porosity since in porous formations hydrogen is concentrated in a porous formation in fluid-filled pores (Rider, 2002).



3.5.4 Density (RHOB) Log

The density log is a porosity log that measures the electron density of the formation and the formation density logging tool is a contact tool that consists of a medium gamma-ray source that emits Gamma Rays into a formation (Serra, 1984). The Gamma Ray emissions collide with the electrons in the formations, resulting in a loss of energy from the Gamma Ray particles and the number of electrons in formations (electron density) is directly proportional to the number of Compton scattering collisions. The density log is easily affected by borehole invasion. Gas affects density logs significantly, unlike hydrocarbon and when formation invasion is shallow, the low density of the formation's hydrocarbons increases density porosity.

According to Schlumberger, 1972, the density log can be used to detect gas-bearing zones, identify evaporate minerals, determine hydrocarbon density and evaluate shaly sand reservoirs and complex lithologies. The units used for the measurement of the density of the formation are in gm/cc.

3.5.5 Resistivity (LLD/ILD/MSFL) Log

Resistivity is the measurement of resistance and the inverse of resistivity is conductivity.

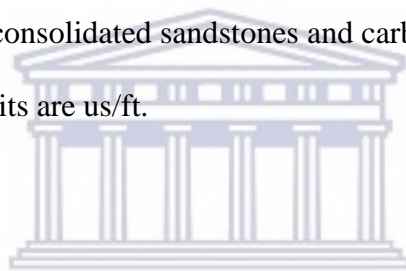
The main application of the resistivity log is to detect hydrocarbons within a reservoir. It can also be used to estimate porosity and aquiferous zones as borehole fluids (water, hydrocarbon) enter porous and permeable zones around the well during drilling. Hydrocarbons, rock and freshwater all act as insulators in the log interpretation and are non-conductive and therefore have lower resistivity. The resistivity is very important for calculating water saturation.

Today, two types of logs measure formation resistivity, an induction log and an electrode log. The former is the most common logging tool (Atlas, 1975) and there are two types of induction devices which include the induction electrode log and the dual induction focused log and the second one is the electrode device. Downhole, the electrodes are connected to the power source, which allows the current to flow from the electrons, which flow through the borehole fluids into the formation.

Electrode resistivity logs include normal, lateral, latero-log, micro-log, microlatero-log and spherically focused logs, and these logs are used in a borehole filled with salt-saturated drilling muds to obtain a more accurate value of the true resistivity of the formation. Also, Induction tools are made up of one or more transmitter coils that emit a high-frequency alternating current at a constant intensity and should be used in non-saline drilling mud to provide an accurate reading of the true resistivity of the formation. The unit for resistivity is ohm-m.

3.5.6 Sonic (DT) Log

The sonic log is a porosity log that measures the interval travel time of a compressional sound wave propagating through a foot of the formation and it depends on lithology and porosity. A reliable value of formation porosity could be extracted from the sonic log if the lithology is known. The sonic device is made up of one or more sound transmitters (sound source) and two or more receivers and the latest sonic logs are Compensated Borehole Device (BHC). The BHC tool has two transmitters and four receivers arranged in two dual receiver sets. These tools are often preferred because they reduce borehole irregularities (Kobesh and Blizard, 1959) and errors caused by sonic tool tilting (Schlumberger, 1972). The sonic velocity can be determined from a chart or using the formula (Wyllie, et al., 1958) and this formula can only be used to determine acoustic porosity in consolidated sandstones and carbonates with intercrystalline or intergranular porosities. The units are us/ft.



3.5.7 Caliper Log (CL)

The caliper logs measure the recently drilled borehole diameter (shape and size) and the measured well size can be used to correct other logs, predict well volume for cementing and also gives an indication of the state of the lithology such as washouts of formation properties (Schroeder, 2004). Within Interactive Petrophysics or related software, the caliper log run is typically displayed within track one and may vary from 6" to 16" depending on the condition of the borehole (i.e. strength of the surrounding formations). The units are inches or cm.

CHAPTER FOUR

4. CONVENTIONAL CORE ANALYSIS AND INTERPRETATION OF WIRELINE LOGS

This chapter focuses on the conventional core analysis and interpretation of the wireline logs within the cored and non-cored intervals of the studied wells.

4.1 INTRODUCTION

Coring is one way to get more detailed samples of a formation, where the formation sample is drilled out utilizing a special bit. According to [Rider, 2002](#), the core sample results are unequivocal. The various ways of obtaining core while drilling includes coring bits systems, wireline side well coring systems, conventional coring systems and special coring systems. The objective of carrying out core analysis is to bring samples of formation and its pore fluids to the surface in an altered state for analysis and to offer information for the advancement of more production of hydrocarbon efficiency via petrophysical and engineering information. The analysis may aim to determine the following: porosity, permeability, correlation, relative permeability, fluid saturation, grain size distribution, etc. The analysis is usually carried out on the core plugs, samples that are taken from the bulk core.

4.2 CONVENTIONAL CORE ANALYSIS

The conventional core analysis was carried out in the petrophysical laboratory on the reservoir rock to measure the following petrophysical properties as permeability, porosity and grain density. This analysis is often performed on homogeneous formations such as sandstones, carbonates, and shaly sand formations at approximately three to four inches from each foot of the core ([Opuwari, 2010](#)). Conventional core analysis reports and well completion reports represent the core data and this analysis was performed on the three (3) wells (F-AH1, F-AH2 and F-AH4) for which core data was available and used for this study.

4.2.1 Intervals Cored

The conventional core analysis results from wells (F-AH1, F-AH2 and F-AH4) used for calibration in this study were obtained from the conventional core report provided by the Petroleum Agency of South Africa (PASA).


4.2.1.1 Well F-AH1

Four (4) cores approximately 3 inches in diameter were cut back-to-back in well F-AH1 and used primarily to evaluate the deposit sands. Core 1 and 2 (2,415-2,433 m and 2,433-2,451 m) fall on the interval of interest and intersected the shallow marine sandstone complex bearing gas from 2,412-2,439 m and hydrocarbon-bearing from 2,439-2,450 m. Cores 1 and 2 consist mainly of fine to medium-grain sandstone. Average core porosity ranges from 9% to 14% but tends to decrease with depth towards the bottom of the core. The permeability values recorded by the core fluctuate erratically between 252 mD and 1 mD at certain locations. Core 2 recorded sandstone with hydrocarbon fluorescence and stains. Cores 3 and 4 (2451-2469 m and 2469-2479 m) intersected an underlying river section containing sandstone with minor siltstone and mud. The upper section of Core 3 begins with a very fine to fine-grained, low permeability dense sandstone, followed by siltstone and mud towards the end of Core 4.

Table 4-1 shows the routine core analysis results for well F-AH1. Core 4 from well F-AH1 was analyzed for a lithology description since the report of conventional core analysis data was not available. K=Permeability, K_{air}= Air permeability, S_w=Water saturation, S_o=Oil saturation, S_g=Gas saturation.

Table 4- 1: Well F-AH1 core analysis results and lithology description

Core	Depth (m)	Porosity (%)	K (mD)	Kair (mD)	Sw	So	Sg	Lithology description
1	2415.1	6.4	3.9	5.2	20	0	80	Massive interval of sandstone. Predominantly medium to fine-grained, clean, grey-white colour, noncalcareous. Lithoclasts in places. Rounded conglomerate towards base of core 1
	2416.61	7.5	27	32	11	0	89	
	2417.82	0.4	0.04	0.063	75	0	25	
	2418.46	5.7	6.1	8	16	0	84	
	2419.86	5.9	14	17	21	0	79	
	2421	6.7	15	19	18	0	82	
	2422.91	3.3	1.2	1.7	16	0	84	
	2424	9.2	66	76	21	0	79	
	2425.2	8.4	35	41	23	0	77	
	2426.04	11.4	160	180	31	0	69	
	2427.03	11.7	232	252	41	0	59	
	2429.47	2.6	0.17	0.28	32	0	68	
	2430.51	6.2	31	37	21	0	79	
	2431.35	2.7	4.7	6.2	42	0	58	
2432.27	8.2	58	67	17	0	83		
2	2433.92	8	17	21	37	0	63	Sandstone. Porous, clean, white-grey, coarse-very coarse in places. Calcite and shell fragments in places. Increased mud influence (green-grey) toward the bottom of the core
	2435	6.7	12	15	41	0	59	
	2435.72	6.9	6	7.8	38	0	62	
	2437	5.4	132	147	36	0	64	
	2438	7.7	121	135	33	19	48	
	2439	8.8	143	159	31	18	51	
	2440.51	6.3	24	29	31	17	52	
	2442	9.3	126	141	29	19	52	
	2449.34	7.1	10	13	48	0	46	

								2.
3	2452.2	6.6	0.19	0.3	57	0	43	Tight sandstone, grey-white, f-m, coarse in places. Green and red mudstones dominate toward the bottom of the core
	2458.5	2	0.07	0.11	76	0	24	
	2459.49	4.1	0.13	0.21	61	0	39	
	2460.52	3.9	0.03	0.05	77	0	23	
4	2470	 <p>N/A</p>						Alternating green silty mudstone (grey-green, argillaceous) and red mudstone (non calcareous) with porous, tight, medium-fine grained, calcareous, light green-grey sandstone containing green mudstone lithoclasts
	2471							
	2472							
	2472.41							
	2472.66							
	2472.82							
	2473							
	2473.3							
	2473.48							
	2473.57							
	2473.7							
2474								

In well F-AH2, six (6) cores (2368-2459 m) were cut back-to-back and were approximately 3 inches in diameter and the six cores were cut primarily to evaluate drilling break and gas resources. Shallow marine sandstones were intersected at a depth of 2368 m to 2445 m that were predominantly fine to medium-grained, although at a depth of 2424 to 2431 m they were coarse to pebbly. A river section was intersected at a depth of 2445 m and consisted mainly of green and interbedded red mudstone with minor siltstone and sandstone below a depth of 2458 m. Within this interval, the sandstones had an average core porosity and permeability of 9.6 percent and 3.4 mD respectively. Permeability, although variable, has generally been accepted as good between 50 and 100 mD. A value of 1388 mD was recorded near the top of the sequence and porosities ranged from 6.5 to 21.5% but averaged about 13%.

Table 4-2 shows the routine core analysis results for well F-AH2. K=Permeability, K_{air} = Air permeability, S_w =Water saturation, S_o =Oil saturation, S_g =Gas saturation.

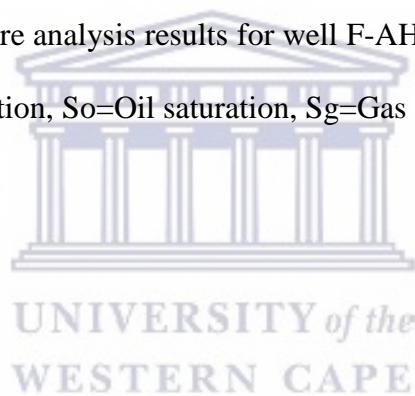


Table 4- 2: Well F-AH2 core analysis results and lithology description

Core	Depth (m)	Porosity (%)	K (mD)	Kair (mD)	Sw	So	Sg	Lithology description
1	2368.62	16	447	507	40	0	60	Fine-med grained sst, non calcareous, with minor siltstone (dark grey, argillaceous, non-calc) bands in places. Becomes coarse grey sst toward the base of core 1
	2369.8	16	497	527	39	0	61	
	2370.69	15	473	503	38	0	62	
	2371.59	9.4	1.3	1.09	48	0	52	
	2372.52	7.7	77	88	39	0	61	
	2373.13	15	491	521				
2	2378.6	14.7	373	403	33	0	67	Med grained grey sst (tight, porous, non- calcareous), coarse in places. Alternates between medium and fine-grained sst toward base of Core 2
	2379.16	10.3	37	44	40	0	60	
	2380.92	6.5	0.69	1.02	35	0	65	
	2381.45	10.7	155	175	23	0	77	
	2382.45	8.8	20	24	43	0	57	
	2383.33	11.4	28	28	42	0	58	
	2384.69	17.2	91	103	40	0	60	
	2386.3	9.4	10	4	41	0	59	
	2387.97	12.6	69	78	39	0	61	
	2388.71	15.5	27	32	42	0	58	
	2390.11	15.8	376	406	43	0	57	
	2390.38	12.3	63	73	43	0	57	
	2391.95	12.1	147	163	33	0	67	
	2392.57	14.8	290	320	41	0	59	
	2393.27	14.1	166	186	43	0	57	
	2395.69	10.6	15	19	45	0	55	
2396.36	6.9	4.5	6	46	0	54		
	2397.09	12.5	24	29	42	0	58	
	2398.43	15.3	254	274	36	0	64	
	2399.47	13	45	53	46	0	54	
	2400.35	14.5	35	42	45	0	55	

3	2401.52	14.2	75	86	45	0	55	Med to fine-grained sst (grey, sorted, rounded, non-calc, argillaceous in places). Becomes intercalated fine sst with silt (argillaceous, non-calc, carbonaceous), and mudstone (non calc, fissile in places, carbonaceous) toward the base of core 3, ending off with coarse sst (medium-grained in places, grey, angular to round fragments, argillaceous in places, silt streaks, mudstone clasts
	2402.54	12.4	20	24	48	0	52	
	2403.44	11.4	20	24	45	0	55	
	2404.4	9	1.0	1.5	54	0	46	
	2406.6	11	3.3	4.4	14	0	86	
	2407.33	14.7	154	170	45	0	55	
	2408.24	9.2	1.3	1.8	42	0	58	
	2409.35	7.7	6.3	8.2	43	0	57	
	2411.23	11.5	47	55	35	0	65	
	2411.76	14.1	139	154	39	0	61	
	2412.91	9.6	30	36	60	0	40	
	2413.39	12.3	31	37	43	0	57	
	2417.05	10.9	26	31	45	0	55	
	2417.89	11.7	12	15	40	0	60	
	2418.85	14.1	163	183	36	0	64	
2419.94	12.1	53	62	40	0	60		
2421.07	14.3	81	92	41	0	59		
2422.16	11.6	73	83	44	0	56		
5	2423.28	9.4	2.9	3.9	46	0	54	Predominantly medium-grained, grey, pebbly sst with mudstone clasts and drapes in places. Becomes silt and clay dominated (non calc) toward the centre of the core and ends with
	2424.18	14.7	35	41	39	0	61	
	2425.19	11.3	11	14	39	0	61	
	2425.95	13.5	325	355	40	0	60	
	2427.06	14.6	35	41	34	0	66	
	2428.04	11.6	23	28	41	0	59	
	2429.31	13	58	67	38	0	62	
	2430.03	8.7	1.6	2.3	35	0	65	
	2430.84	10.6	81	92	39	0	61	
	2431.89	11.4	166	186	35	0	65	
	2433.15	7.7	2.3	3.2	32	0	68	
	2434.35	9.5	32	38	35	0	65	
2435.06	8.3	1.1	1.6	34	0	66		

	2435.9	10.4	11	14	50	0	50	medium grey sst (coarse in places), non- calc.
	2436.82	15.5	2.7	2.9	37	12	51	
	2437.62	14.4	63	73	35	15	50	
	2439.95	9	5	6.6	46	14	40	
	2441.15	10.4	11	14	44	13	43	
6	2441.41	7.5	4.4	5.9	48	14	38	Predominantly medium-grained sst (light green-grey colour, sorted, non-calc in places) with conglomerate matric in places. Becomes intercalated, red and green mudstone (non calc, silty in places) towards centre of core and ends off with medium-grained grey sst (silty in places)
	2442.4	8.4	8.6	11	56	7	37	
	2443.33	10.3	13	16	48	0	52	
	2444.31	14.3	17	21	65	0	35	
	2445.66	13.3	58	45	72	0	28	
	2459.35	9.6	2.5	3.4	54	0	46	

4.2.1.2 WELL F-AH4

Five (5) cores were delineated back-to-back in well F-AH4 (2367 m to 2442 m) and are approximately 3 inches in diameter in massive, relatively clean, porous and intermittently conglomeritic sandstone. Unfortunately, cores 1 and 2 were missing or unavailable for core analysis and information on these specific cores was obtained from previous conventional core reports. Core 1 intersected a massive and probable gas-bearing shallow marine sandstone sequence, and core 2 was also intersected within the shallow marine sandstone sequence but occasionally contained smaller (centimetre-sized) interstitial siltstones. Core 3 intersected with

similar lithology as core 2 but contained a distinct conglomerate horizon and core 4 intersected a massive sandstone sequence similar to that of core 1. Core 5 is believed to have been encountered in embedded marine sandstone and conglomerate overlying a thickened mudstone unit. This was further underlain by a thick layer of sandstone with red and green river mudstones. **Table 4-3** shows the routine core analysis results for well F-AH4. K=Permeability, Kair= Air permeability, Sw=Water saturation, So= Oil saturation, Sg=Gas saturation.



Table 4- 3: Well F-AH4 core analysis results and lithology description

Core	Depth (m)	Porosity (%)	K (mD)	Kair (mD)	Sw	So	Sg	Lithology description
1.	2367.05	20.3	2766.929	2843.186	47	0	53	N/A
	2368.08	17	1141.703	1156.636	39	0	61	
	2371.78	18.7	1067.964	1084.269	42	0	58	
	2372.81	12.8	221.239	221.713	42	0	58	
	2374.68	9.4	3.067	3.453	38	0	62	
	2375.67	10.1	0.362	0.594	50	0	50	
	2376.68	14.7	48.541	51.438	43	0	57	
	2377.66	12.8	51.988	54.068	51	0	49	
	2378.61	12.9	73.969	76.107	48	0	52	
	2379.64	15.3	70.847	74.233	50	0	50	
	2380.61	10.1	4.57	5.303	52	0	48	
	2381.61	15.1	150.168	152.79	50	0	50	
	2382.57	12.3	5.227	6.235	50	0	50	
	2383.63	13.5	23.096	25.226	47	0	53	
2384.63	7	0.084	0.162	33	0	67		
2	2385.62	17.9	814.791	827.3	43	0	57	
	2386.61	16.1	392.403	393.385	50	0	50	
	2387.59	14.3	97.052	99.919	51	0	49	
	2388.58	16.1	498.448	500.622	46	0	54	
	2389.58	18.8	774.924	781.058	50	0	50	
	2390.58	12	12.09	13.114	52	0	48	
	2391.56	12.7	4.367	5.236	45	0	55	
	2392.53	12.2	2.729	3.389	70	0	30	
	2393.53	13.8	34.708	36.932	48	0	52	
	2394.52	16.6	163.247	166.173	50	0	50	
	2395.56	13	43.215	45.014	53	0	47	
	2396.6	15.5	92.504	95.387	51	0	49	
	2397.59	11	3.846	4.54	47	0	53	
	2398.61	9.2	3.387	3.964	51	0	49	
	2399.65	17	258.561	261.766	47	0	53	
	2400.65	13.3	5.631	6.668	44	6	50	
2401.65	10.2	1.156	1.507	38	0	62		

	2402.77	11	0.77	1.079	50	0	50	
3	2403.43	10.2	11.843	12.804	47	0	53	Medium grained sst (with minor cross laminations and mud drapes) becoming fine and silty in places. Core becomes coarser- grained sst (silty mud drapes, quartz pebbles, and shell fragments) with conglomerate (matrix supported, calcareous, well rounded quartz pebbles, shell debris, some scouring) in places toward the base
	2404.76	16.6	446.929	447.412	57	0	43	
	2405.86	14.6	263.201	264.163	50	0	50	
	2406.89	13.2	57.115	59.398	56	0	44	
	2407.74	10.5	18.335	19.401	49	0	51	
	2408.76	13.5	99.985	101.809	50	0	50	
	2409.73	13.1	147.289	148.374	39	0	61	
	2410.71	11.8	48.71	50.331	51	0	49	
	2411.76	10.8	0.766	1.069	50	0	50	
	2412.72	16.6	610.851	614.495	52	0	48	
	2413.72	14.1	361.656	361.755	46	0	54	
	2414.75	14.6	202.211	204.177	49	0	51	
	2415.74	9.2	12.418	13.358	50	0	50	
	2416.74	9.4	8.241	9.045	52	0	48	
	2417.73	13.2	297.21	928.201	46	0	54	
2418.73	14.9	679.651	685.683	39	0	61		
2419.75	12.4	298.934	300.956	33	0	67		
2420.75	16	985.714	987.754	48	0	52		
4	2421.78	13.9	384	386	43	0	57	predominantly medium coarse grained sst (rounded pebbles in places, streaks of calcite cementation, cross bedding, shell fragments throughout)
	2422.78	14.9	842	851	44	0	56	
5	2424.43	11.9	45.53	47.26	39	0	61	Alternating medium grained sst (poor sorting, glauconite, mudstone rip-up clasts, often
	2425.58	6.1	0.07	0.15	45	0	55	
	2428.46	12.4	9.05	10.08	35	8	57	
	2429.73	14.6	5.56	6.95	53	0	47	
	2430.46	12.4	9.81	11.09	40	13	47	
	2431.21	6.6	0.2	0.34	37	0	63	
	2431.49	3.4	0	0.02	65	0	35	

	2432.51	12	0.3	0.52	66	0	34	calcareous) and conglomerate (matrix supported, rounded quart pebbles, shale, shell fragments) toward top half of the core. Core becomes medium to fine grained sst (noncalcareous, horizontal laminations) with olive green mudstone (slightly silty, calcareous concretions) toward base.
	2433.51	7.6	0.01	0.04	80	0	20	
	2434.68	12	0.3	0.53	65	0	35	
	2435.68	11.4	0.52	0.81	65	0	35	
	2436.67	13.5	1.27	1.77	67	0	33	
	2437.66	11.5	0.34	0.58	66	0	34	
	2438.67	6.7	0.13	0.23	59	0	41	
	2439.66	8.3	0.01	0.02	72	0	28	



4.3 CORE-LOG DEPTH MATCH


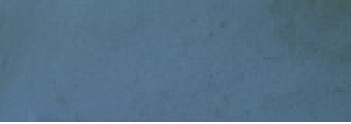

Core and wireline logging are different processes used to verify log interpretation models. Adams, (2005) stated that using the core data to verify the log interpretation models allows for the log and core data to be compared and the uncertainties in the log-derived properties to be quantified. In this study, the core data and log data were placed side-by-side in separate tracks in Interactive Petrophysics (IP 4.7) © 2021 software for comparison. The Gamma Ray log was used for comparison to the core data. It easily identified the sandy and shale formations. In addition, shale boundaries were established and then compared with core data to check for discrepancies. A well-core depth shift was only carried out in well F-AH4 as the well logs indicate that the logger's depth is 2.45m deeper than the driller's depth over the cored interval and a match between the logger's depth and the driller's depth was observed F-AH1 and F-AH2.

4.4 LITHOFACIES DESCRIPTION



The facies is simply a body of rock characterized by a particular combination of lithology, physical and biological structure and presents a different appearance from the body of rock above, below, and laterally adjacent (Roger and Noel, 1992). According to Moore, 1949, sedimentary facies is defined as any areally restricted part of a designated stratigraphic unit that exhibits characters significantly different from those of other parts of the units.

This study uses an existing core sedimentological description of the routine core analysis. The lithofacies of the rock units were grouped by structural, textural features and grain sizes based on the approach of Nieto and Rojas (1998) to lithofacies groupings within the studied wells (F-AH1, F-AH2, and F-AH4). A total of nine lithofacies were identified and ranging from A1 to A9, with varying reservoir quality. **Table 4-4** shows the lithofacies classifications of rock units grouped into nine (9) different facies and the photographs in the table below have been chosen to represent each of the nine identified facies.

Table 4- 4: Litho-facies description and classification of reservoir facies

Facies	Description	Reservoir quality	Facies photos
A1	Sandstone, mostly massive, medium grained, grey-white colour, well-sorted, micaceous grains present. Rare mud drapes (~2mm) present	Good	
A2	Sandstone, predominantly fine grained, grey with occasional yellow discolouration.	Moderate	
A3	Very fine sandstone intercalated with occasional mud laminations. Locally rippled and cross laminated. Occasional mud drapes (~2mm) present.	Poor	

A4	Coarse-grained sandstone (occasional >0.5mm grains), poorly sorted, locally emplaced rounded to subrounded mud clasts and pebbles (3-5mm).	Good	
Facies	Description	Reservoir quality	Facies photos
A5	Very coarse-grained sandstone (1mm grain size), moderate to poorly sorted, grey in colour, locally emplaced subrounded mud clasts (brown-black colour) and pebbles (~5mm)	Moderate-Good	
A6	Granule (2-4mm) to pebble (>5mm) conglomerate (apparently monomict), individual rounded to subrounded clasts of mud (brown-black) set in a medium-coarse grained grey sandstone matrix.	Good	
A7	Intercalated medium sandstone (grey colour)	Fair	

	and silt (grey-light brown, gritty but often becoming muddy) laminated, occasionally cross laminated.		
A8	siltstone, dark grey colour, with occasional mud drapes (1-3mm)	Poor	
A9	Mudstone, massive but often laminated, colour variations of dark grey/green/red colour, burrowing evident.	Non-Reservoir	

4.4.1 Well F-AH1 Litho-facies Description

In well F-AH1, nine (9) litho-facies were identified within the studied well and comprise facies A1 to A9. Facies A1 to A4 consisted largely of sandstone, which was generally well sorted and varied in size from coarse to very fine. The A1 and A2 facies were interpreted as having the best deposit quality sandstones as they were minimally affected by clay content based on texture, grain size, shape and sedimentary structures as they were extended throughout the study area and were well sorted to allow possible free flow of hydrocarbons. Facies A6 was a conglomerate with black\brown subrounded mud clasts and poor sorting. Facies A7 consists of intercalated medium-grained sandstone and fine silt particles and has been described as acceptable reservoir quality, but depends largely on where the sandstone content is predominant and of sufficient thickness. The A8 and A9 facies are siltstones and mudstones and both facies comprise non-reservoir-type lithology with extremely fine grain sizes. Facies A9 were extended and interpreted as a potential sealing mechanism if found to be of sufficient

thickness and unfractured. **Table 4-5** presents the summary of identified lithofacies for well F-AH1 and **Figure 4-1** shows the facies identified in well F-AH1. The Gamma Ray curve is shown in track 1, the depth reference is shown in the second track, the resistivity curve is shown in the third track, the caliper log is shown in the fourth track and the neutron and density curves are shown in the fifth track, and the facies are in the sixth track shown. The core intervals examined were mostly sandstones with silt and mud intercalations.

Table 4- 5: Summary of identified lithofacies for well F-AH1

Well Name	Lithofacies	Lithology	Grain class	Grain size (mm)	Sorting	Colour
F-AH1	A1	Sandstone	Medium	0.27	Well	Grey/white
	A2	Sandstone	Fine	0.128	Very well	Grey/yellow
	A3	Sandstone	Very fine	0.1	Very well	Grey/white
	A4	Sandstone	Coarse grained	0.6	Poor	Grey
	A5	Sandstone	Very Coarse	1	Moderate to poor	White
	A6	Conglomerate	Granule-Pebble	2-10	Very poor	Grey matrix, brown/black pebbles
	A7	Mixed Sand and Silt	Medium and fine	0.01-0.26	Well to very well	Grey/light brown
	A8	Siltstone	Fine-very fine	0.01		Dark grey
	A9	Mudstone	Very fine	>0.003		Dark grey/green/red

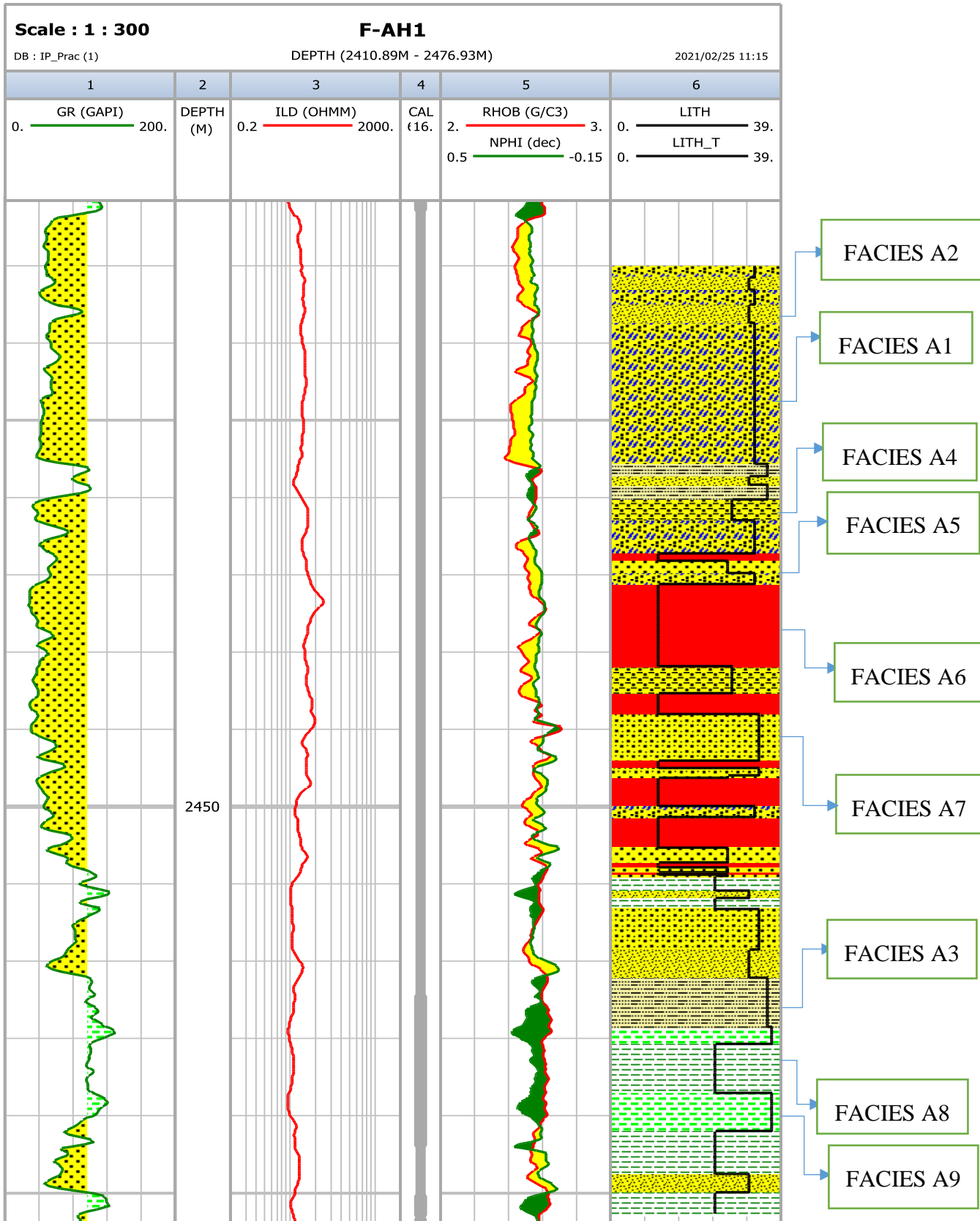


Figure 4- 1: Well F-AH1 showing core facies in track 6

4.4.2 Well F-AH2 Litho-facies Description

Eight (8) lithofacies were identified within the study well (F-AH2) and they are facies A1 to A5 and A7 to A9. Facies A1 to A4 consisted largely of sandstone, which was generally well-sorted and varied in size from coarse to very fine. The A1 and A2 facies were interpreted as having the best reservoir quality sandstones as they were minimally affected by clay content based on texture, grain size, shape and sedimentary structures as they were extended throughout the study area and were well sorted to allow possible free flow of hydrocarbons. Facies A7 consists of intercalated medium-grained sandstone and fine silt particles and has been described as acceptable reservoir quality, but depends largely on where the sandstone content is predominant and of sufficient thickness. The A8 and A9 facies are siltstones and mudstones and both facies comprise non-reservoir-type lithology with extremely fine grain sizes. Facies A9 were extensive and interpreted as a potential sealing mechanism if found to be of sufficient thickness and unfractured. **Table 4-6** presents the summary of identified lithofacies for well F-AH2 and **Figure 4-2** shows the facies identified in well F-AH2. The core intervals examined were mostly sandstones with silt and mud intercalations.

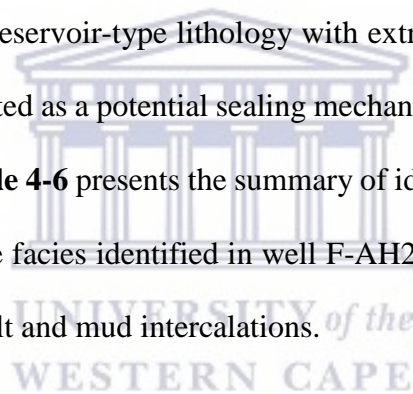
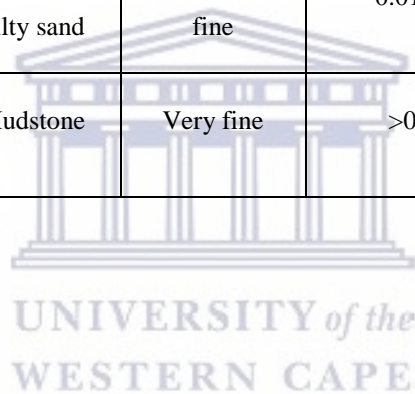


Table 4- 6: Summary of identified lithofacies for well F-AH2

Well Name	Lithofacies	Lithology	Grain class	Grain size (mm)	Sorting	Colour
F-AH2	A1	Sandstone	Medium	0.27	Well	Grey/white
	A2	Sandstone	Fine	0.128	Very well	Grey/yellow
	A3	Sandstone	Very fine	0.1	Very well	Grey/white
	A4	Sandstone	Coarse grained	0.6	Poor	Grey
	A5	Sandstone	Very Coarse	1	Moderate to poor	White
	A7	Silty sand	Medium and fine	0.01-0.26	Well to very well	Grey/light brown
	A9	Mudstone	Very fine	>0.003		Dark grey/green/red



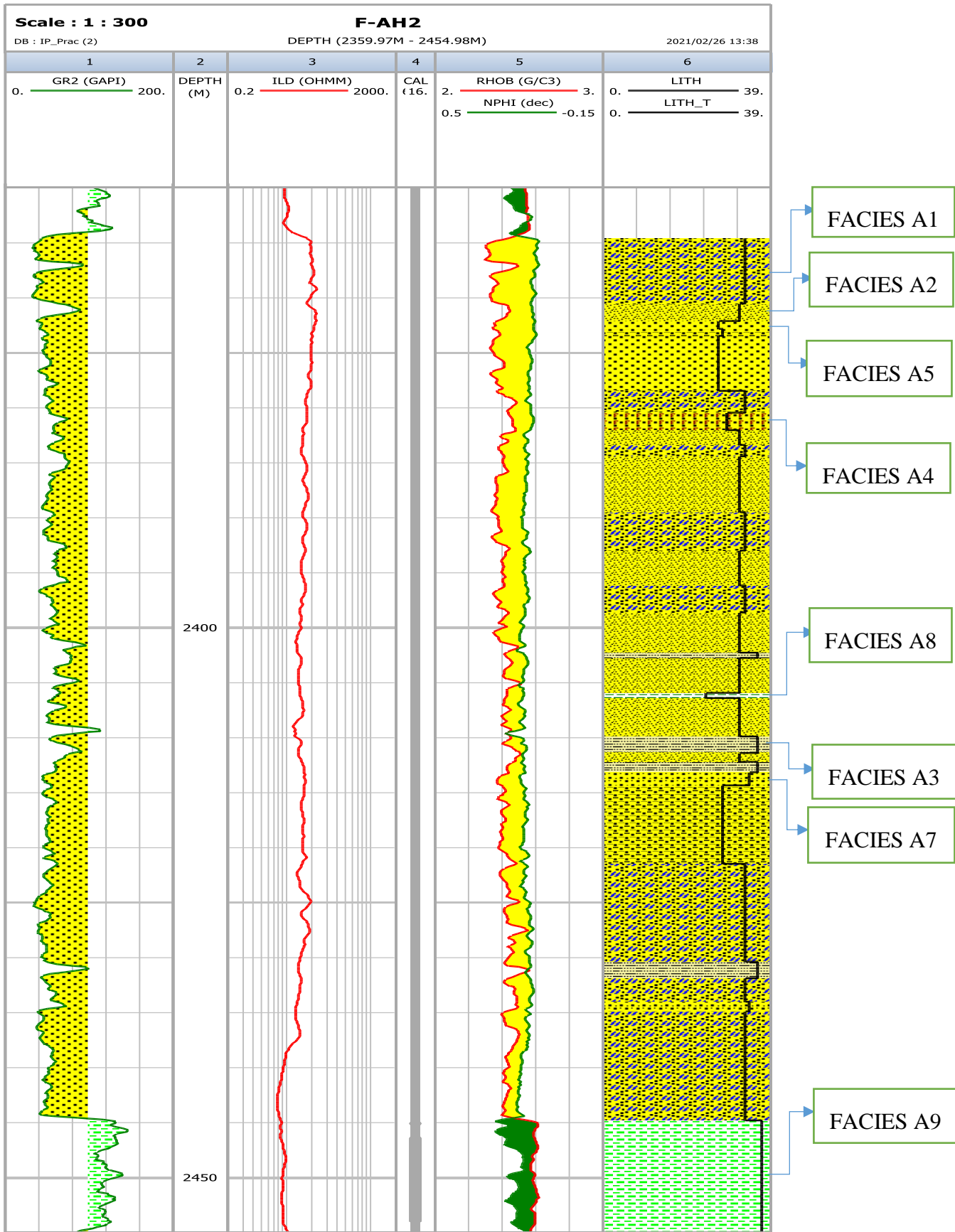


Figure 4- 2: Well F-AH2 showing core facies in track 6

4.4.3 Well F-AH4 Litho-facies Description

In well F-AH4, nine (9) litho-facies were identified within the study well, namely facies A1 through A6 and A9. . Facies A1 to A4 consisted largely of sandstone, which was generally well sorted and varied in size from coarse to very fine. The A1 and A2 facies were interpreted as having the best reservoir quality sandstones as they were minimally affected by clay content based on texture, grain size, shape and sedimentary structures as they were extensive throughout the study area and were well sorted to allow possible free flow of hydrocarbons. Facies A6 was a conglomerate with brown\black subrounded mud clasts and poor sorting. The A9 facies are siltstones and mudstones and comprise a non-reservoir-type lithology with extremely fine grain sizes. The A9 facies was also extensive and was interpreted as a potential sealing mechanism if found to be of sufficient thickness and unfractured. **Table 4-7** presents the summary of identified lithofacies for well F-AH4 and **Figure 4-3** shows the facies identified in well F-AH4. The core intervals examined were mostly sandstones with silt and mud intercalations.

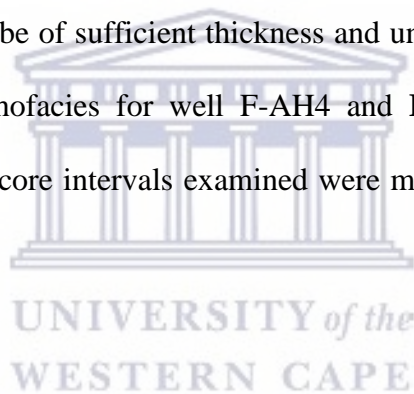


Table 4- 7: Summary of identified lithofacies for well F-AH4

Well Name	Lithofacies	Lithology	Grain class	Grain size (mm)	Sorting	Colour
F-AH4	A1	Sandstone	Medium	0.27	Well	Grey/white
	A2	Sandstone	Fine	0.128	Very well	Grey/yellow
	A3	Sandstone	Very fine	0.1	Very well	Grey/white
	A4	Sandstone	Coarse grained	0.6	Poor	Grey
	A5	Sandstone.	Very Coarse	1	Moderate to poor	White
	A6	Conglomerate	Granule- Pebble	2-10	Very poor	Grey matrix, brown/black pebbles
	A9	Mudstone	Very fine	>0.003		Dark grey/green/red

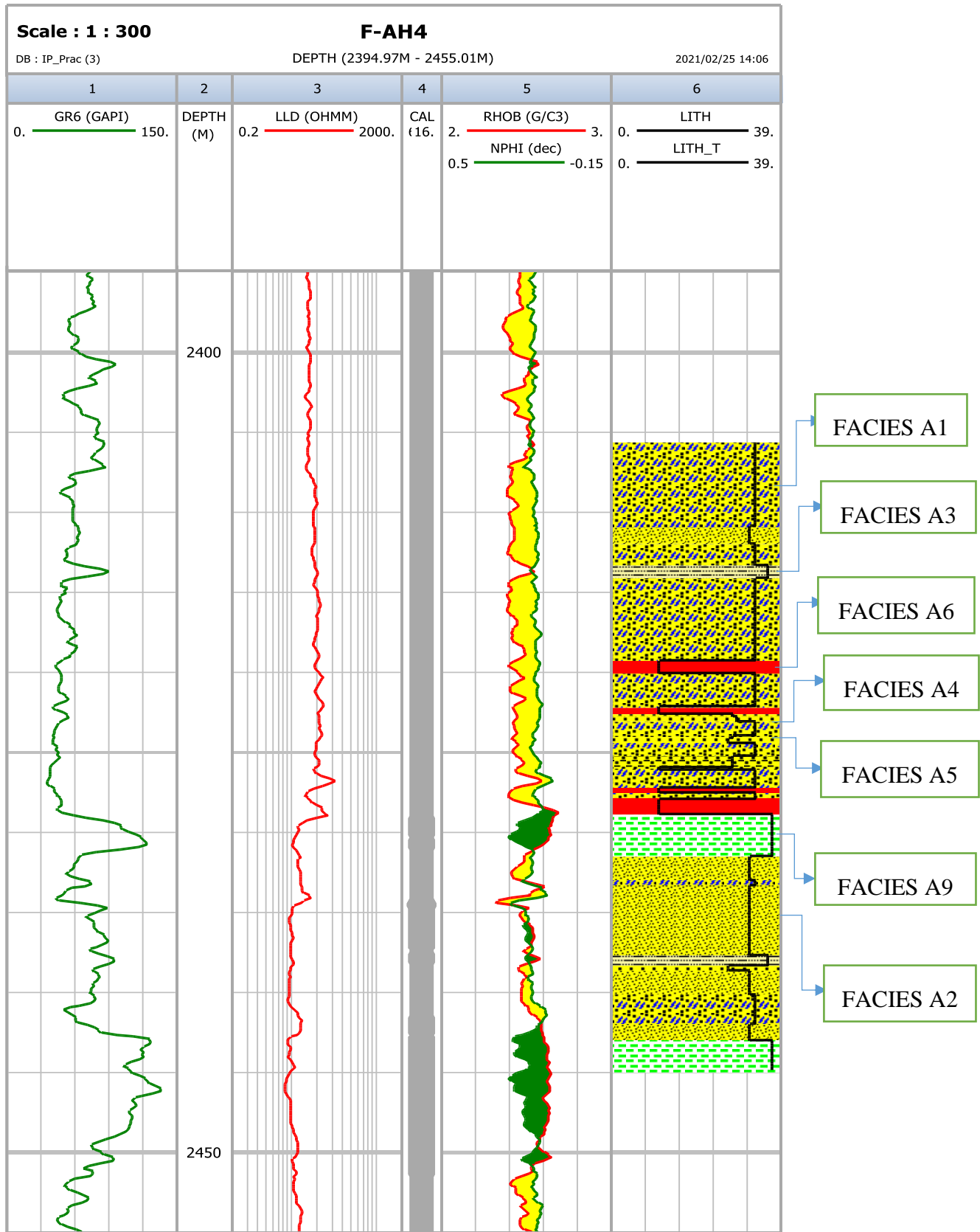


Figure 4- 3: Well F-AH4 showing core facies in track 6

4.5 RESULTS AND INTERPRETATION

4.5.1 Well Correlation

The well correlation was performed for this study using Gamma Ray, sonic, neutron and resistivity logs of the wells loaded into Petrel ® 2014 software. **Figures 4-4 and 4-5** show the general well correlation scenario of geological horizons across the three wells (F-AH1, F-AH2 and F-AH4). Well correlation was performed to define the stratigraphic horizons bounding the main geological sequence trend and depth correlating across wells along the study sequence, allowing for well-to-well correlation. Gamma Ray (GR), Acoustic (Sonic) (DT), Neutron (NPHI), and Resistivity (LLD/ILD) were the wireline logs used for correlation purposes. The GR log was used to identify the lithology and the limit for the logs used was 0-150 API. The high Gamma Ray values of 75-150 API units indicate the presence of shale while the low Gamma Ray values (0-75 API units) indicate the presence of sand. The top (1AT1) and bottom (BUSM) of these sands were correlated. The top of the 1AT1 sand contains hydrocarbon. The 1AT1 sands are of similar thickness in all three wells in the field.

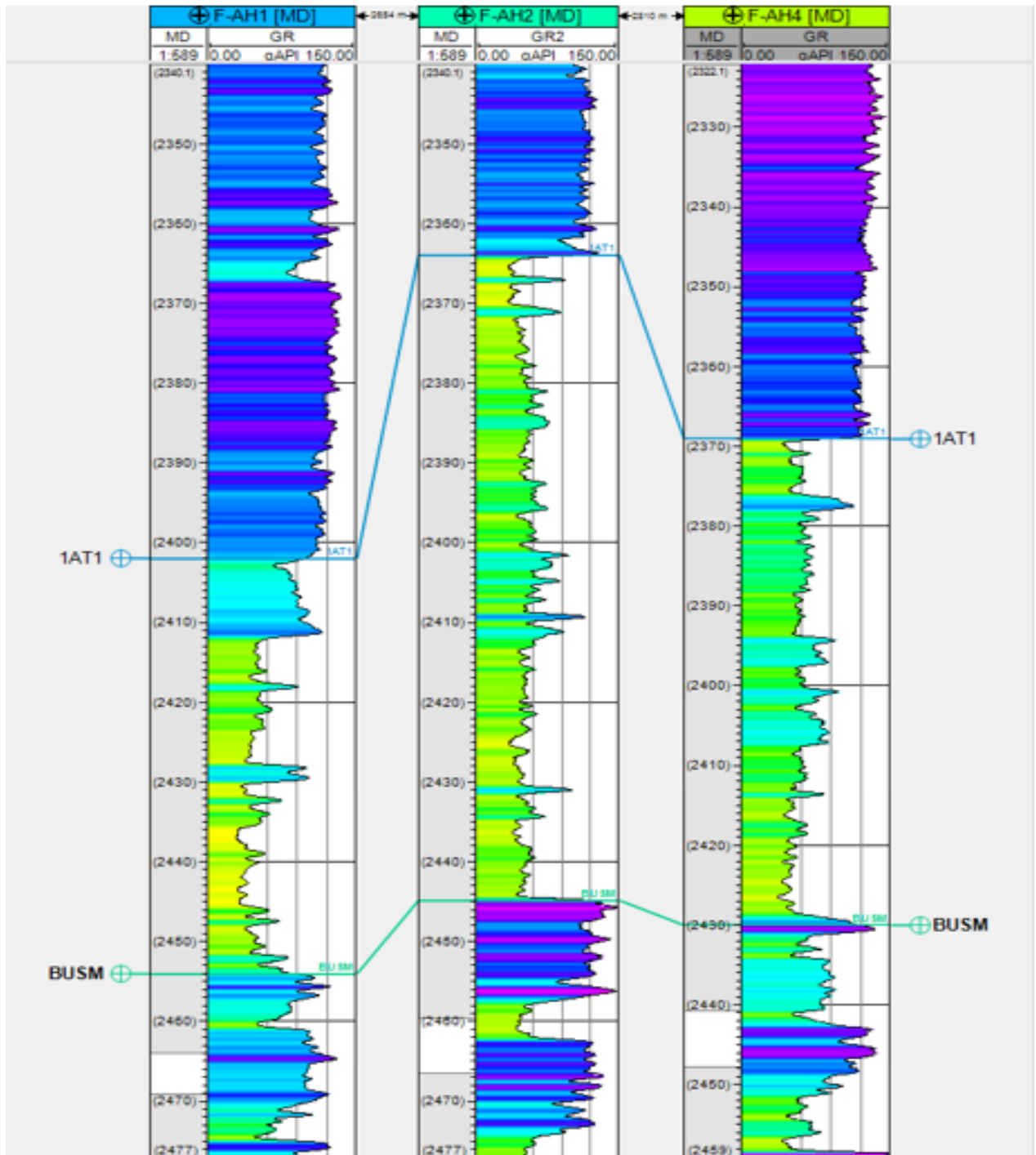


Figure 4- 4: Well correlation between well F-AH1, F-AH2 and F-AH4 using Gamma Ray log.

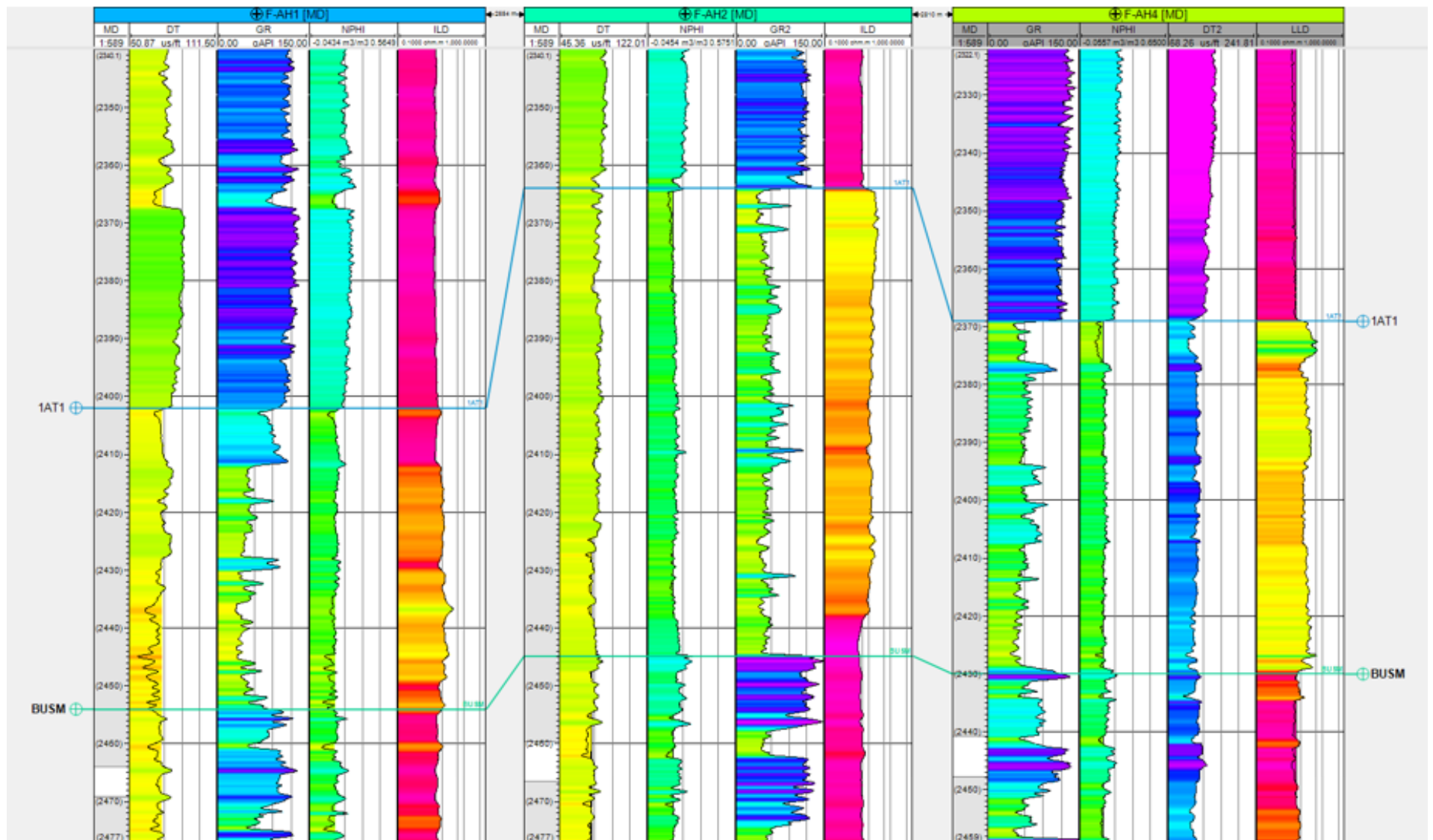


Figure 4- 5: Well correlation between well F-AH1, F-AH2 and F-AH4 using Gamma Ray, neutron porosity, sonic and resistivity log

4.5.2 Grain Density

Grain density is a measure of the density of a non-porous rock (grains), or mineral contained in the core sample, omitting the contained liquids and voids. Schlumberger, 2013 states that in formation evaluation, the grain density is characterized as the density of grains in a formation or core sample. This grain density is derived from measured dry weight divided by grain volume and is also determined from density logs using a porosity assessment and liquid content information. The matrix densities of some common lithologies are given in **Table 4-8**.

Table 4- 8: Matrix density of common lithology (Source: Schlumberger, 2013)

Lithology	Matrix value (g/cm ³)
Clay Minerals	2.02-2.81
Chlorine	2.81
Illite	2.61
Kaolinite	2.55
Smectite	2.02
Coal	1.19
Halite	2.04
Sandstones (quartz)	2.65
Limestones	2.17
Dolomites	2.85
Orthoclase	2.57
Plagioclase	2.59
Anhydrite	2.98
Siderite	3.88
Pyrite	4.99

In this study, F-AH4 was the only well that contained recorded core plug grain density data, therefore histograms were plotted on a core-to-core basis to observe interval variations within the well. See **Appendix 1**. The grain density results of core 1 (**Appendix 1**) show a range of 2.61 g/cc to 2.77 g/cc and in core 2 the grain density ranged from 2.64 g/cc to 2.67 g/cc. The grain density of core 3 ranged from 2.57 g/cc to 2.66 g/cc and core 4 was a short section of

only 2 core boxes and only two measurements were taken of 2.65 g/cc and 2.66 g/cm³, indicating quartz-rich sand. With exception of core 3, which had an average grain density of 2.64 g/cc, the averages across each core section were relatively constant at 2.65 g/cc, and the average of 2.65 g/cc confirmed that the core sections were largely clean quartz sandstones and could potentially be of reservoir quality as shown in **Table 4-8**. The standard deviation value of cores 1 to 3 and 5 are 0.02317, 0.00865, 0.01945, and 0.01676 respectively.

However, the variation in grain density was relatively small and indicated that the lithology was not highly variable across core sections. This observation was expected as the cored intervals all belonged to the same well and were cut in sandstone. Also, the off-mean values represented variable clays or calcite that were mixed with the sandstone. In core 1, calcite impact where a reading of 2.73 g/cc was interpreted at a depth of 2383.86 m. Calcite cement forms between the grains and can negatively affect porosity and permeability. A clay-sand mixture was observed in core 3 where a recurring value of 2.63 g/cc was found over a depth range of 2406.89 m to 2410.71 m. This was confirmed by the clay-type streaks and drapes seen on the core at these depths.

Calcite and dolomite appear to be low, reflecting low occurrences of calcium carbonate cement. Core 1 had the highest standard deviation, possibly explaining the calcite influence of the formation of a broader spectrum of lithology present. It should be noted that only 2 readings were taken for core 4, representing a skewed response compared to the mean values for the rest of the core section. Core grain density data and core characterization are commonly used together to confirm the projected lithology. If a visual core description is not available, grain density analysis can be used to identify the entire lithology. Grain density statistics across the 5 cores from well F-AH4 are presented in **Table 4-9**.

Table 4- 9: Summarised grain density statistics of Well F-AH4 core sections

Well F-AH4				
Core	Grain density (g/cc)			
	Minimum	Maximum	Mean	Standard deviation
Core 1	2.61	2.77	2.65	0.02317
Core 2	2.64	2.67	2.65	0.00865
Core 3	2.57	2.66	2.64	0.01945
Core 4	2.65	2.66	---	---
Core 5	2.55	2.66	2.65	0.01676

4.5.3 Sediment Logs

SedLog is a software program for drawing graphic sedimentary structures for wells and multi-platform software for creating graphical sediment logs. It offers an intuitive graphical user interface that makes it very easy for anyone to use with minimal effort. In this study, the graphical sediment logs were generated by SedLog. See **Appendix 4** for the graphic sedimentary structures for wells F-AH, F-AH2 and F-AH4 respectively.

4.6 INTERPRETATION OF WIRELINE LOGS

The interpretation of the wireline logs commenced with the identification of zones of interest (clean sand with a sizable quantity of hydrocarbons) and the possible sandstone reservoir was identified using the GR log (Gamma Ray log) with reference to the sand/shale baseline. The baseline is the line used to demarcate the shale formation from the sand formation since a maximum deviation to the right indicates a shale formation and a maximum deviation to the left indicates clean sandstone.

In this study, a suite of composite well logs were presented from wells F-AH1, F-AH2, and F-AH4 comprises of Gamma Ray (GR), resistivity (ILD/LLD), Bulk density (RHOB), neutron (NPHI) and sonic (DT) logs. The identification of a possible sandstone reservoir (clean sand) is usually the first step in log interpretation and the application of the baseline interval allows better distinction between sandstone and shale and clarifies the reservoir seal. **Figure 4-5** shows the identification of the Sandstone reservoir in well F-AH1.



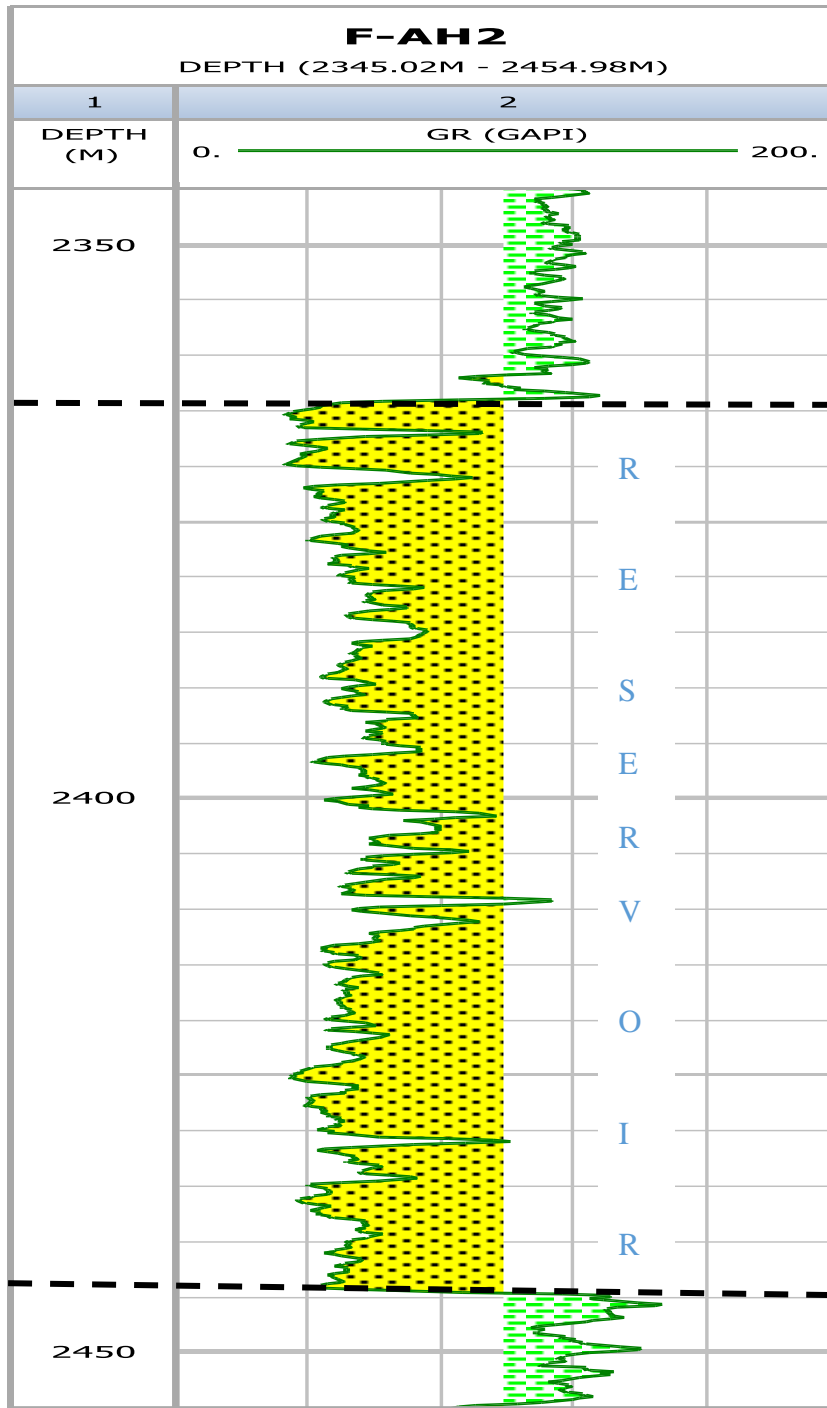


Figure 4- 6: Example of a potential Sandstone Reservoir in well F-AH2

Figure 4-6 show the Gamma Ray log (green curve) on track 2 and the reservoir interval. The maximum right deflection of the Gamma Ray indicates shale formation and reservoir seal and the minimum left deflection of the Gamma Ray log indicates a clean baseline of sandstone and

shale (Jensen et al., 2013). The well logs were used to identify the reservoir intervals and lithology in the three wells (F-AH1, F-AH2, and F-AH4) and the Gamma Ray logs and a combination of density and neutron logs were used to classify the reservoir interval into distinct zones and the Deep Induction Resistivity (ILD) log was used to identify the formation fluid (water/hydrocarbon) and possible fluid contacts in all the wells.

4.6.1 Well F-AH1 wireline logs interpretation

Well F-AH1 was drilled to test hydrocarbons in an independent dome lock formed by the F-AH structure at the Horizon C (1At1) level, located 3.5 km northwest of F-AR3. Four (4) reservoir zones were identified within the zone of interest on the evaluated interval in well F-AH1, which has varied from depth 2411.5m – 2428.1m, 2429.5m – 2454.2m, 2495.8m – 2503.0m and 2560.8m – 2569.5m respectively. Hydrocarbon zones are indicated by high downhole resistivity readings. Reservoir zone 1 which was selected from the Gamma Ray log ranges from 2411.5m to 2428.1m with a thickness of 16.6m representing Core 1, 2, 3 and 4 as shown in **Figure 4-7** shows the resistivity log (ILD) in track 4, density log (RHOB) in track 5, neutron log (NPHI) in track 6 and sonic log (DT) in track 7.

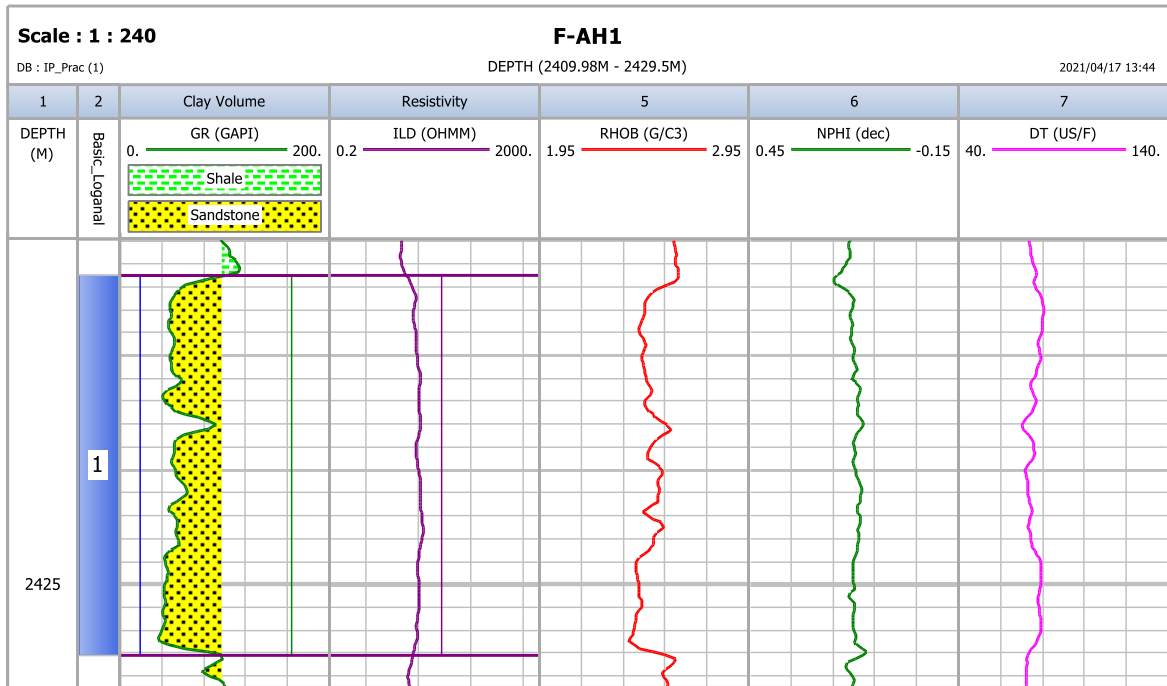


Figure 4- 7: Reservoir interval in well F-AH1 (Zone 1, 2411.5 – 2428.1 m depth)

Reservoir zone 2 which was selected from the Gamma Ray log ranges from 2429.5m to 2454.2m representing cores 5 and 6 and has a thickness of 24.7m as shown in **Figure 4-8**.

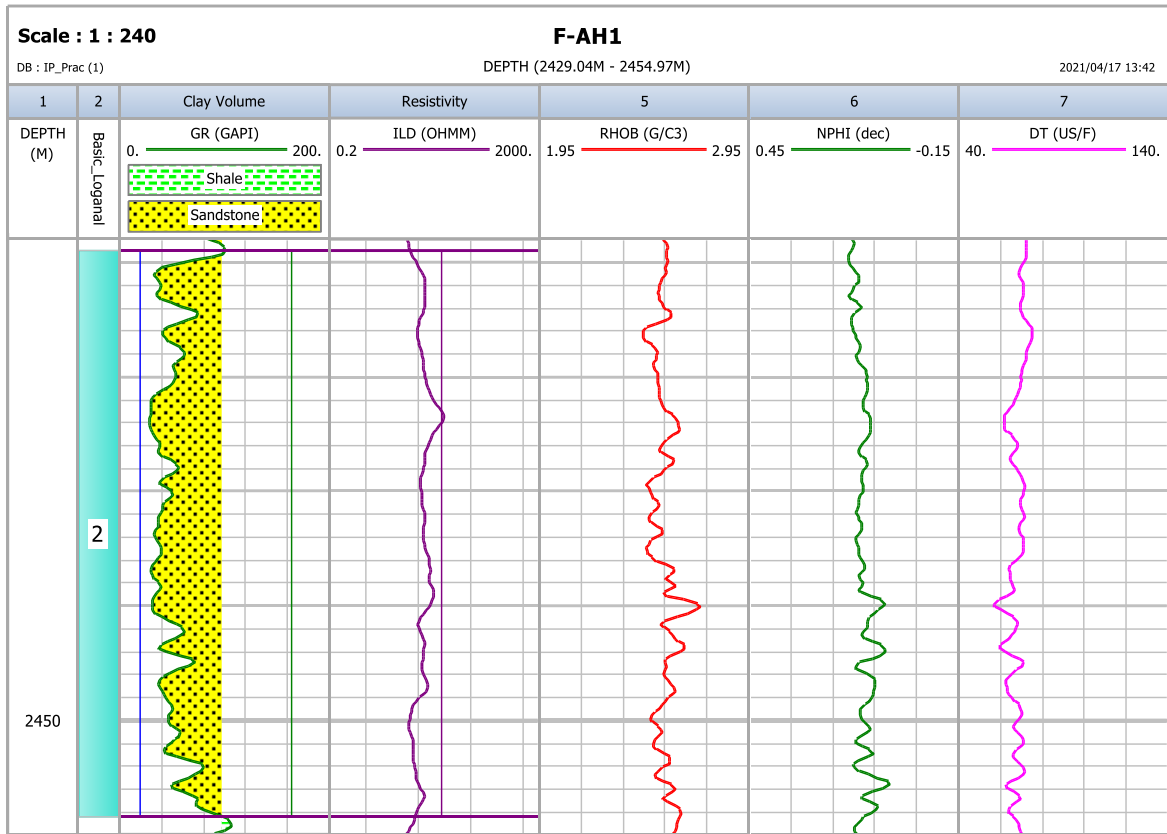


Figure 4- 8: Reservoir interval in well F-AH1 (Zone 2, 2429.5 – 2454.2 m depth)

Reservoir zone 3 is the selected potential reservoir interval ranging from 2495.8m to 2503.0m with a thickness of 7.2m as shown in **Figure 4-9**.

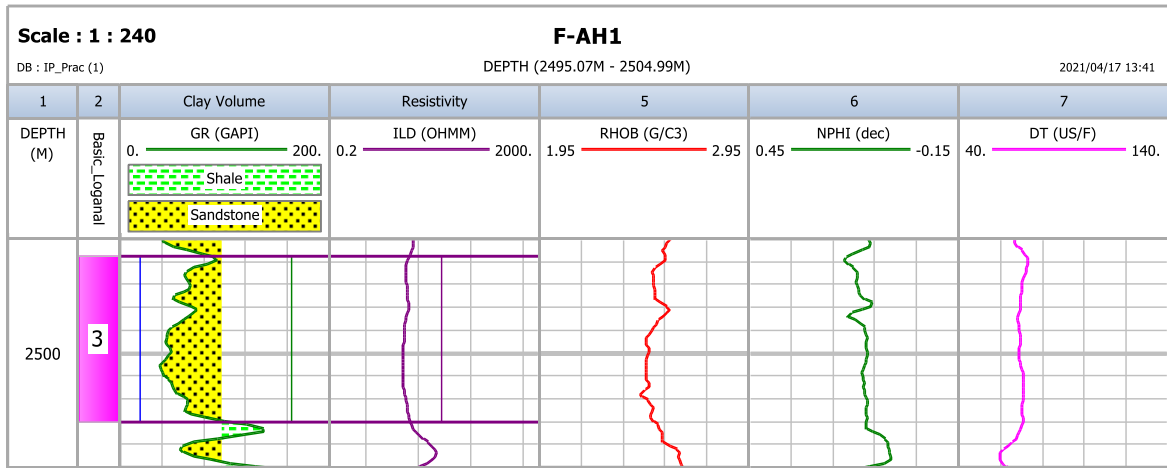


Figure 4- 9: Reservoir interval in well F-AH1 (Zone 3, 2495.8 – 2503.0 m depth)

Reservoir zone 4 is the selected potential reservoir interval that ranges from 2560.8m to 2569.5m and has a thickness of 8.7m as shown in **Figure 4-10**.

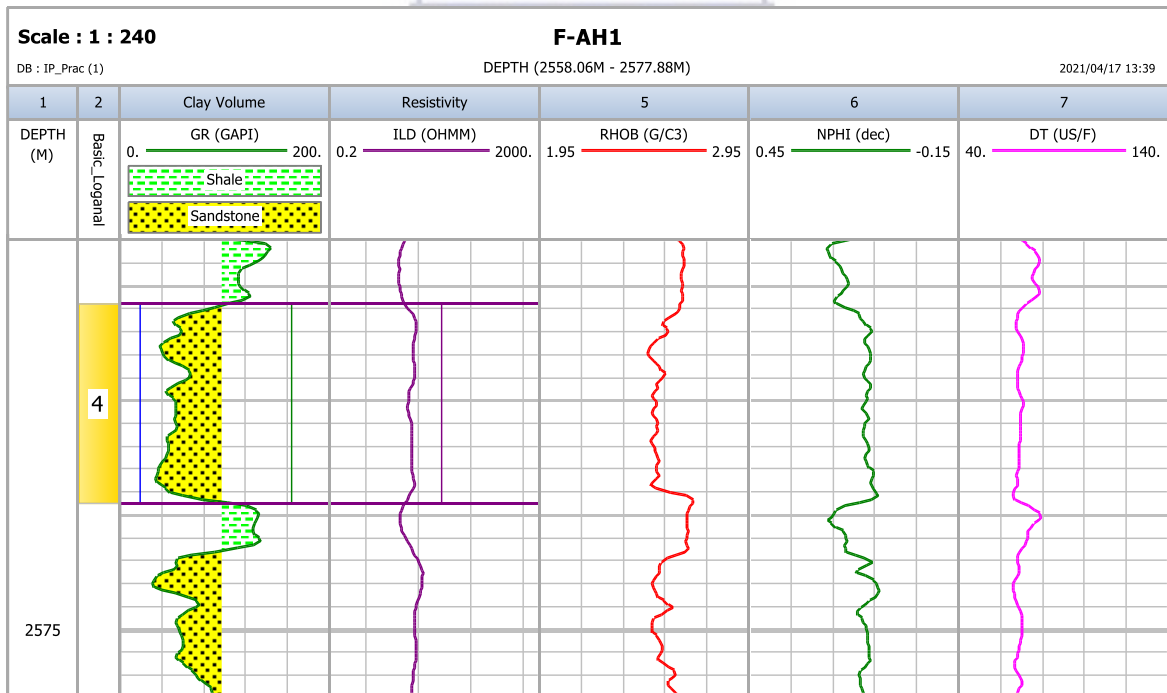
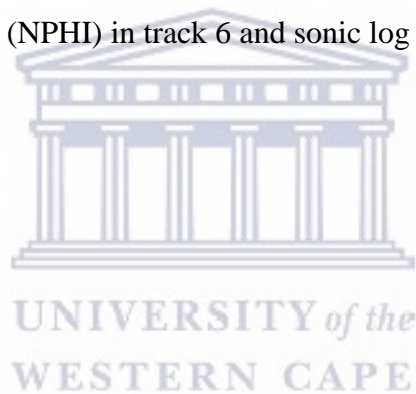


Figure 4- 10: Reservoir interval in well F-AH1 (Zone 4, 2560.8 – 2569.5 m depth)

4.6.2 Well F-AH2 wireline logs interpretation

Well F-AH2 is located 78 km south-southwest of Mossel Bay and 7.5 km east of borehole E-S3 and according to [Bell and Van Heerden 1986](#), the well was also recommended to test for hydrocarbons in an independent area of the Domal Closure Northwest of well F-AH1. Four (4) reservoir zones were identified within the zone of interest in the studied interval in well F-AH2 varying from depth 2363.9m – 2444.7m, 2457.1m – 2462.3m, 2487.2m – 2490.5m, 2553.8m – 2557.9m respectively. These zones were selected based on Gamma Ray behaviour and a combination of density and neutron logs. Reservoir zone 1 which was selected from the Gamma Ray log ranges from 2363.9m to 2444.7m with a thickness of 80.75m representing Core 1, 2, 3, 4, 5 and 6 as shown in **Figure 4-11** shows the resistivity log (ILD) in track 4, density log (RHOB) in track 5, neutron log (NPHI) in track 6 and sonic log (DT) in track 7.



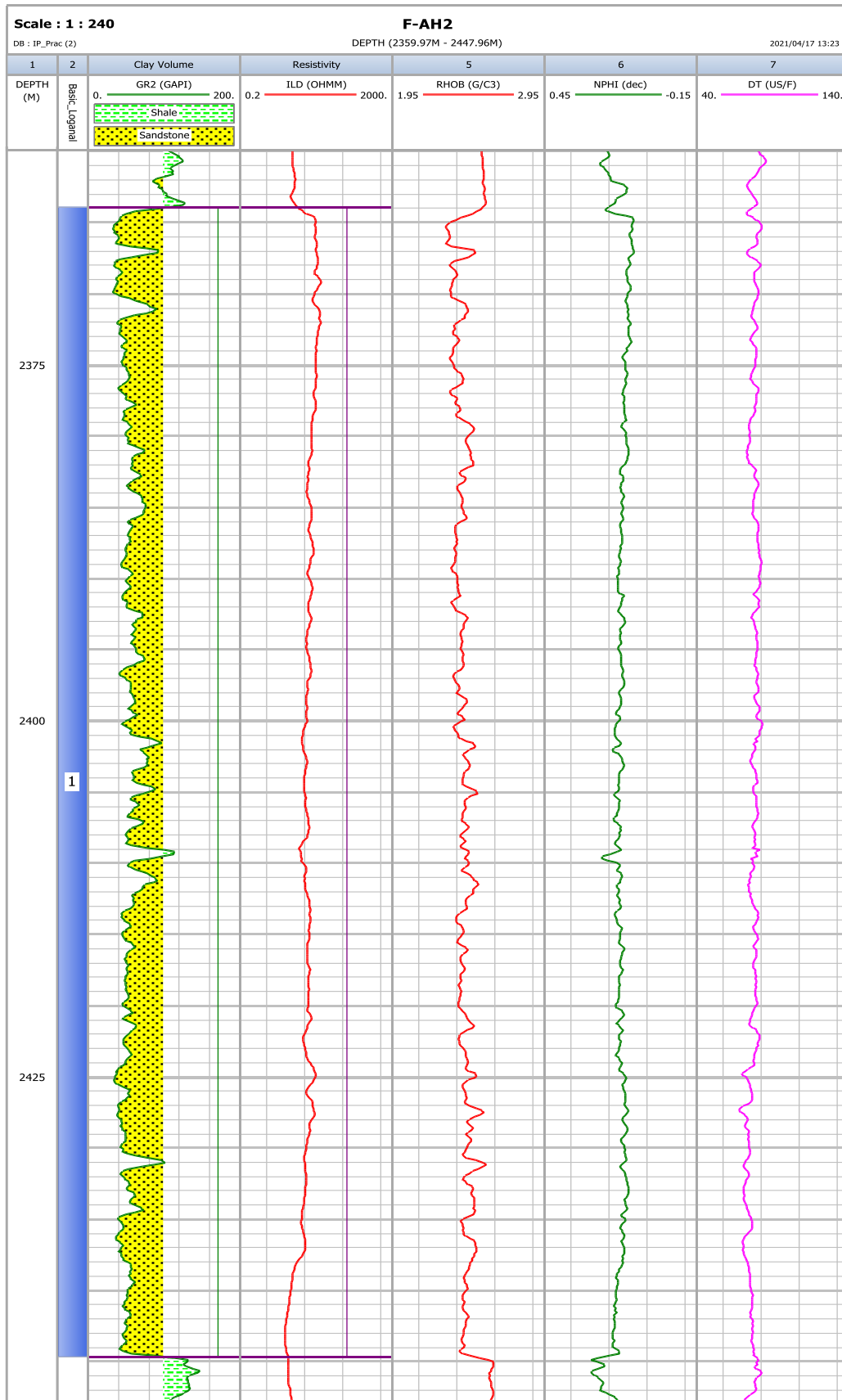


Figure 4- 11: Reservoir interval in well F-AH2 (Zone 1, 2363.9 – 2444.7 m depth)

Reservoir zone 2 which was selected from the Gamma Ray log ranges from 2457.1m to 2462.3m and has a thickness of 5.2m as shown in **Figure 4-12**.

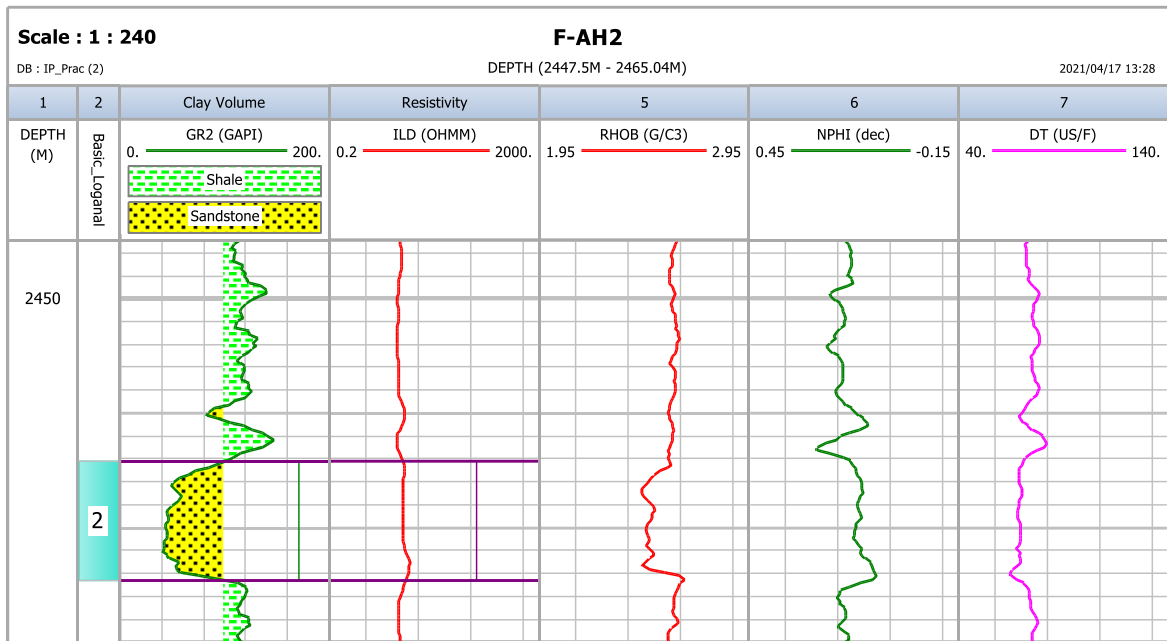
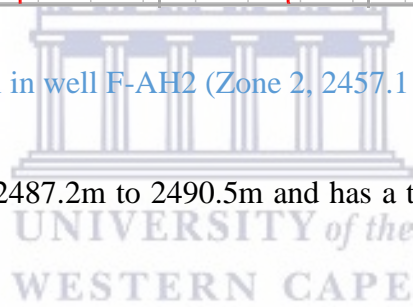


Figure 4- 12: Reservoir interval in well F-AH2 (Zone 2, 2457.1 – 2462.3 m depth)

Reservoir zone 3 ranges from 2487.2m to 2490.5m and has a thickness of 3.3m as shown in **Figure 4-13**.



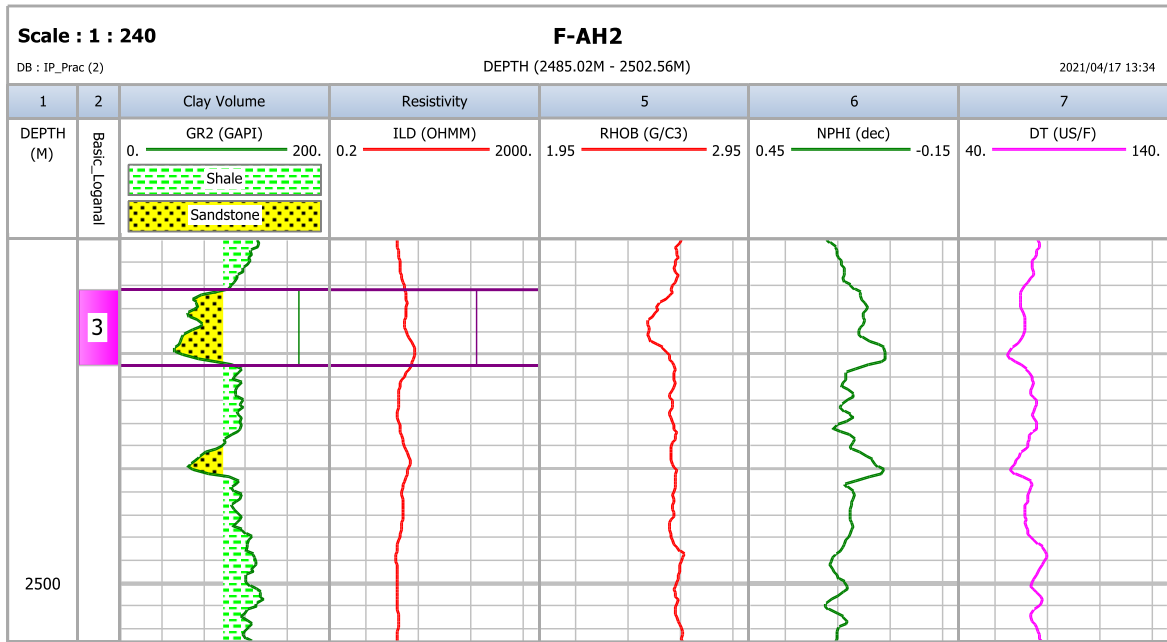


Figure 4- 13: Reservoir interval in well F-AH2 (Zone 3, 2487.2 – 2490.5 m depth)

Reservoir zone 4 ranges from 2553.8m to 2557.9m and has a thickness of 4.1m as shown in

Figure 4-14.

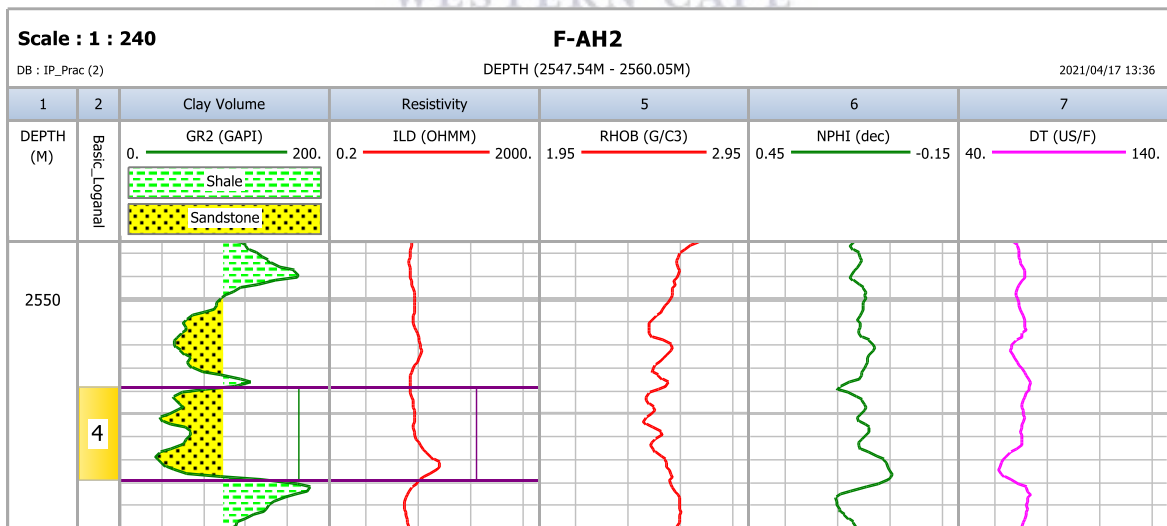
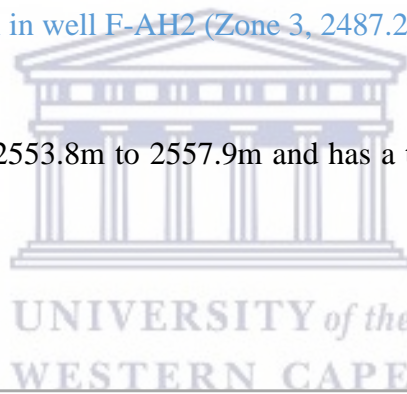


Figure 4- 14: Reservoir interval in well F-AH2 (Zone 4, 2553.8 – 2557.9 m depth)

4.6.3 Well F-AH4 wireline logs interpretation

Eight reservoir zones were identified within the zone of interest in the studied interval in well F-AH4 with depth ranges of 2369.1m – 2376.7m, 2377.7m – 2429.4m, 2450.1m – 2458.4m, 2476.7m – 2483.8m, 2516.4m – 2524.8m, 2526.8m – 2535.6m, 2545.1m – 2550.0m and 2557.7m – 2561.1m respectively. Reservoir zone 1 which was selected from the Gamma Ray log ranges from 2369.1m to 2376.7m with a thickness of 7.6m representing Core 1 as shown in **Figure 4-15**.

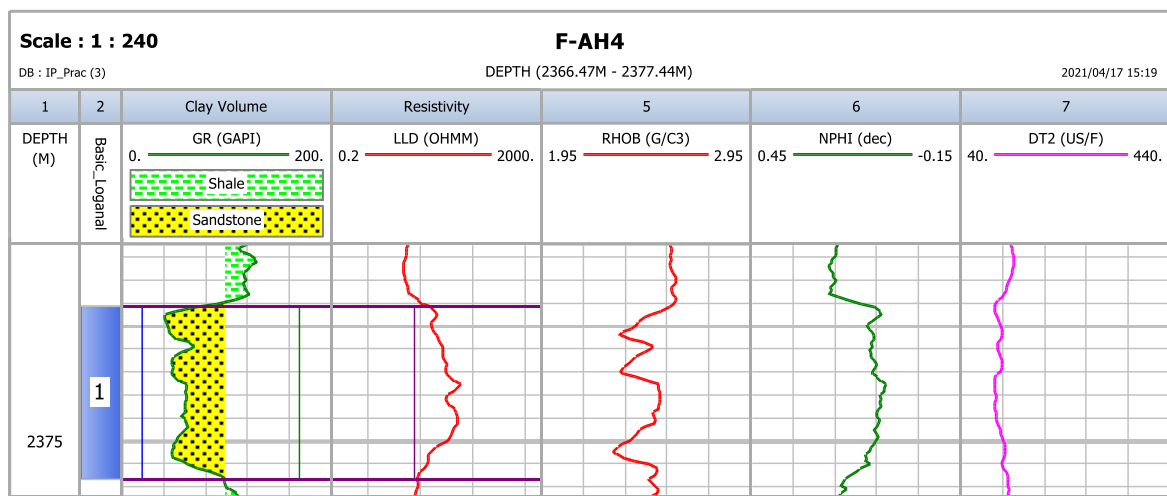


Figure 4- 15: Reservoir interval in well F-AH4 (Zone 2, 2369.1 – 2376.7 m depth)

Reservoir zone 2 ranges from 2377.7m to 2429.4m representing cores 2, 3, 4, 5 and has a thickness of 51.7m as shown in **Figure 4-16** shows the resistivity log (ILD) in track 4, density log (RHOB) in track 5, neutron log (NPHI) in track 6 and sonic log (DT) in track 7.

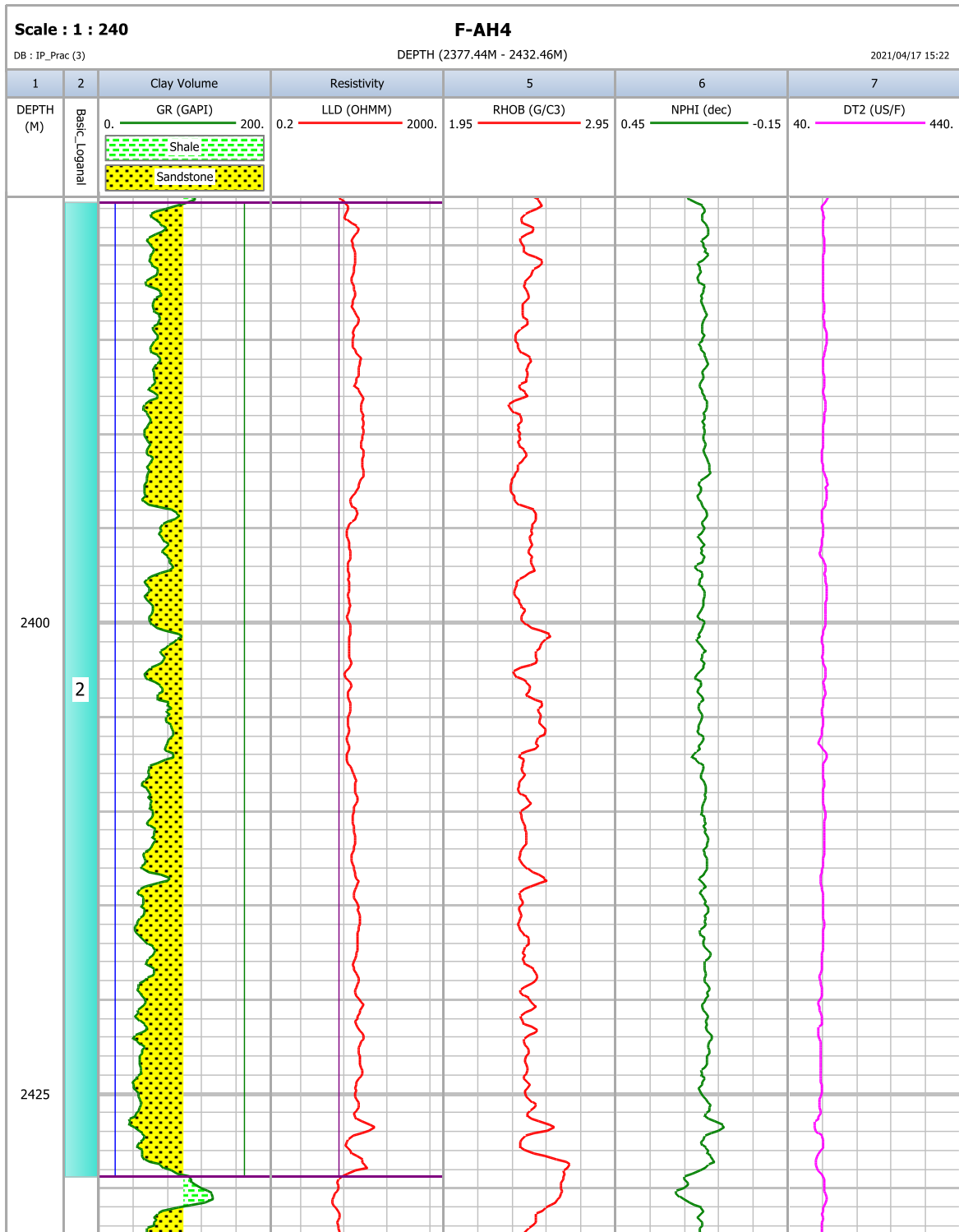


Figure 4- 16: Reservoir interval in well F-AH4 (Zone 2, 2377.7 – 2429.4 m depth)

Reservoir zone 3 ranges from 2450.1m to 2458.4m and has a thickness of 8.3m as shown in **Figure 4-17**.

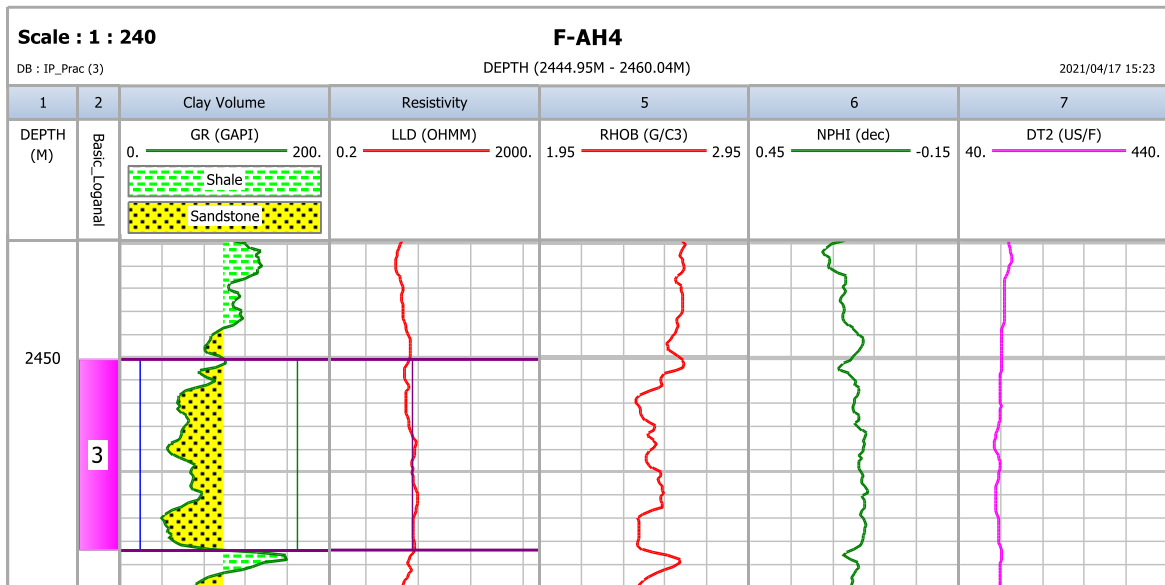
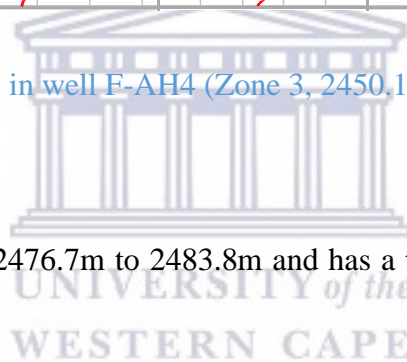


Figure 4- 17: Reservoir interval in well F-AH4 (Zone 3, 2450.1 – 2458.4 m depth)

Reservoir zone 4 ranges from 2476.7m to 2483.8m and has a thickness of 7.1m as shown in **Figure 4-18**.



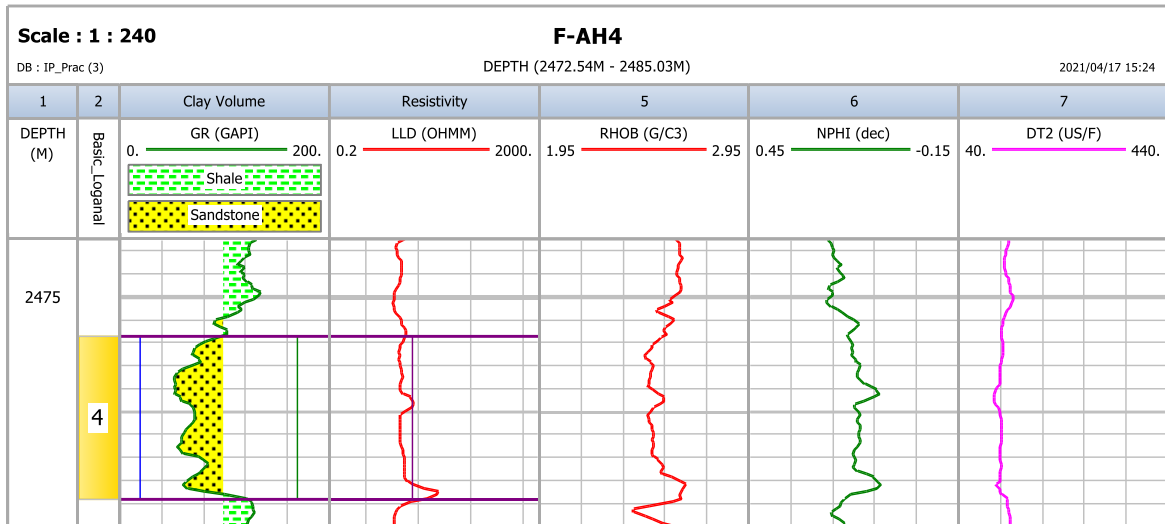


Figure 4- 18: Reservoir interval in well F-AH4 (Zone 4, 2476.7 – 2483.8 m depth)

Reservoir zone 5 ranges from 2516.4m to 2524.8m and has a thickness of 8.4m as shown in

Figure 4-19.

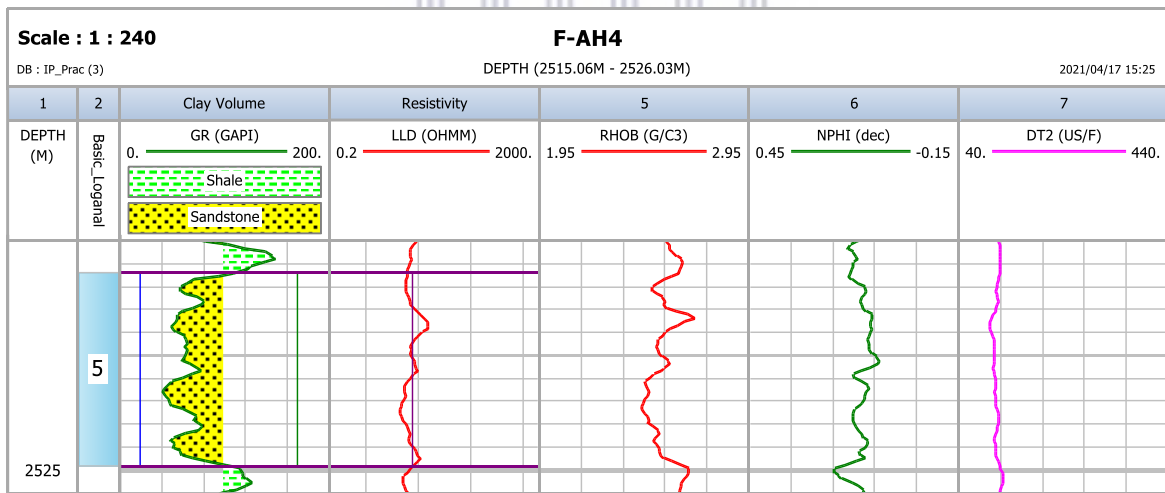


Figure 4- 19: Reservoir interval in well F-AH4 (Zone 5, 2516.4 – 2524.8 m depth)

Reservoir zone 6, 7 and 8 range from 2526.8m to 2561.1m, 2545.1m to 2550.0m and 2557.7m to 2561.1m with the respective thickness of 8.8m, 4.9m and 3.4m as shown in **Figure 4-20**

shows the resistivity log (LLD) in track 4, density log (RHOB) in track 5, neutron log (NPHI) in track 6 and sonic log (DT) in track 7.

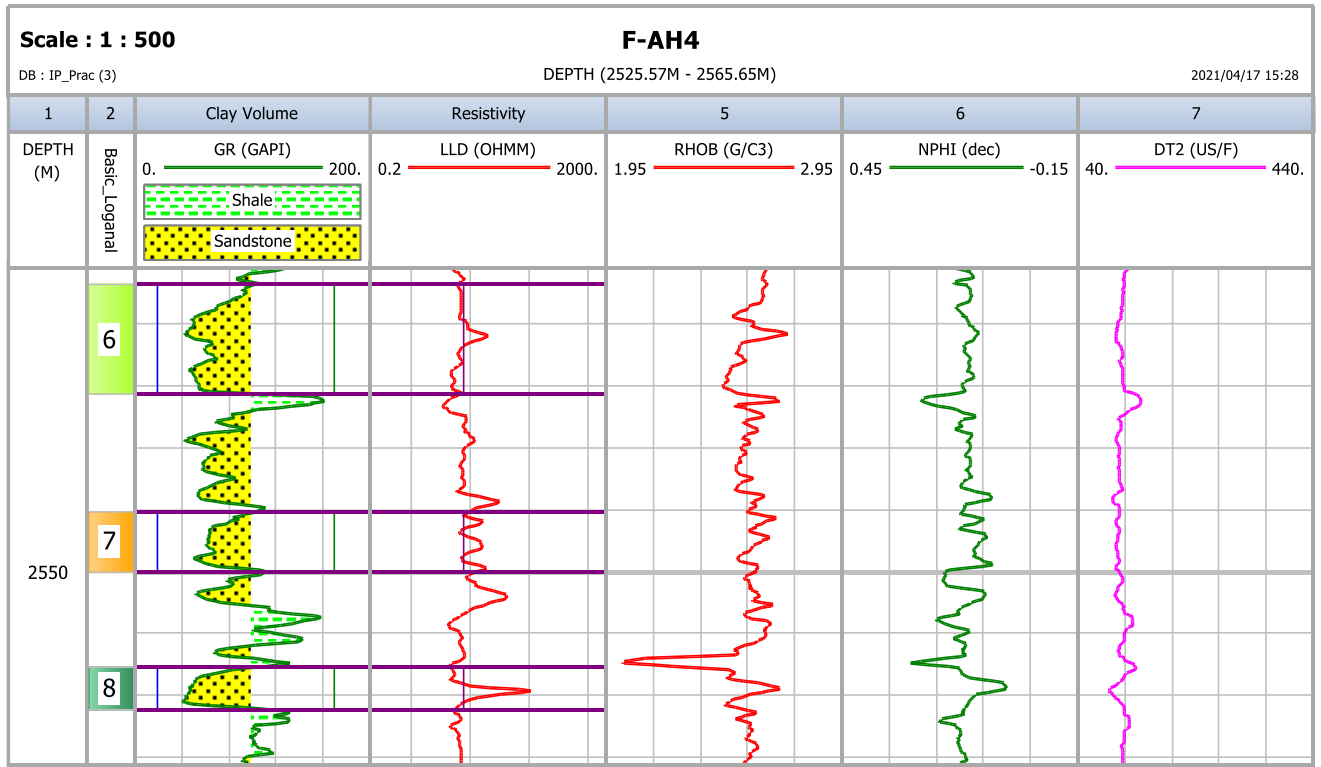


Figure 4- 20: Reservoir interval in well F-AH4 (Zone 6,7 and 8, 2526.8 – 2561.1 m depth)

CHAPTER FIVE

5. PETROPHYSICAL MODEL

This chapter describes the petrophysical model used to obtain the results of the following parameters: the volume of shale, porosity, permeability and water saturation determinations.

5.1 ESTIMATION OF THE SHALE VOLUME

Shale volume is the volume of wetted shale per unit volume of the reservoir rock. Szabo, 2010, defined shale volume as the ratio of the volume of clay and other fine-grained particles (particularly silt particles) to the total volume of the rock. It is expressed in percent or decimal fractions and the presence of shale in sand formations (shaly sand) reduces the accuracy of porosity and water saturation values and affects the response of logging tools. However, an essential technique in formation evaluation is to accurately determine the volume of shale present in the wage intervals. The most commonly used shale indicators are the Gamma Ray and spontaneous potential logs. In this study, the Gamma Ray method was used to define shale volume.

5.1.1 Gamma Ray Shale Volume

The most common shale volume indicator is the Gamma Ray log. The volume of silt or other inclusions within the shales cannot be measured by the Gamma Ray log. Crain, 2004 states that a minor setback for the Gamma Ray log is that it does not measure non-radioactive inclusions in the clay, namely debris that has been mixed with mud and silt.

In calculating the Gamma Ray clay indicator, two methods can be used to identify clay (Dresser Atlas, 1979):

- 1.) Linear method
- 2.) Non-linear method

In this study, the linear method was used as a clay indicator because it was sufficient for this type of analysis. The following linear equation is used to determine the Gamma Ray index:

$$\text{Volume of shale (Vsh)} = \frac{\text{GR value (log)} - \text{GR}(\text{min})}{\text{GR}(\text{max}) - \text{GR}(\text{min})} \dots\dots\dots(5.1)$$

Where:

GR value (log) = GR log value reading of the formation

GR (min) = Lowest GR value (clean formation)

GR (max) = Maximum shale reading of the formation

The following parameters (**Table 5-1**) were used to estimate the clay volume.

Table 5- 1: Parameters for clay volume estimation

Well	GR max (API)	GR min (API)
F-AH1	172	20
F-AH2	184	12
F-AH4	172	16

Figures 5-1, 5-2 and 5-3 show the log-derived volume of the clay model for wells F-AH1, F-AH2, and F-AH4 respectively. Histogram plots of the Gamma Ray measurements were made on each well and the maximum and minimum readings of which were interpreted as shown in **Figures 5-4, 5-5 and 5-6**.

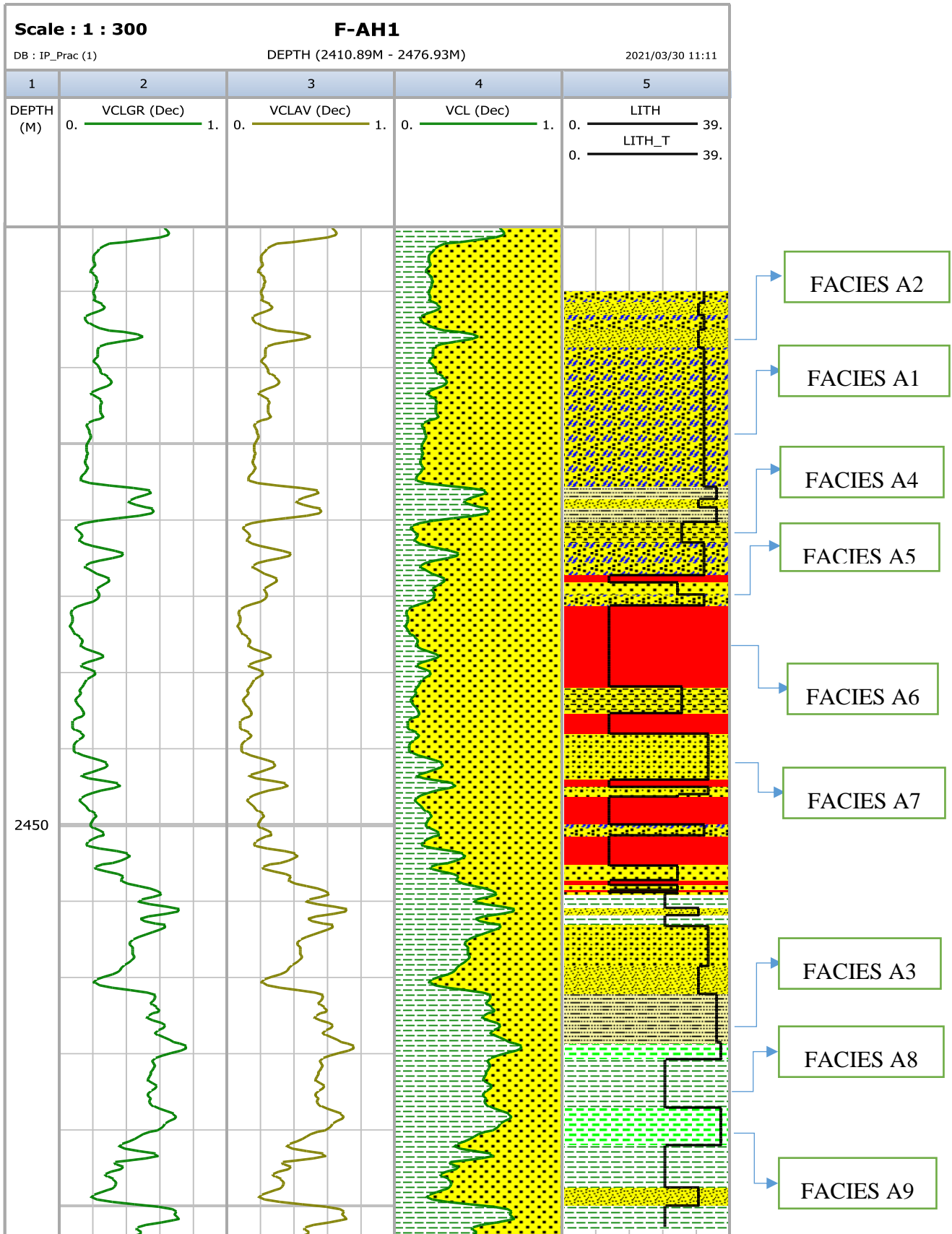


Figure 5- 1: Log-derived volume of clay models of well F-AH1

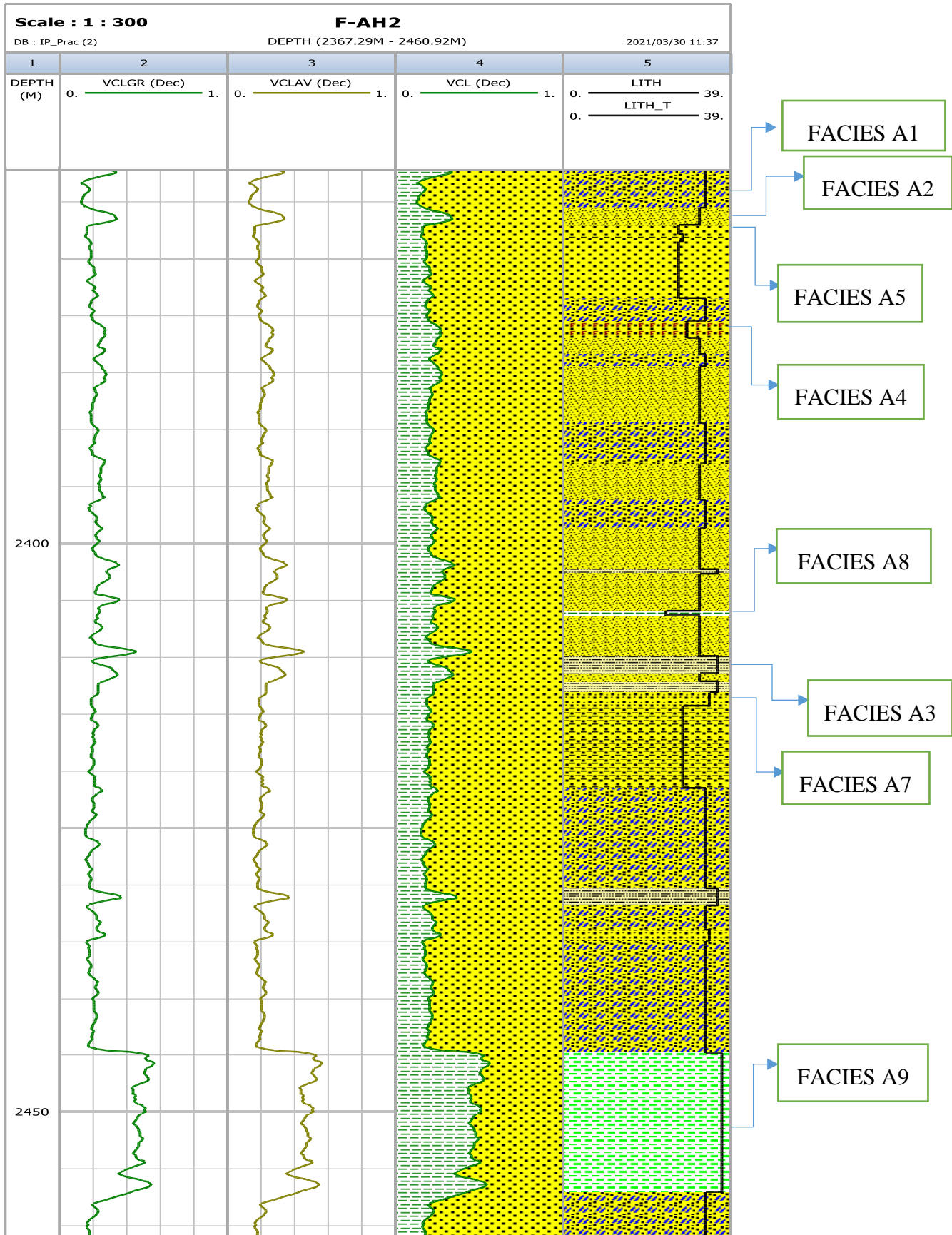


Figure 5- 2: Log-derived volume of clay models of well F-AH2

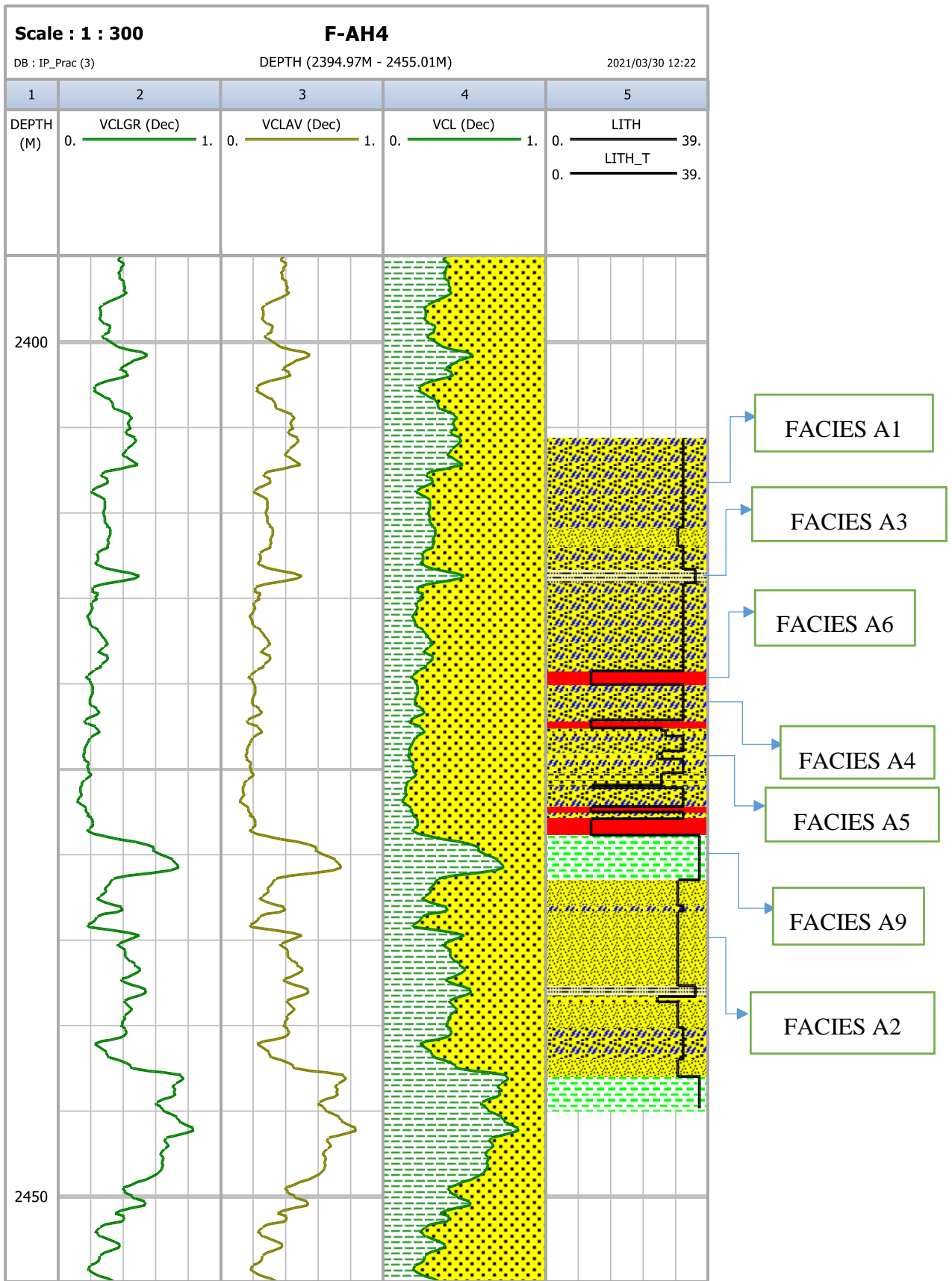


Figure 5- 3: Log-derived volume of clay models of well F-AH4

The clay model volumes for the study wells (F-AH1, F-AH2 and F-AH4) derived from the log data are based on the linear Gamma Ray method. The green VCLGR curve in track 2 represents the linear Gamma Ray method shown. The grey VCLAV curve in track 3 represents an average clay volume. However, the green-shaded left side of the VCL curve in trace 4 represents the clay volume of the formation, while the yellow-shaded right side of the VCL curve represents the sand influence of the formation.

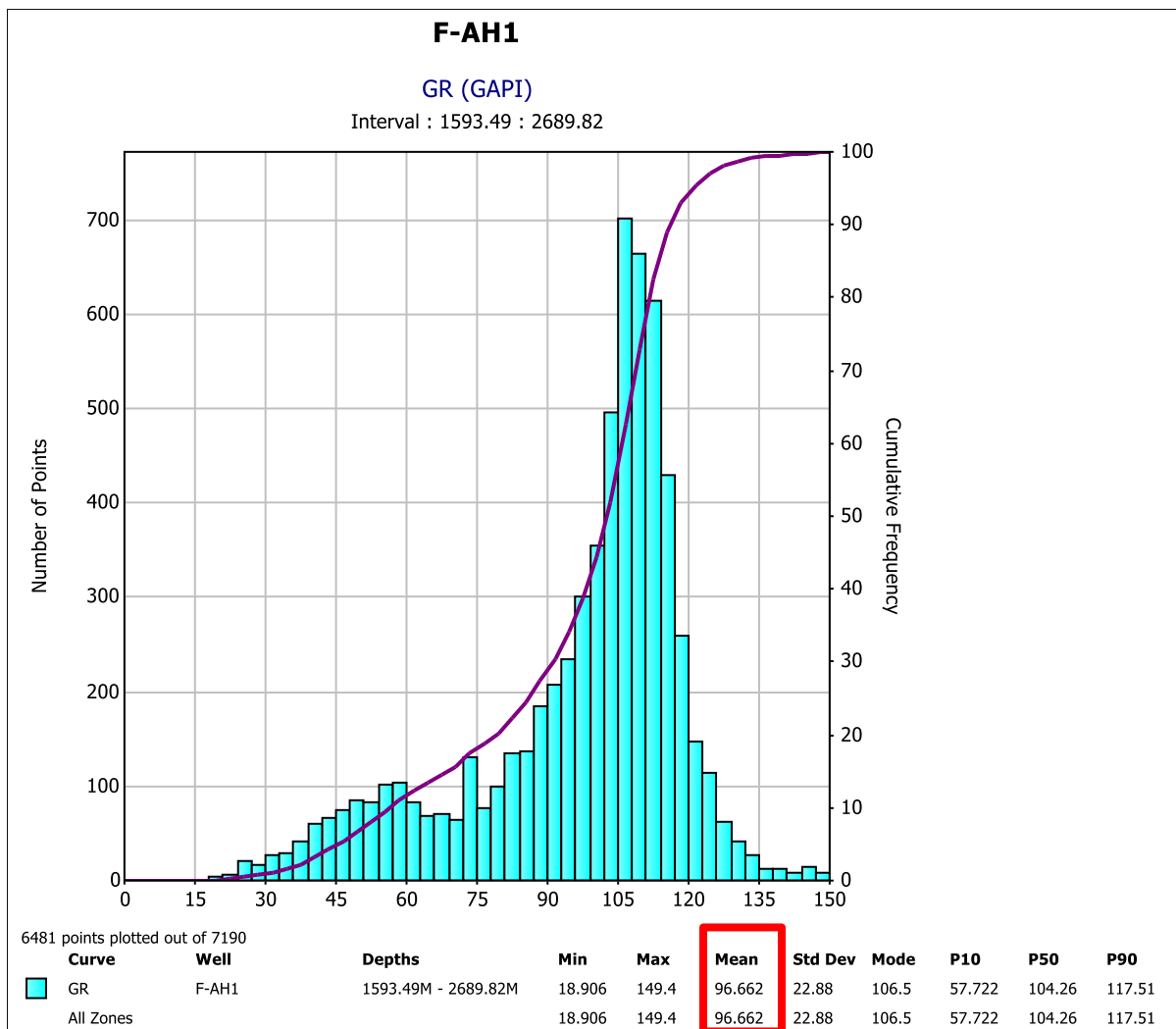


Figure 5- 4: Well F-AH1 Gamma Ray Histogram plot

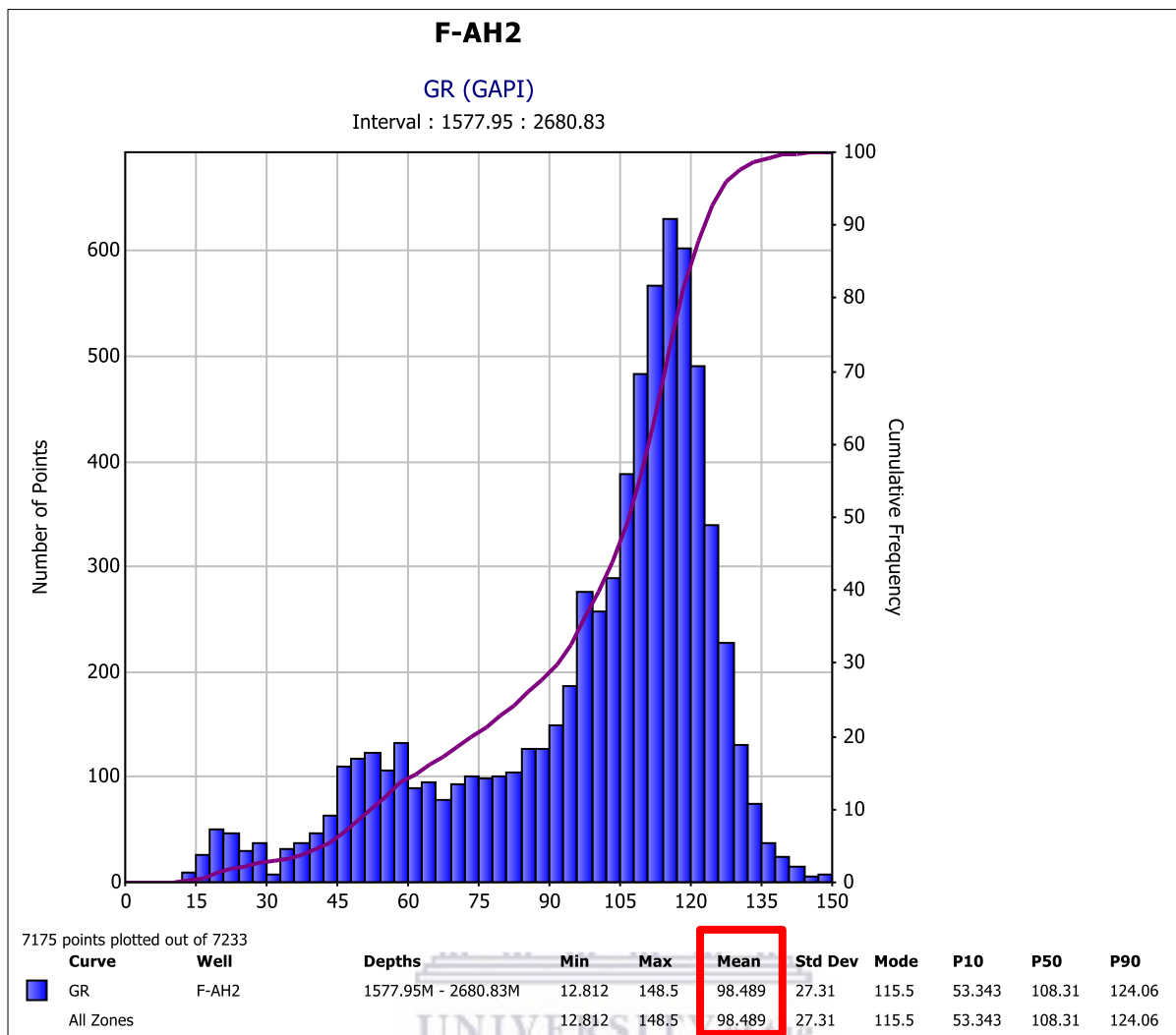


Figure 5- 5: Well F-AH2 Gamma Ray Histogram plot

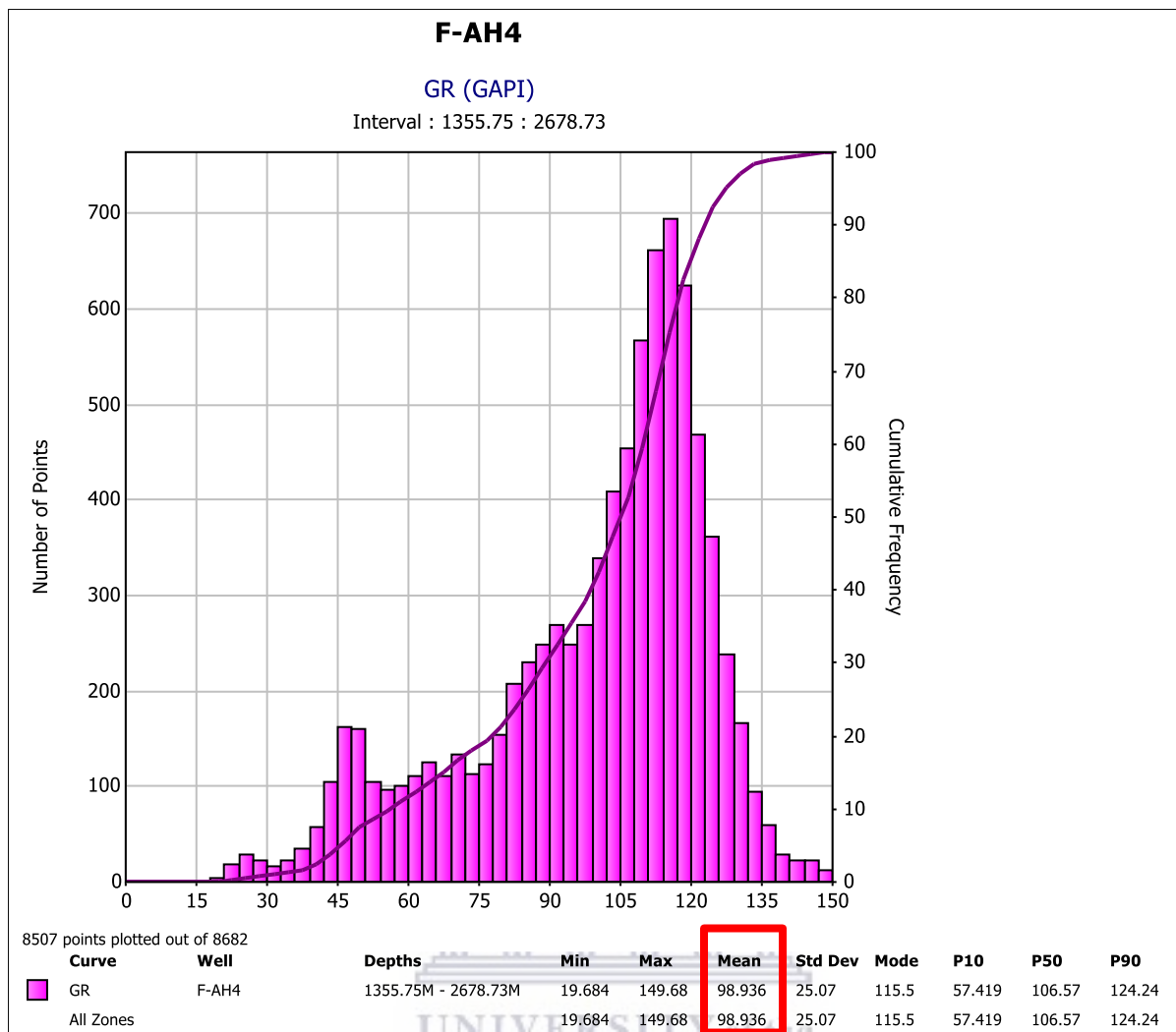


Figure 5- 6: Well F-AH4 Gamma Ray Histogram plot

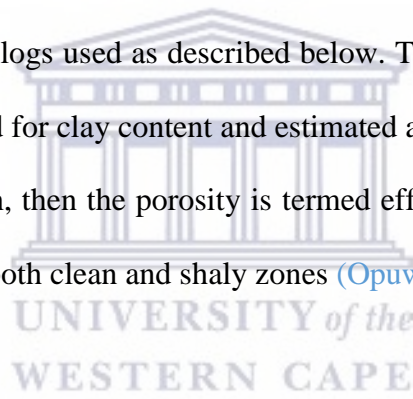
The Gamma Ray histogram plots for each of the wells (F-AH1, F-AH2 and F-AH4) showed the mean values of 96, 98 and 98 API, respectively. The baseline or cut-off line was obtained from the mean (API unit) of the histogram of Gamma Rays plotted for each of the wells.

5.2 DETERMINATION OF THE POROSITY

Porosity is an important rock property and can be expressed as the ratio or percentage of void space to solid rock (Lucia, 2007). Selly, 2000, defined porosity as the ratio of the pore space volume not occupied by the solid components to the total volume. The percentage or fraction of porosity is denoted by the Greek lowercase letter phi (ϕ) and can be expressed mathematically as:

$$\text{Porosity } (\phi) = \frac{\text{Volume of Voids}}{\text{Total volume of rock}} \times 100 \dots\dots\dots(5.2)$$

Various logs can be used in determining porosity and in this study, density, neutron and sonic logs were the porosity-derived logs used as described below. This log derived porosity (raw) must in most cases be corrected for clay content and estimated as total porosity and if the clay effect is removed by correction, then the porosity is termed effective porosity. However, log porosity can be determined in both clean and shaly zones (Opuwari, 2010).



5.2.1 Porosity from Density Log

Wyllie, 1963 states that the porosity derived from the density log (Φ Density) is defined by the following relationships and expressed in the equation:

$$\Phi \text{ Density} = \frac{\rho_{matrix} - \rho_{log}}{\rho_{matrix} - \rho_{fluid}} \dots\dots\dots(5.3)$$

Where:

Φ Density = Porosity derived from Density log

ρ_{matrix} = Matrix/grain density measured by the tool

ρ_{log} = Bulk density measured by the tool

ρ_{fluid} = Fluid density

Fluid mud densities vary with the type of fluid and pressure in the formation at the time and maybe freshwater mud (1 g/cc), saltwater mud (1.1 g/cc), or gas mud (0.7 g/cc) and the most commonly encountered reservoir rocks are sandstone, limestone, and dolomite with typical matrix densities of 2.65 g/cc, 2.71 g/cc, and 2.87 g/cc, respectively.

Dresser Atlas, 1979 states that the formation may contain a significant amount of shale and can therefore be accounted for using the following equation:

$$\Phi_{DenCorr} = \frac{\rho_{matrix} - \rho_{log}}{\rho_{matrix} - \rho_{fluid}} - V_{sh} \frac{\rho_{matrix} - \rho_{shale}}{\rho_{matrix} - \rho_{fluid}} \dots \dots \dots (5.4)$$

Where:

$\Phi_{DenCorr}$ = Porosity derived from Density corrected for shale effect

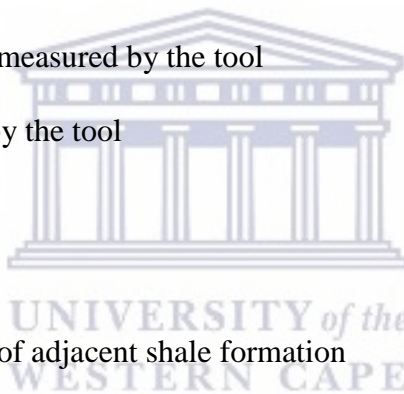
ρ_{matrix} = Matrix/grain density measured by the tool

ρ_{log} = Bulk density measured by the tool

ρ_{fluid} = Fluid density

V_{sh} = Volume of shale

ρ_{shale} = Density measurement of adjacent shale formation



5.2.2 Porosity from Neutron Log

A neutron log is a porosity log that measures the hydrogen ion concentration in a formation influenced by borehole impacts and mineralogy and is popular in combination with a density log for estimating total porosity. According to Hamada and Abushanab, 2008, the method is typically used in the gas reservoir to compensate for the effect of gas on neutron and density logs. The effect of shale on the neutron log can be corrected by the following equation:

$$\Phi_{Ncorr} = \Phi_{Nlog} - V_{sh} \times \Phi_{Nsh} \dots \dots \dots (5.5)$$

Where:

ΦN_{corr} = Corrected neutron porosity

ΦN_{log} = Neutron log reading of the interval

V_{sh} = Volume of shale

ΦN_{sh} = neutron log reading of the adjacent shale formation

5.2.3 Porosity from Sonic (acoustic) Log

The sound log is time dependent for a sound wave to traverse a foot of the formation and depends on lithology and porosity. The following equations may be required to calculate sonic porosity in consolidated and compacted formations (Wyllie et al., 1958).

Wyllie Time – Average Equation:

$$\Phi_{sonic} = \frac{DT - DT_{Ma}}{DTF1 - DT_{Ma}} * \frac{1}{B_{cp}} \dots \dots \dots (5.6)$$

Where:

Φ_{sonic} = Porosity derived from sonic/acoustic log

DT = Acoustic travel time from the log

DT_{Ma} = Acoustic travel time in matrix

B_{cp} = Compaction correction = $DT_{Shale}/100 > 1$

Raymer-Hunt Gardner (1980) equation:

$$\Phi_{sonic} = \frac{5}{8} * \frac{DT - DT_{Ma}}{DT} \dots \dots \dots (5.7)$$

Where:

Φ_{sonic} = Porosity derived from sonic/acoustic log

DT = Acoustic travel time from the log

DT_{Ma} = Acoustic travel time in matrix

Hilchie, 1978, proposed the following empirical correction for the hydrocarbon effects on sound-derived porosity in a gas formation:

$$\Phi_{corr} = \Phi_{sonic} * 0.7 \dots \dots \dots (5.8)$$

5.2.4 Effective Porosity

Effective porosity is when the total effect is removed by correction (Opuwari, 2010). It excludes all bound water associated with clays but includes all associated pores in the pore system that may contribute to flow. In this study, the effective porosity was determined using the density protocol and is expressed by the following equation:

$$Eval\ Phie = \left(\frac{\rho_{ma} - \rho_{log}}{\rho_{ma} - \rho_{fl}} \right) - V_{clay} * \left(\frac{\rho_{ma} - \rho_{clay}}{\rho_{ma} - \rho_{fl}} \right) \dots \dots \dots (5.9)$$

Where:

Eval Phie = Effective porosity from density log

ρ_{ma} = Matrix density (g/cc) from core

ρ_{log} = Log bulk formation density (g/cc)

A summary of the parameters used for effective porosity calculation for the study wells is presented in **Table 5-2**.

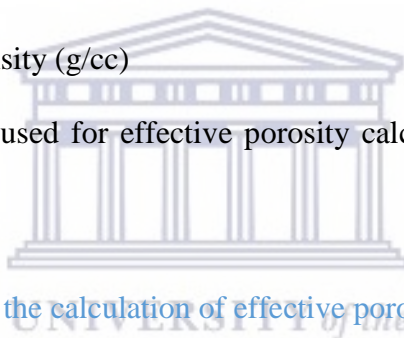


Table 5- 2: Parameters used for the calculation of effective porosity

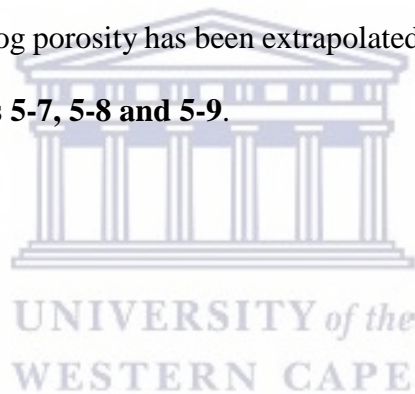
	PARAMETERS				
WELL	MATRIX DENSITY $\rho_{ma}(g/cc)$	CLAY (g/cc)	WATER DENSITY (g/cc)	HYDROCARBON DENSITY(g/cc)	Vclay (v/v)
F-AH1	2.65	2.58	1	0.2	VCLGR
F-AH2	2.67	2.54	1	0.2	VCLGR
F-AH4	2.65	2.59	1	0.2	VCLGR

The matrix density (ρ_{ma}) measurements were only available for well F-AH4, while at room conditions the matrix density values for wells F-AH1 and F-AH2 were taken as average values

from special core analysis reports. The fluid densities for water and gas were taken as constants of 1 g/cm³ and 0.2 g/cm³, respectively, while the sound volume (VGLGR) was estimated from the Gamma Ray log using the linear method.

5.2.5 Comparison of Log and Core Porosity

The log-derived porosities were calibrated with the conventional core and the overburden-corrected core properties were measured. The comparison of the log and core-derived porosities aims to identify a log curve that best fits the core-derived porosities. Core porosity measurements are only available for the core intervals of interest, while the log-derived porosity curve that best fits the core porosity, therefore represents the best overall estimate of porosity for the entire well, as log porosity has been extrapolated beyond the core interval. The results are presented in **Figures 5-7, 5-8 and 5-9.**



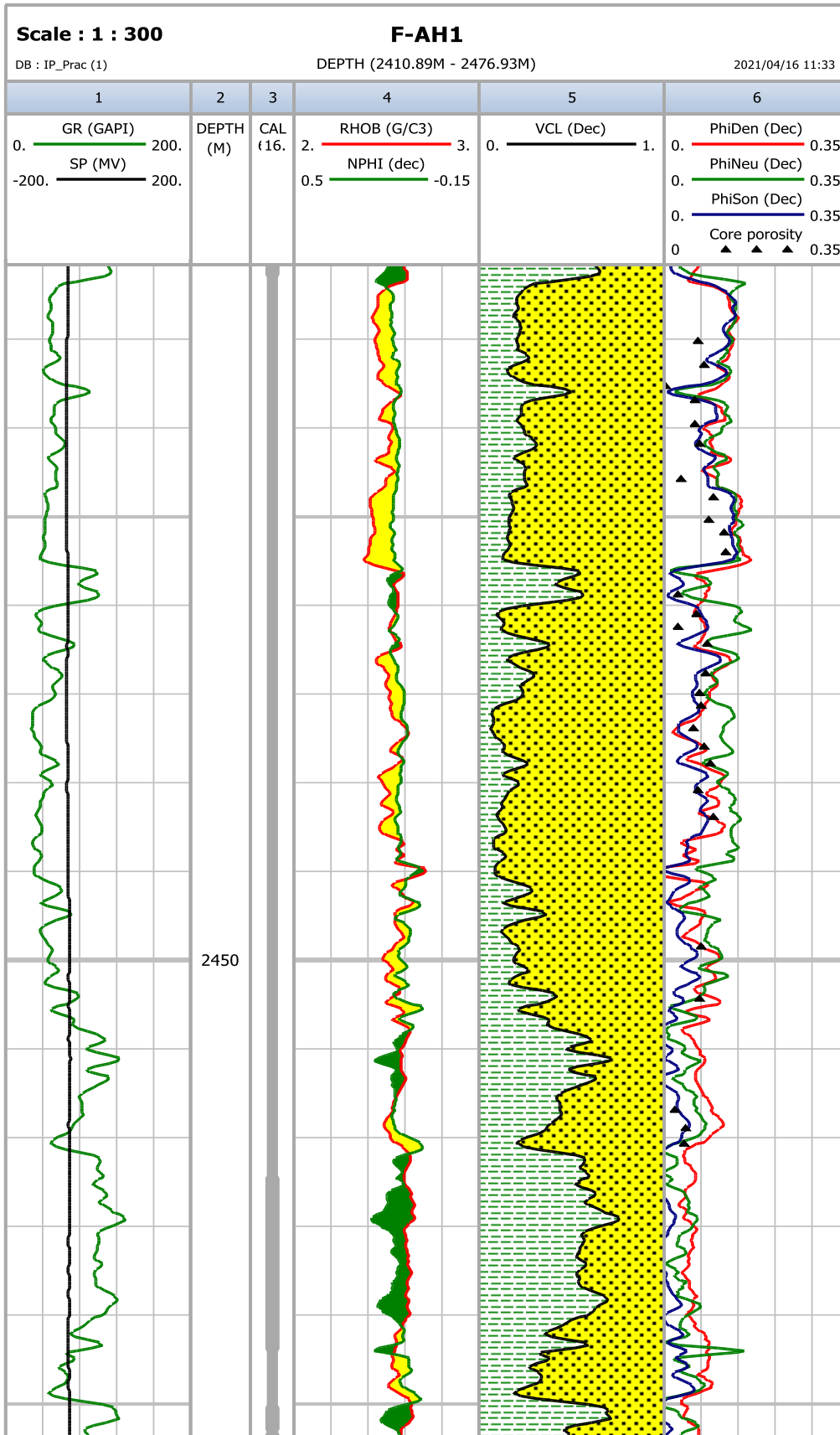


Figure 5- 7: Well F-AH1 comparison of log and core porosity

Track 6 in **Figure 5-7** shows the log-derived porosity from the density (Phi-Density- red curve), neutron porosity (PhiNeu- green curve), and sonic porosity (PhiSon- blue curve), as well as the overburden, corrected porosity measurements (core porosity- black triangles). The plot for well F-AH2 is presented in **Figure 5-8**.



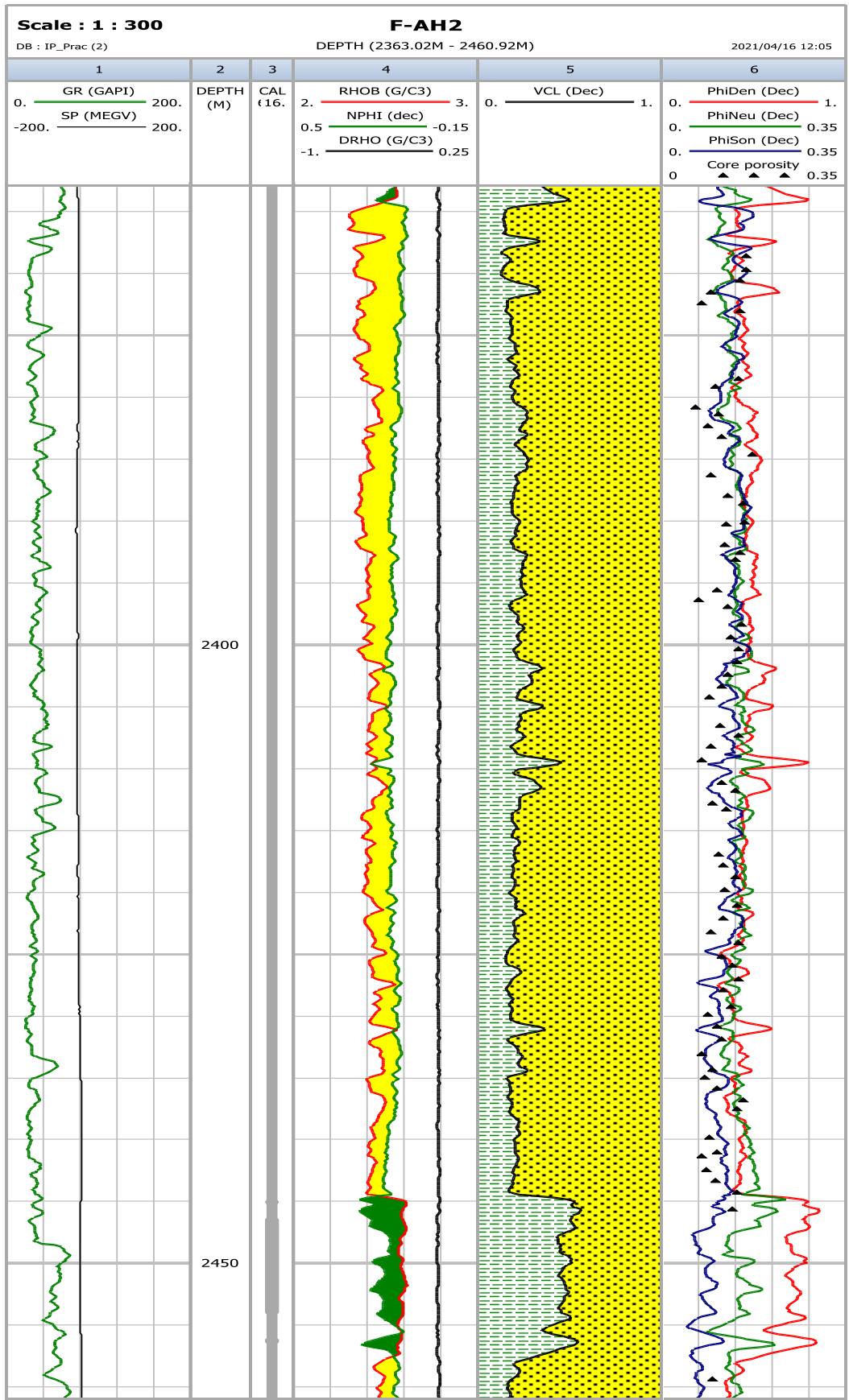


Figure 5- 8: Well F-AH2 comparison of log and core porosity

In track 6 of **Figure 5-8**, the log of density porosity (PhiDen red curve), neutron porosity log (PhiNeu green curve) and sonic porosity (PhiSon blue curve) are plotted. The porosity logs were plotted against the overburden corrected porosity or core porosity measurements (solid triangles) for comparison. The plot for well F-AH4 is presented in **Figure 5-9**.



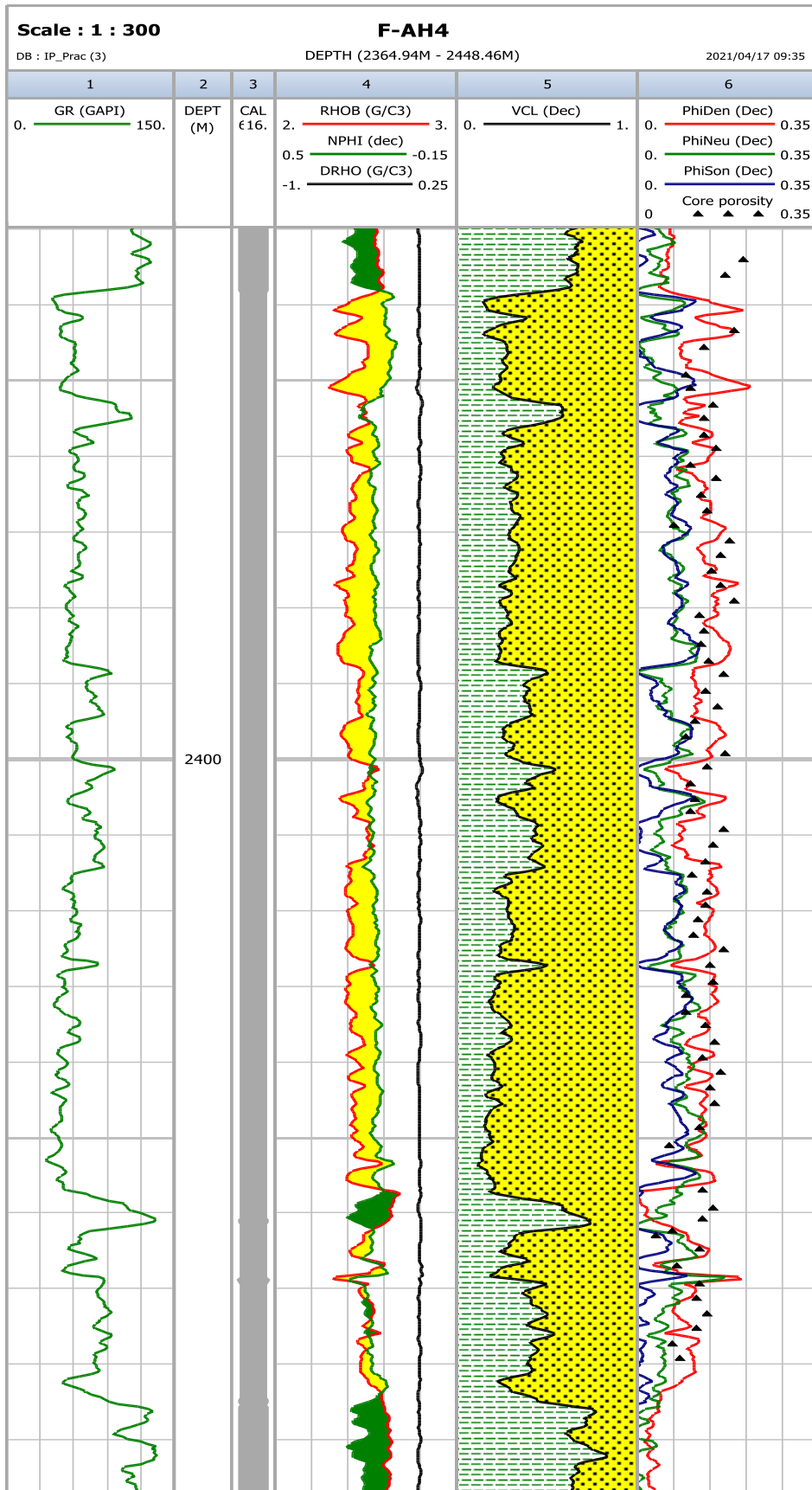


Figure 5- 9: Well F-AH4 comparison of log and core porosity

Track 6 in **Figure 5-9** shows the log-derived porosity from the density (Phi-Density- red curve), neutron porosity (PhiNeu- green curve), and sonic porosity (PhiSon- blue curve), as well as the overburden, corrected porosity measurements (core porosity- black triangles). The resulting interpretation was a selection of a porosity log curve that best matched the overburden corrected measurements in each of the F-AH wells.

5.3 PERMEABILITY

Permeability is the property of a reservoir rock characterized by the flow of fluid through its interconnected pore spaces and its conductivity measured. Permeability can be estimated using data from porosity, resistivity, water saturation, and hydrocarbon density. Permeability is calculated or determined but can be measured vertically or horizontally. Vertical permeability is measured across the bedding plane, while horizontal permeability is measured parallel to the bedding plane structure. Vertical permeability is generally lower than horizontal permeability and grain sorting and size are more susceptible to vertical changes with depth.

Therefore, horizontal permeability is widely used and according to [Halliburton, 2001](#), most permeability calculations are made from horizontal measurements. In this study, the core permeability and the estimated permeability curve are derived from the cross plot of the core porosity versus the core permeability because the comparison of the core permeability and the derived permeability is an important analysis as it allows the log-generated data to be calibrated with the actual core measurements ([Parker, 2014](#)).

5.3.1 Permeability from Core Analysis (Porosity-Permeability Crossplot)

The permeability from the core analysis section provides a correlation between the core permeability and Log porosity measurements. Estimating and forecasting the permeability in non-cored interval sections of the wells are the main objectives and then the estimated

permeability curve is generated in each well section and later compared to the core permeability results. **Figures 5-10, 5-11, 5-12 and 5-13** show the core porosity-permeability cross plots for wells F-AH1, F-AH2 and F-AH4. In this study, the core permeability distribution across all studied wells ranged from 0.001 mD to 2767 mD. Hydrocarbon was recorded within the core intervals of the well. Average hydrocarbon saturations of 3%, 1.1% and 0.2% were encountered in wells F-AH1, F-AH2 and F-AH4.



WELL F-AH1

Porosity versus permeability & facies plot

Interval : 2415 : 2474

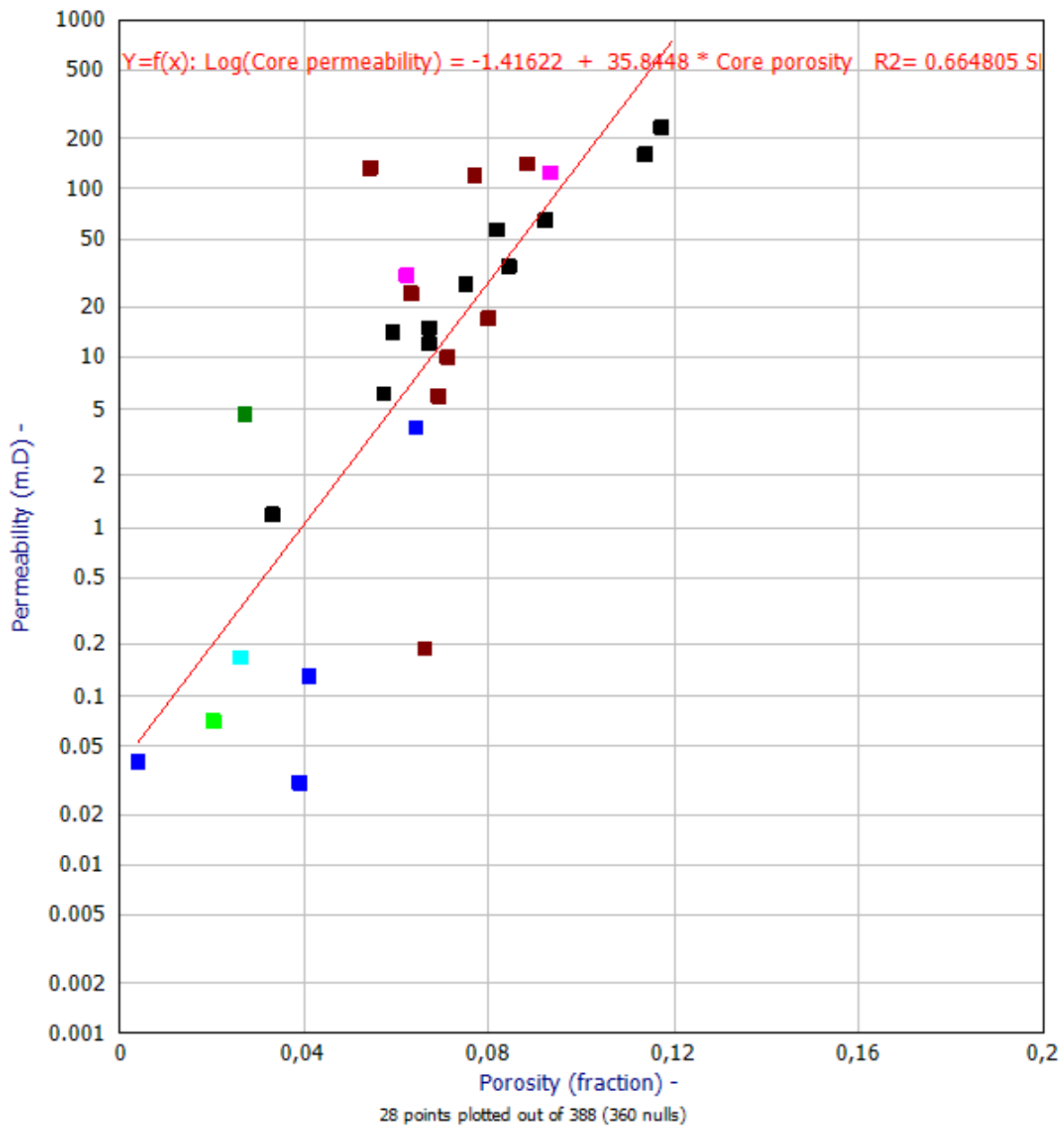


Figure 5- 10: Porosity-permeability cross-plot relationships for well F-AH1

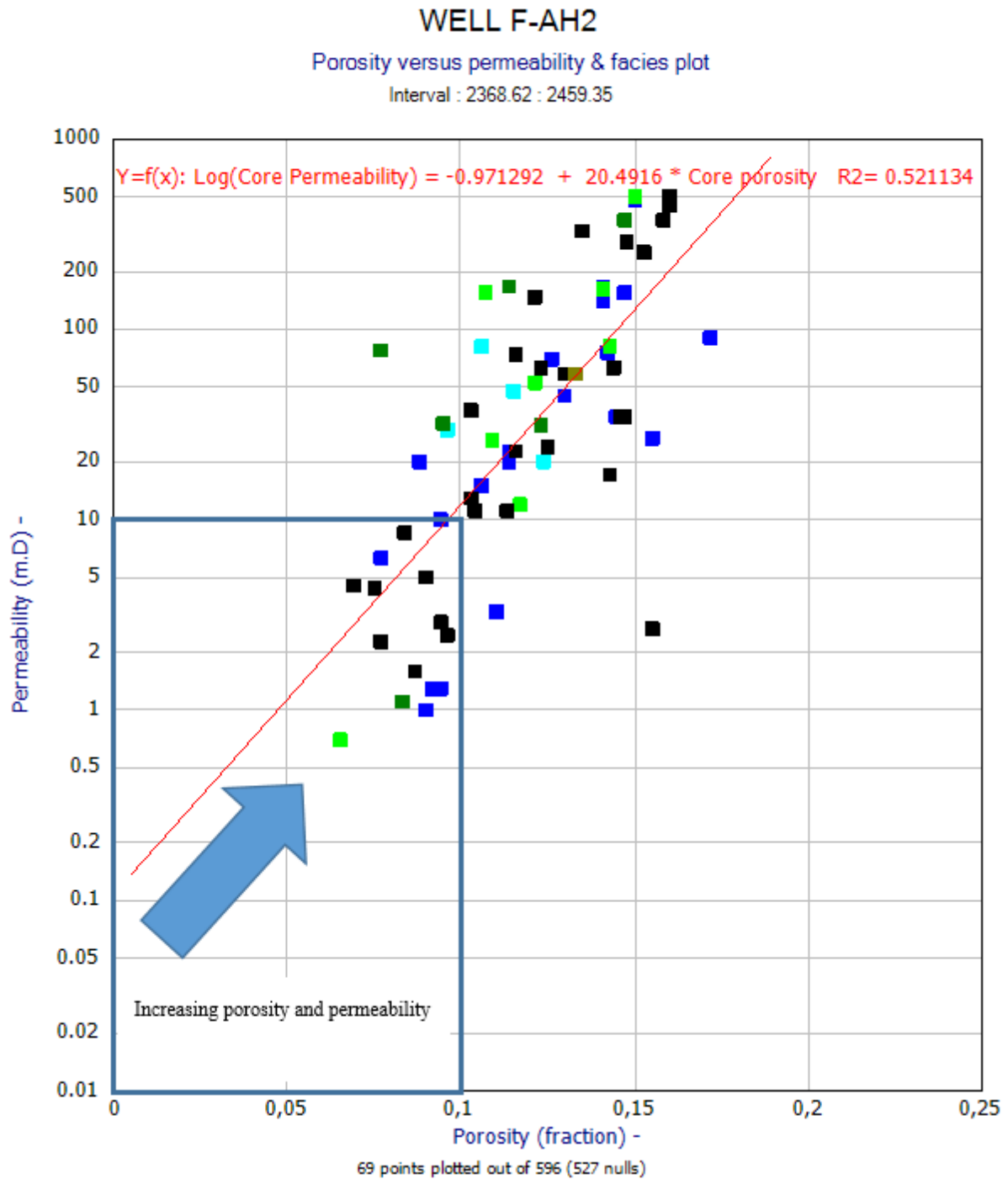


Figure 5- 11: Porosity-Permeability cross-plot relationships for well F-AH2

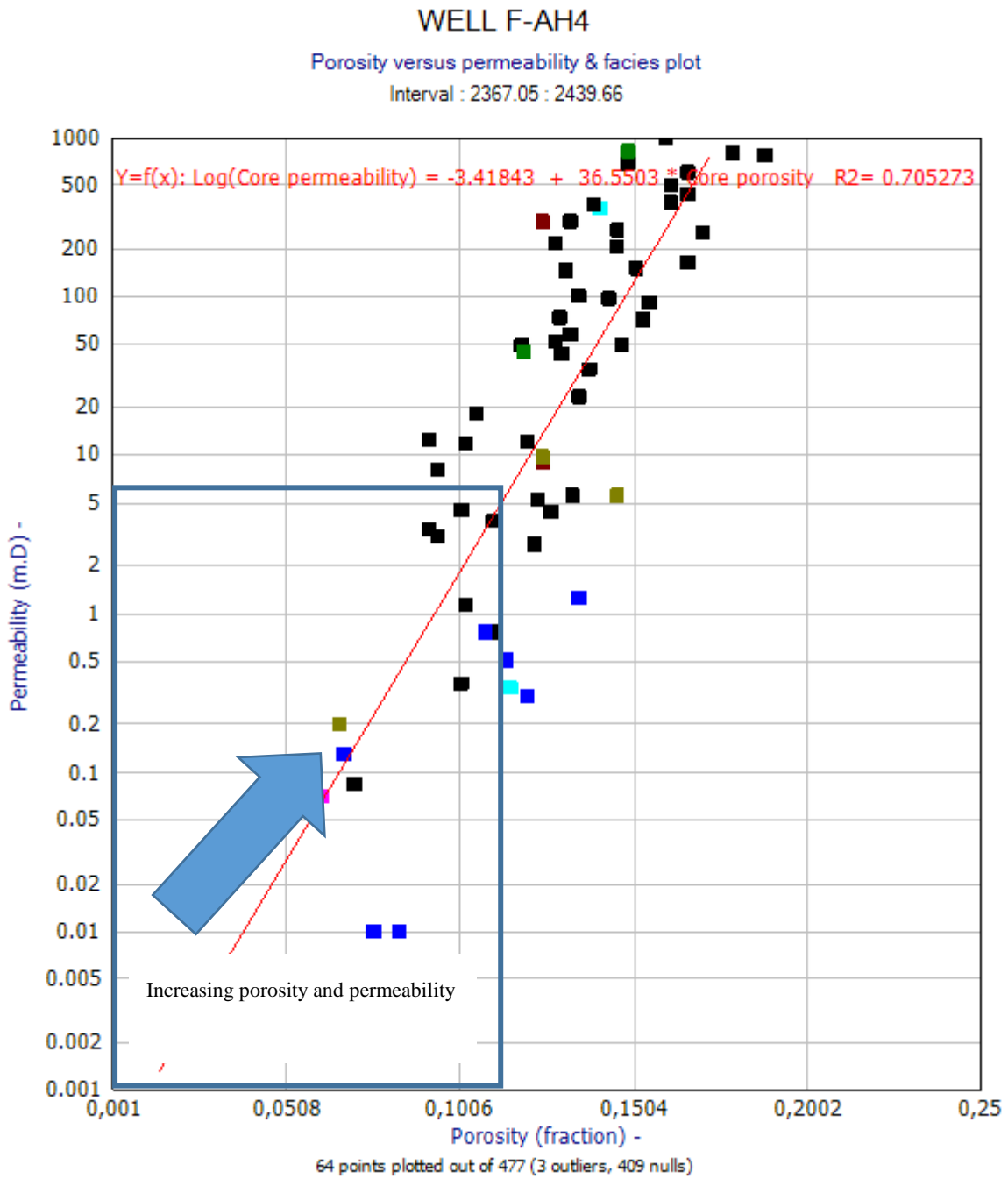


Figure 5- 12: Porosity-permeability cross-plot relationships for well F-AH4

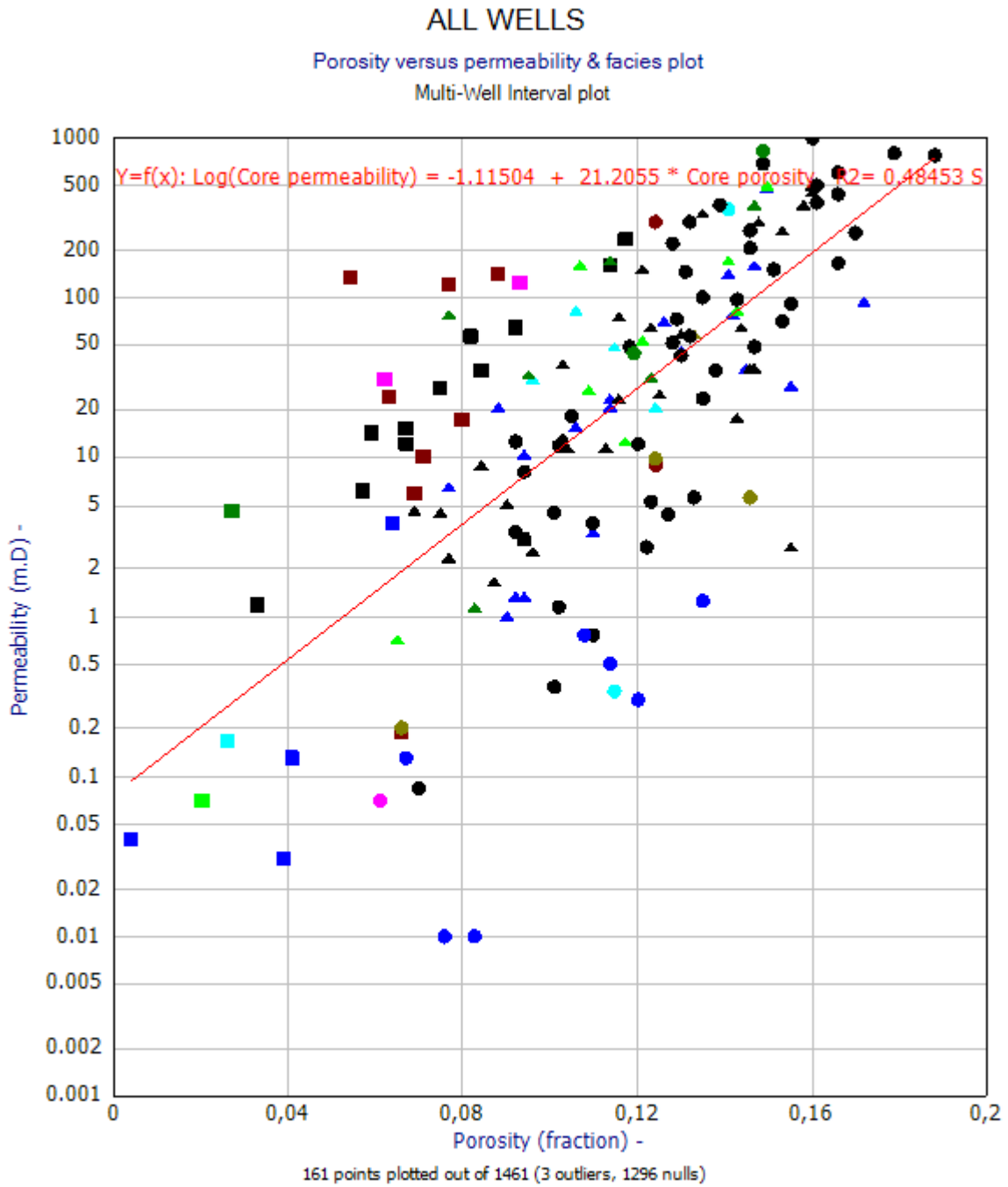


Figure 5- 13: Porosity-permeability cross-plot relationships for all wells

5.3.2 Comparison of Estimated Log Permeability with Core Permeability

Table 5- 3: Porosity-permeability functions per wells

Well	Porosity-permeability function	Correlation coefficient (R ²)
F-AH1	$\text{Log}(K) = -1.41622 + 35.8448 * \text{Porosity}$	0.6648
F-AH2	$\text{Log}(K) = -0.971292 + 20.4916 * \text{Porosity}$	0.5211
F-AH4	$\text{Log}(K) = -3.41843 + 36.5503 * \text{Porosity}$	0.7053
ALL WELLS	$\text{Log}(K) = -1.11504 + 21.2055 * \text{Porosity}$	0.4845

The functions in **Table 5-3** were used to generate the predicted permeability curve for each well and validated against core permeability. The primary objective of the Estimated Permeability was to identify permeability throughout the well as core measurements are limited to only the core interval. The comparison of the predicted permeabilities (red curve in tract 6) along with the core permeability (green squares in tract 6) for wells F-AH1, F-AH2 and F-AH4, respectively, are shown in **Figures 5-14, 5-15 and 5-16**.

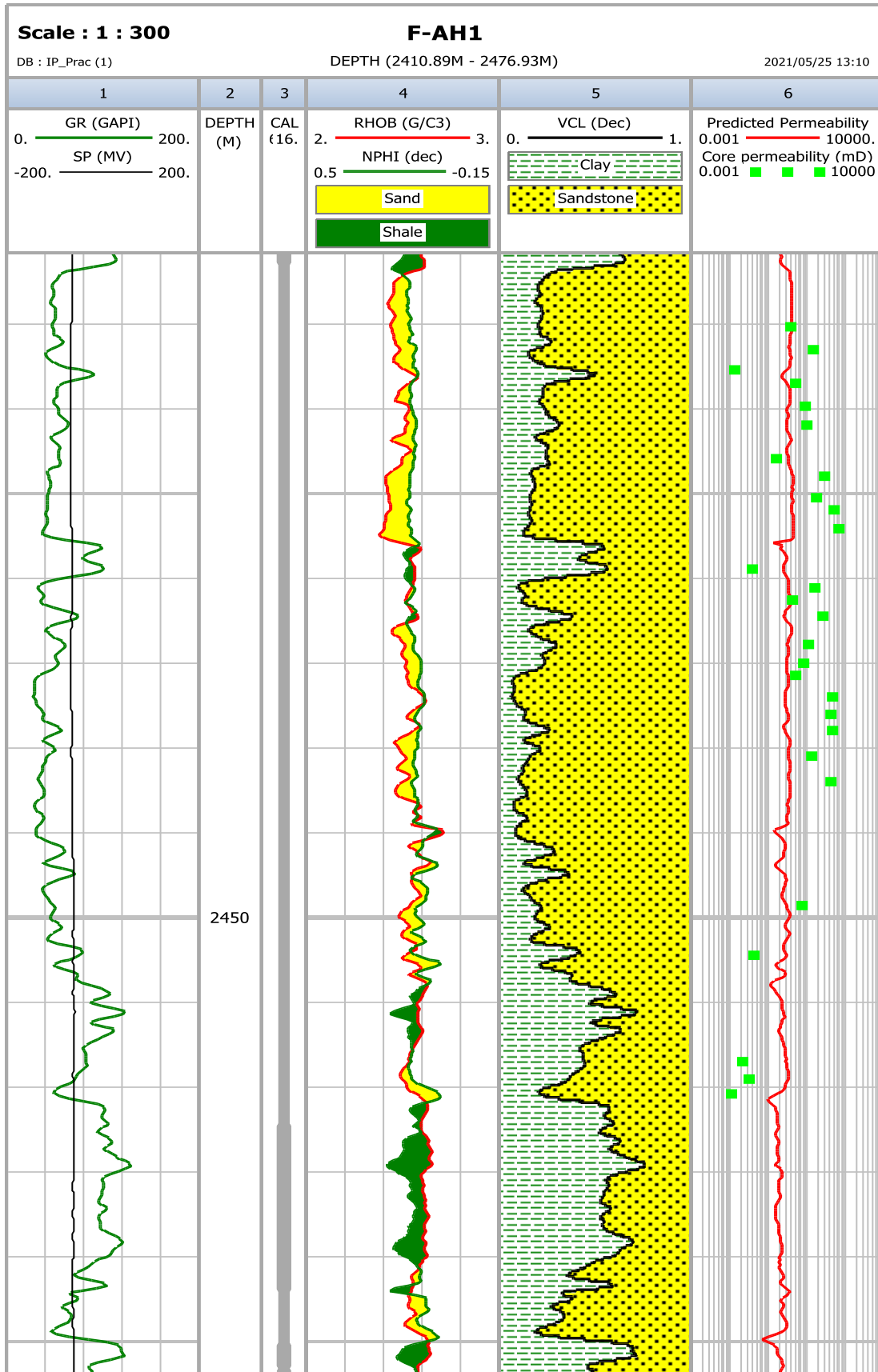


Figure 5- 14: Predicted permeability together with core permeability for Well F-AH1

In well F-AH1 (**Figure 5-14**), the predicted permeability values in tract 6 (red) from the porosity-permeability function were broadly consistent with the core permeability results (tract 6 green dots). The predicted permeability plot for well F-AH2 is shown in **Figure 5-15**.



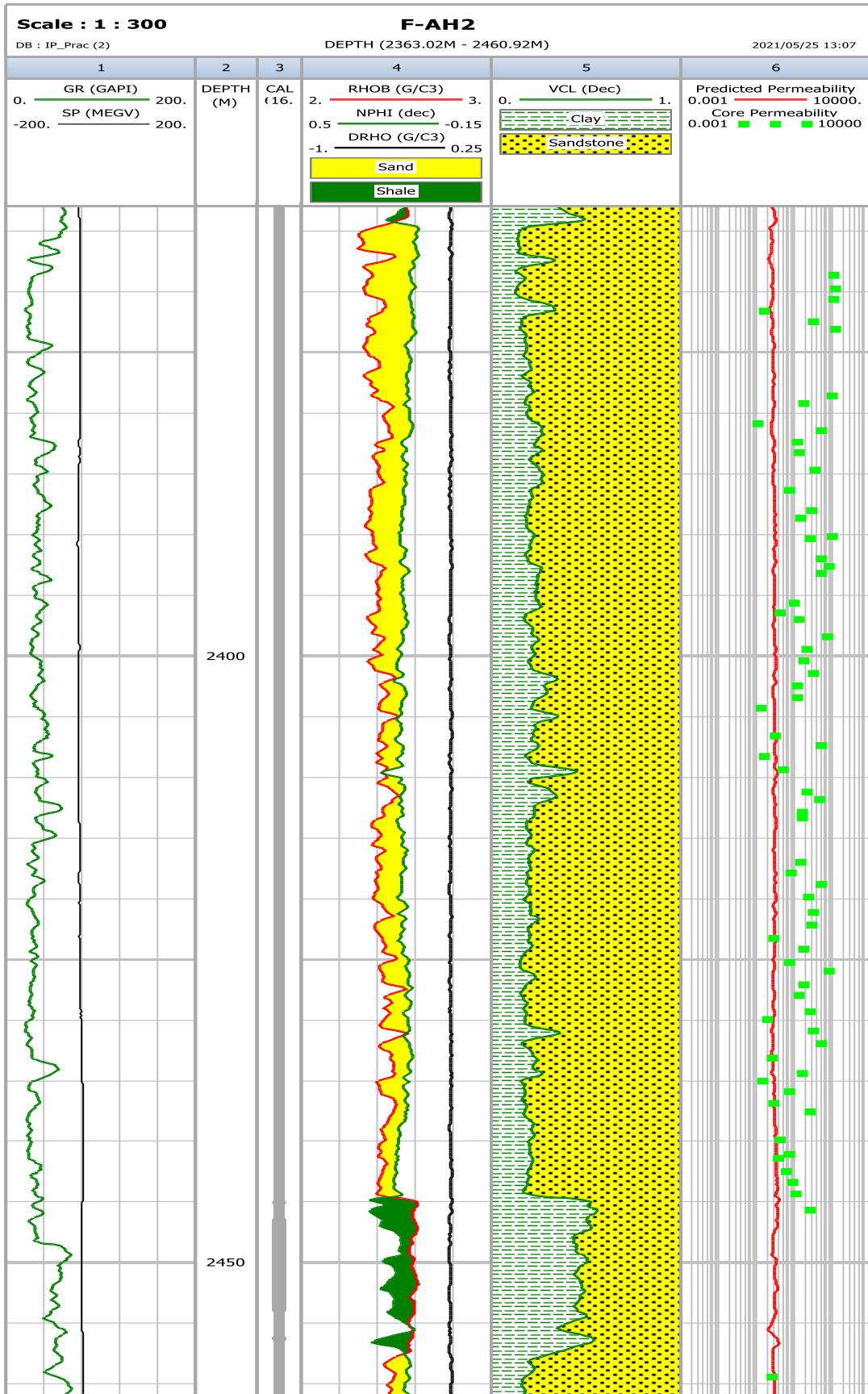


Figure 5- 15: Predicted permeability together with core permeability for Well F-AH2

For well F-AH2 (**Figure 5-15**), the predicted permeability values in tract 6 (red) from the porosity-permeability function were broadly consistent with the core permeability results (tract 6 green dots). **Figure 5-16** shows the predicted permeability plot for well F-AH4.



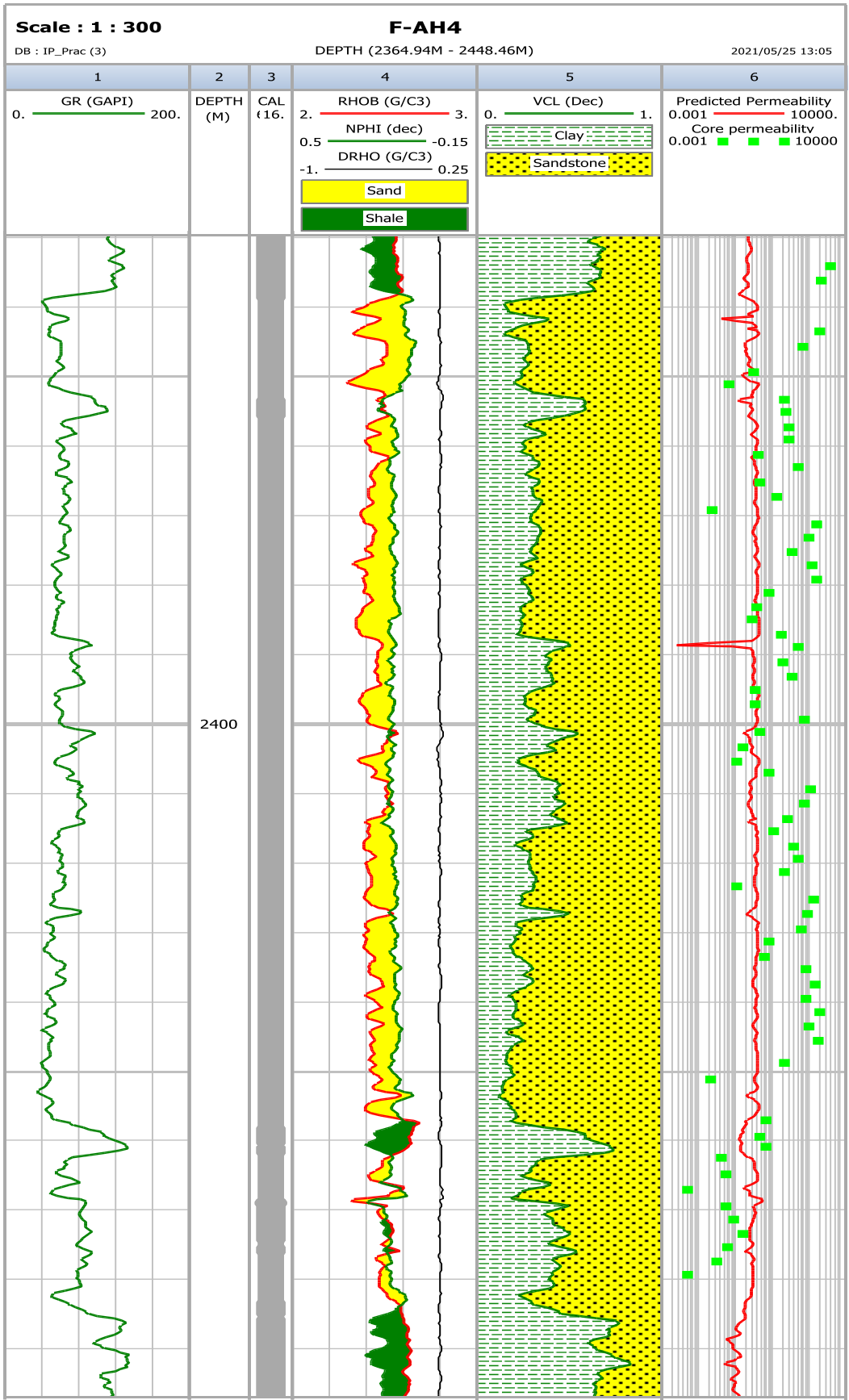


Figure 5- 16: Predicted permeability together with core permeability for Well F-AH4

In well F-AH4 (**Figure 5-16**), the predicted permeability values in track 6 (red) from the porosity-permeability function were broadly consistent with the core permeability results in track 6 (green dots). Wells (F-AH1, F-AH2 and F-AH4) used to construct permeability estimation curves generally showed an acceptable correlation to core permeability results. Because the log-generated curves are models and relied on correlation equations to estimate permeability, areas of discrepancy between the estimated and core-derived permeabilities were evident and expected. In summary, the permeability for the non-cored intervals was estimated from the permeability of the core porosity and is within an acceptable level of correlation and confidence. A set of core and log permeability estimates for each well are presented in **Appendix 2**.



5.4 WATER SATURATION MODEL

Water saturation is an essential parameter in the evaluation of reservoir rocks and formations. It can be determined from the calibration of core data using a log-derived water saturation model, although other methods can be used to determine water saturation in a formation and these include cable logs and core data etc. Water saturation of reservoir rocks for log-derived curves was grouped into two models: shaly-sand and clean-sand (shale-free) models. In this study, the shale-sand models were determined from Simandoux and Indonesia models and the clean-sand model was determined from the Archie relationship

5.4.1 Parameters

5.4.1.1 Formation Temperature Determination

The static formation temperature in this study was taken at the bottom of the well report for each well and then loaded into the Interactive Petrophysics (IP 4.7) 2021 workstation to calculate and generate a temperature gradient. These temperature calculations were output as temperature curves for later use in the Formation Water Resistivity from SP (Self Potential) log calculations.

5.4.1.2 Determination of Formation Water Resistivity (R_w)

Formation temperature is needed to accurately predict hydrocarbon saturation because the salinity of formation water is controlled by temperature. Therefore, the resistivity of the formation water decreases with increasing temperature. In this study, the Spontaneous Potential (SP) log was used to determine the Formation Water Resistivity

5.4.1.2.1 SP method for determination of formation water resistivity (Rw)

The static spontaneous potential of the log spontaneous potential (SP) in aquiferous clean sand can be used to estimate the water formation resistivity value. In this study, formation temperature was entered as a parameter and generated from the temperature gradient module in the Interactive Petrophysics (IP 4.7) 2021 workstation. The output curves are the water resistivity from the SP curve (RwSP) and the salinity curve. An example of an RwSp generated curve for well FAH1 is shown in **Figure 5-17**. The water resistance of SP (RwSP) and the formation salinity curves are shown in trace 5.



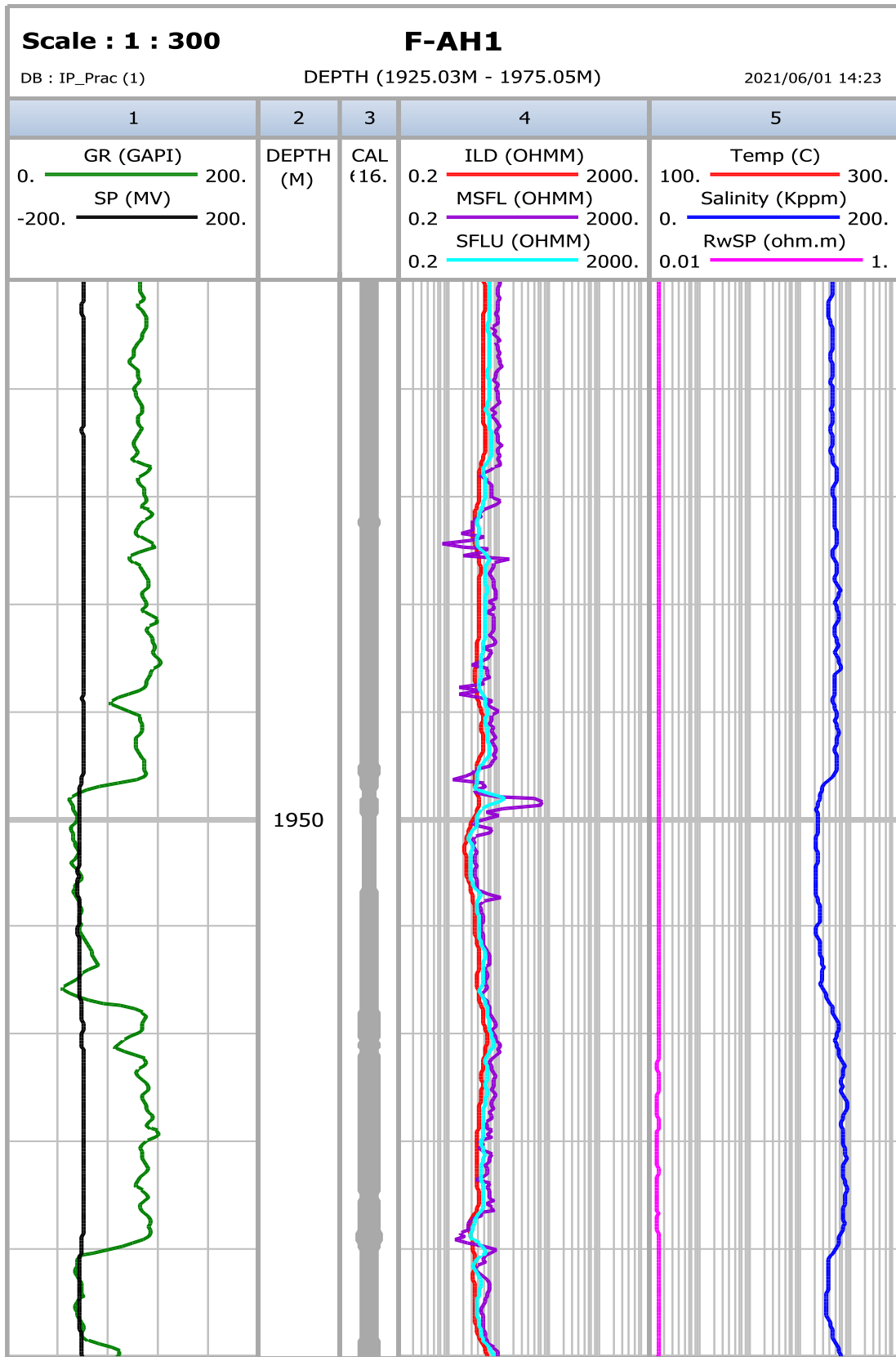


Figure 5- 17: Example of resistivity of water from SP method

5.4.2 Water Saturation (Sw) Models

Estimates of water saturation are required when evaluating the potential of a reservoir. Three (3) water saturation models (the clean Sand Archie model, Simandoux and the Indonesian model) were used in this study and the comparison of these models to best fit each well was analyzed below.

5.4.2.1 Clean Sand model

5.4.2.1.1 Archie's model

Archie (1942) provided the most used and popular clean sand model for electrical measurements and saturation. His model characterized the conductivity of a porous medium with a non-conductive matrix as a function of the porosity and the conductivity of the saturating fluids

Archie's equation is shown below.

$$S_w^n = R_w / (\phi^m * R_t) \dots\dots\dots(5.10)$$

Where:

S_w = Water saturation of the un-invaded zone

R_w = Formation water resistivity at formation temperature= 0.1 Ohm-m

R_t = True resistivity of the formation corrected for invasion, borehole, thin bed, and other effects

m = Cementation exponent

n = Saturation exponent

ϕ = Porosity

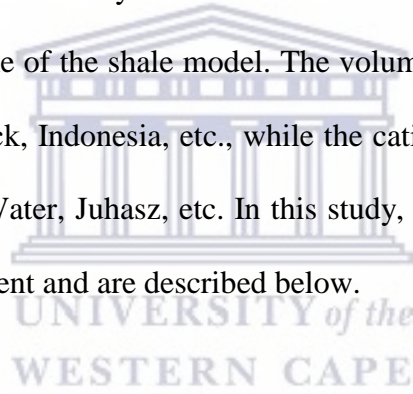
Table 5-4 shows the cementation exponent (m), and saturation exponent (n) taken as averages from the SCAL reports for wells F-AH1, F-AH2 and F-AH4.

Table 5- 4: Porosity –permeability functions per well

Well	Cementation Exponent (m)	Saturation Exponent (n)	Comment
F-AH1	1.79	1.69	Averages from SCAL report
F-AH2	1.68	1.78	Averages from SCAL report
F-AH4	1.77	1.81	Averages from SCAL report

5.4.2.2 Shaley-Sand models

In contrast to the Archie's model, the Shaley-Sand models consider the Formation water as well as the conductivity of shale. The Shaley sand models are divided into the cation exchange capacity models and the volume of the shale model. The volume of the shale model includes Simandoux, Fertl and Hammock, Indonesia, etc., while the cation exchange capacity models include Waxman-Smit, Dual-Water, Juhasz, etc. In this study, the Simandoux and Indonesia models were considered sufficient and are described below.



5.4.2.2.1 Simandoux model

Simandoux's (1963) model, based on the experimental work on homogeneous mixtures of sand and shale, expressed the following relationship:

$$S_w = \frac{aR_w}{2\phi^m} - \left(\frac{V_{sh}}{R_{sh}} + \sqrt{\left(\frac{V_{sh}}{R_{sh}}\right)^2 + \frac{4}{F}} * R_w * R_t \right) \dots \dots \dots (5.11)$$

S_w = Water saturation

a = Equation coefficient

R_w = Resistivity of water

m = cementation exponent

ϕ = Effective porosity in fraction

V_{sh} = Volume of shale

R_{sh} = Resistivity of shale

F = Formation resistivity factor

R_t = True formation resistivity from corrected deep resistivity log.

5.4.2.2.2 Indonesian model

Poupon and Leveaux (1971) proposed the above empirical model based on the properties of high shale freshwater present in the Indonesian Formation. The empirical relationship was described as follows:

$$\frac{1}{\sqrt{R_t}} = \frac{\sqrt{\Phi_e^m}}{a \cdot R_w} + \frac{V_{cl}^{(1-V_{cl}/2)}}{\sqrt{R_{cl}}} * S_w^{n/2} \dots\dots\dots(5.12)$$

Where:

R_t = Resistivity curve from deep log reading

R_{cl} = Resistivity of wet clay

Φ_e = Effective porosity

S_w = Water saturation, fraction

V_{cl} = Volume of shale, fraction

R_w = Formation water resistivity

m = Cementation exponent

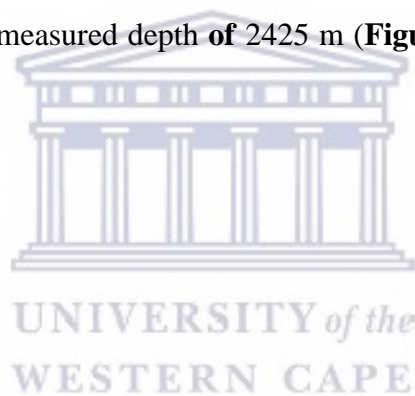
a = Tortuosity factor

n = Saturation exponent



5.4.3 Comparison of Conventional Core and Log-Derived Water Saturation

Water saturation was estimated by three (3) focal methods and compared per well. In this study, the estimation aimed to define which log-derived curve (Archie, Simandoux, or Indonesian) best fitted the conventional core and free-water saturation measurements. The conventional core water saturation measurements and log-calculated water saturation models were provided for the three wells (F-AH1, F-AH2 and F-AH4). The Interactive Petrophysics (IP 4.7) 2021 software used in this study only generates the log water saturation models for intervals that have been flagged as reservoir zones. Calculated water saturation models of the three (3) wells studied comparing the conventional core and free water saturation measurements are shown in **Figures 5-18, 5-19, 5-20 and 5-21**. In this study, one possible gas-water contact (GWC) was identified in well F-AH 1 at a measured depth of 2425 m (**Figures 5-18**). This result will be confirmed with the log data.



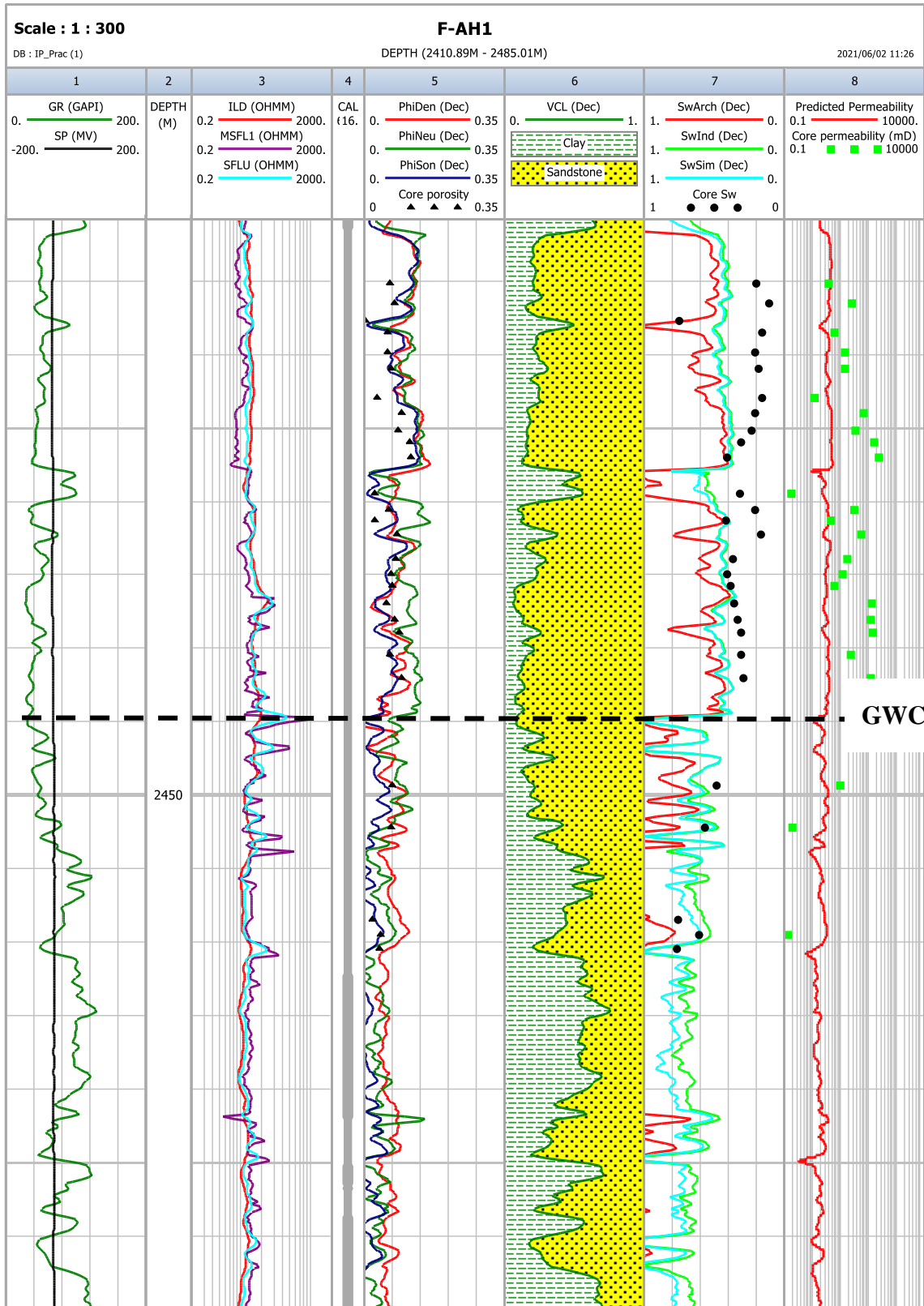


Figure 5- 18: Comparison of core and log water saturation models for well F-AH1

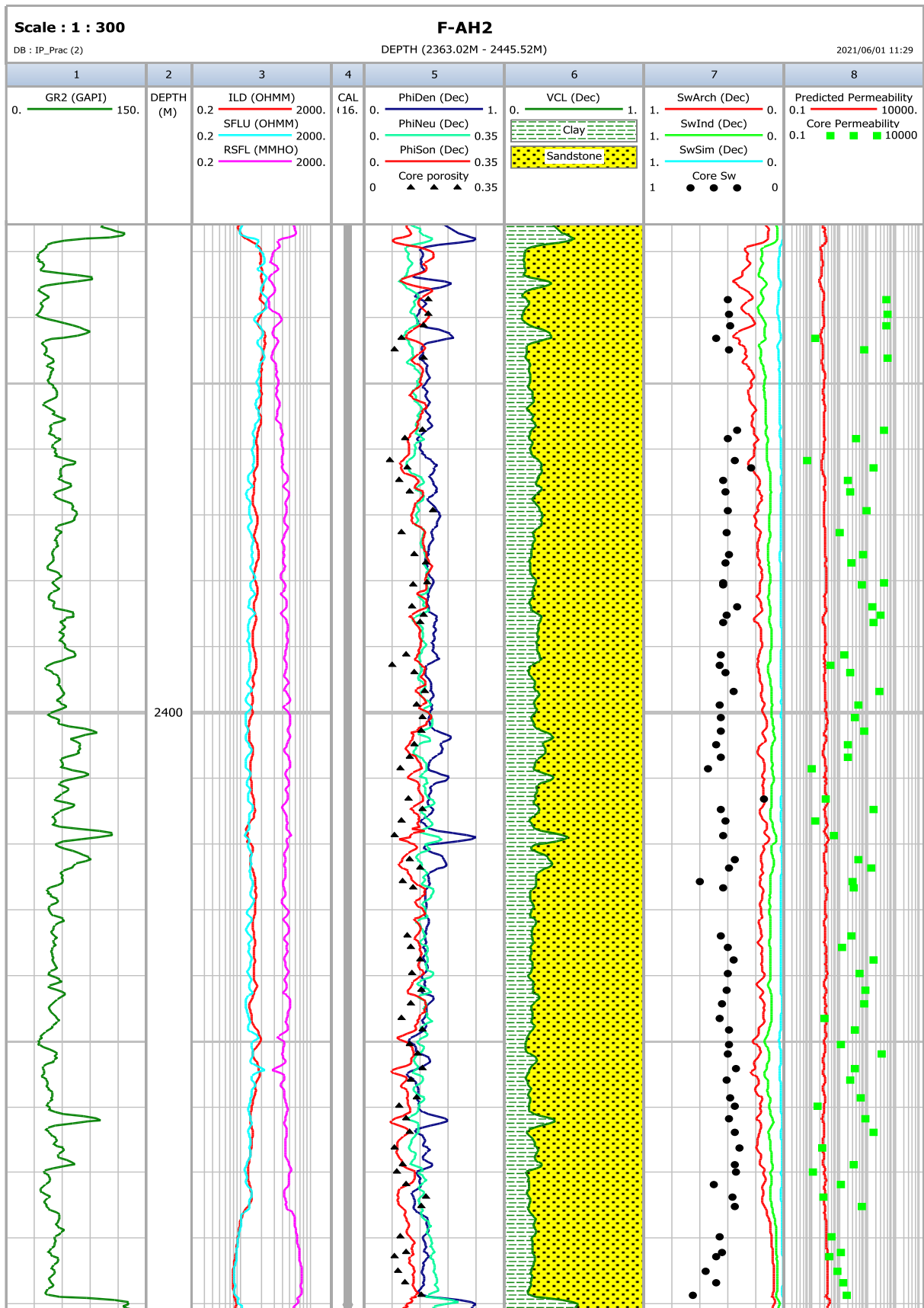


Figure 5- 19: Comparison of core and log water saturation models for well F-AH2

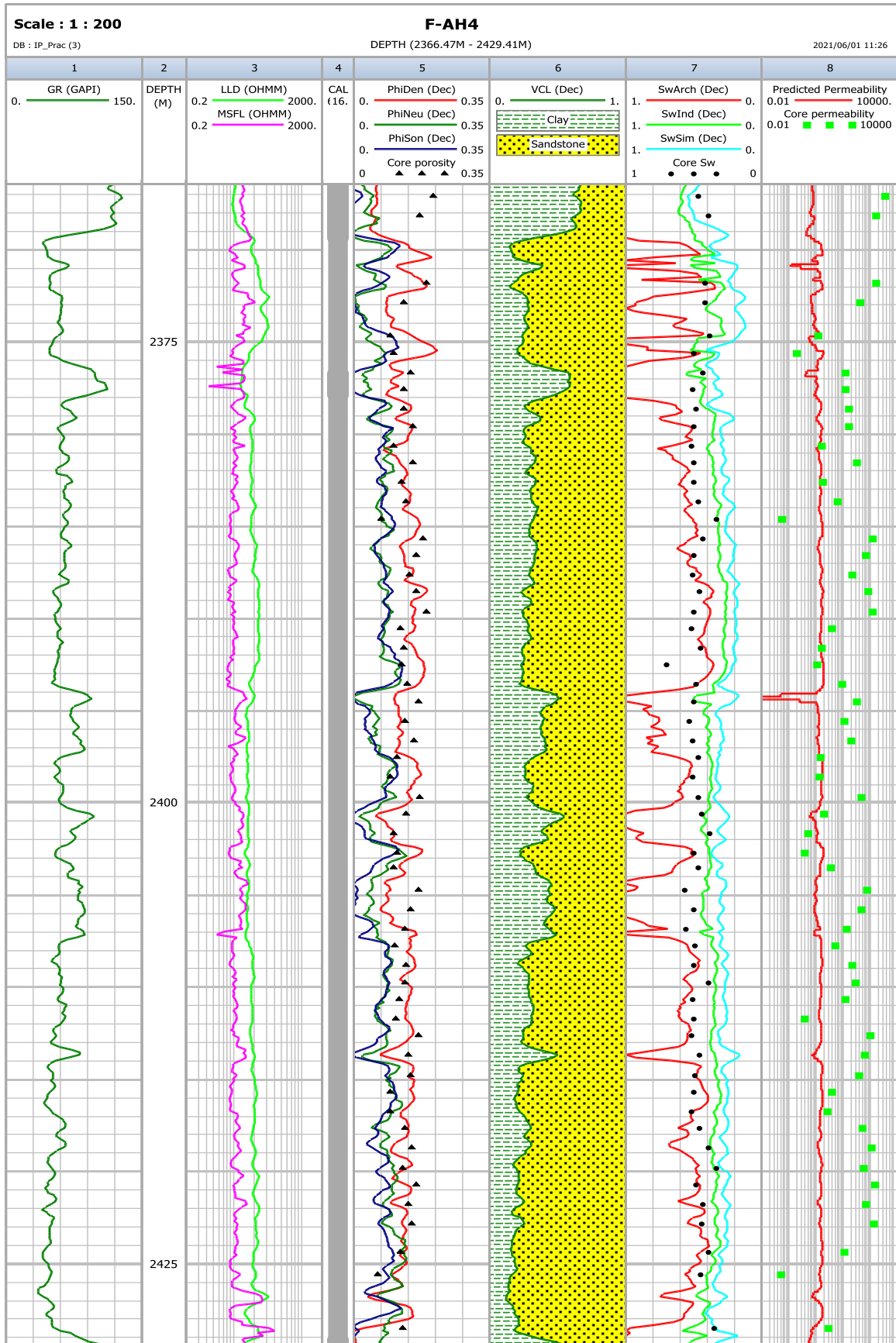


Figure 5- 20: Comparison of core and log water saturation models for well F-AH4

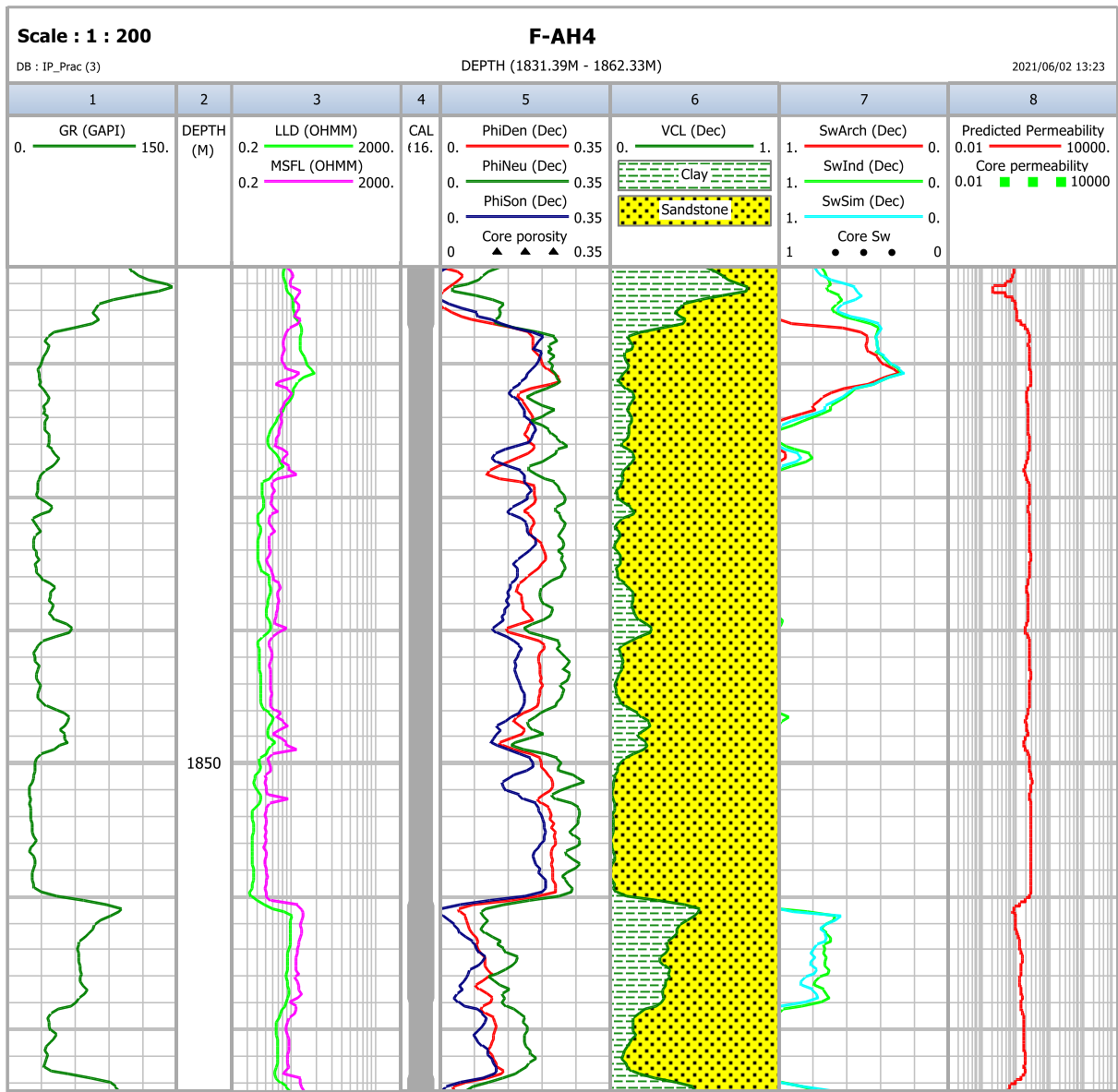


Figure 5- 21: Comparison of log water saturation over hydrocarbon zone for well F-AH4

CHAPTER SIX

6. CUT-OFF AND NET PAY DETERMINATION AND ESTIMATION OF STORAGE AND FLOW CAPACITIES.

This chapter first discusses the cut-off and net pay determination used to attain the desired results and finally discusses the estimation of storage and flow capacities and the effect of minerals on the flow units in the northeastern Bredasdorp Basin, offshore of South Africa.

6.1 INTRODUCTION

The concept of cut-off aims to define the effective petrophysical properties of a given geological unit in the presence of poor reservoir zones. In order to assess the efficiency of reservoir recovery mechanisms, the initial hydrocarbon volume must be related to the reservoir rock. Where this is not the case, the hydrocarbons stand little chance, may not contribute to reservoir dynamics, and should not be included in the accumulation volume against which recovery is to be evaluated (Worthington, 2008). The starting point in determining the cutoff is to identify reference parameters that allow us to distinguish between intervals with reservoir potential and intervals without reservoir potential. There is no single universally applicable approach to determining the cut-off (Worthington & Cosentino, 2005). One of the most important steps is to establish the link between a conventional drill core log and a reference parameter that distinguishes between the reservoir and non-reservoir rocks.

Evaluation of hydrocarbon volumes requires cut-offs so that net reservoir intervals (net pay) can be identified that contain sufficient hydrocarbon potentials and allow for reasonable hydrocarbon flow. The net pay is defined according to flow criteria and liquids produced. Rocks with sufficient permeability to flow fluids at commercially significant rates are classified as a net reservoir or net sandstone. If they produce hydrocarbons at a commercially acceptable hydrocarbon/water ratio, they are classified as net pay (Suzanne & Robert, 2004).

The storage capacity calculations help give an idea of how much the production interval is capable of storing the hydrocarbons. This is obtained simply by multiplying net thickness by porosity while using flow capacity to determine how well the hydrocarbon can flow within the reservoir simply by multiplying net thickness by permeability.

6.1.1 Determination of Petrophysical Properties in Non-cored wells

The petrophysical models of the volume of shale, porosity, permeability, and water saturation were derived from the cored reservoir sections of wells F-AH1, F-AH2 and F-AH4 and later applied throughout the non-cored sections of each well. Clay volume was estimated for the non-cored intervals of each well using the linear Gamma Ray method. This method was considered sufficient for the scope of this study. As discussed in Chapter 5, the linear volume of the clay model showed good agreement with the observed facies for each well. The log-calculated porosities were derived using the three main logs, primarily sonic, neutron and density porosity. The log that best matched conventional core porosity results was accordingly used as the best-fit analysis per well. Each log calculated porosity curve per well was compared to the overburden porosity measurements. The cover layer porosity measurements were calculated by plotting the SCAL measured cover layer porosity versus the conventional core porosity to obtain a pore reduction equation. In well F-AH1 the density log best matched the core analysis results, in well F-AH2 the neutron log, and in well FAH4 the neutron log. Core porosity and permeability measurements were cross-plotted per well to derive individual correlation equations. The correlation equations were used along with identified log-porosity curves to derive an estimated permeability curve. The estimated per-well permeability curves were then displayed for comparison to the core permeability results. In the water saturation study, the Archie, Simandoux, and Indonesian water saturation models were used. In well F-AH1 the Indonesian model was the best fit for the water saturation results of the core analysis,

in well F-AH2 the Simandoux model and in well F-AH4 the Archie model was the best fit for core water saturation. All selected models that best fit the core analysis results were used as an extrapolation to estimate the petrophysical properties in the non-cored zones.

6.2 CUT-OFF DETERMINATION

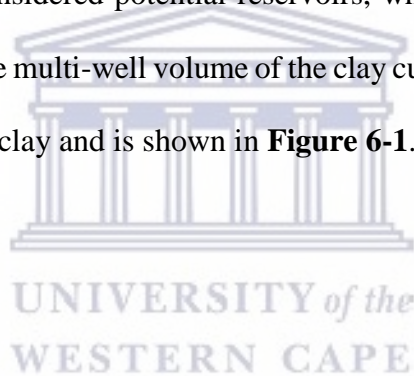
Cut-off parameters are typically applied to wells to distinguish between the reservoir and non-reservoir zones to provide baseline criteria for determining the presence of hydrocarbons. This differentiation becomes important in knowing the boundaries of a reservoir and in estimating how efficiently a reservoir can recover potential hydrocarbons. Non-reservoirs do not contribute well to reservoir dynamics and recovery mechanisms and therefore become a challenge in evaluating prospects. Identifying hydrocarbon volumes also requires the use of parameters so that the gross reservoir package and the net hydro-carbonaceous section can be identified. The net reservoir zones are rocks that have sufficient porosity and permeability to allow fluids (particularly hydrocarbons) to flow at economically viable rates (Suzanne and Robert, 2004). It was further explained that if these sections are shown to contain hydrocarbons, they will be classified as net pay zones.

There are different types of reservoirs. In an example of an unconventional reservoir, shale can contain large amounts of organic material and host hydrocarbons therein. These rocks act as both a source and reservoir for shale gas, but do not allow the flow of these hydrocarbons to the surface. In these situations, porosity and permeability are generally very low and sometimes inconvenient to produce hydrocarbon. Sandstones are a different case (conventional type) and can have high porosity and permeability. These sandstones could be reservoirs for hydrocarbons provided there is evidence of hydrocarbon existence. The lithology is a controlling factor to consider in most cases and the permeability is another control factor as it relates to how easily the fluids can flow through the formation. In this study, the volume of

clay, porosity, water saturation and permeability were the primary parameters used for the formation evaluation and are described below.

6.2.1 Volume of Clay Cut-off Determination

In each well, the amount of clay content per formation can be used to distinguish between the reservoir and non-reservoir rocks. A rock containing large amounts of clay (mudstone) is usually a poor reservoir rock by conventional standards, as these rocks have low porosity and permeability. Rocks with low or near zero grades of clay are generally considered suitable reservoirs as they usually have good porosity and permeability. Clay cut-off volume is used to distinguish between the reservoir and non-reservoir rocks by assigning a cut-off value. Rocks falling below this value are considered potential reservoirs, while rocks above the value are identified as non-reservoirs. The multi-well volume of the clay cut-off versus porosity was used to determine the volume of the clay and is shown in **Figure 6-1**.



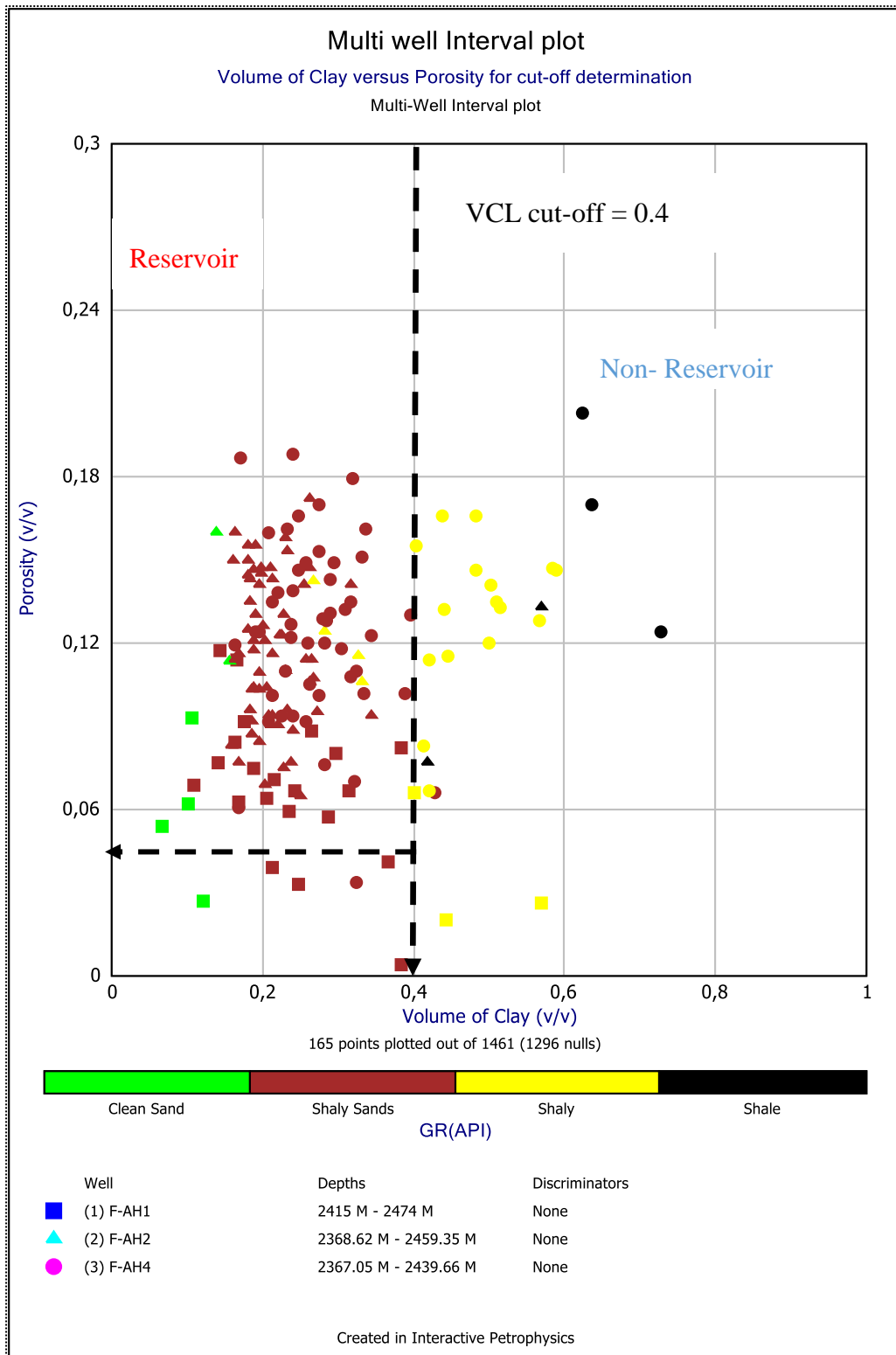


Figure 6- 1: Multi-well Volume of Clay-Porosity plot for cut-off determination

The Volume of Clay-Porosity plot in **Figure 6-1** shows that the clay volume (VCL) cut-off value that distinguishes between reservoir and non-reservoir was set at 0.4. This means that any rock with a clay volume greater than 40% is classified as non-reservoir, while clay volumes equal to or less than 40% are considered potential reservoirs. The reservoir interval may be associated with zones of good porosity-permeability where the clay content is low. Fine clays and silts can seal pore spaces and reduce porosity and permeability. The non-reservoir section represents areas of a relatively higher volume of clay content and lower porosity-permeability relationships than the reservoir section.

6.2.2 Porosity Cut-off Determination

To distinguish between the reservoir and non-reservoir intervals, a porosity cut-off must be established. Rocks with low porosity are mostly non-reservoir rocks and rocks with high porosity are generally capable rocks. To establish a cut-off, a cross-plot of core porosity versus permeability corrected for overburden conditions and facies was generated by combining all wells in this study. This cross plot allows the determination of the lowest porosity and equivalent permeability capable of hydrocarbon flow. **Figure 6-2** presents such a cross plot for combined wells where the parameters have been determined.

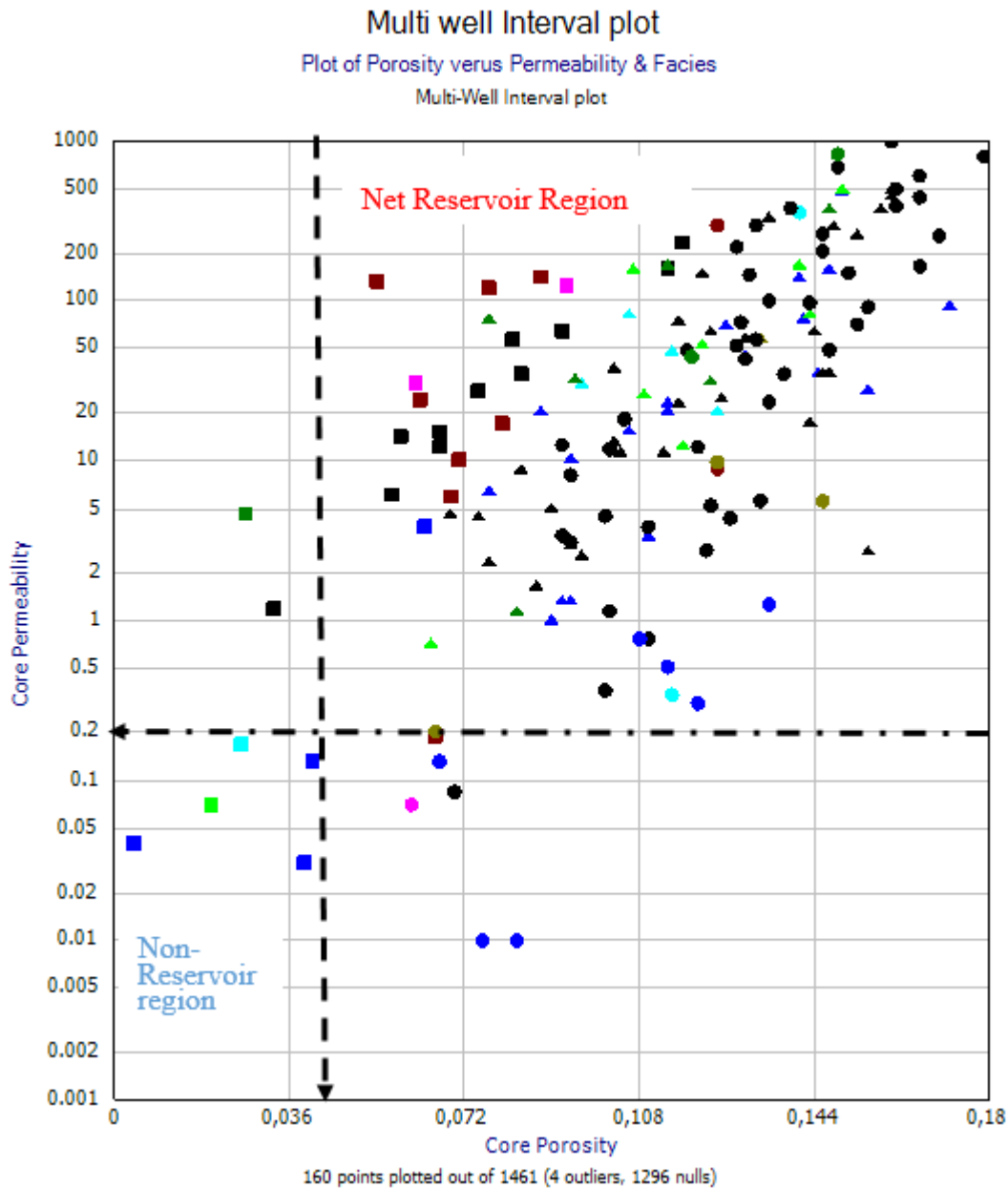


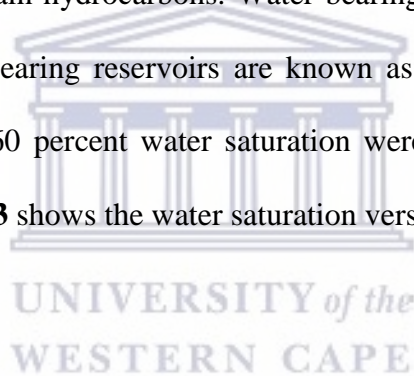
Figure 6- 2: Multi-well porosity-permeability plot for cut-off determination

The porosity-permeability relationships in **Figure 6-2** show 4% porosity and 0.2 mD permeability as boundaries between the reservoir and non-reservoir sections. The points on the y-axis and the x-axis represent the permeability and porosity limits, respectively. In the net reservoir region, variable facies types are predominant. Overall, the F1 (medium sandstone), F2 (fine sandstone), and F11 (intermixed fine and medium sandstone) facies appear to be the

dominant groupings, presenting good porosity and permeability (above cut-off values). Non-reservoir facies such as F8 (siltstone) and F9 (mudstone) exist in the net reservoir region with good porosity-permeability relationships. This could be explained by fractured sections of mud and silt representing sections of high porosity-permeability relationships. Variable facies types also exist within the non-reservoir region, mainly F1 (medium sandstone), F2 (fine sandstone), and F3 (very fine sandstone). These sand-type facies may be relatively more argillaceous than their reservoir counterparts, which may explain poor porosity-permeability relationships

6.2.3 Water Saturation Cut-off Determination

The water saturation cut-off is useful to differentiate between reservoirs that contain water and reservoirs that potentially contain hydrocarbons. Water-bearing reservoirs are known as wet intervals, while hydrocarbon-bearing reservoirs are known as pay intervals. Intervals with water saturation greater than 60 percent water saturation were assumed to be wet or non-productive intervals. **Figure 6-3** shows the water saturation versus porosity cross-plot.



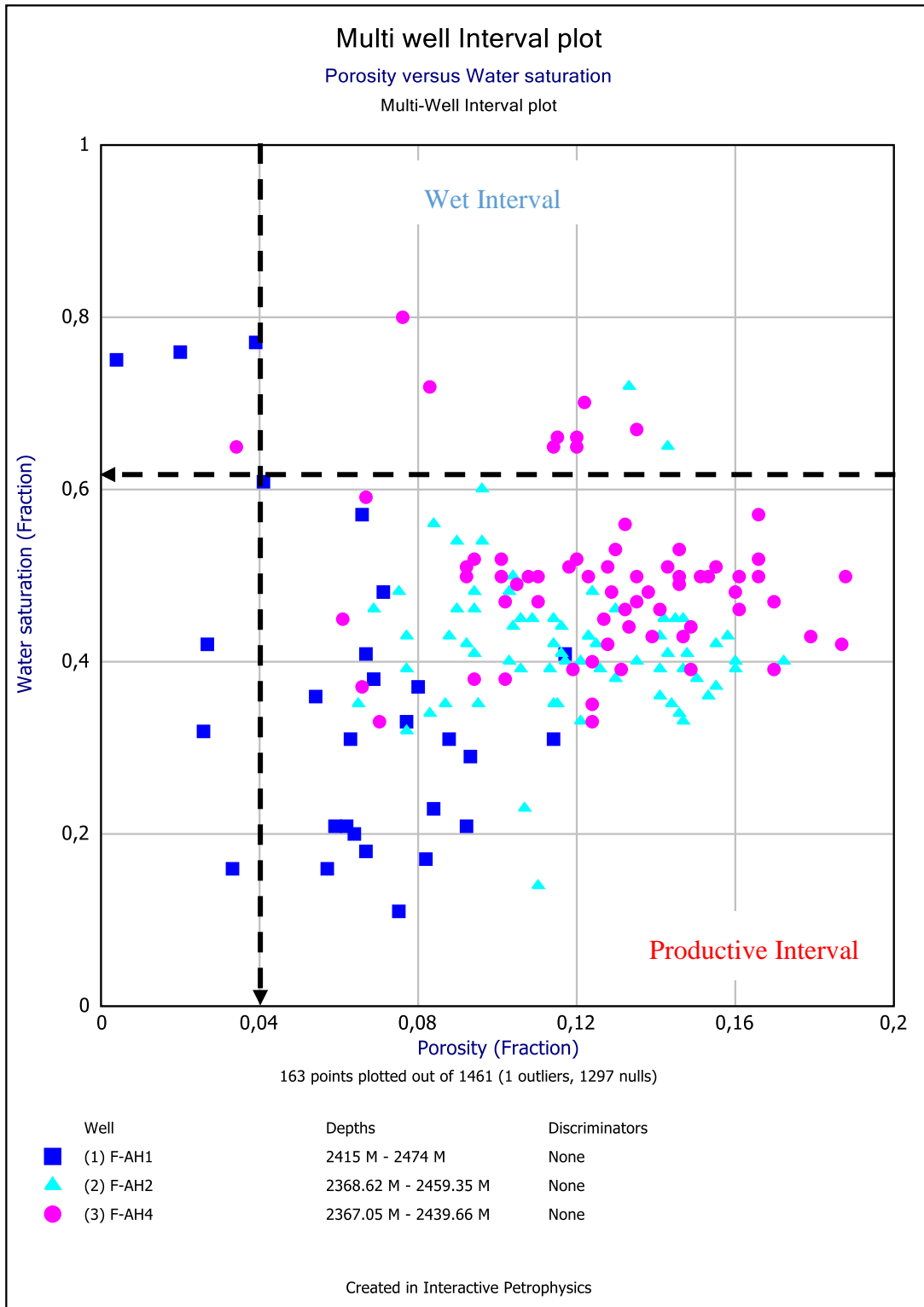


Figure 6- 3: Multi-well Water saturation plot for cut-off determination

6.3 NET PAY DETERMINATION

To determine net pay zones per well, potential reservoir zones per well must be identified along with the application of cut-off parameters in the petrophysical analysis. The gross zone is the interval of thickness that contains hydrocarbons along with intervals that are not contributing to hydrocarbon production but are still reservoir intervals. A reservoir's net pay zone is the interval that contains recoverable hydrocarbon (adequate hydrocarbon saturation, storage space, and mobility) at an economically viable price for an allocated production process (Opuwari, 2010). Net pay is primarily used in volumetric calculations to estimate the total hydrocarbon present, whether it is a hydrocarbon. These hydrocarbons can be mobile or non-mobile within the reservoir.

The distinction between net pay and gross is made by applying cut-off values in the petrophysical analysis. In this study, cut-off values for porosity (≥ 0.04), volume of clay (≤ 0.4), and water saturation (≤ 0.65) were used to identify pay intervals. I.e., intervals with porosity equal to or greater than 40 percent and volume of clay less than or equal to 40 percent and water saturation less than or equal to 65 percent were considered net pay intervals. The net-to-gross ratio is the net sand thickness divided by the gross sand thickness. This ratio is often used to represent the quality of a reservoir zone and for volumetric hydrocarbon calculations. Using the cut-off limits, flag curves were constructed in the database for the net reservoir interval (red) and the gross deposit interval (green). The volume of gas originally available could be calculated from the determined net-to-gross ratio. **Tables 6-1 to 6-3** show the calculated net pay summaries for wells with the corresponding graphics in **Figures 6-4 to 6-20**.

Table 6- 1: Summary of calculated net pay parameters for Well F-AH1

Zone Name	Top(m)	Bottom (m)	Gross (m)	Net (m)	N/G	Av Phi (v/v)	Av Sw (v/v)	Av Vcl (v/v)
Reservoir 1	2411.5	2428.1	16.60	9.46	0.570	0.132	0.446	0.193
Reservoir 2	2429.5	2454.2	24.70	5.49	0.222	0.113	0.453	0.143
Reservoir 3	2495.8	2503.0	7.20	0.00	0	---	---	---
Reservoir 4	2560.8	2569.5	8.70	0.00	0	---	---	---

Two reservoir intervals were encountered within well F-AH1 and the two were found to have net pay (Reservoirs 1 and 2). Reservoir 1 had the highest net pay (9.46 m) and had an average porosity of 13 %, water saturation of 45 % and a clay volume of 19 % as presented in **Table 6-1** and **Figures 6-4, 6-5, 6-6 and 6-7**.

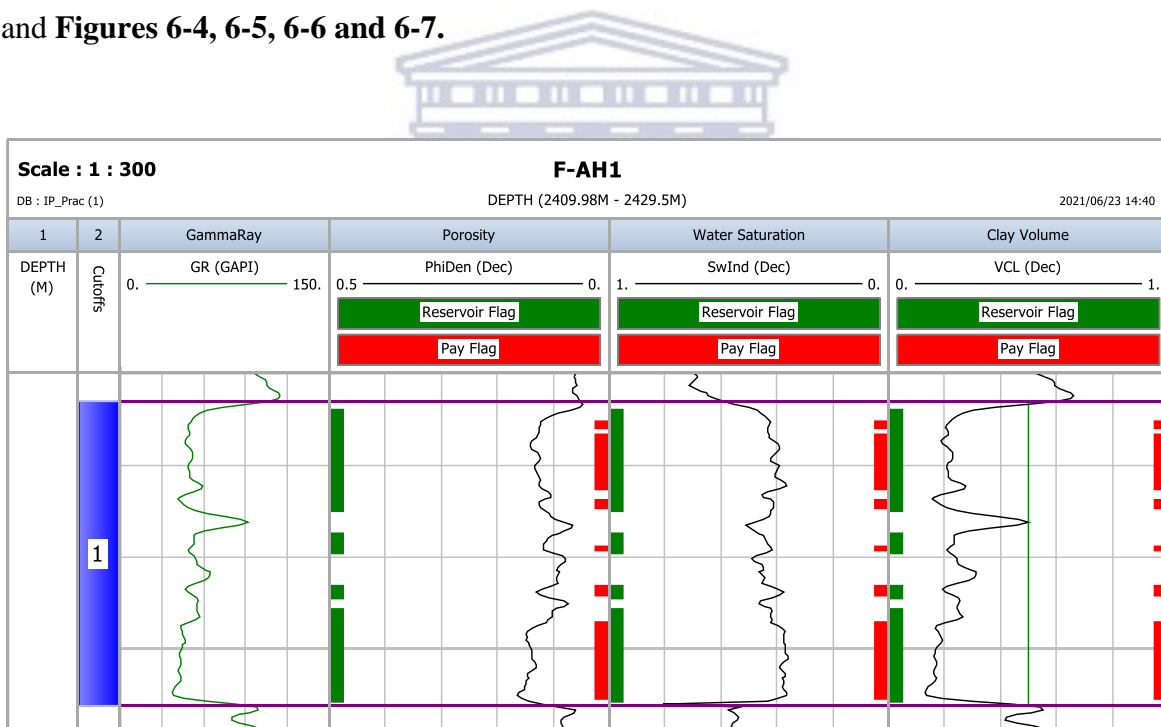


Figure 6- 4: Well F-AH1 showing calculated reservoir parameters and pay flags in reservoir 1

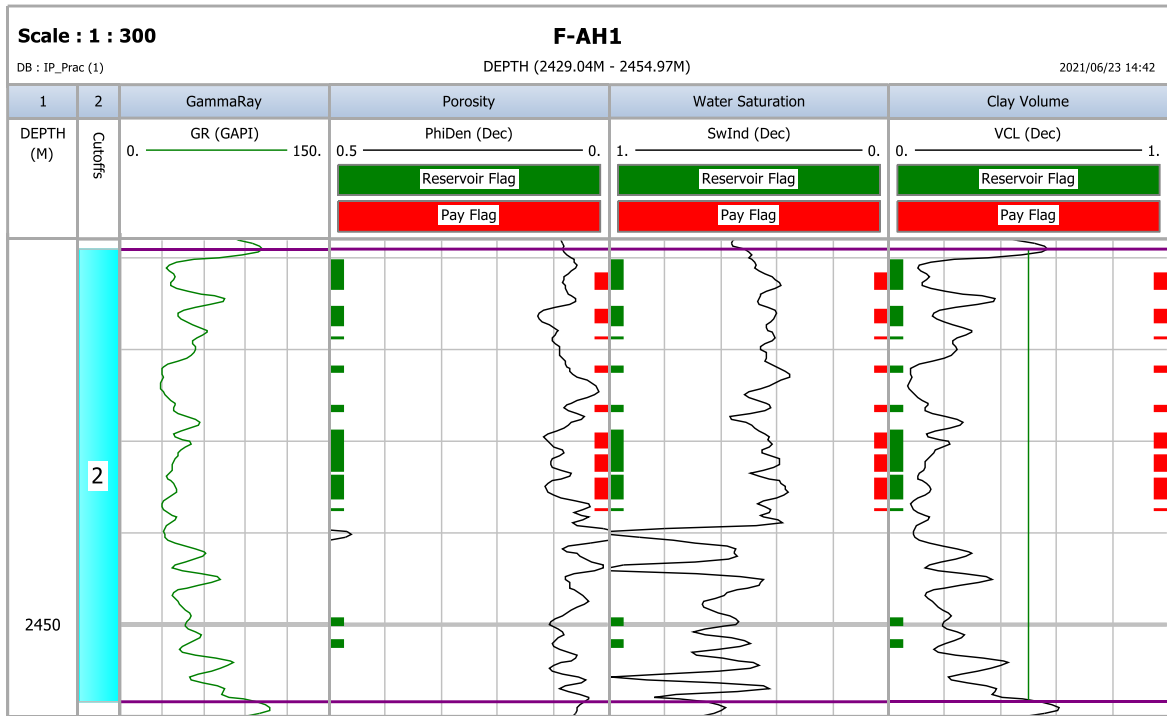


Figure 6- 5: Well F-AH1 showing calculated reservoir parameters and pay flags in reservoir 2

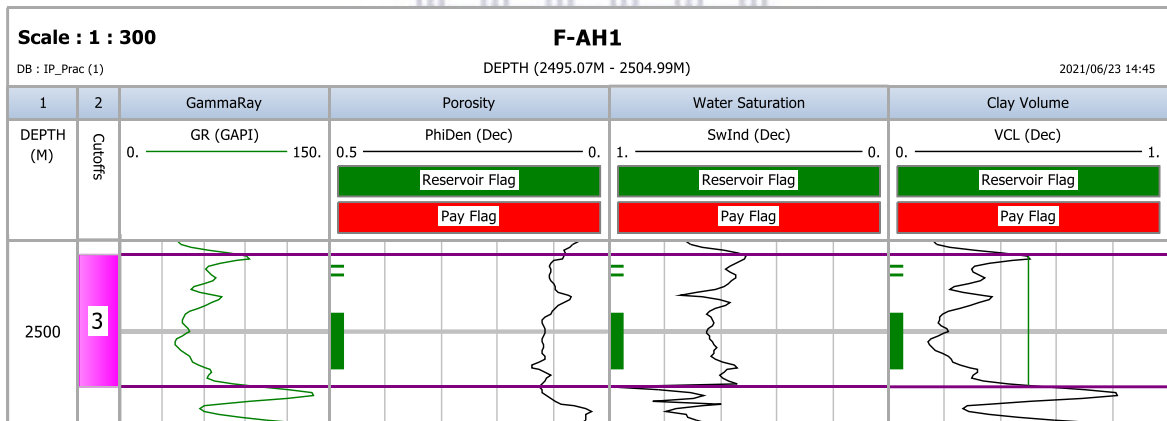


Figure 6- 6: Well F-AH1 showing calculated reservoir parameters and pay flags in reservoir 3

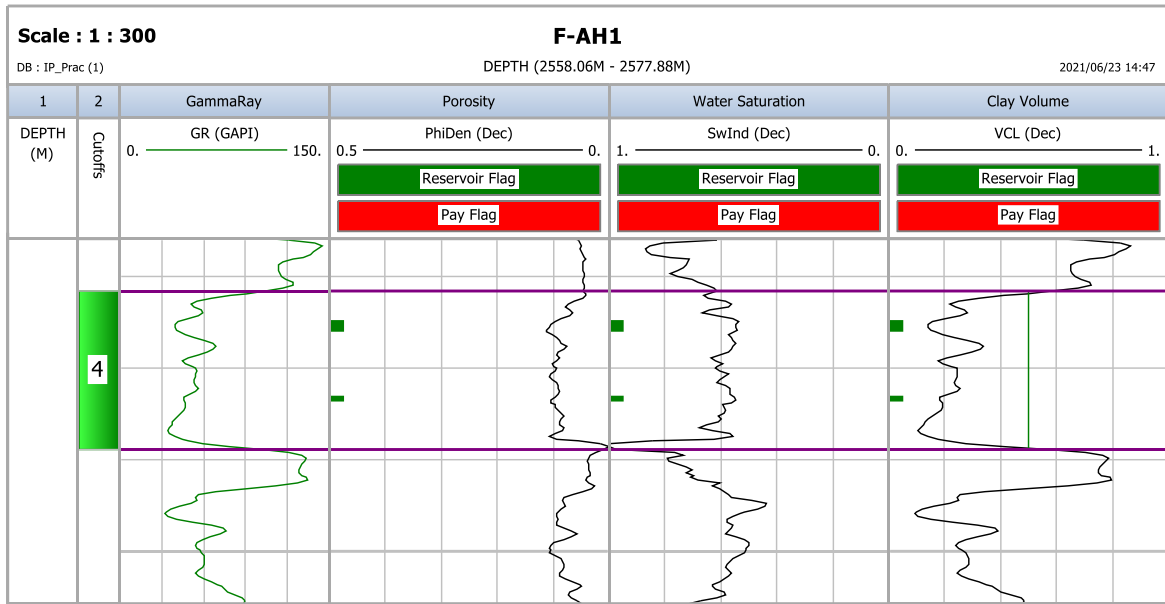


Figure 6- 7: Well F-AH1 showing calculated reservoir parameters and pay flags in reservoir 4

In well F-AH2, four reservoirs were evaluated and all were found to have net pay potential (reservoirs 1 to 4). The net thickness ranges from 2.32 m to 79.84 m and average porosity from 11 to 15 %, water saturation from 11 to 16 % and clay volume from 21 to 28 % as presented in **Table 6-2** and **Figures 6-8, 6-9, 6-10 and 6-11.**

Table 6- 2: Summary of calculated net pay parameters for Well F-AH2

Zone Name	Top(m)	Bottom (m)	Gross (m)	Net (m)	N/G	Av Phi (v/v)	Av Sw (v/v)	Av Vcl (v/v)
Reservoir 1	2363.9	2444.7	80.75	79.84	0.989	0.145	0.162	0.220
Reservoir 2	2457.1	2462.3	5.20	4.51	0.867	0.135	0.112	0.214
Reservoir 3	2487.2	2490.5	3.30	2.32	0.703	0.114	0.137	0.282
Reservoir 4	2553.8	2557.9	4.10	2.82	0.687	0.129	0.148	0.247

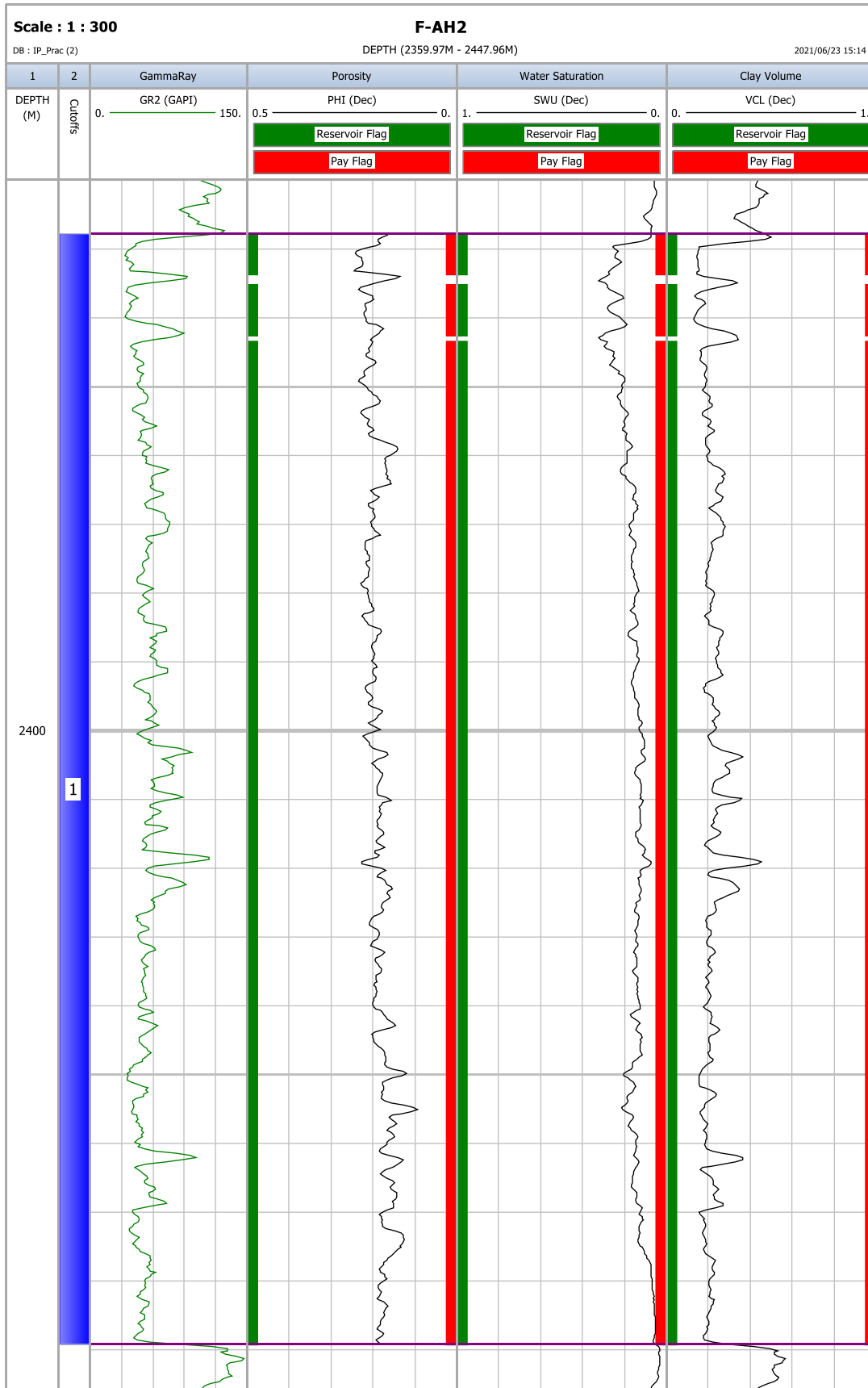


Figure 6- 8: Well F-AH2 showing calculated reservoir parameters and pay flags of reservoir 1

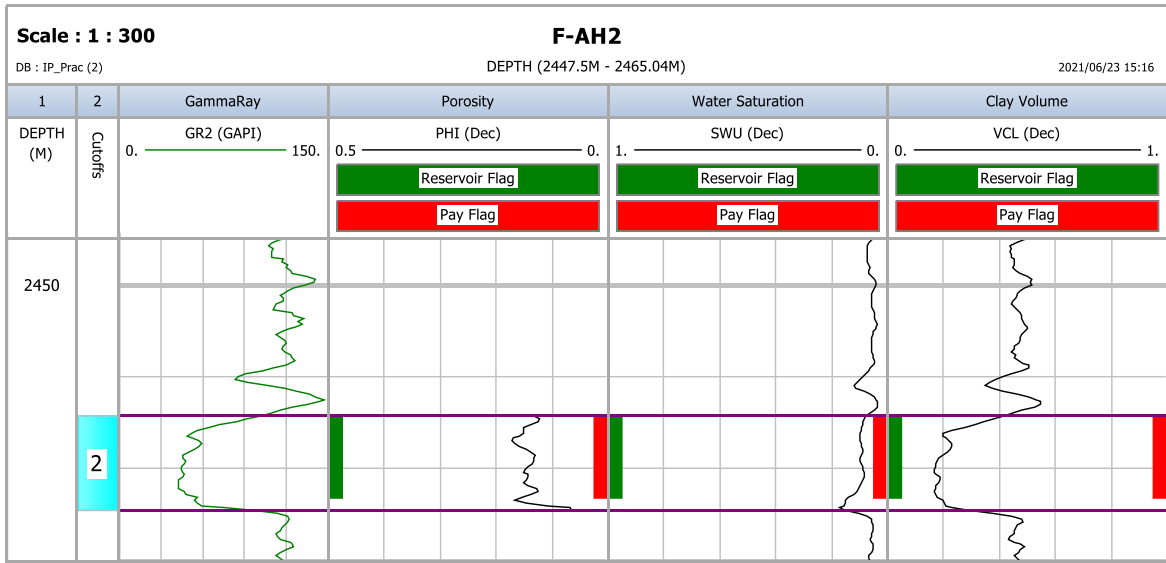


Figure 6- 9: Well F-AH2 showing calculated reservoir parameters and pay flags of reservoir 2

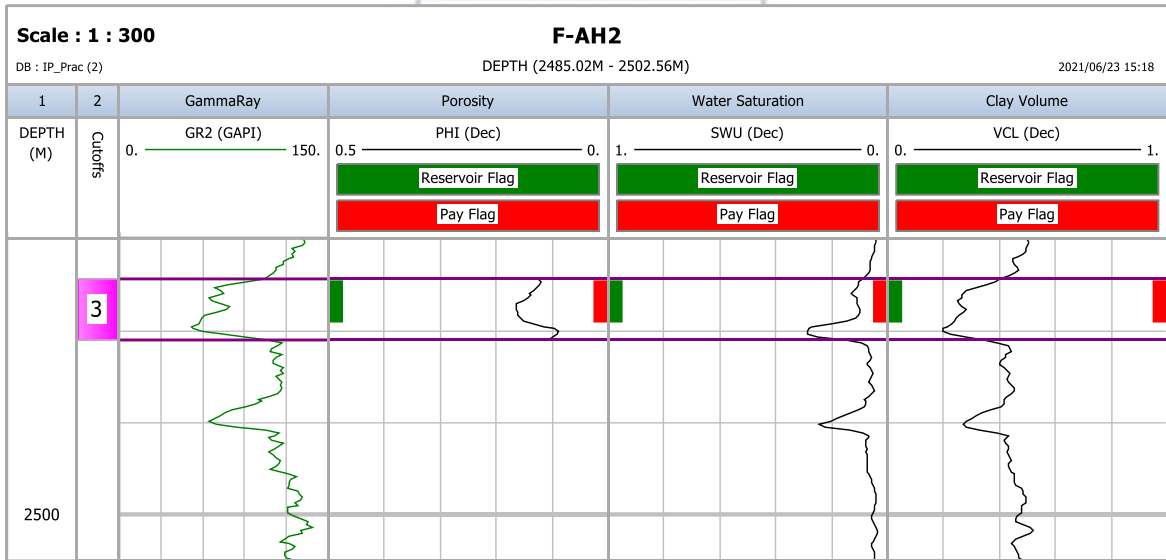


Figure 6- 10: Well F-AH2 showing calculated reservoir parameters & pay flags of reservoir 3

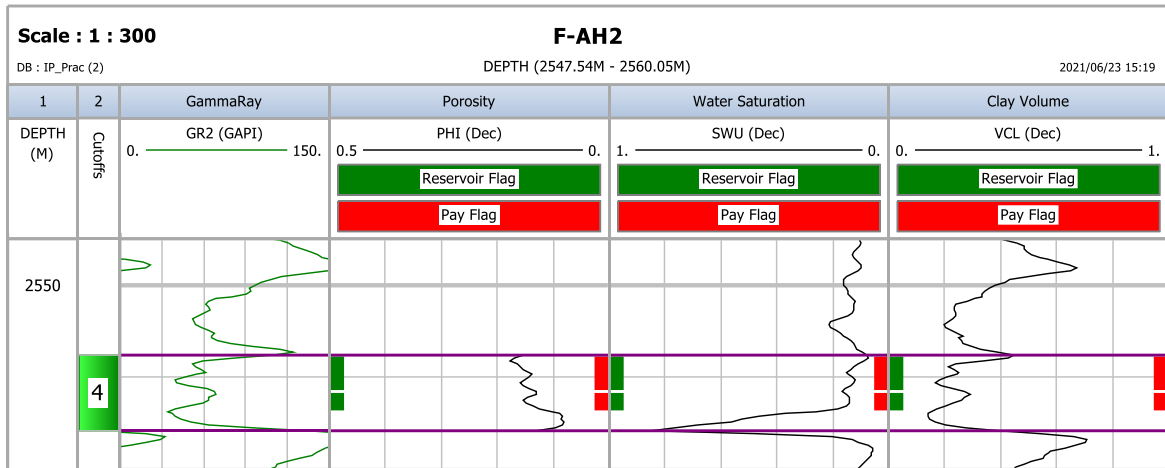


Figure 6- 11: Well F-AH2 showing calculated reservoir parameters & pay flags of reservoir 4

Nine reservoirs were evaluated in well F-AH4, three of which proved to have net pay (Reservoirs 1 to 3). The net thickness ranges from 1.68 m to 29.11 m and average porosity from 13 to 22 %, water saturation from 40 to 43% and clay volume from 11 to 25 %, as presented in **Table 6-3** and **Figures 6-12, 6-13, 6-14, 6-15, 6-16, 6-17, 6-18, 6-19** and **6-20**.

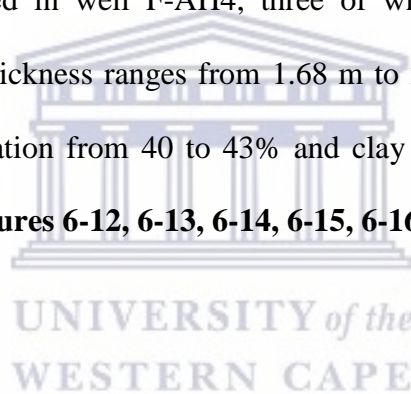


Table 6- 3: Summary of calculated net pay parameters for Well F-AH4

Zone Name	Top(m)	Bottom (m)	Gross (m)	Net (m)	N/G	Av Phi (v/v)	Av Sw (v/v)	Av Vcl (v/v)
Reservoir 1	1832.6	1876.8	44.20	2.13	0.048	0.219	0.414	0.105
Reservoir 2	2369.1	2376.7	7.60	1.68	0.221	0.127	0.402	0.192
Reservoir 3	2377.7	2429.4	51.70	29.11	0.563	0.124	0.428	0.251
Reservoir 4	2450.1	2458.4	8.30	0	0	---	---	---
Reservoir 5	2476.7	2483.8	7.10	0	0	---	---	---
Reservoir 6	2516.4	2524.8	8.40	0	0	---	---	---
Reservoir 7	2526.8	2535.6	8.80	0	0	---	---	---
Reservoir 8	2545.1	2550.0	4.90	0	0	---	---	---
Reservoir 9	2557.7	2561.1	3.40	0	0	---	---	---

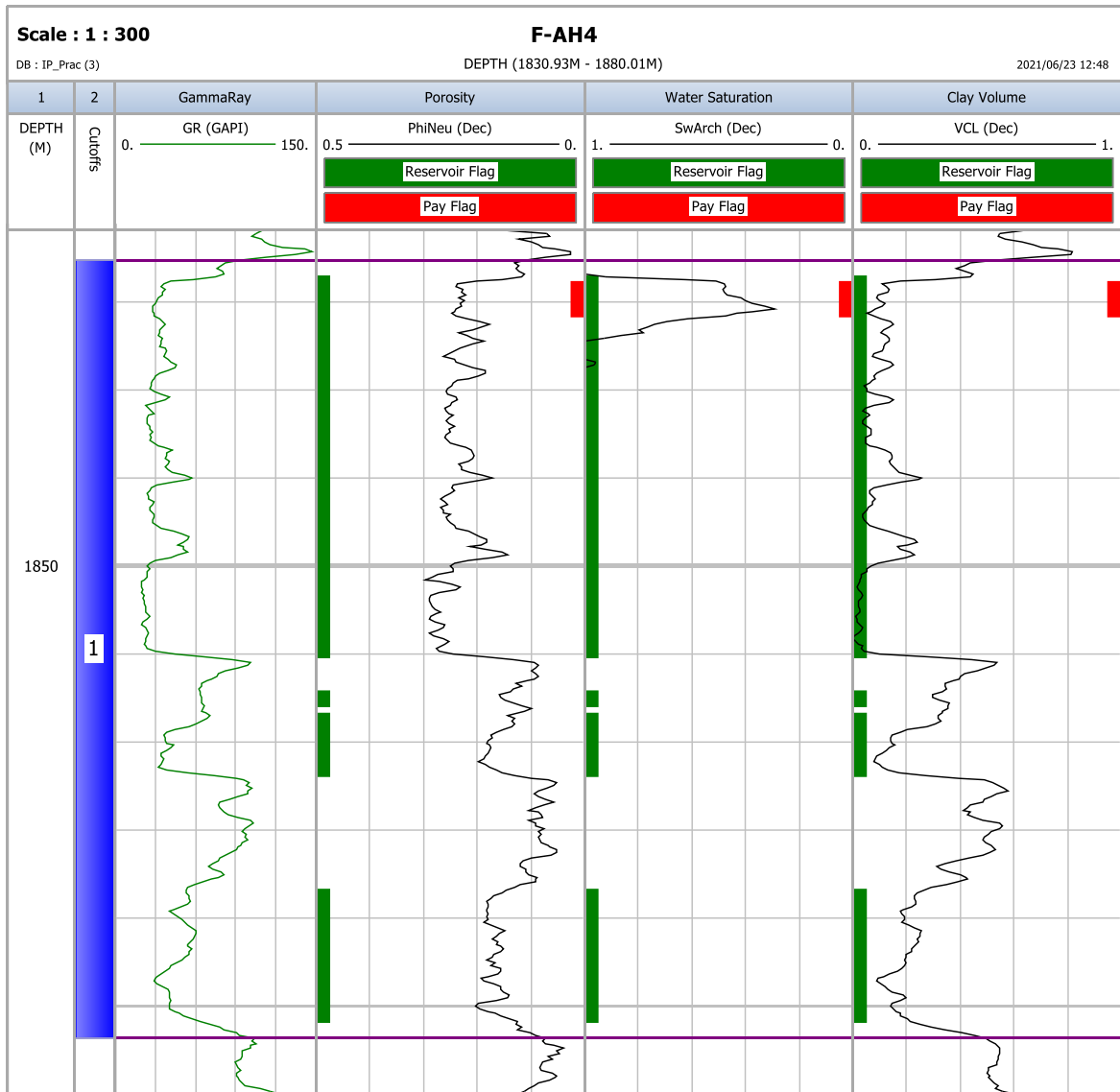


Figure 6- 12: Well F-AH4 showing calculated reservoir parameters & pay flags of reservoir 1

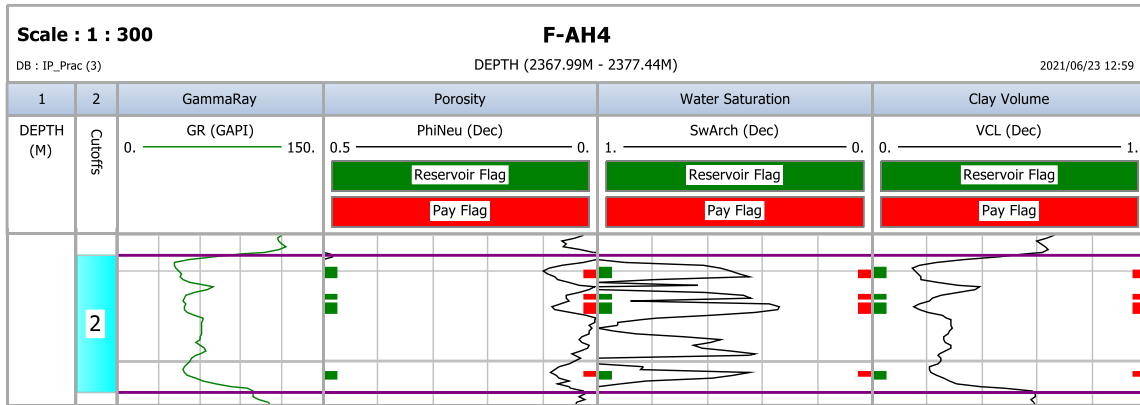


Figure 6- 13: Well F-AH4 showing calculated reservoir parameters & pay flags of reservoir 2



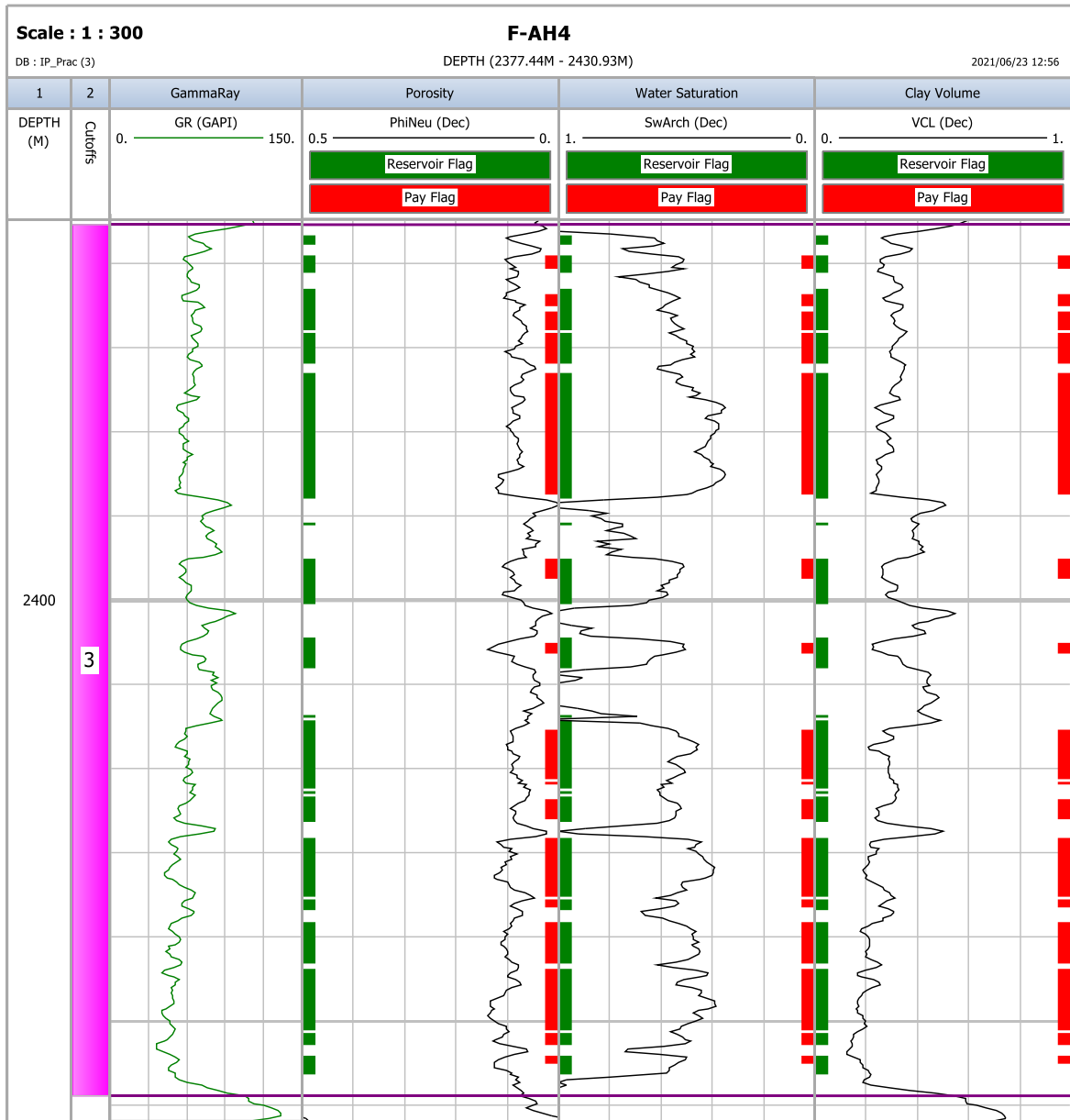


Figure 6- 14: Well F-AH4 showing calculated reservoir parameters & pay flags of reservoir 3

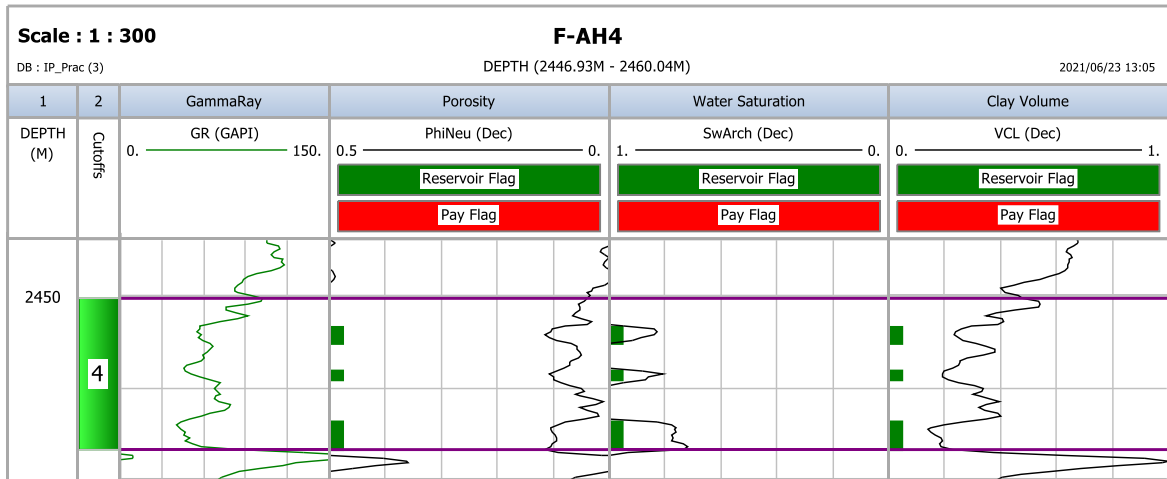


Figure 6- 15: Well F-AH4 showing calculated reservoir parameters & pay flags of reservoir 4

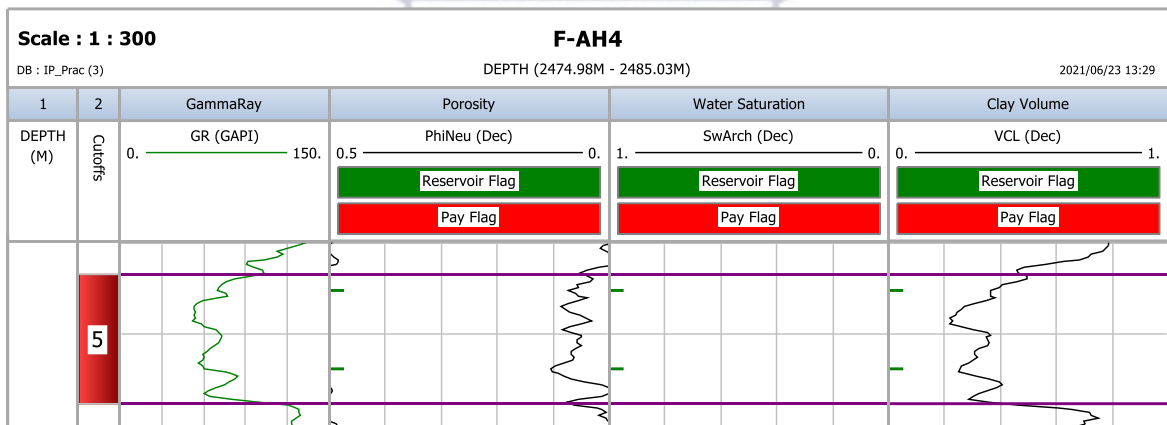


Figure 6- 16: Well F-AH4 showing calculated reservoir parameters & pay flags of reservoir 5

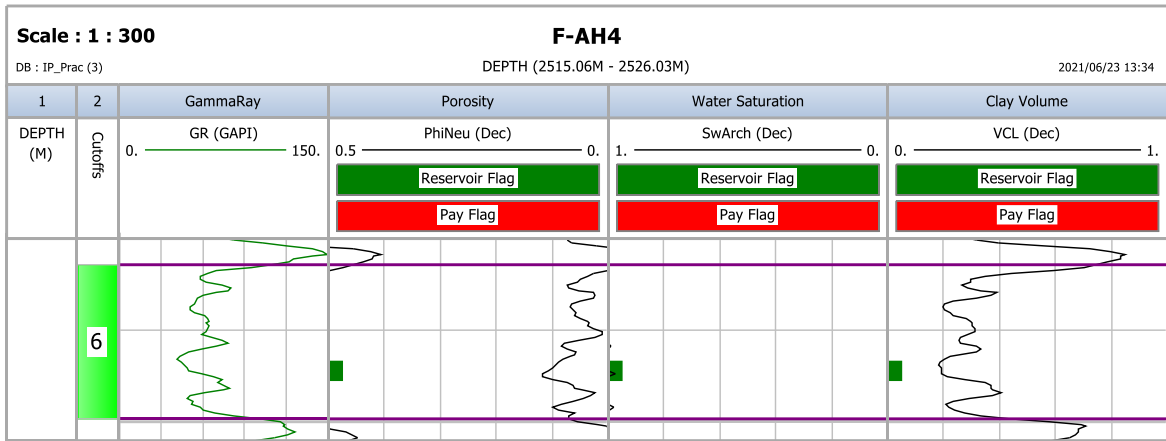


Figure 6- 17: Well F-AH4 showing calculated reservoir parameters & pay flags of reservoir 6

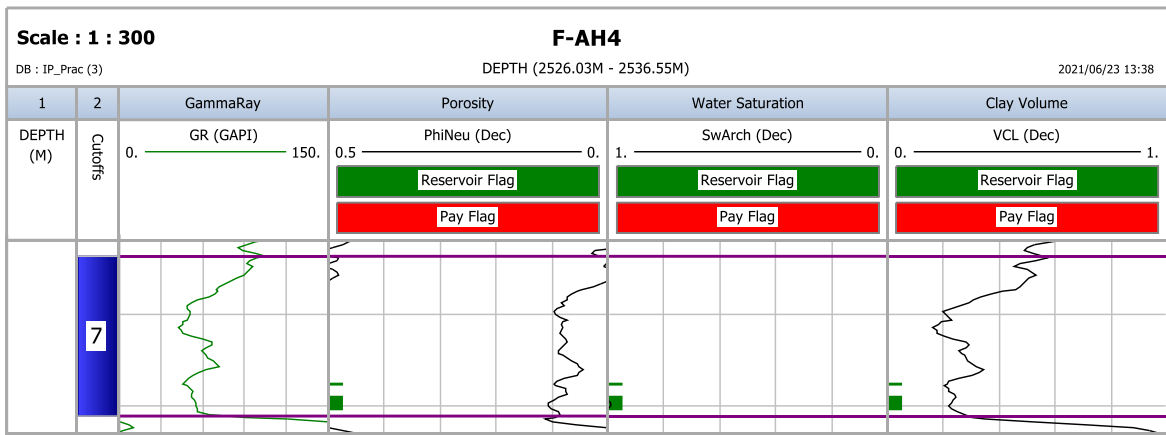


Figure 6- 18: Well F-AH4 showing calculated reservoir parameters & pay flags of reservoir 7

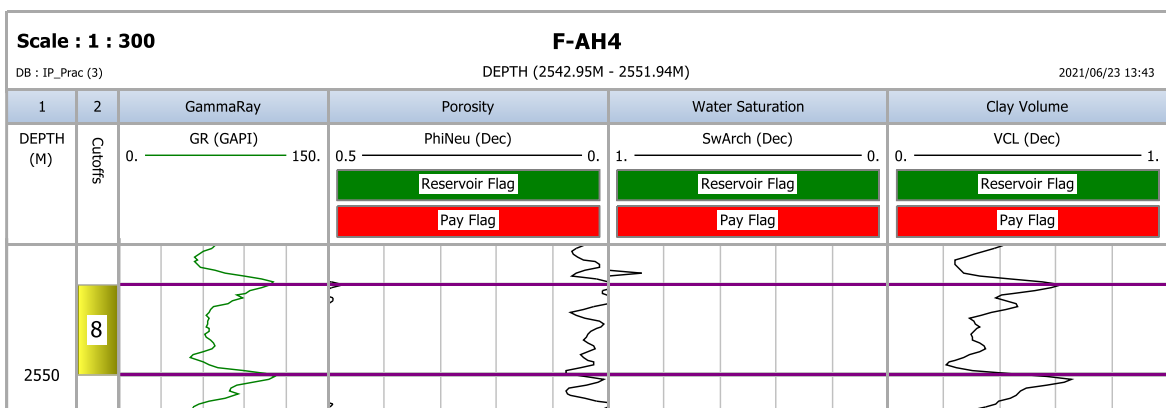


Figure 6- 19: Well F-AH4 showing calculated reservoir parameters & pay flags of reservoir 8

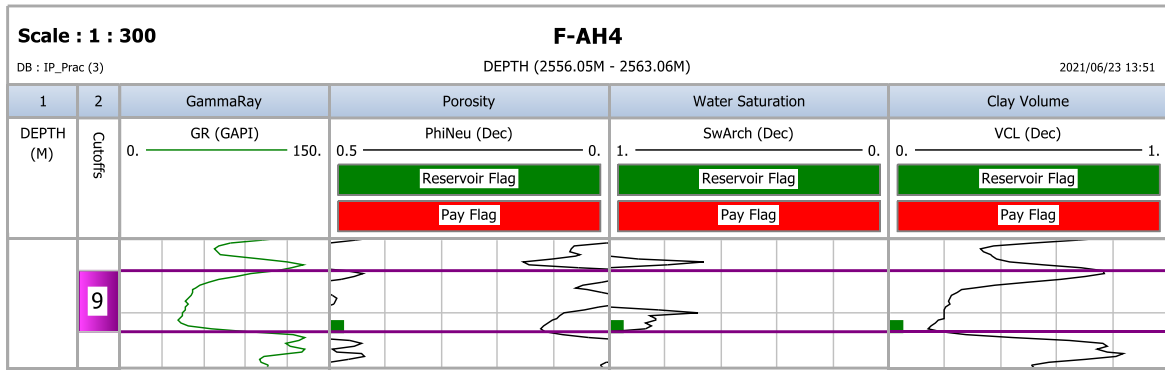
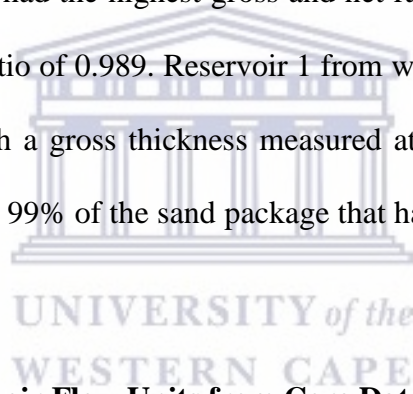


Figure 6- 20: Well F-AH4 showing calculated reservoir parameters & pay flags of reservoir 8

All wells range in gross thickness from 3.30 m to 80.75 m and net thickness from 0 m to 79.84 m. Reservoir 1 of well F-AH2 had the highest gross and net ratios of 80.75 m and 79.84 m, respectively with a net/gross ratio of 0.989. Reservoir 1 from well F-AH2 showed the highest net-to-gross ratio of 0.989 with a gross thickness measured at 80.75m and net thickness at 79.84m. This represents almost 99% of the sand package that has the potential to be occupied by hydrocarbons.



6.3.1 Determination of Reservoir Flow Units from Core Data

K/Φ ratio was used to determine the flow units within the cored sections and reservoir permeability and porosity were the two most important parameters for predicting flow units based on the method proposed by Amaefule et al., 1993 for the evaluation and identification of the flow units. In this study, three petrophysical parameters were identified when predicting flow units using the K/Φ ratio method and each distinct reservoir unit has a unique Flow Zone Indicator (FZI), Reservoir quality index (RQI), and Normalized Porosity Index (NPI) values (Al-Dhafeeri and Nasr-El-Din, 2006). These parameters are based on the calculation of two terms, RQI and NPI as defined below (Amaefule et al., 1993):

$$RQI = 0.0314\sqrt{K/\Phi}$$

$$\text{NPI} = \Phi / (1 - \Phi)$$

$$\text{FZI} = \text{RQI} / \text{NPI}$$

Where:

K = Permeability (mD)

Φ = Porosity (Fraction)

RQI and FZI are in microns.

Appendix 3 presents the results of the calculated RQI, NPI and FZI values for the three Wells (F-AH1, F-AH2, and F-AH4).

6.4 FLOW ZONE MODELLING

6.4.1 Windlandr35

The results of the pore throat radius calculated by the Winland r35 pore throat radius methods are shown in **Table 6-4**. The calculated mean of the pore throat radius of an interval was used to represent the flow zone denoted as (PRTs) based on the following criteria:

Megaoporous rock ($\geq 10 \mu\text{m}$) = PRT1.

Macroporous rock (from 4.0 to 10 μm) = PRT2.

Mesoporous rock (from 2.0 to 4 μm) = PRT3.

Microporous rock (from 1 to 2 μm) = PRT4.

Nanoporous rock ($\leq 1 \mu\text{m}$) = PRT5.

Table 6- 4: Results of calculated petrophysical rock types and flow zone indicators used to classify rocks into different flow zones
(Modified after Porras et al., 1999 and Opuwari et al., 2020)

Well	Top Depth (m)	Bottom Depth (m)	Thickness (m)	HU/ PRT	Porosity %	Permeability mD	r35 (μm)	FZI (μm)	Zone/ Units	Rock Type	Ranking
				1	12-22	200-1000	> 10	≥ 6	High	Megaporous	Very Good
				2	10-12	20-100	4-10	3-6	Moderate	Macroporous	Good
				3	5-10	5-20	2-4	2-3	Low	Mesoporous	Fair
				4	5-10	1-5	1-2	1-2	Very low	Microporous	Poor
				5	< 5	<1.0	< 1	≤ 1	Tight	Nanoporous	Impervious
F-AH1	2415.1	2418.0	2.9	4	6.0	2.1	3.4	2.2	Very Low	Microporous	Poor
	2418.0	2429.3	31.3	2	7.8	29.8	8.3	4.9	Moderate	Macroporous	Good
	2429.3	2435.7	6.4	3	5.9	10.8	4.1	2.3	Low	Mesoporous	Fair
	2435.7	2443.3	7.6	4	7.3	53.8	10.6	5.8	Moderate	Macroporous	Good
	2443.3	2446.6	3.1	5	4.9	0.5	1.2	0.9	Tight	Nanoporous	Impervious
F-AH2	2368.2	2380.1	11.9	1	13.7	273.0	15.2	8.1	High	Megaporous	Very Good
	2380.1	2396.0	15.9	2	12.2	65.0	7.0	4.9	Moderate	Macroporous	Good
	2396.0	2417.6	21.6	2	11.5	29.0	5.0	3.2	Moderate	Macroporous	Good
	2417.6	2436.8	19.2	2	11.7	42.0	5.8	3.9	Moderate	Macroporous	Good
	2436.8	2445.2	8.4	3	11.2	18.0	3.3	2.6	Low	Mesoporous	Fair
F-AH4	2369.2	2376.2	7.0	1	16.8	842.0	27.0	11.6	High	Megaporous	Very Good
	2376.2	2378.2	11.0	3	12.2	27.51	4.3	3.0	Low	Mesoporous	Fair
	2378.2	2393.3	6.1	1	15.3	300.0	14.0	6.8	High	Megaporous	Very Good
	2393.3	2419.3	26.0	2	12.8	43.0	6.7	4.2	Moderate	Macroporous	Good
	2419.3	2428.2	8.9	1	12.9	277.0	16.0	10.0	High	Megaporous	Very Good
	2434.0	2442.4	14.2	5	10.1	0.5	0.7	0.8	Tight	Nanoporous	Impervious

Figure 6-21 shows five different PRTs (PRT1-5). The lower calculated value of r35 (PRT1 and 2) represents smaller pore throats and lower permeability values. In contrast, the high r35 values (PRT4-5) resulted in higher pore throats and permeability. PRT3 is an intermediary rock type between the higher and lower pore throats. From **Figure 6-22**, it was also observed that with porosity in the range of 12-21%, higher permeability values from 20 to 1000 mD indicate better reservoir qualities (PRT1 and 2). PRT1 is the best rock type while PRT5 is the lowest rock type.

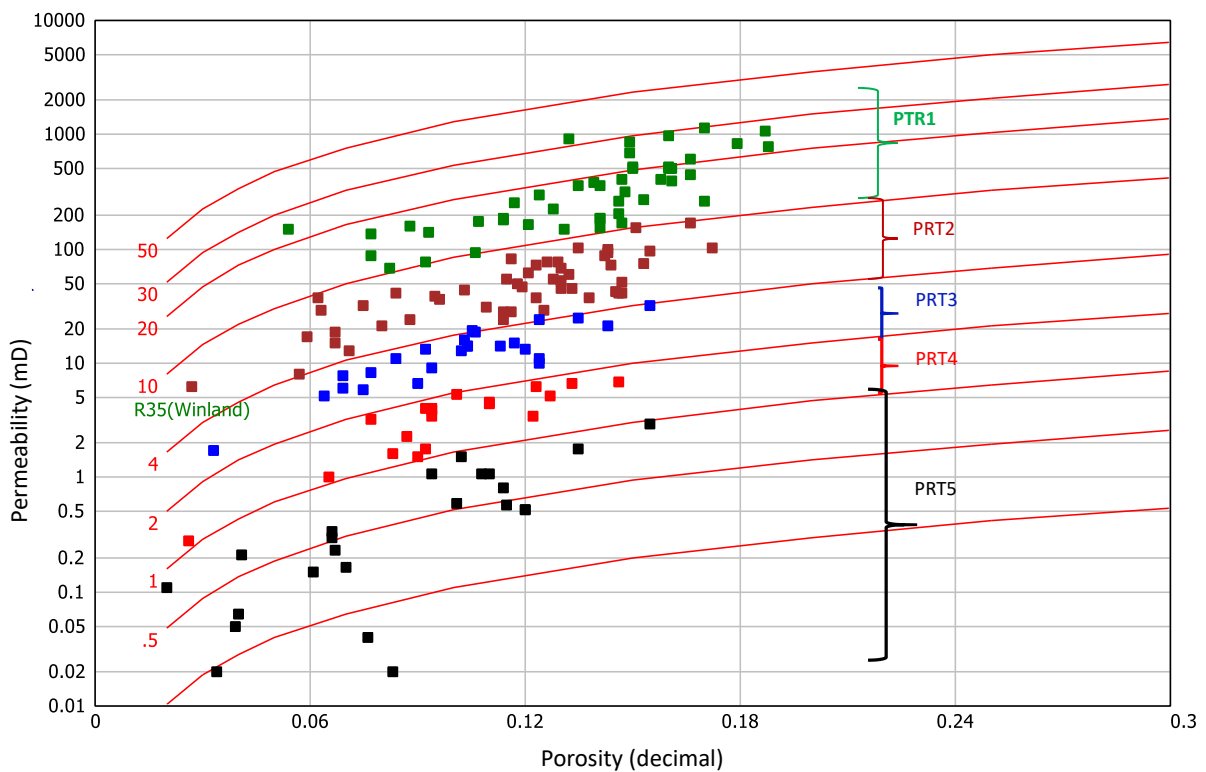


Figure 6- 21: Calculated Windland r35 pore throat radius showing five different petrophysical rock types (PRT1-5) plotted on the standard Windland graph on permeability against porosity

6.4.2 Flow Zone Indicator

The results of calculating the FZI for the wells examined using the modified classification criteria from (Nabawy et al., 2015) yielded five different HFUs from 0.8 to 11.6 μm , as shown in **Table 6-4**. The criteria used to classify the flow zones are:

$$\text{HFU1} = \geq 6 \mu\text{m}$$

$$\text{HFU2} = 3\text{--}6 \mu\text{m}$$

$$\text{HFU3} = 2\text{--}3 \mu\text{m}$$

$$\text{HFU4} = 1\text{--}2 \mu\text{m}$$

$$\text{HFU5} = \leq 1 \mu\text{m}$$

Looking at **Table 6-4**, we can deduce that HFU5 correlates with PRT5, the impervious rock type; HFU4 to PRT4, a poor rock type; HFU3 to PRT3, classified as a fair type of rock; HFU2 to PRT2, which is good reservoir rock; and HFU1 to PRT1, a very good reservoir rock.

The highest FZI value of 11.2 μm was recorded in well F-AH4 which has a thickness of 7.0m, a porosity of 17.2% and an average permeability of 942mD. The lowest FZI value of 0.8 μm was measured in well F-AH4 with a thickness of 14.1m, a porosity of 10% and a permeability of 0.5mD (**Table 6-4**). By visual observation, the RQI versus NPI plot on a log-log scale generally showed five distinguishable HFUs with some overlap (**Figure 6-22**). The permeability, porosity, and FZI of each type of flow unit are shown in **Figure 6-23**. **Figure 6-23** illustrates a significant difference in the permeabilities of the flow units reflecting differential fluid transmissibility. However, porosity does not clearly distinguish between flow units, except for HFU5, which generally had porosity values less than 12%. Hence, for low-permeability sandstone gas reservoirs, which include the eastern Bredasdorp Basin, we propose a 8% porosity cut-off be used to distinguish between impervious rock and reservoir rock, with a corresponding permeability of 1 mD to distinguish impervious rock exclude rocks from our reservoir rock units.

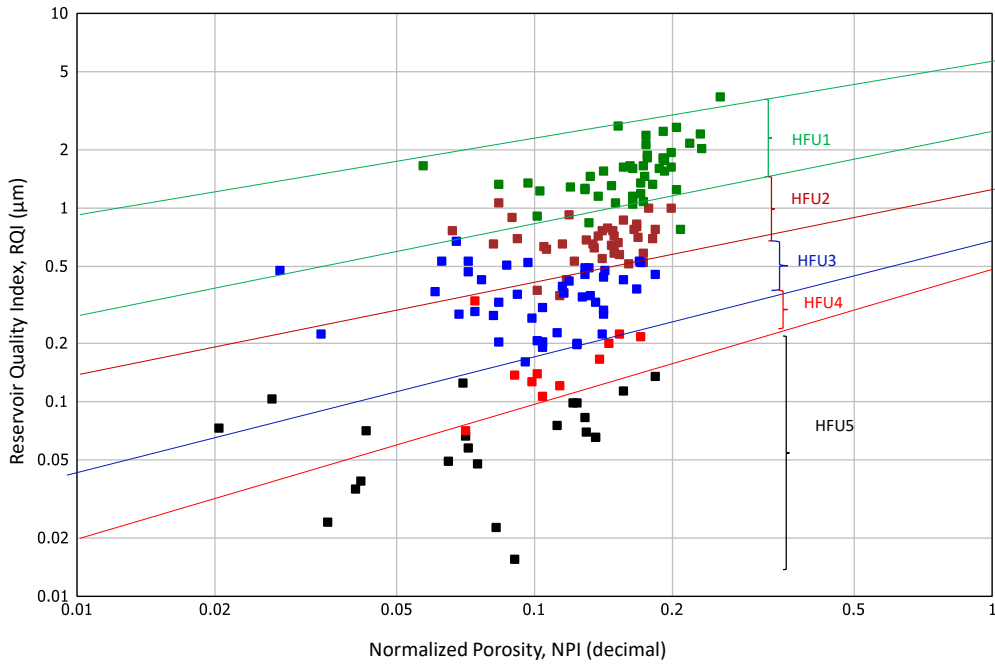


Figure 6- 22: Calculated FZI used to identify different HFUs from RQI versus NPI

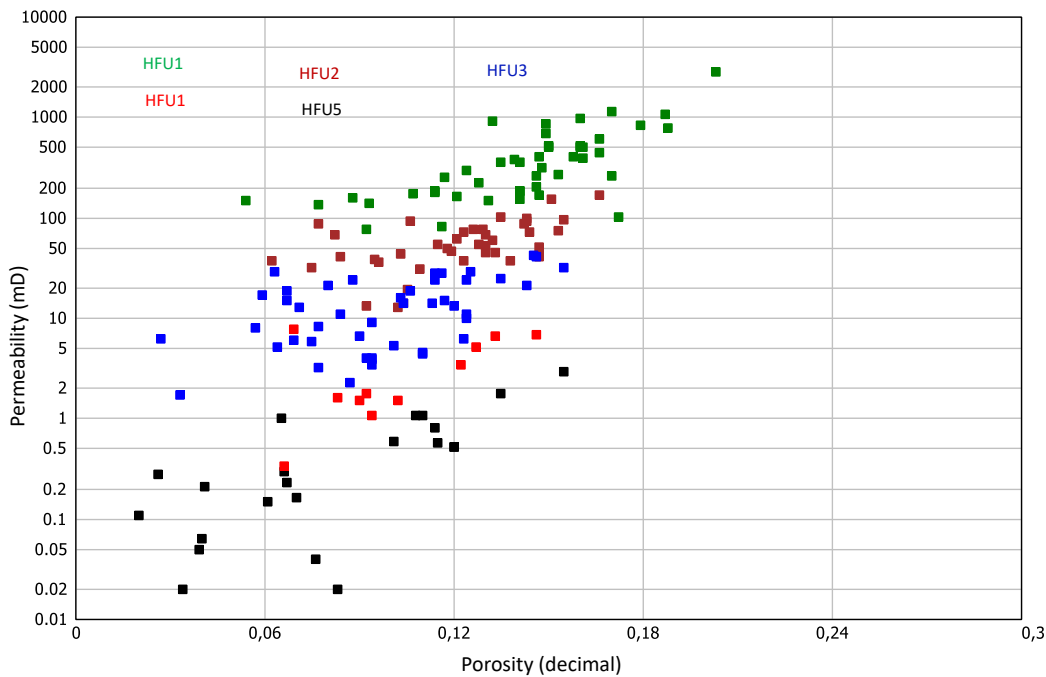


Figure 6- 23: Permeability versus porosity plot showing different hydraulic flow units, HFU 1-5.

Based on the differences between the HFUs, it was concluded that HFU1 had the best reservoir quality, while HFU5 was classified as poor quality. The combination of the calculated Windland r35 and FZI petrophysical zoning methods for rock types culminated in five different flow zones classified into high (PRT1), moderate

(PRT2), low (PRT3), very low (PRT4) and tight (PRT5) zones were grouped (**Table 6-4**). The SMLP method is used to estimate the storage and flow capacities in the flow zones.

6.5 ESTIMATION OF STORAGE AND FLOW CAPACITIES

6.5.1 Stratigraphy-Modified Lorenz Plot (SMLP)

To understand the storage and flow capacities as well as the petrophysical behaviour of the HFUs and PRTs forming a flow zone within a reservoir, the SMLP method was applied in the studied wells. The SMLP method is based on porosity and permeability core data multiplied by their respective bed thicknesses, normalized. Results provided cumulative storage capacity (porosity multiplied by bed thickness) and cumulative flow capacity (permeability multiplied by bed thickness). Cumulative flow capacity is plotted on the vertical axis against cumulative storage capacity on the horizontal axis to create a chart used to estimate storage and flow capacities. Line segments and slopes of the graph separated by an inflection point are used to represent flow and storage capacities. The steeper the slope, the higher the flow capacity, while the flattened slope presents a barrier or has insignificant flow capacity. In this study, five different flow units, FU1-5 for well F-AH1, FU1-3 for well F-AH2 and FU1-5 in well F-AH4 are identified in **Figure 6-24** and **Table 6-5**. The best flow units identified for individual wells are FU2 for well F-AH1 contributing 28% and 50% storage and flow capacities, and FU1 in wells F-AH2 (16% storage and 51% flow capacities) and well F-AH4 (14% and 44% storage and flow capacities). Concurrently, FU5 makes a small contribution to the storage and flow capacities identified in well F-AH1 (13% and 1% storage and flow capacity) and well F-AH4 (6% and 1% storage and flow capacity).

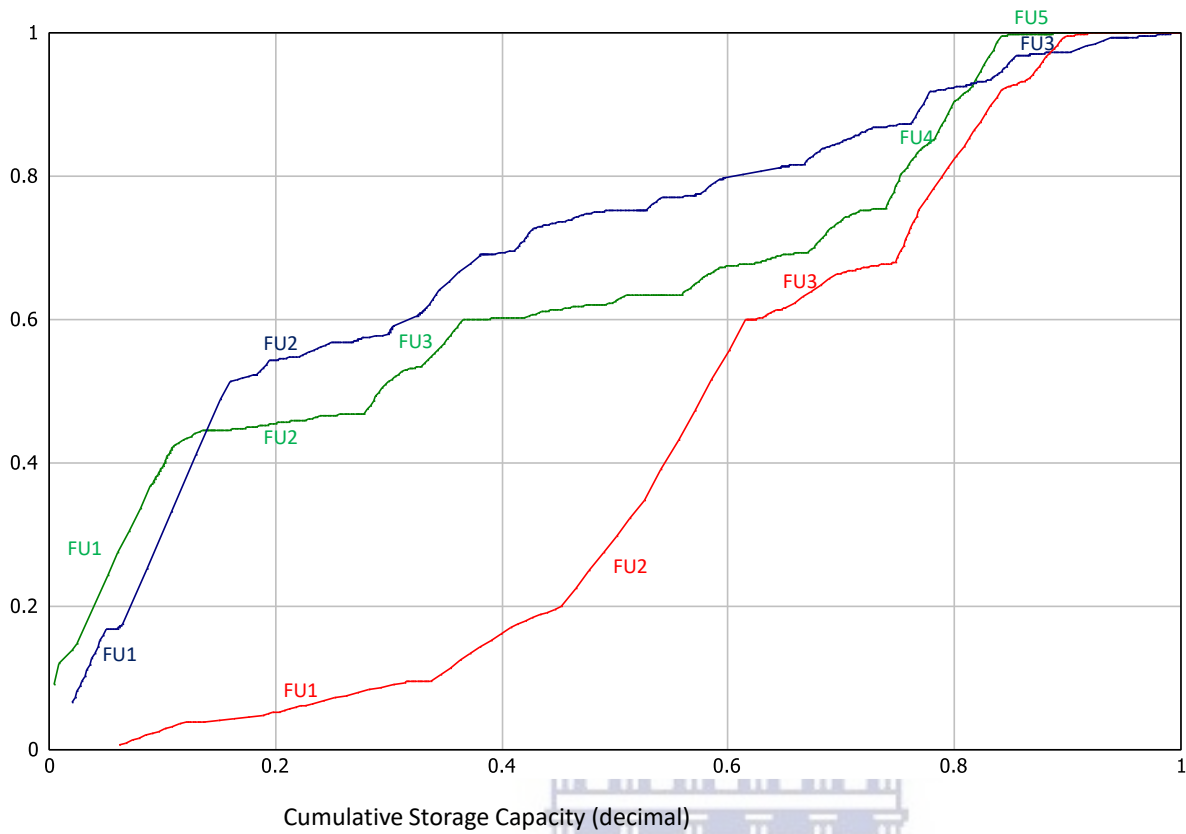


Figure 6- 24: Plot of cumulative flow and storage capacities for wells showing five different flow units, FU1-5

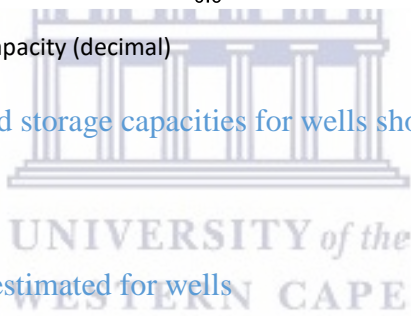


Table 6- 5: Storage and flow capacities estimated for wells

FLOW UNIT	F-AH1		F-AH2		F-AH4	
	Storage Capacity (%)	Flow Capacity (%)	Storage Capacity (%)	Flow Capacity (%)	Storage Capacity (%)	Flow Capacity (%)
1	34.0	9.5	16.0	51.0	14.0	44.0
2	28.0	50.5	70.0	45.0	14.0	3.0
3	10.0	8.0	14.0	4.0	9.0	13.0
4	15.0	31.0	-	-	47.0	39.0
5	13.0	1.0	-	-	6.0	1.0

6.5.2 Effect of Mineral on Flow Units

The XRD and SEM petrographic results have been integrated with the flow zones. Quantitative results from XRD show that the mineral composition of the four (4) samples from different flow zones (high, moderate, low and tight) is dominated by quartz and plagioclase (**Table 6-6**). Quartz content varies between 75.8% and 95.3% while plagioclase ranges from 2.6% to 12.1%. Carbonate fragments of dolomite (7.5%) and calcite (8.5%) were observed in the low and tight flow zones. Muscovite varies from 0.4% in the high flow zone sample to 1.3% in the tight flow zone sample, while the highest microcline of 2.4% is in the moderate and low flow zones and 1.5% and 1.7% were recorded in the tight and high flow zones. In addition, the samples showed low levels of pyrite and kaolinite. The effect of minerals on flow zones becomes evident as the content of plagioclase and muscovite increases. An accompanying decrease in quartz grade is observed, implying that a low plagioclase grade of $\leq 4\%$ and a muscovite grade of $\leq 1\%$ correspond to the low, moderate and high flow zones, while a plagioclase grade of $\geq 4\%$ and a muscovite grade of $\geq 1\%$ belong to the Tight Flow Zone. However, the amount of plagioclase and muscovite can be used as a proxy to identify better reservoir quality rocks and the flow zones are generally controlled by a combination of facies and diagenetic factors.

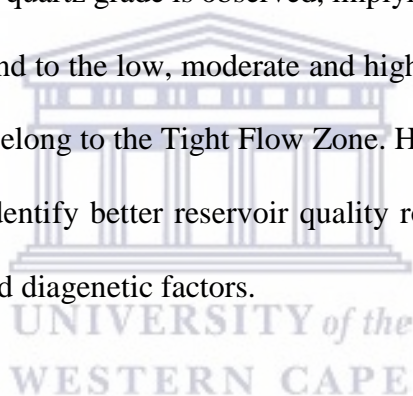


Table 6- 6: Qualitative XRD results showing the mineral content of different minerals

Well	Depth (m)	Zone Name	Quartz (%)	Dolomite (%)	Plagioclase (%)	Muscovite (%)	Calcite (%)	Microcline (%)	Pyrite (%)	Kaolinite (%)
F-AH1	2427	Moderate	93.7	0	3.2	0.6	0	2.4	0	0.1
F-AH1	2430	Low	84.6	7.5	3.8	1.4	0	2.4	0.2	0.2
F-AH4	2369	High	95.3	0	2.6	0.4	0	1.5	0	0.1
F-AH4	2442	Tight	75.8	0	12.1	1.3	8.5	1.7	0	0.7



CHAPTER SEVEN

7. CONCLUSION AND RECOMMENDATIONS

The F-AH Gas Field of the northeastern Bredasdorp Basin, offshore, South Africa, was evaluated from the study of three wells (F-AH1, F-AH2 and F-AH4). The petrophysical approach, petrographic evaluation and integration of the sandstone reservoir zonation were used for the identification of flow zones. It was later correlated with the identified zones in the other parts of the basin in the Gas Field with the use of core data. Generation of rock units grouping from core permeability and porosity uses two graphic methods; Petrophysical Rock Type (PRT) from the Winland r35 and Flow Zone Indicator (FZI) and Stratigraphic Modified Lorenz Plot (SMLP) with the integration of mineralogy composition analyses that plays an important role in understanding the factors that control reservoir behaviour. Detailed analysis and interpretation of well logs and core data are available. The clay volume was calculated using the linear Gamma Ray method. Across the reservoir interval, well F-AH1 had an average clay volume of 16.8 %, well F-AH2 had an average volume of 24.1% and well F-AH4 had 18.3% all of which are relatively clean sand formations with little clay and silt impact. Log-derived porosity was calculated using density, neutron and sonic log data with an emphasis on estimating porosity within the non-reservoir sections of each well. These wells returned good average log-derived porosities of 12.3%, 13.1% and 15.7%. The core permeability distribution across the studied wells ranged from 0.001 mD to 2767 mD. Water and gas were recorded within the core intervals of the well. Well F-AH1 through F-AH4 had average gas saturation of 61%, 57% and 27% respectively. Average core water saturations of 39%, 43% and 73% were measured per well. The average log-derived water saturations for the three wells were 45 %, 14 % and 42 %. Cut-off parameters were established to distinguish between pay and non-pay intervals. Pay potential intervals must have a porosity of at least 4 %, clay volume less than 40 %, and water saturation less than 65 %. Nine of seventeen reservoirs met the cut-off criteria

for net pay potential. Gross thicknesses of the reservoir intervals ranged from 3.30 –80.62 m and net thicknesses ranging from 0-79.84 m respectively. Reservoir 1 of well F-AH2 had the highest gross and net thicknesses of 80.75 m and 79.84 m at a net/gross ratio of 0.989. The lithofacies were interpreted based on geological setting and core data based on the five flow zones interpreted by flow zone calculations as high, moderate, low, very low, and tight. The high flow zone showed a storage capacity of 16% well F-AH2 and 14% in well F-AH4 and a flow capacity of 51% in well F-AH2 and 44% in well F-AH4. The very good petrophysical characteristics of the high flow zone indicate that significant amounts of gas can be produced from it, which is comparable to a high flow zone identified in well PA1 in the central Bredasdorp Basin. The diagenetic process reducing rock quality can be attributed to quartz overgrowth, accumulation of mica flakes in the pore spaces and high levels of plagioclase and muscovite. The fracture observed in the high flow zone is interpreted as an improvement in the reservoir quality-enhancing process. The flow zones are generally controlled by a combination of facies and diagenetic factors. This study has provided investigators with the opportunity to examine the vertical and lateral extent of the flow zone that extends to all well surveyed.

7.1 RECOMMENDATIONS

I strongly recommend that the Nuclear magnetic resonance (NRM) laboratory measurements be performed on the core samples of interest on the wells in the future to understand the reasons for the variety of the saturated exponent and better results. This will help to estimate the reservoir's initial water saturation accurately.

REFERENCES

- Adams S. J. (2005).** Core-to-log Comparison-What's a good match? Society of Petroleum Engineers Annual Technical Conference and Exhibition, Dallas, Texas.
- Adegbite, J.O.; Belhaj, H.; Bera, A. (2021).** Investigations on the Relationship among the Porosity, Permeability and Pore Throat Size of Transition Zone Samples in Carbonate Reservoirs Using Multiple Regression Analysis, Artificial Neural Network and Adaptive Neuro-Fuzzy Interface System. *Pet. Res.*, 6, 321–332.
- Al-Dhafeeri AM, Nasr-El-Din HA (2006)** Characteristics of high-permeability zones using core analysis and production logging data. *Journal of Petroleum Science and Engineering*, doi: 10.1016.
- Alger, R. P. (1980).** Geological use of wireline logs in development in petroleum geology. Applied science publication London, 2nd edition.
- Ali, M.; Abdelhady, A.; Abdelmaksoud, A.; Darwish, M.; Essa, M.A. (2020).** 3D Static Modeling and Petrographic Aspects of the Albian/Cenomanian Reservoir, Komombo Basin, Upper Egypt. *Nat. Resour. Res.*, 29, 1259–1281.
- Allogo, A.M., (2006).** Sedimentology and Stratigraphy of deep-water reservoirs in the 9A to 14A Sequences of the central Bredasdorp Basin, offshore South Africa: MSc. Thesis, University of Stellenbosch, pp. 20-30.
- Alqubalee, A.; Babalola, L.; Abdullatif, O.; Makkawi, M. (2019).** Factors Controlling Reservoir Quality of a Paleozoic Tight Sandstone, Rub'al Khali Basin, Saudi Arabia. *Arab. J. Sci. Eng.*, 44, 6489–6507.
- Amaefule JO, Altunbay M, Tiab D, Kersey DG, Keelan DK (1993):** Enhanced reservoir description: Using core and log data to identify hydraulic flow units and predict permeability in uncored intervals/wells. Society of Petroleum Engineers, paper 26436, 88th Annual Technical Conference and Exhibition; 205-220.
- Archie, G.E., (1942).** The Electrical resistivity log as an aid in determining some reservoir characteristics. *Transaction of AIME* pp.54, 146.
- Asadi, A.; Rahimpour-Bonab, H.; Aleali, M.; Arian, M. (2022).** Geologically Based Integrated Approach for Zonation of a Late Jurassic– Early Cretaceous Carbonate Reservoir, a Case from Persian Gulf. *J. Pet. Explor. Prod. Technol.*, 12, 1265–1283.
- Ayodele, O.L.; Chatterjee, T.K.; Opuwari, M. (2021).** Static Reservoir Modeling Using Stochastic Method: A Case Study of the Cretaceous Sequence of Gamtoos Basin, Offshore, South Africa. *J. Pet. Explor. Prod. Technol.*, 11, 4185–4200.
- Ayodele, O.L.; van Bever Donker, J.M.; Opuwari, M. (2016).** Pore Pressure Prediction of Some Selected Wells from the Southern Pletmos Basin, Offshore South Africa. *S. Afr. J. Geol.*, 119, 203–214.

Basin Offshore in South Africa. *Nat Resour Res* (2020). <https://doi.org/10.1007/s11053-020-09722-3>.

Bassiouni, Z., (1994) Theory, measurement, and interpretation of well logs (Vol. 4). Henry L. Doherty Memorial Fund of AIME, Society of Petroleum Engineers.

Bear J (1972): Dynamics of fluids in porous Media, Elsevier, New York.

Bell, C.P.T., Van Heerden, M., (1986). Geological well completion report of borehole FAH2: *a SOEKOR report*, pp.3.

Bell, C.P.T., Van Heerden, M., Wolmarans, C., Van Wyk, C., (1986). Geological well completion report of borehole F-AH1: *a SOEKOR report*, pp.4-8.

Boyer, J., Duvail, C., Le Strat, P., Gensous, B. and Tesson, M., (2005). High resolution stratigraphy and evolution of the Rhône delta plain during Postglacial time, from subsurface drilling data bank. *Marine Geology*, pp. 222-223, 267-298.

Broad, D., Jungslager, E., McLachlan, I. & Roux, J. (2006) "Offshore Mesozoic basins", *The Geology of South Africa. Geological Society of South Africa/Council for Geoscience, Pretoria*, pp. 553-571.

Brown, L.F., Brown Jr., L.F., Benson, J.M., Brink, G.J., Doherty, S., Jollands, A., Jungslager, E.H.A., Keenan, J.H.G., Muntingh, A and Van Wyk, N.J.S. (1995). Sequence stratigraphy in offshore South African divergent basins: an Atlas on Exploration for Cretaceous Lowstand Traps by SOEKOR Limited. AAPG Studies. Geol. 41, p 83–137 (SOEKOR (Pty) Ltd.).

Catuneanu, O., (2002). Sequence Stratigraphy of clastic systems: concept, merits, and pitfalls, *Journal of Earth Sciences*, 35, pp. 1-43.

Crain, 2014. www.spec2000.net/14-swbasics.htm

Dar, Q.U.; Pu, R.; Baiyegunhi, C.; Shabeer, G.; Ali, R.I.; Ashraf, U.; Sajid, Z.; Mehmood, M. (2022). The Impact of Diagenesis on the Reservoir Quality of the Early Cretaceous Lower Goru Sandstones in the Lower Indus Basin, Pakistan. *J. Pet. Explor. Prod. Technol.* **2022**, *12*, 1437–1452.

Davies, C.P.N., (1997). Hydrocarbon Evolution of the Bredasdorp Basin, offshore South Africa: from Source to Reservoir: Ph.D. thesis, University Stellenbosch, pp. 286.

Dingle, R.V., Siesser, W.G. and Newton, A.R. (1983). "Mesozoic and tertiary geology of South Africa". A.A. Balkema, Rotterdam, 375, pp. 22.

Dresser Atlas (1979): Log Interpretation Charts; Houston, Dresser Industries Inc.

Du Toit, S. R. (1976). "Mesozoic geology of the Agulhas Bank, South Africa". Ph.D. Thesis. Faculty of Science, University of Cape Town South Africa.

Ebanks, W.J., Jr.; (1987). AAPG. *Flow Unit Concept-Integrated Approach to Reservoir Description for Engineering Projects*; AAPG: Tulsa, OK, USA; Volume 71.

El Sharawy, M.S.; Nabawy, B.S. (2019). Integration of Electrofacies and Hydraulic Flow Units to Delineate Reservoir Quality in Uncored Reservoirs: A Case Study, Nubia Sandstone Reservoir, Gulf of Suez, Egypt. *Nat. Resour. Res.*, 28, 1587–1608.

Galloway, W.E., (1989). Genetic stratigraphic sequences in basin analysis I: Architecture and genesis of flooding-surface bounded depositional units. *American Association of Petroleum Geologists Bulletin*, 73 (2), pp. 125-142.

Gibbons, K., Hellem, T., Kjemperud, S.D.N. and Veibenstad K., (1993). Sequence architecture, facies development and carbonate-cemented horizons in the Troll Field reservoir, offshore Norway, In Ashton, M. (eds.), *Advances in reservoir Geology, Geological Society Special Publication*, 69, pp. 1-31.

Glover, P. (2009). Petrophysics course notes, University of the Aberdeen, Scotland

Gluyas, J., Swarbrick, R., (2004). *Petroleum Geoscience*. Blackwell Publishing, UK. 3-4.

Gunter, G.W.; Finneran, J.M.; Hartmann, D.J.; Miller, J.D. (1997). Early Determination of Reservoir Flow Units Using an Integrated Petrophysical Method. In *Proceedings of the SPE Annual Technical Conference and Exhibition*, San Antonio, TX, USA.

Guo, S.; Focke, W.W.; Tichapondwa, S.M. (2020). Sn/Mn/Bi₂O₃ Ternary Pyrotechnic Time Delay Compositions. *ACS Sustain. Chem. Eng.*, 8, 14524–14530.

Halderson, H.H., Damsleth, E., (1993). Challenges in reservoir characterization. *Amer. Assoc. Pet. Geol. Bull.*, 77, 541-551.

Halliburton (2001). *Basic Petroleum Geology and Log Analysis*; 35, 72.

Hamada, G. and Abushanab, M. (2008). Better porosity estimate of gas sandstone reservoirs using density and nmr logging data. *Emirates Journal for Engineering Research*, 13(3):47_54.

Hearn, C.L.; Ebanks, W.J.; Tye, R.S.; Ranganathan, V. (1984). Geological Factors Influencing Reservoir Performance of the Hartzog Draw Field, Wyoming. *J. Pet. Technol.*, 36, 1335–1344.

Hilchie, D.W. (1978). *Applied open-hole log interpretation*. Golden, Colorado: D.W. Hilchie. Inc.

Hseih, B., Lewis, C., Lin, Z. (2005). Lithological identification of aquifers from geophysical well logs and fuzzy logic analysis: Shui – Lin Area, Taiwan. *Computers & Geosciences*, 31, 263 – 275.

Hunt, D., and Tucker, M.E., (1995). Stranded parasequence and the forced regressive wedge systems tract: deposition during base-level fall-reply, *Sedimentary Geology*, 95, pp.147-160.

J.C., Bertram, G.T. (eds.), Sequence Stratigraphy of foreland basin deposits. *American Association of Petroleum Geologists Memoir*, 64, pp. 9-21.

Jarvis, K., (2006). Integrating well and Seismic data for Reservoir Characterization: Risks and rewards. Australia, Australia Earth Sciences Convention (ASEG) Extended Abstracts, July, 2006(1), Geological Society of Australia. Pp.1-4.

Jawoodien, A. (2011). Basic Petrophysics presentation (unpublished).

Jensen, E.H., Johansen, T.A., Avseth, P and Bredesen, K. (2016). Quantitative interpretation using inverse rock-physics modelling on AVO data. *The leading edge*, 35(8), 677-683.

Jungslager, E.H. (1999). Petroleum Habitats of the Atlantic Margin of South Africa. *Geol. Soc. Lond. Spec. Publ.*, 153, 153–168.

Kassab, M.A.; Hashish, M.F.A.; Nabawy, B.S.; Elnaggar, O.M. (2017). Effect of Kaolinite as a Key Factor Controlling the Petrophysical Properties of the Nubia Sandstone in Central Eastern Desert, Egypt. *J. Afr. Earth Sci.*, 125, 103–117.

Khalid, M.; Desouky, S.E.-D.; Rashed, M.; Shazly, T.; Sediek, K. (2020). Application of Hydraulic Flow Units' Approach for Improving Reservoir Characterization and Predicting Permeability. *J. Pet. Explor. Prod. Technol.*, 10, 467–479.

Kobesh, F.P and Blizard, R.B. (1959.) Geometric factors in sonic logging. *Geophysics*, Volume 24, pp. 64-76.

Kolodzie, S. (1980). Analysis of Pore Throat Size and Use of the Waxman-Smiths Equation to Determine OOIP in Spindle Field, Colorado. In Proceedings of the SPE Annual Technical Conference and Exhibition, Dallas, TX, USA.

Leila, M.; Moscariello, A.; Šegvić, B. (2019). Depositional Facies Controls on the Diagenesis and Reservoir Quality of the Messinian Qawasim and Abu Madi Formations, Onshore Nile Delta, Egypt. *Geol. J.*, 54, 1797–1813.

Li, Y.; Chen, J.; Elsworth, D.; Pan, Z.; Ma, X. (2022). Nanoscale Mechanical Property Variations Concerning Mineral Composition and Contact of Marine Shale. *Geosci. Front.* 2022, 13, 101405.

Li, Y.; Chen, J.-Q.; Yang, J.-H.; Liu, J.-S.; Tong, W.-S. (2022). Determination of Shale Macroscale Modulus Based on Microscale Measurement: A Case Study Concerning Multiscale Mechanical Characteristics. *Pet. Sci.*, 19, 1262–1275.

Li, Y.; Gao, X.; Meng, S.; Wu, P.; Niu, X.; Qiao, P.; Elsworth, D. (2019). Diagenetic Sequences of Continuously Deposited Tight Sandstones in Various Environments: A Case Study from Upper Paleozoic Sandstones in the Linxing Area, Eastern Ordos Basin, China. *AAPG Bulletin*, 103, 2757–2783.

Li, Y.; Wang, Z.; Pan, Z.; Niu, X.; Yu, Y.; Meng, S. (2019). Pore Structure and Its Fractal Dimensions of Transitional Shale: A Cross-Section from East Margin of the Ordos Basin, China. *Fuel*, 241, 417–431.

Lucia, F.J., (2007). Carbonate reservoir characterisation: an integrated approach. Berlin: Springer.

Magoba, M.; Opuwari, M. (2020). Petrophysical Interpretation and Fluid Substitution Modelling of the Upper Shallow Marine Sandstone Reservoirs in the Bredasdorp Basin, Offshore South Africa. *J. Pet. Explor. Prod. Technol.*, 10, 783–803.

Magoon, J.B. and W.G. Dow, (1994). The petroleum system-from source to trap. AAPG Memoir, 60: 619.

Magoon, L. B., and Beaumont, E. A., (1999). Petroleum systems, in Exploring for oil and gas traps edited by E. A. BEAUMONT and N. H. FOSTER: Tulsa, Oklahoma, USA, American Association of Petroleum Geologists, Treatise of Petroleum Geology, pp. 59–92.

Makeen, Y.M.; Shan, X.; Lawal, M.; Ayinla, H.A.; Su, S.; Yelwa, N.A.; Liang, Y.; Ayuk, N.E.; Du, X. (2021). Reservoir Quality and Its Controlling Diagenetic Factors in the Bentiu Formation, Northeastern Muglad Basin, Sudan. *Sci. Rep.*, 11, 18442.

Masindi, R.; Trivedi, K.B.; Opuwari, M. (2022). An Integrated Approach of Reservoir Characterization of Y Gas Field in Central Bredasdorp Basin, South Africa. *J. Pet. Explor. Prod. Technol.*, 1–19.

Mavko G, Tapan M, Dvorkin J (2009). The Rock Physics Handbook, 2 edn. Cambridge University Press, New York.

McMillan, I.K. (1990). Foraminiferal biostratigraphy of the Barremian to Miocene rocks of the Kudu 9A-1, 9A-2 and 9A-3 boreholes. Communications of the Geological Survey of Namibia, 6, 23 - 29.

McMillan, I.K.; Brink, G.I.; Broad, D.S.; Maier, J.J. (1997). Late Mesozoic Sedimentary Basins off the South Coast of South Africa. In *Sedimentary Basins of the World*; Elsevier: Amsterdam, The Netherlands; Volume 3, pp. 319–376.

Mitchum, R.M., Vail, P.R., Todd, R.G., Widmier, J.M., Thompson, S., Sangree, J.B., Bubb, J.N., and Hatlelid, W.G., (1977). Seismic stratigraphy and changes of sea-level, Part 1: Glossary of terms used in seismic stratigraphy. In: Payton, C.E. (eds.), Seismic stratigraphy and application to hydrocarbon exploration. *American Association of Petroleum Geologists Memoir*, 26, pp. 205-212.

Mode, A.W.; Anyiam, O.A.; Onwuchekwa, C.N. (2014). Flow Unit Characterization: Key to Delineating Reservoir Performance in “Aqua-Field”, Niger Delta, Nigeria. *J. Geol. Soc. India*, 84, 701–708.

Mohammadian, E.; Kheirollahi, M.; Liu, B.; Ostadhassan, M.; Sabet, M. (2022). A Case Study of Petrophysical Rock Typing and Permeability Prediction Using Machine Learning in a Heterogenous Carbonate Reservoir in Iran. *Sci. Rep.*, 12, 4505.

Moore, R.C. (1949). Meaning of facies. Memoir Geological Society of America 39. Mountain Association of Geologists 2004 Guidebook; pp. 226-227.

Nabawy, B.S. (2021). An Improved Stratigraphic Modified Lorenz (ISML) Plot as a Tool for Describing Efficiency of the Hydraulic Flow Units (HFUs) in Clastic and Non-Clastic Reservoir Sequences. *Geomech. Geophys. Geo-Energy Geo-Resour.*, 7, 67.

Nabawy, B.S.; Al-Azazi, N.A. (2015). Reservoir Zonation and Discrimination Using the Routine Core Analyses Data: The Upper Jurassic Sab'atayn Sandstones as a Case Study, Sab'atayn Basin, Yemen. *Arab. J. Geosci.*, 8, 5511–5530

Nabawy, B.S.; Elgendy, N.T.; Gazia, M.T. (2020). Mineralogic and Diagenetic Controls on Reservoir Quality of Paleozoic Sandstones, Gebel El-Zeit, Northeastern Desert, Egypt. *Nat. Resour. Res.*, 29, 1215–1238.

Nieto and Rojas, N. (1998). Geological and petrophysical reservoir in Apiay K2, Freedom Fields Suria and characterization. Ecopetrol, Internal report.

Opuwari, M. (2021). An Integrated Approach of Fluid Contact Determination of the Albian Age Sandstone Reservoirs of the Orange Basin Offshore South Africa. *Mar. Georesour. Geotechnol.*, 39, 876–888.

Opuwari, M., (2010). Petrophysical evaluation of the Albian age gas bearing sandstone reservoir of the O-M field, Orange Basin, South Africa, Ph.D.Thesis, South Africa: University of the Western Cape.

Opuwari, M., Amponsah-Dacosta, M., Mohammed, S., & Egesi, N. (2020a). Delineation of sandstone reservoirs of Pletmos Basin offshore South Africa into Flow Units using Core Data. *South African Journal of Geology*, 123(4), 479–492.

Opuwari, M.; Afolayan, B.; Mohammed, S.; Amaechi, P.O.; Bareja, Y.; Chatterjee, T. (2022). Petrophysical Core-Based Zonation of OW Oilfield in the Bredasdorp Basin South Africa. *Sci. Rep.*, 12, 510.

Opuwari, M.; Amponsah-Dacosta, M.; Mohammed, S.; Egesi, N. (2020). Delineation of Sandstone Reservoirs of Pletmos Basin Offshore South Africa into Flow Units Using Core Data. *S. Afr. J. Geol.* 2020, 123, 479–492.

Opuwari, M.; Dominick, N. (2021). Sandstone Reservoir Zonation of the North-Western Bredasdorp Basin South Africa Using Core Data. *J. Appl. Geophys.*, 193, 104425.

Opuwari, M.; Kaushalendra, B.T.; Momoh, A. (2019). Sandstone Reservoir Zonation Using Conventional Core Data: A Case Study of Lower Cretaceous Sandstones, Orange Basin, South Africa. *J. Afr. Earth Sci.*, 153, 54–66.

Opuwari, M.; Mohammed, S.; Ile, C. (2021). Determination of Reservoir Flow Units from Core Data: A Case Study of the Lower Cretaceous Sandstone Reservoirs, Western Bredasdorp Basin Offshore in South Africa. *Nat. Resour. Res.*, 30, 411–430.

Parker, I. (2014). Petrophysical evaluation of sandstone reservoirs of the Central Bredasdorp Basin, Block 9, Offshore South Africa. MSc. Thesis. The University of the Western Cape. Pp 198-200

Paton, D.A.; Di Primio, R.; Kuhlmann, G.; Van Der Spuy, D.; Horsfield, B. (2007). Insights into the Petroleum System Evolution of the Southern Orange Basin, South Africa. *S. Afr. J. Geol.*, 110, 261–274.

Petroleum Agency of South Africa (2003). Petroleum Exploration Information and Opportunities. In *Petroleum Agency South Africa Report*; Petroleum Agency of South Africa: Cape Town, South Africa.

Petroleum Agency SA, (2004/2005). Petroleum Exploration Information and Opportunities: Petroleum Agency SA Brochure, p15-20.

Petroleum Agency South Africa. (2012). Petroleum Exploration in South Africa.

Porras JC, Campos N (2001). Rock typing: A key Approach for Petrophysical characterization and definition of flow Units, Santa Barbara field, Eastern Venezuela Basin. SPE 69458.

Porras, J.C.; Barbato, R.; Khazen, L. (1999). Reservoir Flow Units: A Comparison between Three Different Models in the Santa Barbara and Pirital Fields, North Monagas Area, Eastern Venezuela Basin. In Proceedings of the Latin American and Caribbean Petroleum Engineering Conference, Caracas, Venezuela.

Posamentier, H.W., Jersey, M.T. and Vail, P.R., (1988). Eustatic controls on clastic deposition I. Conceptual framework. In: Wilgus, C.K., Hastings, B.S., Kendall, C.G.S.C.,

Poupon, A., and Leveaux, J., (1971). Evaluation of water saturation in shaly formations; Trans. SPWLA 12th Annual Logging Symposium; pp. 2.

Pranter, M.J.; Hurley, N.F.; Davis, T.L. (2004). *Sequence-Stratigraphic, Petrophysical, and Multicomponent Seismic Analysis of a Shelf-Margin Reservoir: San Andres Formation (Permian), Vacuum Field, New Mexico, United States*; ACS Publishers: Washington, DC, USA Press

Radwan, A.E.; Nabawy, B.S.; Kassem, A.A.; Hussein, W.S. (2021). Implementation of Rock Typing on Waterflooding Process during Secondary Recovery in Oil Reservoirs: A Case Study, El Morgan Oil Field, Gulf of Suez, Egypt. *Nat. Resour. Res.*, 30, 1667–1696.

Ramiah, K.; Trivedi, K.B.; Opuwari, M. (2019). A 2D Geomechanical Model of an Offshore Gas Field in the Bredasdorp Basin, South Africa. *J. Pet. Explor. Prod. Technol.*, 9, 207–222.

Rider, M. (2002). The Geological interpretation of well logs. Second edition, p1

Rider, M. H., (1996). The geological interpretation of well logs. 3rd Revised edition ed. New York: Petroleum Exploration consultant Rider-French consultant Ltd Cambridge and Sutherland. Halsted press, a division of John Wiley and Sons.

Roger GW, Noel PJ (1992). Facies Models response to sea level change. Geological Association of Canada. Love Printing services Ltd, Stilts Ville, Ontario, pp2.

Opuwari, M.; Manzi, M.S.; Durrheim, R.J. (2020). Geomechanical Characterization of CO₂ Storage Sites: A Case Study from a Nearly Depleted Gas Field in the Bredasdorp Basin, South Africa. *J. Nat. Gas Sci. Eng.*, 81, 103446.

Schalkwyk, H.J., (2005). Assessment controls on reservoir performance and the effects of granulation seam mechanics in the Bredasdorp Basin, South Africa: MSc. Thesis, University of the Western Cape, pp. 24.

Schlager, W. (1999). Type 3 sequence boundaries. In: Harris, P, Saller, A. and Simo, A. (eds), Carbonate sequence stratigraphy: application to reservoirs, outcrops and models. Society of Sedimentary Geology, Spec. Pub. 63, p. 35-46.

Schlumberger, (1972). *Log interpretation/charts*. Houston: Schlumberger well services.

Schlumberger Ltd (2013). Grain density classification: Houston, Texas.

Schroeder, F. (2004). *Well Log Data*, s.l.: American Association of Petroleum Geologists.

Serra, O. (1984). *Fundamentals of Well-Log Interpretation: The acquisition of logging data*. Vol.1 ed. Amsterdam: Elsevier.

Simandoux, P. (1963). Dielectric Measurements on Porous Media: Application to measurement of water saturation. Study of the behaviour of argillaceous formation. SPWLA, Houston, vol; 97-124.

Sixsmith, P.J., (2000). Stratigraphic development of a Permian turbidite system on a deforming basin floor: Laingsburg Formation, Karoo Basin, South Africa, Unpublished Ph.D. thesis. University of Liverpool, pp. 229.

Slath, R. M., (2009). Stratigraphic Reservoir Characterization for petroleum Geologists, Geophysics and Engineers. Elsevier, the Netherlands, UK. 1-2.

Slatt, R.M.; Hopkins, G.L. (1990). Scaling Geologic Reservoir Description to Engineering Needs. *J. Pet. Technol.*, 42, 202–210.

Suzanne, G.C., and Robert, M.C., (2004). Petrophysics of the Lance Sandstone Reservoirs in Jonah Field, Sublette County, Wyoming. AAPG Studies in Geology 52 and Rocky Mountain Association of Geologists 2004 Guidebook; pp. 226-227.

Szabo, N.P., (2010). Shale volume estimation based on the factor analysis of well-logging data. University of Miskolc, Department of Geophysics, 3515 Miskolc-Egyetemváros, Hungary, pp 1-4.

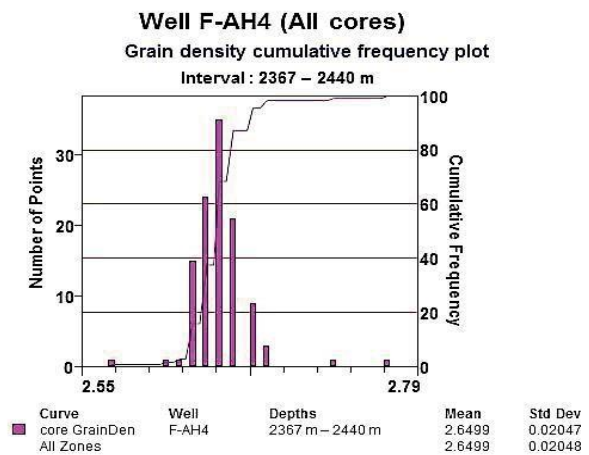
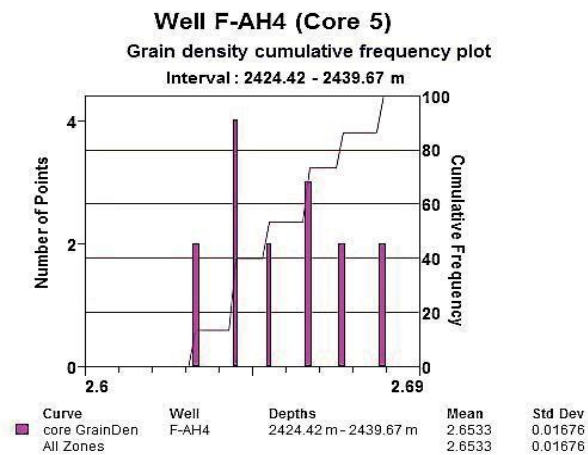
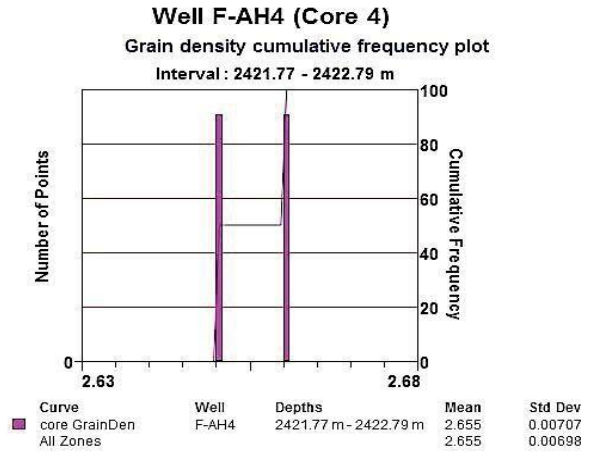
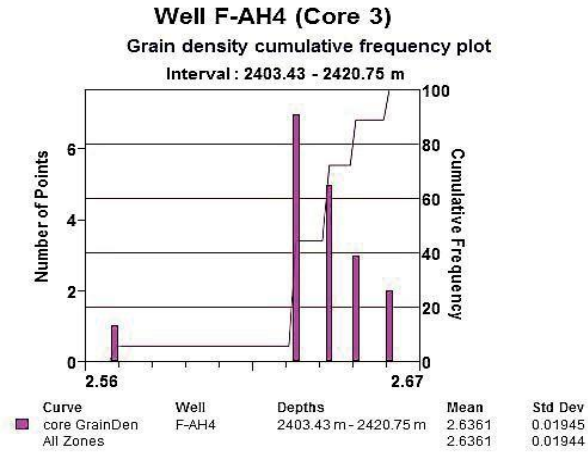
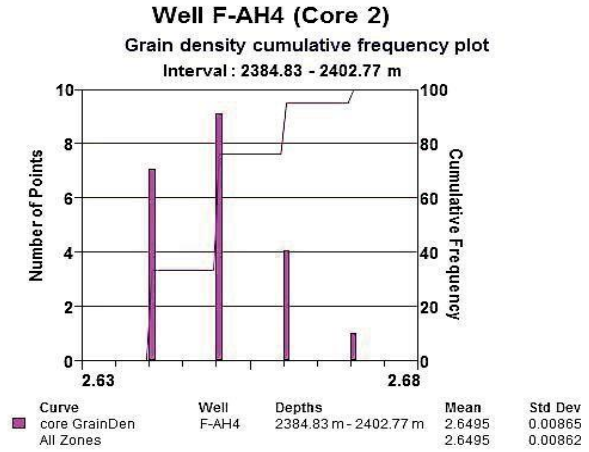
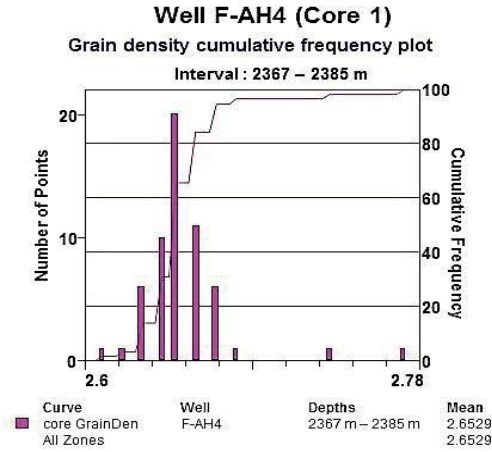
Turner, J.R., Grobber, N. and Sontudu, S. (2000). Geological modelling of the Aptian and Albian sequences within Block 9, the Bredasdorp Basin, offshore South Africa. *Journal of African sciences*, 31(1), 80.

Van der Spuy, D., (2000). Potential source rocks and modelled maturity levels in the southern Outeniqua Basin, offshore South Africa.

- Van Wagoner, J.C., (1995).** Overview of sequence stratigraphy of foreland basin deposits: terminology, a summary of papers, and glossary of sequence stratigraphy. *In: Van Wagoner.*
- Walker, R.G., (1992).** Wave- and storm-dominated shallow marine systems. *Facies Models- response to sea-level change. Geological Association of Canada: 200-238. St. Johns.*
- Wang, W.; Jiang, Y.; Swennen, R.; Yuan, J.; Liu, J.; Zhang, S. (2018).** Pore-Throat Characteristics of Tight Sandstone Reservoirs Composed of Gravity Flow Sediments: Yingcheng Formation, Longfengshan Sag, China. *J. Pet. Sci. Eng., 171, 646–661.*
- Williams, A. (2014).** *Identifying compartmentalization of the E-M field, Bredasdorp Basin (South Africa) using well logs and core data.* Structured Petroleum Geology MSc Mini-thesis, University of Western Cape (Unpublished). Cape Town.
- Winland, H.D. (1972).** Amoco Production Research Report No. F72-G25 1972. In *Oil Accumulation in Response to Pore Size Changes, Weyburn Field, Saskatchewan;* Amoco: London, UK.
- Wyllie, M.R.J., (1963).** The fundamentals of Well Log Interpretation. New York Academic Press
- Wyllie, M.R.J., Gregory, A.R., and Gardner, G.H.F., (1958).** An experimental investigation of factors affecting elastic wave velocities in porous media. *Geophysics, vol.23.*
- Yu, P. (2021).** Hydraulic Unit Classification of Un-Cored Intervals/Wells and Its Influence on the Productivity Performance. *J. Pet. Sci. Eng., 197, 107980.*
- Zhang, Z.; Zhang, H.; Li, J.; Cai, Z. (2021).** Permeability and Porosity Prediction Using Logging Data in a Heterogeneous Dolomite Reservoir: An Integrated Approach. *J. Nat. Gas Sci. Eng., 86, 103743.*

APPENDICES

APPENDIX 1- GRAIN DENSITY HISTOGRAM



APPENDIX 2 - RANGE OF CORE AND LOG ESTIMATED PERMEABILITY

WELL F-AH1

Well	Reservoir	Top Depth (m)	Bottom Depth (m)	Data type	Min (mD)	Max (mD)	Mean (mD)
F-AH1	1	2411.883	2427.885	Est. K	0.338	4676.31	365.139
				Core K	0.04	232	50.931
	2	2430.17	2454.25	Est. K	0	214.883	13.621
				Core K	0.19	143	52.684
	3	2498.598	2502.865	Est. K	10.658	486.259	105.016
				Core K	N/A	N/A	N/A
	4	2561.082	2569.312	Est. K	0.004	66.984	14.02
				Core K	N/A	N/A	N/A

WELL F-AH2

Well	Reservoir	Top Depth (m)	Bottom Depth (m)	Data type	Min (mD)	Max (mD)	Mean (mD)
F-AH2	1	2364.029	2444.648	Est. K	0.476	202.541	29.257
				Core K	0.69	497	89.94
	2	2457.45	2462.174	Est. K	0.562	47.519	15.467
				Core K	2.5	2.5	2.5
	3	2487.32	2490.216	Est. K	0.215	5.593	1.912
				Core K	N/A	N/A	N/A
	4	2554.072	2557.577	Est. K	0.124	28.931	6.772
				Core K	N/A	N/A	N/A

WELL F-AH4

Well	Reservoir	Top Depth (m)	Bottom Depth (m)	Data type	Min (mD)	Max (mD)	Mean (mD)
F-AH4	1	2369.363	2376.373	Est. K	0.01	7.192	1.033
				Core K	0.08	1221.547	360.386
	2	2378.05	2428.646	Est. K	0.123	244.858	16.246
				Core K	0.07	985.714	182.42
	3	2451.202	2458.212	Est. K	0.067	29.799	6.005
				Core K	N/A	N/A	N/A
	4	2476.957	2482.291	Est. K	0.065	14.04	3.729
				Core K	N/A	N/A	N/A
	5	2517.038	2524.658	Est. K	0.018	12.39	2.432
				Core K	N/A	N/A	N/A
	6	2528.469	2535.631	Est. K	0.459	15.707	5.008
				Core K	N/A	N/A	N/A
	7	2546.299	2549.5	Est. K	0.008	9.232	1.182
				Core K	N/A	N/A	N/A
	8	2557.882	2560.7	Est. K	0.002	12.229	3.513
				Core K	N/A	N/A	N/A



APPENDIX 3 - CALCULATED VALUES FOR RQI, NPI AND FZI

WELL F-AH1

Depth(m)	Porosity	Kair (mD)	RQI	NPI	FZI
2415.1	0.064	5.2	0.28	0.07	4.00
2416.61	0.075	32	0.65	0.08	8.13
2417.82	0.004	0.063	0.12	4.02	0.03
2418.46	0.057	8	0.37	0.06	6.17
2419.86	0.059	17	0.53	0.06	8.83
2421	0.067	19	0.53	0.07	7.57
2422.91	0.033	1.7	0.23	0.03	7.67
2424	0.092	76	0.90	0.10	9.00
2425.2	0.084	41	0.69	0.09	7.67
2426.04	0.114	180	1.25	0.13	9.62
2427.03	0.117	252	1.46	0.13	11.23
2429.47	0.026	0.28	0.10	0.03	3.33
2430.51	0.062	37	0.77	0.07	11.00
2431.35	0.027	6.2	0.48	0.03	16.00
2432.27	0.082	67	0.90	0.09	10.00
2433.92	0.08	21	0.51	0.09	5.67
2435	0.067	15	0.47	0.07	6.71
2435.72	0.069	7.8	0.33	0.07	4.71
2437	0.054	147	1.64	0.06	27.33

2438	0.077	135	1.31	0.08	16.38
2439	0.088	159	1.33	0.10	13.30
2440.51	0.063	29	0.67	0.67	1.00
2442	0.093	141	1.22	0.10	12.20
2449.34	0.071	13	0.42	0.08	5.25
2452.2	0.066	0.3	0.07	0.07	1.00
2458.5	0.02	0.11	0.07	0.02	3.50
2459.49	0.041	0.21	0.07	0.04	1.75
2460.52	0.039	0.05	0.04	0.04	1.00



WELL F-AH2

Depth(m)	Porosity	Kair (mD)	RQI	NPI	FZI
2368.62	0.16	507	1.77	0.19	9.32
2369.8	0.16	527	1.80	0.19	9.47
2370.69	0.15	503	1.82	0.18	10.11
2371.59	0.094	1.09	0.11	0.10	1.10
2372.52	0.077	88	1.06	0.08	13.25
2373.13	0.15	521	1.85	0.18	10.28
2378.6	0.147	403	1.64	0.17	9.65
2379.16	0.103	44	0.65	0.11	5.91
2380.92	0.065	1.02	0.12	0.07	1.71
2381.45	0.107	175	1.27	0.12	10.58
2382.45	0.088	24	0.52	0.10	5.20
2383.33	0.114	28	0.49	0.13	3.77
2384.69	0.172	103	0.77	0.21	3.67
2386.3	0.094	4	0.20	0.10	2.00
2387.97	0.126	78	0.78	0.14	5.57
2388.71	0.155	32	0.45	0.18	2.50
2390.11	0.158	406	1.59	0.19	8.37
2390.38	0.123	73	0.76	0.14	5.43
2391.95	0.121	163	1.15	0.14	8.21
2392.57	0.148	320	1.46	0.17	8.59
2393.27	0.141	186	1.14	0.16	7.13
2395.69	0.106	19	0.42	0.12	3.50

2396.36	0.069	6	0.29	0.07	4.14
2397.09	0.125	29	0.48	0.14	3.43
2398.43	0.153	274	1.33	0.18	7.39
2399.47	0.13	53	0.63	0.15	4.20
2400.35	0.145	42	0.53	0.17	3.12
2401.52	0.142	86	0.77	0.17	4.53
2402.54	0.124	24	0.44	0.14	3.14
2403.44	0.114	24	0.46	0.13	3.34
2404.4	0.09	1.5	0.13	0.10	1.30
2406.6	0.11	4.4	0.20	0.12	1.67
2407.33	0.147	170	1.07	0.17	6.29
2408.24	0.092	1.8	0.14	0.10	1.40
2409.35	0.077	8.2	0.32	0.08	4.00
2411.23	0.115	55	0.69	0.13	5.31
2411.76	0.141	154	1.04	0.16	6.50
2412.91	0.096	36	0.61	0.11	5.55
2413.39	0.123	37	0.54	0.14	3.86
2417.05	0.109	31	0.53	0.12	4.42
2417.89	0.117	15	0.36	0.13	2.77
2418.85	0.141	183	1.13	0.16	7.06
2419.94	0.121	62	0.71	0.14	5.07
2421.07	0.143	92	0.80	0.17	4.71
2422.16	0.116	83	0.84	0.13	6.46
2423.28	0.094	3.9	0.20	0.10	2.00

2424.18	0.147	41	0.52	0.17	3.06
2425.19	0.113	14	0.35	0.13	2.69
2425.95	0.135	355	1.61	0.16	10.06
2427.06	0.146	41	0.53	0.17	3.12
2428.04	0.116	28	0.49	0.13	3.77
2429.31	0.13	67	0.71	0.15	4.73
2430.03	0.087	2.3	0.16	0.10	1.60
2430.84	0.106	92	0.93	0.12	7.75
2431.89	0.114	186	1.27	0.13	9.77
2433.15	0.077	3.2	0.20	0.08	2.50
2434.35	0.095	38	0.63	1.04	0.61
2435.06	0.083	1.6	0.14	0.09	1.56
2435.9	0.104	14	0.36	0.12	3.00
2436.82	0.155	2.9	0.14	0.18	0.78
2437.62	0.144	73	0.71	0.17	4.18
2439.95	0.09	6.6	0.27	0.10	2.70
2441.15	0.104	14	0.36	0.12	3.00
2441.41	0.075	5.9	0.28	0.08	3.50
2442.4	0.084	11	0.36	0.09	4.00
2443.33	0.103	16	0.39	0.11	3.55
2444.31	0.143	21	0.38	0.17	2.24
2445.66	0.133	45	0.58	0.15	3.85
2459.35	0.096	3.4	0.19	0.12	1.58

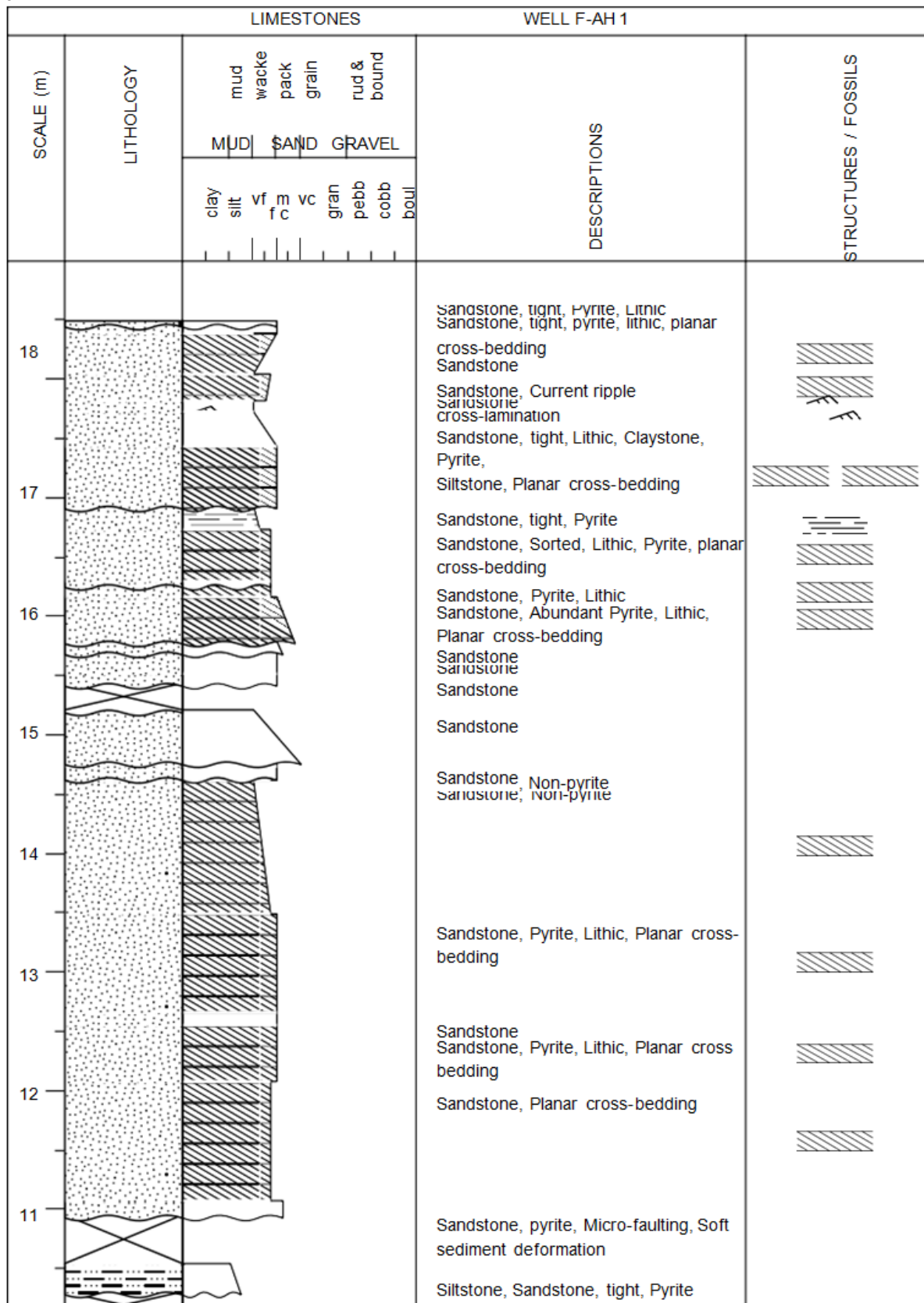
WELL F-AH4

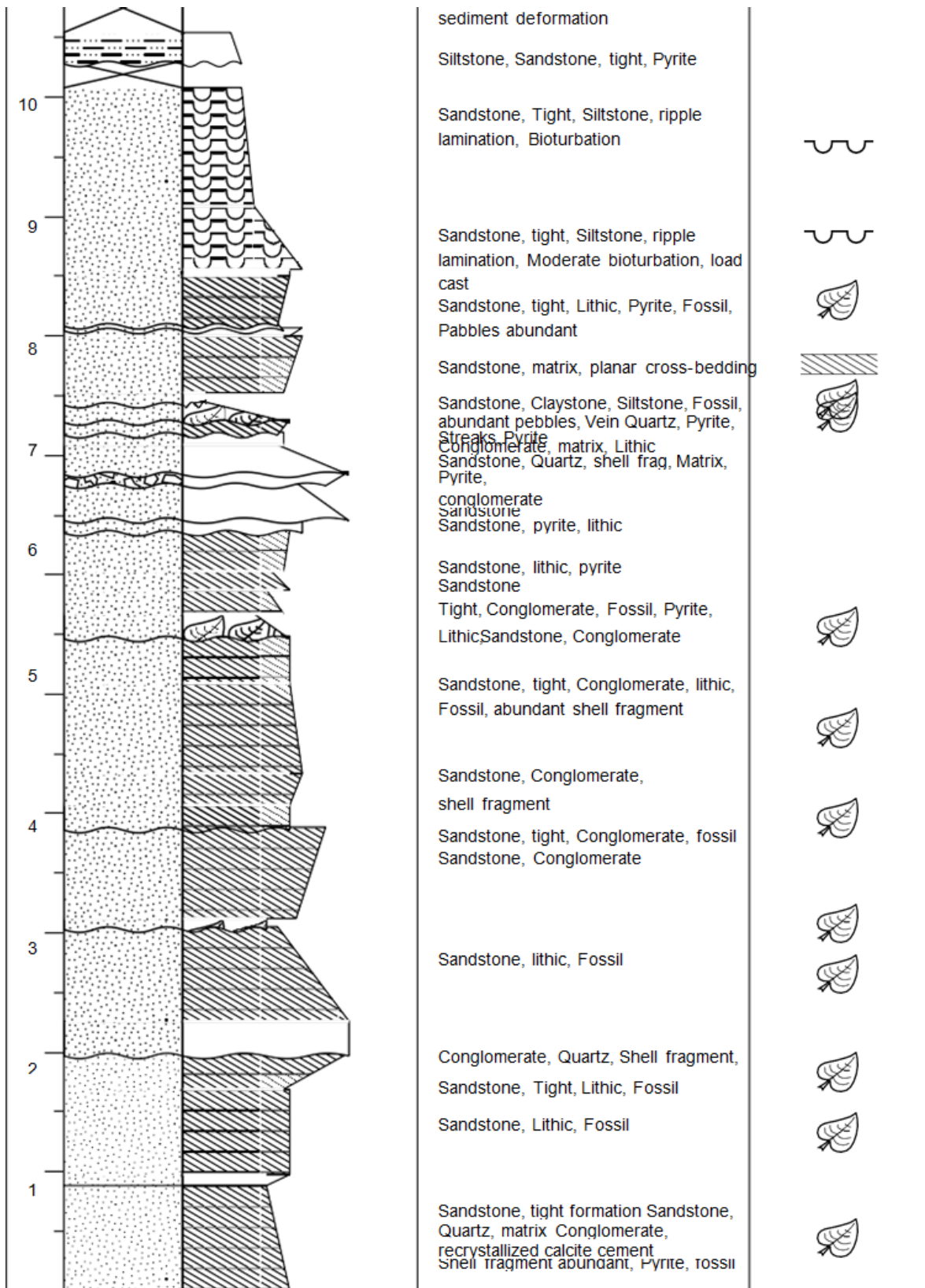
Depth(m)	Porosity	Kair (mD)	RQI	NPI	FZI
2367.05	0.203	2843.16	3.72	0.25	14.59
2368.08	0.17	1156.66	2.59	0.20	12.65
2371.78	0.187	1084.29	2.39	0.23	10.40
2372.81	0.128	221.713	1.31	0.15	8.90
2374.68	0.094	3.453	0.19	0.10	1.83
2375.67	0.101	0.594	0.08	0.11	0.68
2376.68	0.147	51.438	0.59	0.17	3.41
2377.66	0.128	54.068	0.65	0.15	4.40
2378.61	0.129	76.107	0.76	0.15	5.15
2379.64	0.153	74.233	0.69	0.18	3.83
2380.61	0.101	5.303	0.23	0.11	2.03
2381.61	0.151	152.79	1.00	0.18	5.62
2382.57	0.123	6.235	0.22	0.14	1.59
2383.63	0.135	25.226	0.43	0.16	2.75
2384.63	0.07	0.162	0.05	0.08	0.63
2385.62	0.179	827.3	2.13	0.22	9.79
2386.61	0.161	393.385	1.55	0.19	8.09
2387.59	0.143	99.919	0.83	0.17	4.97
2388.58	0.161	500.622	1.75	0.19	9.12
2389.58	0.188	781.058	2.02	0.23	8.74
2390.58	0.12	13.114	0.33	0.14	2.41
2391.56	0.127	5.236	0.20	0.15	1.39

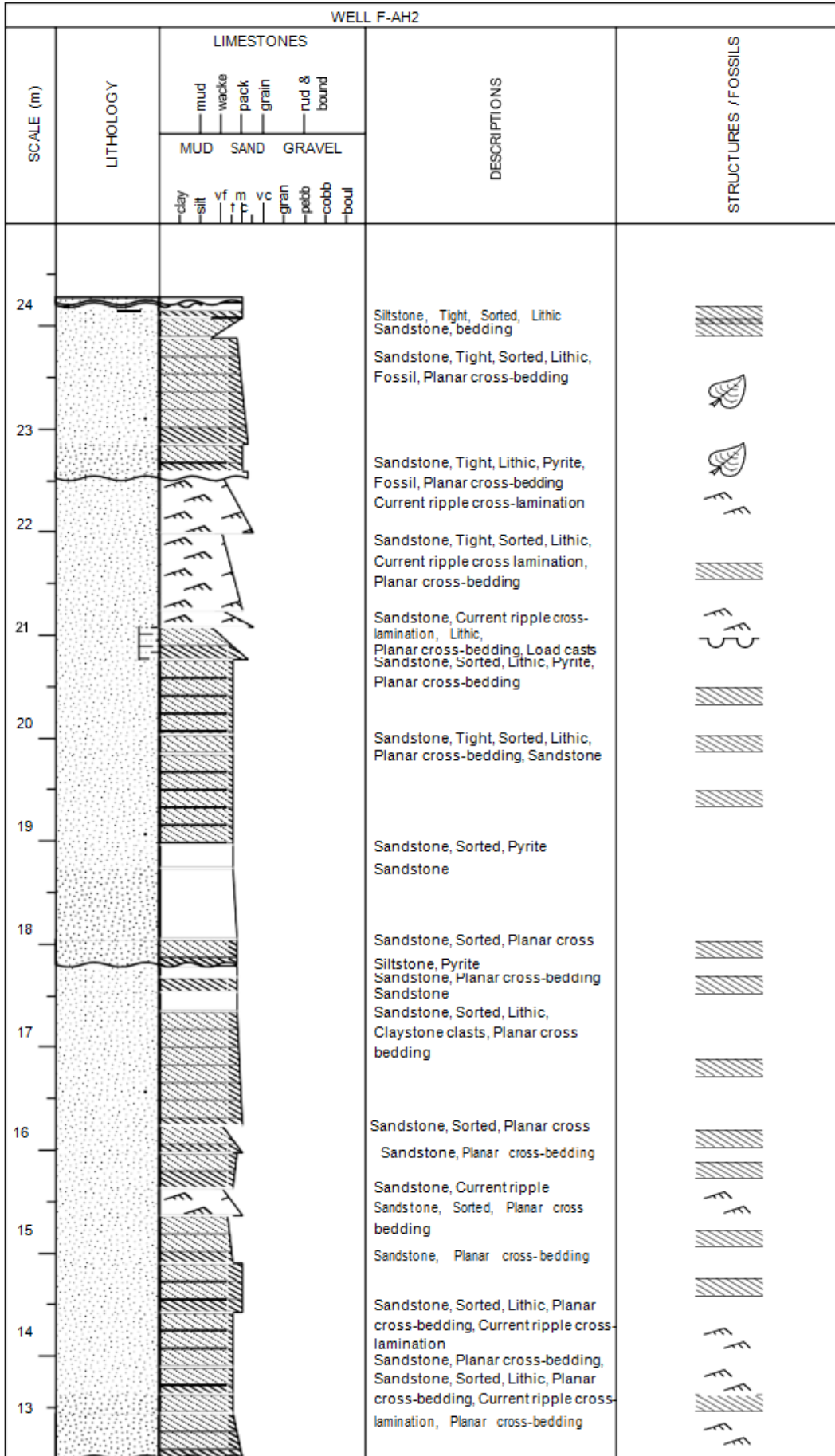
2392.53	0.122	3.389	0.17	0.14	1.19
2393.53	0.138	36.932	0.51	0.16	3.21
2394.52	0.166	166.173	0.99	0.20	4.99
2395.56	0.13	45.014	0.58	0.15	3.91
2396.6	0.155	95.387	0.78	0.18	4.25
2397.59	0.11	4.54	0.20	0.12	1.63
2398.61	0.092	3.964	0.21	0.10	2.03
2399.65	0.17	261.766	1.23	0.20	6.02
2400.65	0.133	6.668	0.22	0.15	1.45
2401.65	0.102	1.507	0.12	0.11	1.06
2402.77	0.11	1.079	0.10	0.12	0.80
2403.43	0.102	12.804	0.35	0.11	3.10
2404.76	0.166	447.412	1.63	0.20	8.19
2405.86	0.146	264.163	1.34	0.17	7.81
2406.89	0.132	59.398	0.67	0.15	4.38
2407.74	0.105	19.401	0.43	0.12	3.64
2408.76	0.135	101.809	0.86	0.16	5.53
2409.73	0.131	148.374	1.06	0.15	7.01
2410.71	0.118	50.331	0.65	0.13	4.85
2411.76	0.108	1.069	0.10	0.12	0.82
2412.72	0.166	614.495	1.91	0.20	9.60
2413.72	0.141	361.755	1.59	0.16	9.69
2414.75	0.146	204.177	1.17	0.17	6.87
2415.74	0.092	13.358	0.38	0.10	3.73

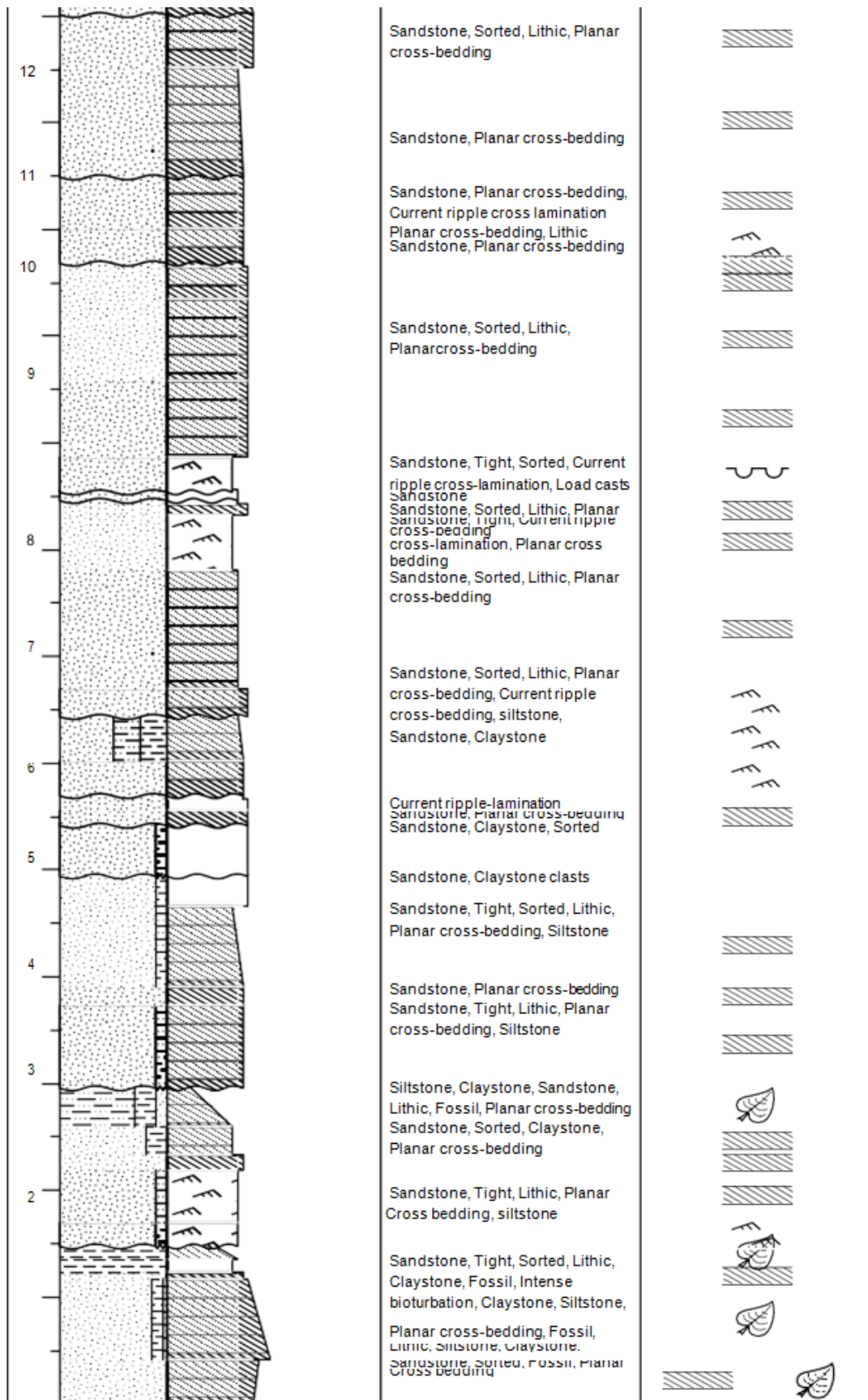
2416.74	0.094	9.045	0.31	0.10	2.97
2417.73	0.132	928.201	2.63	0.15	17.31
2418.73	0.149	685.683	2.13	0.18	12.17
2419.75	0.124	300.956	1.55	0.14	10.93
2420.75	0.16	987.754	2.47	0.19	12.95
2421.78	0.139	386	1.65	0.16	10.25
2422.78	0.149	851	2.37	0.18	13.55
2424.43	0.119	47.26	0.63	0.14	4.63
2425.58	0.061	0.15	0.05	0.06	0.76
2428.46	0.124	10.08	0.28	0.14	2.00
2429.73	0.146	6.95	0.22	0.17	1.27
2430.46	0.124	11.09	0.30	0.14	2.10
2431.21	0.066	0.34	0.07	0.07	1.01
2431.49	0.034	0.02	0.02	0.04	0.68
2432.51	0.12	0.52	0.07	0.14	0.48
2433.51	0.076	0.04	0.02	0.08	0.28
2434.68	0.12	0.53	0.07	0.14	0.48
2435.68	0.114	0.81	0.08	0.13	0.65
2436.67	0.135	1.77	0.11	0.16	0.73
2437.66	0.115	0.58	0.07	0.13	0.54
2438.67	0.067	0.23	0.06	0.07	0.81
2439.66	0.083	0.02	0.02	0.09	0.17

APPENDIX 4 - GRAPHIC SEDIMENTARY STRUCTURE









WELL F-AH4													
SCALE (m)	LITHOLOGY	LIMESTONES							DESCRIPTIONS	STRUCTURES / FOSSILS			
		mud	wacke	pack	grain	rud &	bound						
		MUD		SAND		GRAVEL							
		clay	silt	vf	m	vc	gran	pebb	cobb	boul			
59													
58													
57													
56													
55													

